EFFICIENT SOLAR ENERGY HARVESTING USING IMAGE PROCESSING AND SOFT COMPUTING TECHNIQUE

A Thesis Submitted

IN PARTIAL FULFILLMENT OF THE REQUIREMENTS

FOR THE DEGREE OF

DOCTOR OF PHILOSOPHY
IN
Electrical Engineering
Department of Electrical, Electronics and Communication Engineering

By

KANHAIYA KUMAR

Regd. No. – 18SECE3010001

Under the supervision of

Dr. Lokesh Varshney (Supervisor)
Dr. A. Ambikapathy (Co-supervisor)

GALGOTIAS UNIVERSITY
UTTAR PRADESH

[2022]

STATEMENT OF THESIS PREPARATION

1. Thesis title: Efficient Solar Energy Harvesting using Image Processing and Soft Computing Technique.

2. Degree for which the thesis is submitted: Doctor of Philosophy in Electrical Engineering, Department of Electrical, Electronics and Communication Engineering.

3. Thesis Guide was referred to for preparing the thesis.

4. Specifications regarding thesis format have been closely followed.

5. The contents of the thesis have been organized based on the guidelines.

6. The thesis has been prepared without resorting to plagiarism.

7. All sources used have been cited appropriately.

8. The thesis has not been submitted elsewhere for a degree.

(Signature of the Student)

Name: Kanhaiya Kumar

Roll No: 18SECE3010001

APPROVAL SHEET

This thesis entitled “Efficient Solar Energy Harvesting using Image Processing and Soft Computing Technique” by Mr. Kanhaiya Kumar is approved for the degree of Doctor of Philosophy.

Examiners

Supervisor (s)

Chairman

Date: ----------
Place: ----------

CANDIDATE'S DECLARATION

I hereby certify that the work which is being presented in the thesis, entitled "**Efficient Solar Energy Harvesting using Image Processing and Soft Computing Technique**" in fulfillment of the requirements for the award of the degree of Doctor of Philosophy in Faculty and submitted in Galgotias University, Greater Noida is an authentic record of my own work carried out during a period from 28/09/2018 to 04/04/2022 under the supervision of Dr. **Lokesh Varshney** (Supervisor) and Dr. **A. Ambikapathy** (Co-Supervisor**).**

The matter embodied in this thesis has not been submitted by me for the award of any other degree of this or any other University/Institute.

(Kanhaiya Kumar)

This is to certify that the above statement made by the candidate is correct to the best of our knowledge.

(**Dr. Lokesh Varshney)**	(**Dr. A. Ambikapathy**)
Supervisor	Co-Supervisor
Deptt. of DEECE	Deptt. of EEE

The Ph.D. Viva-Voice examination of_____Research Scholar has been held on_____.

Sign. of Supervisor(s) Sign. of Co-Supervisor(s) Sign. of External Examiner

ABSTRACT

Electricity is a vital power source for the world's rapidly rising population, and its usage of conventional resources is hazardous to the world environs. This cause is related to the destruction of the atmosphere and environs, so effective decision is essential to overcome these challenges, which resulted in the rapid development of sustainable. Geothermal, Hydropower, Solar, Biofuels & wind energy are the main renewable resources with contributed to the development of our country and their market have been growing at rapid pace since the Indian government introduce different economic policies to reduce the generation of greenhouse gasses. Beyond this renewable energy, solar energy is most favourable energy regarding India where on average 245 days of clear sky out of 365 days. Sun energy is gaining popularity and is poised to be among the most essential components of the future of the planet power harvesting and financial growth. The use of low-cost, energy-efficient solar power systems is one strategy to upsurge the usage of Sun power schemes, particularly in rural and underdeveloped areas. There are various types of solar power system to extract electricity or heat energy.

This report dispenses the design, working and result analysis of a two-axis soft computing and GPS based solar energy harvesting system. This Nobel method improved result compare to various solar power extractors like, Stable panel system, one axis LDR centred Sun tracer, two axis LDR centred Sun tracer. The above said Sun energy extractor system have various draw back which is remove in applied system. LDR sensor based sun followers have low tracking accuracy and because of an electrical part low sensitivity to climate and can damage by lightning discharge, It works on the sensor so its tracker is obstructed which produce hampers in energy production and System require continuously monitored. We have also simulated the hybrid system and performance parameter is evaluated.

This project consists of three major parts, hardware, software and electronics and electrical. Two stepper motor carried out the rotate of solar panels and GPS, Soft computing and image processing used to monitor panel orientation. Here detail introduction of hardware design consideration dimension (U-shaped solar panel supporter, Solar panel base support, Metallic stand for system, Threaded metallic rod, Vertical tracking rod, Horizontal tracking pipe, Metallic Angle joint, Vertical tracking Rod stopper, DC motor support, Flange Linear Ball Bearing, Flanged Coupler, Pillow Thrust Bearing, Angular support for DC motor),

electronics part (DC geared motor & driver, Image sensor, GPS, LDR, Raspberry PI, Semi flexible Photovoltaic panel, Power supply, Voltage regulator and Personal computer) and software used (MATLAB Simulink, Python software and Arduino Software (IDE)). The proposed sun energy systems are as follows

1. A hybrid power generating system based on renewable wind turbine energy and solar PV dependable sources outlined in Chapter 4 is simulated, modelled, and designed. The principal system is a solar electric generator that consists of six-models that are linked in series centred on predictive P&O and is connected to an MPPT controller and AC/DC converter. The system is linked to a Permanent Magnet Synchronous Generator. The major goal of this project is to connect systems so that they can create the increased power for single auxiliary phase loads through solar PV generators and wind turbine systems. The simulation is performed using Simulink/MatLab for the hybrid power system for increasing efficiency and stability. The Array-power Predictive-PO Method appears to reach the maximum point significantly sooner than the Array-power PO Method. In this experiment, a buck-booster DC-DC converter is used for conversion, and a MOSFET switch is used to turn on and off the energy storage circuit. It is also found that the proposed approach has the least fluctuation variance and reaches higher stability in peak value sooner than the conventional PO method.

2. The proposed work deal with image based solar tracker utilizing raspberry pi 4B discussed in Chapter 5. The system works fine with a webcam supporting the digital image processing within the raspberry pi model 4B board which manages to arrest the Sun's Image during hazy days due to cloud. India is the country that acquires Sunlight all-round the year. Sunlight can be utilized as substitute energy to fossil fuels or hydroelectricity for the generation of electricity. There are numerous methods which are available to expand the harvesting of solar energy but few are expensive and others can't provide accurate position of the Sun during hazy Sunlight. Raspberry Pi is the foremost board which is used to replace the CPU (central processing unit) to develop and process the Sun image. The two servo motors consisting of tilt & pan are helping to position the web camera to trace the trajectory of the Sun path. The system provides easy execution of Sun follower with the ability to find the centroid of the Sun on sky picture. Raspberry board then sends the instruction to the driver and it rotates in line with the trajectory of the Sun. The result state that tracking error reduced on haze or cloudy day with the use of raspberry pi model 4B.

3. Electricity is a vital source of energy for a rapidly rising population, and its consumption is hazardous to the environment. This reason is harmful to the environment, so immediate action is needed to address the issues that have arisen as a result of the development of solar energy. In this work the production of a solar energy is maximizing by using solar follower discussed in Chapter 6. The main component of panels is a micro-controller with an LDR sensor setup that is used to track the sun. However, due to the poor sensitivity of LDR sensors, they are less effective in tracking the sun. With the use of both LDR sensors and image processing, we propose a way for tracking the sun more effectively. This type of mechanism can track the sun using image processing software that combines the results of LDR sensors with a processed image of the sun to operate the solar panel. In solar farming, a combination of software and hardware can be employed.

4. In this work energy harvesting assessments were piloted between a Static base PV arrangement and a two orientation Sun follower module with 10 watt solar panels experimented in Chapter 7. The Global positioning centred Sun follower arrangement was designed to confirm highest possible power production from the solar radiation. The GPS-based two-orientation sun following system was able to capture sunlight intensity from 6:00 to 17:00 solar time by following the sun's trajectory across the sky during the day. The engrossed power of the sun follower module using GPS was more than that of the LDR based two axis follower and static base panel, with the energy generated for two days by 10 watt panel on sun shine, hazy or cloudy and rainy day at 147.4Wh, 83.9Wh and 42.87Wh, respectively. The average amount of energy produced by the two axis-GPS sun following system was 4.021754Wh/day in 2021, which was 45.85% more than the average energy produced from the static base PV system.

5. The importance of solar energy is to increase the effectiveness of the Sun Panel by employing a primitive solar tracking system. We proposed a solar positioning system using the global positioning system (GPS), artificial neural network (ANN), and image processing (IP) as described in Chapter 8. The sun's azimuth angle is calculated using GPS data, which includes latitude, date, longitude, and time. The image processing is utilised to find a sun image, from which the centroid of the sun is determined, and then the centroid of the sun is compared to the GPS quadrate to choose the best tracking point. Weather conditions and situations are monitored using AI decision-making and IP algorithms. Experimental effects are used to analyse and establish the offered advance adaption, which might then be stored on

the cloud carrier's memory for systematisation. When compared to a stable system and a two-axis solar following system, the proposed method improves power gain by 59.21% and 10.32%, respectively. The azimuth angle error of the IoT-based Two-axis solar following system has been lowered as a result of the reduced tracking error.

DEDICATION

This thesis is dedicated to three primitive persons who have meant a lot to me and continue to do so. Despite the fact that my father and father-in-law are no longer with us, their memories continue to guide my life. First and foremost, to my father, Late Sriniwas, whose love for me had no bounds and who cultivate in me the importance of smart work. "Papa," thank you so much; I shall never forget you.

Next, my father in law Late Chatti Lal who always inspired me to be focus to your work and always happy about what you have and start your day with joy and end with happiness.

I also want to remember my mother Chanda Devi who’s blessed makes me where I am today.

ACKNOWLEDGEMENTS

Research work for award of the degree of Ph.D. requires dedicated and sustained efforts and its accomplishment is not possible without proper guidance and inspiration from experts in relevant area of research. I am grateful to my supervisor, Dr. Lokesh Varshney, for his invaluable advice and guidance in accomplishment of this task. I am also thankful to him for providing me an extremely conducive research environment based on trust and creative collaboration which helped me to develop and refine my skills.

I am respectfully indebted to my co-supervisor, Dr. A. Ambikapathy for her continuous motivation, advice and guidance throughout out this research work. Her critical evaluation of my work due to her deep knowledge and dedication to research helped me in completing this work. She provided me a healthy environment for discussion on relevant and diverse topics.

I wish to thank members of my Ph.D. committee for constructively evaluating my thesis and offering their valuable feedback. I had pleasure to work in an environment where I received a lot of help and support. Thus, my sincere gratitude goes to Dean, Department of Electrical, Electronics and Communication Engineering, Prof. (Dr.) Baibaswata Mahapatra.

I would like to express my deep gratitude to Dr. Preeti Bajaj, Vice Chancellor, Dr. Naresh Kumar, Dean, Ph.D. and other respectable authorities of Galgotias University for providing me opportunity to register and complete requirements for accomplishing the Ph.D. work.

I wish to thank Prof. (Dr.) R. K. Saket, Indian Institute of Technology (Banaras Hindu University) for his valuable guidance on research paper writing and providing me in-site into

specific subject area with his vast knowledge in this field of research. His advice helped me in refining my concepts and focusing on right path.

I also produce my great thanks to Pradeep kumar (Workshop Superintendent, GCET) who helped me to design my project hardware.

I feel blessed for having unconditional love and support of my family members and I thank them for always being next to me. I am wholeheartedly grateful to my wife and my dainty daughter for being with me always during course of this research work.

Greater Noida, 2021 **(Kanhaiya Kumar)**

TABLE OF CONTENTS

LIST OF FIGURES

LIST OF TABLES

LIST OF ABBREVIATIONS AND SYMBOLS

ABBREVIATIONS

IDE	Integrated Development Environment
P&O	Perturb & Observe
MPPT	Maximum Power Point Tracking
MATLAB	Matrix Laboratory
MOSFET	Metal-Oxide Semiconductor Field Effect Transistor
IGBT	Insulated-Gate Bipolar Transistor
DC	Direct Current
AC	Alternating Current
VDC	Voltage Direct Current
CPU	Central Processing Unit
LDR	Light Dependent Resister
GPS	Global Positioning System
ANN	Artificial Neural Network
IP	Image Processing
IoT	Internet of Thing
IRENA	International Renewable Energy Agency
USD	United State Dollar
TWh	Terawatt-hour
ARCO	Atlantic Petroleum and the Richfield Oil Corporation
IR	Infrared Radiation
OL	Open Loop
CL	Closed Loop
CSP	Concentrated Solar Power System
DNI	Direct Normal Radiation
LCOE	Levelized Charge of Energy
ISN	Inclined South-North Single-Axis
TLBO	Teaching Learning based Optimization

JLBO	Jaya and Teaching Learning based Optimization
TAC	Total Annual Cost
LPSP	Loss of Power Supply Probablity
SD	Standard Deviation
HEV	Hybrid Electrical Vehicle
LLC	Low Level Controller
HLC	High Level Controller
PV	Photovoltaic
CPV	Concentrated Photovoltaic
DLD	Digital Logic Design
SOLOPS	Solar Position
CMPPT	Centralized Maximum Power Point Tracking
DMPPT	Distributed Maximum Power Point Tracking
GSO	Gold Section Optimization
GMPPT	Global Maximum Power Point Tracking
MRFO	Manta Ray Foraging Optimization
TFSC	Triple-junction thin-film silicon solar cell
CSA	Crow Search Algorithm
DE	Differential Evolution
ANFIS	Adaptive Neuro-Fuzzy Inference
BIO	Bio-Inspection Optimization
SSA	Squirrel Search Algorithm
ISSA	Improved Squirrel Search Algorithm
GA	Genetic Algorithm
PSO	Particle Swarm Optimization
PWM	Pulse Width Modulation
TV	Television
CD	Compact Disc
HDMI	High-Definition Multimedia Interface
USB	Universal Serial Bus
LMS	Least Mean Square
DSP	Digital Signal Processing
AF	Adaptive Filter

PMSG	Permanent Magnet Synchronous Generator
DIP	Digital Image Processing
DRAM	Dynamic Random Access Memory
LED	Light Emitting Diode
PCB	Printed Circuit Board
RGB	Red Green Blue
OASFS	One Axis Sun Following System
TASFS	Two Axis Sun Following System
RTC	Remote Time Clock
SCL	Serial Clock Line
SDA	Serial Data Line
SFS	Solar Follower System
NISE	National Institute of Solar Energy
MNRE	Ministry of New and Renewable Energy
GND	Ground
I/P	Input/output
UART	Universal Asynchronous Receiver-Transmitter
TXD	Transmitter
RXD	Receiver
AHF	Adaptive Frequency Hopping
Wi Fi	Wireless Fidelity
LAN	Local Area Network
GPIO	General Purpose Input / Output
EEPROM	Electronically Erasable Programmable Read-Only Memory
LPDDR	Low-Power Double Data Rate
SDIO	Secure Digital Input Output
DPI	Dots Per Inch
GPCLK	General Purpose Clock
SSD	Solid State Device

SYMBOLS

I_d	Saturation Current of Diode
I_{Sh}	Shunt Current in Single Diode ckt
R_{Sh}	Shunt Resistance in Single Diode ckt
R_P	Shunt Resistance in Double Diode ckt
R_S	Series Resistance in Double Diode ckt
I	Photovoltaic Current of Double Diode ckt
I_{SC}	Short ckt Current
V_{OC}	Open ckt Voltage
V	Output Voltage of Double Diode ckt
V_T	Diode Thermal Voltage
I_{PV}	Current Created by Light
V_m	Maximum Power Point Voltage
I_m	Maximum Power Point Current
P_m	Maximum Power Point
G	Irradiation
I_{d1} , I_{d2}	Saturation Current of Diode one eaual to Diode two
STC	Typical Test Condition
K1	Variable
T	Temperature
t_{STC}	Temperature on Test Condition
$I_{SC\text{-}STC}$	Short ckt Current on Test Condition
$I_{PV\text{-}STC}$	Current Created by Light on Test Condition
G_{STC}	Irradiation on Test Condition
K_V	Temperature Factor
F	Length of Adaptive Filter
y(n)	Output Signal
X(n)	Input Signal
Pm	Power Generated by Wind Turbine
w	Wind Speed
A	Turbine Blade Area

C_P	Turbine Performance Coefficient
¥	Angle of Blade Pitch
€	Density of Air
λ	Rotor Blade Tip Velocity Ratio to Wind Velocity
P(n+1)	Prediction Power
dp	Inverse Ratio of Accumulator Resolution
©	Latitude angle
®	Declination Angle
η	Solar Hour Angle
d	Date
H	Beijing Time
E	Jet leg
t_a	Time
Þ	Local Longitude
T_a	After Ta Time
$Ât_a$, $Èt_a$	Sun Current Location
ΔÂ, ΔÈ	Sun New Location
A_C, B_C	Centroid Co-ordinate of Sun
TQ	Equation of Time
Ω	Fractional Year
Hr	Hour
YSD	Year's Day
OT	Offset Time
IT	Standard Time of India
ST	Solar Time
H	0 – 233 Hours
MN	0 – 59 Minutes
SC	0 – 39 Seconds
η	Sun or Solar Hour Angle
©	Latutude Angle
j	Zenith Angle
Ĝ	Azimuth Angle
Ʊ	Altitude Angle

n_{Avg}	Efficiency od Average Power Output
BO	Tilt-Angle
BSN	Tilt-Angle of ISN-Axis
OPTM	Optimal Value
SS	Yearly Maximum Amass Sun Ray of Stable Solar Array
SA	Yearly Maximum Amass Sun Ray of Single Axis Sun Tracker
TA	Yearly Maximum Amass Sun Ray of Two Axis Sun Tracker
FT	The ISN Axis is Four Times Annually Tuned
NC, OPTM	Tilt-Angle Modification Date of An ISN - Axis, Days from the Equinoctial Point
A, OPTM	ISN-Axis Tilt-Angle Modification for each change
V	Geographic Latitude (Degree)
б	Panel Rotation Angle
$\overrightarrow{M}$	Panel Normal Unit Vector
$\overrightarrow{N}$	Unit Vector Perpendicular to and Lagging behind the Normal Vector of Panel by 90^0
θew	Instantaneous Incident Angle of Sunlight to Panel (Degree)
It	Global Sun Radiation on Angled Panel (J/M^2)
Ibb	Clear Sky Beam on Horizontal Surface (J/M^2)
Idd	Clear Sky Diffusion on Horizontal Surface (J/M^2)
Rb	Ratio of Beam Rays
$\hat{Y}$	Reflection Coefficient
$\overrightarrow{P}$	Sun Seeming Location
б	Sun Following Device Angle
Ic	Clear Sky Radiation on Horizontal Surface (J/M^2)
I_{GB}	Total Terrestrial Sun Rays Intercept by The One-Axis Follower
Wst	South Fronting Morning or Evening Hour Angle
Wtr	Daylight Hour Angle at Any Sloping
Wts	Evening Hour Angle at Any Sloping
H”tt	Daily Radiation
Hbt1	Direct Radiation
Hbt2	Sky Diffracted Radiation

Hbt3	Ground Radiation
sigma	Reflection Coefficient
Hbh	Straight Incident Irradiation Of Horizontal Plane (MJ/M^2 H)
Hdh	Diffuse Irradiance Sun Incident on Horizontal Plane (MJ/M^2 H)
ETh	Horizontal Surface Entire Irradiance (MJ/M^2 H)
ρ	Reflection Coefficient, Dimensionless
β	Tilt Angle Of Plane to Ground (Degree)
α	Elevation Angle

LIST OF PUBLICATIONS

During this Ph.D., I published and communicated seven papers in different journals and conferences. This section presents the detail of research articles published during this Ph. D., which are listed below.

1) Modelling and Simulation of Hybrid System published in International Journal of Advanced Science and Technology (IJAST) , Vol. 29, Issue No. 4s, (2020), pp. 2857 - 2867. Publisher: Science and Engineering Research Support Society, ISSN 2005-4238, SCOPUS indexed Journal.

2) Soft Computing & IoT based Solar Tracker published in International Journal of Power Electronics and Drive System (IJPEDS). Article DOI: 10.11591/ijpeds.v12.i3.pp1880-1889, Vol. 12, No. 3, September 2021, pp. 1880~1889. Publisher: Institute of Advanced Engineering and Science (IAES), ISSN: 2088-8694, SCOPUS indexed Journal, SJR Q2 on Electrical and Electronics Engineering.

3) Vision based solar tracking system for efficient energy Harvesting published in International Journal of Power Electronics and Drive System (IJPEDS). Article DOI: 10.11591/ijpeds.v12.i3.pp1431-1438, Vol. 12, No. 3, September 2021, pp. 1431~1438. . Publisher: Institute of Advanced Engineering and Science (IAES), ISSN: 2088-8694, SCOPUS indexed Journal, SJR Q2 on Electrical and Electronics Engineering.

4) Solar Tracker Transcript – A Review, Kumar K, Varshney L, Ambikapathy A, Saket RK, Mekhilef S. Int Trans Electr Energ Syst. 2021;e13250. doi:10.1002/2050-7038.13250, SCI indexed Journal.

5) Soft computing based Solar Follower using Raspberry Pi 4B, presented in International Conference on Advance Computing and Ingenious Technology in Engineering Science, Dec 30-31 2021, AIP, SCOPUS indexed Conference.

6) Image Denoising by Wavelet Based Thresholding Method, presented in International Conference on Advance Computing and Innovative Technologies in Engineering, April 28-29 2022, IEEE, SCOPUS indexed Conference.

CHAPTER 1
INTRODUCTION

1.1. Overview

Traditional energy supplies are becoming scarce as consumption continues to rise due to continual population intensification, putting them on the verge of depletion gradually. This consequence forces investigators and academics to focus on another resource that is abundantly present and easily accessible on the Earth. Sun power is an excellent choice among various renewable options for meeting the demand. So-called "green energy" is renewable, inexhaustible, and limitless. If traditional resources are consumed at the current speed for the next three or four decades, it is estimated that the remaining conventional resources will be end up. As a result, the entire planet would face an energy catastrophe. In addition to harmful pollutants like carbon mono-oxide, nitrous-oxide, carbon di-oxide, Sulphur di-oxide, and others, the ignition of fossil fuels causes global warming. Since energy consumption will never decrease, it is the current situation's obligation to shift to clean and renewable resources of energy like wind, hydro, thermal, sun, tidal, and bio energy. The International Renewable Energy Agency (IRENA) states that, the overall electricity power produced by non-conventional energy in the world, Asia, China, and India is 2538441 MW, 1118705 MW, 758869 MW, and 128237 MW, respectively, with hydro power contributing the most and bio-energy contributing the least, as shown in Figure 1.1. Bio, hydro, wind, and marine energy all have geographical limitations, and their energy production is location-specific. In India, almost 245 days of clear bright days are accessible out of 365 days because of its location near tropic of cancer, is available almost everywhere in India.

Renewable energy resources like the sun, biogas, wind, etc. are among the most promising technological developments in the advanced world. The request for renewable energy sources is growing, while traditional fossil fuel energy is rapidly decreasing [2]. The annual change in production of renewable energy for different countries is shown in Figure 1.2 [3].

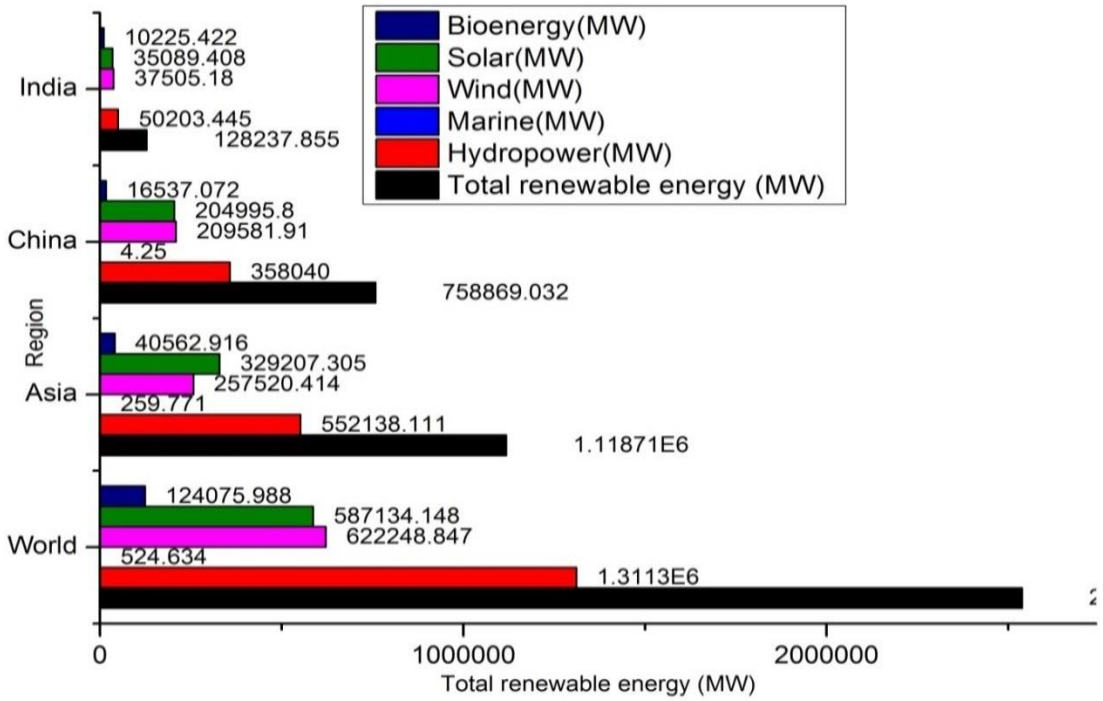

Figure 1.1 Data of different region's electricity production from different renewable energy sources.

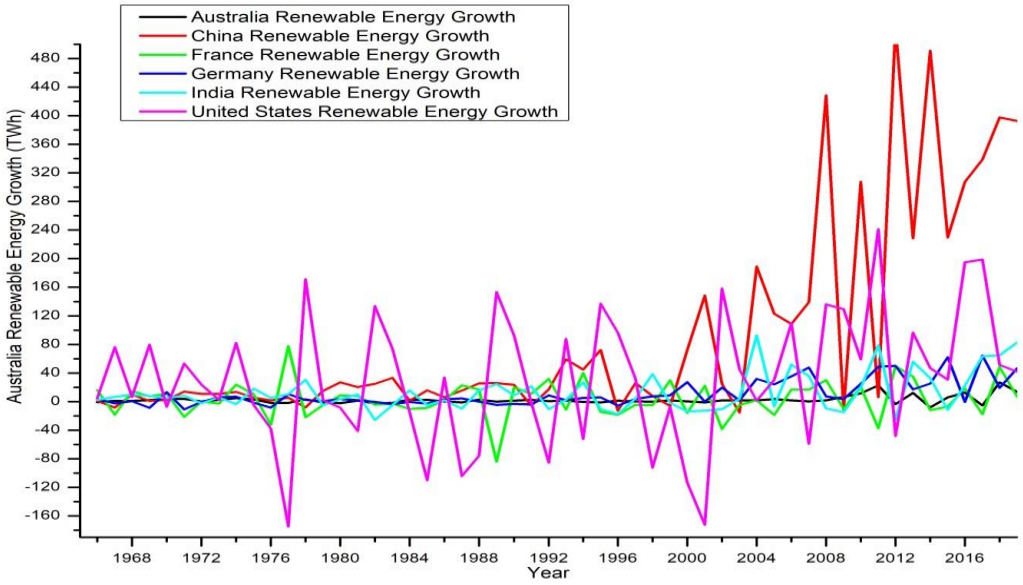

Figure 1.2 Annual changes in production of renewable energy

Solar PV energy systems have an advantage over other renewable energy systems due to their ease of installation and maintenance, as well as the fact that India has nearly 245 days of clear sky per year. The annual change in solar energy generation for China, France, Germany, USA, India, and Australia is compared in Figure 1.3 [4].

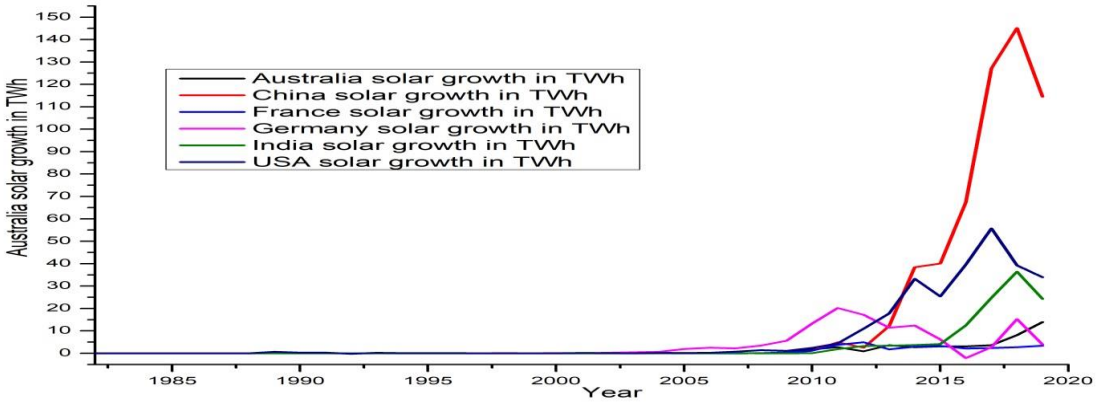

Figure 1.3 Annual changes in solar energy generation

Renewable energy expansion has successfully captured worldwide interest in the energy production industry these days. The three main elements that contribute to their relevance are the continued rapid utilisation of world-wide non-renewable resources, the finite nature of non-renewable fuel reserves, and the need to regulate pollution control. India has 245 days of clear and sunny skies, so we may simply reduce our reliance on fossil fuels. Sun power in our country is projected to be over 750 GWp [5] by MNRE (Ministry of New and Renewable Energy) and NISE (National Institute of Solar Energy) at the highest level. However, India nearly achieved a grid connected Sun energy capacity of about 37 GW through 31 October 2020 [6], and different Indian states' power production capabilities are analysed in Figure 1.4.

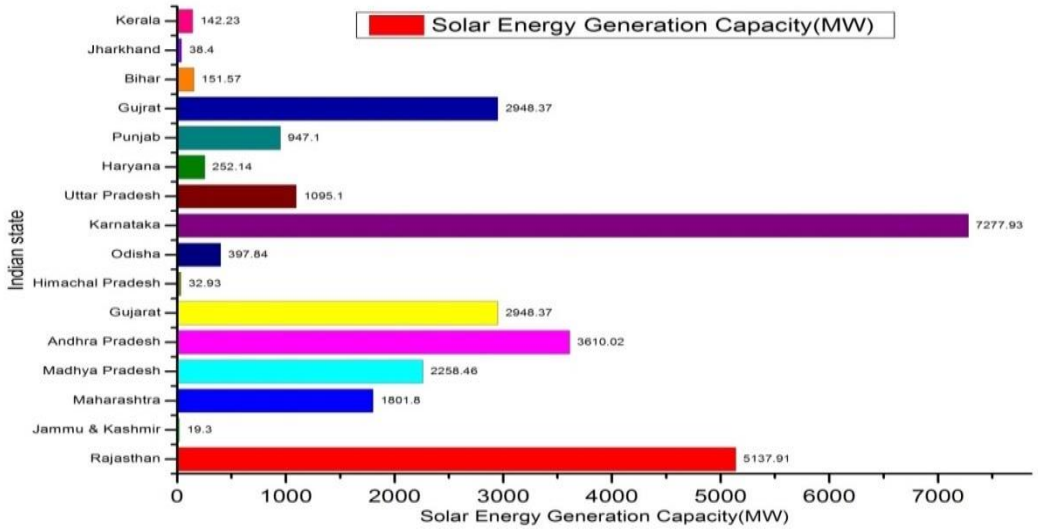

Figure 1.4 State wise Power generations by solar energy

Solar radiation is among the most affordable and readily available energy sources that can really meet these needs. By 1950, significant research on photovoltaic had resulted in a continuous improvement in their efficacy, from 15% in 1950 to 17% in 1970 to 46% in 2019 [7]. To extract the sun's energy, various technologies and procedures have been developed. The sun follower market is worth USD 9.30 billion in 2019 and is anticipated to reach USD 49.21 billion by 2026, according to a new report by Reports and Data [8]. According to the IRENA (International Renewable Energy Agency) [9], energy from the sun is predicted to power roughly 13% of the worldwide by 2030. Various studies and research [10] were underway to determine the best site for the Sun's following system around the planet, as illustrated in Figure 1.5. We've been studying the Sun's following system for a long time, and we've come to the conclusion that there's been a lot of interest in this area for the past six years, as seen in Figure 1.6.

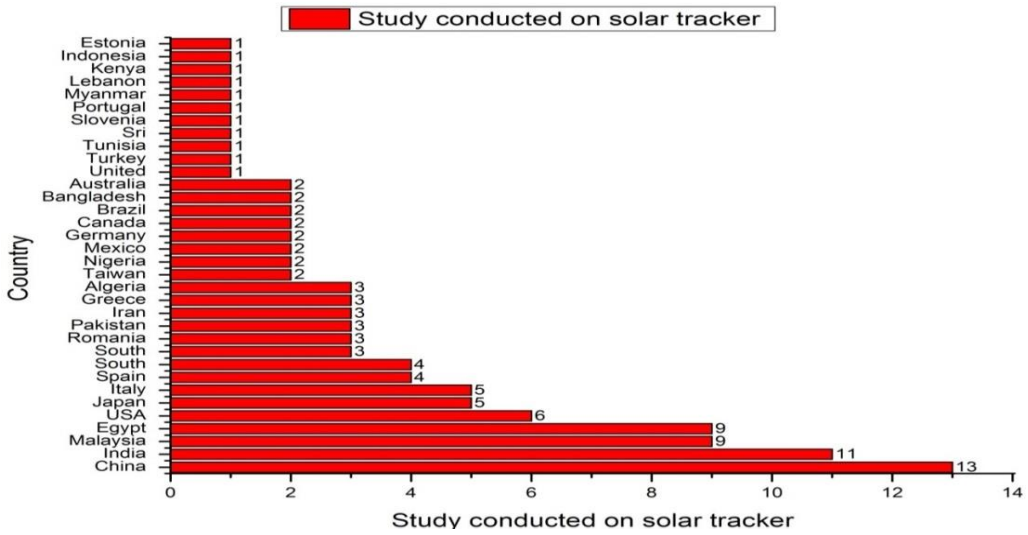

Figure 1.5 Number of solar tracker studies conducted by country

The overall sun energy production of the world has been steadily growing for the past 26 years, as shown in Figure 1.6 [11], which compares data on world and India's electric energy generation from the sun represented in TWH (Terawatt-hours). Figure 1.7 [12] demonstrates that India is now far behind in solar energy output, but that it is leading in solar energy generation yearly percentage change in 2019. As a result, various solar electricity producing systems are constantly emerging in order to

increase the system efficiency.

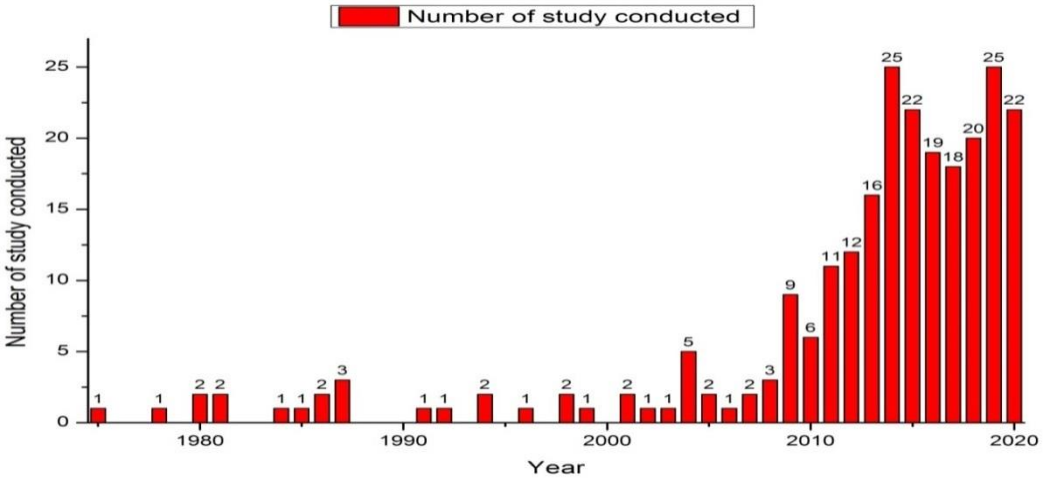

Figure 1.6 Number of solar follower studies conducted by year

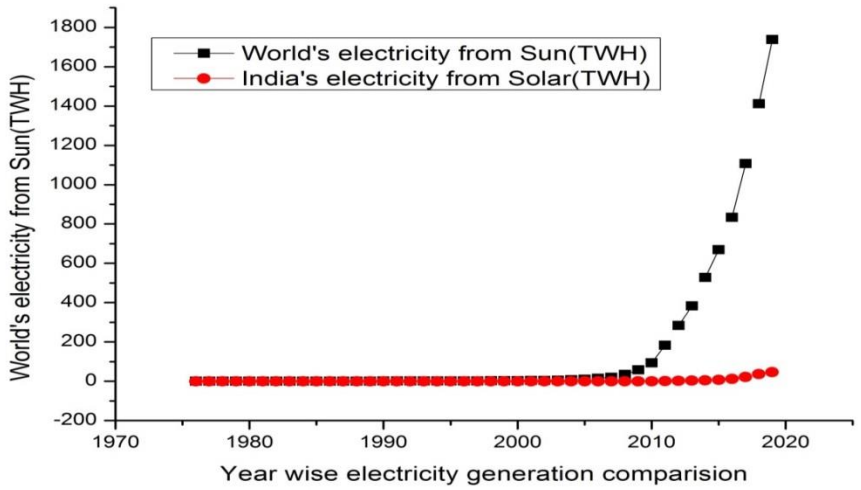

Figure 1.7 Graphs comparing India's and the world's annual electricity generation by solar energy expressed in Terawatt-hours (TWh)

Photovoltaic (PV) module transform the sun's visible radiation energy into electricity, but their conversion is not efficient. Its conversion efficiency is influenced by the sun's visible irradiation, temperature, velocity of wind, system optimal matching with the load, azimuth, altitude, and the horizontal plane.

Sun followers trace the sun's route throughout the day and orientate PV modules, reflectors, glass lenses or another photosensitive device headed towards the sun. Since the sun location changes continuously in the sky corresponding with time (15 degrees

per hour), the azimuth angle and altitude angle differ continuously. The sun follower continuously lines up the whole module to improve power generation. Various categories of one-axis and two-axis followers have been designed in the previous decade after the birth of optical sensitive transducers and sensors.

Solar follower with intermediate to large scale electricity generation facilitates protection of huge power wastage if tracking were performed. The everyday average output power of the photovoltaic module can be boosted by a sun follower, which focuses sun radiation directly onto the photovoltaic panel whole through the day [13]. The value of using a Sun-following system results from the advantage that the incidence radiation angle of the PV of sun irradiation is more promising than the angular radiation incidence that corresponds to a stable PV module. The ratio of the diffracted module for both systems is nearly equal; the immediate sun irradiation absorbed by the PV systems is higher than the stable system. Various tests have been achieved upon the advantage of the Sun's following module, enlightening that up to 40% to 60% gain in power can be achieved by implementing the Sun's following scheme [14]. The utilisation of Sun followers boosts the accessibility of everyday Sun power as well as the Sun radiance threshold.

The conventional Sun follower was developed by using LDR (light dependent resistors) sensors, photo diode sensors, and photo transistor sensors [15-18]. All these sensors need bias electricity for processing and energy consumption. Single axis requires more than two transducers or sensors. If anyone's sensors' responses differ from the other because of weather conditions, time, unexpected effects, or cloud cover, then the follower flops to trace the Sun's path.

On the other hand, with this new approach to image sensor, GPS, and LDR, the above error possibility is completely removed. The change in sensor response does not alter the sensing algorithm because it removes the false triggering. Since this thesis work concentrates on the maximisation of solar energy achievement with the least tracking error, the theory and discussion will revolve around the design of the solar harvesting system and its implementation.

1.2 Problem statement

The sun shifts its position from east to west. Solar panels are designed to focus on the sun's centroid. A solar following system is aimed at adjusting the direction of the solar panel accordingly to the movement of the sun with minimum tracking error and maximum sun energy.

1.3 Objective

The foremost objective of this project is to implement and design a solar following system centred on image processing (image sensor), soft computing, GPS, Raspberry Pi 4B, Arduino, flexible solar panel, and DC motor to minimise the drawbacks generated in stable and LDR-based two axis solar harvesting systems.

1.4 Thesis outline

This thesis consists of ten chapters. This chapter contains a brief overview of the project, a problem statement, and the thesis layout.

Chapter 1 deals with the main reason behind the reforms to non-conventional sources of energy. In this section, we deliberate the main aspects of renewable energy in the world and what different renewable energies are, most prominently solar energy and how much they contribute to energy production. Here we also discuss the electricity generation by various renewable energy sources, the annual change in renewable energy growth and solar energy growth, the solar energy generation capacity of India’s different states and how many studies have been conducted on solar followers.

Chapter 2 states the introduction to solar tracking systems, solar geometry, and the different classifications of solar trackers and their literature review till present.

Chapter 3 includes the project hardware, electronics, and software details. In this section, the tracker hardware specification and design details are discussed. The different software used in implementing the methodology with electronics and electrical parts is also discussed.

Chapter 4 discusses the simulation, modelling, and design of a hybrid energy system that uses renewable sources like solar PV and wind turbine energy systems.

Chapter 5 deals with an image-based solar tracker utilising the Raspberry Pi 4B. The system works fine with a webcam supporting the digital image processing within the Raspberry Pi model 4B board, which manages to arrest the sun's image during hazy days due to clouds and can track the sun.

Chapter 6 elaborates on a method for tracking the sun more effectively using both LDR and IP. This mechanism can trace the sun using IP software that combines the results of the LDR sensors' output with an IP-based processed image of the sun to operate the solar panel. In solar farming, a combination of software and hardware can be employed.

Chapter 7 detailed energy harvesting assessments were piloted between a Static base PV arrangement and a two orientation Sun follower module with 10 watt solar panels. The Global positioning centred Sun follower arrangement was designed to confirm highest possible power production from the solar radiation.

Chapter 8 discusses the importance of solar energy in raising the efficacy of the solar panel by using a primitive solar following system. In this work, the experiments were done with a Sun locating system by using GPS (global positioning system), ANN (artificial neural networks), and IP (image processing).

Chapter 9 discusses results obtained as part of the research work carried out and described in previous chapters. The result is analysed and discussed in the context of addressing the problem of energy harvesting.

Chapter 10 presents the summary of the research work carried out in contrast to the work. Conclusions drawn from the logical analysis, results and discussions are described. Future scope of work is also indicated to further address the problem of energy harvesting using emerging technologies.

CHAPTER 2

HISTORICAL BACKGROUND

2.1 Contextual

The Solar follower based research travelled through five decade from the time of its beginning. The first fruitful Sun follower (passive) was erected in 1968. It was a motor less pole and top follower that based on refrigerant and Al (aluminum) optical reverberators to move photovoltaic module to focus along the sun. In spite of first tracker still no tracker comes commercially in market till 1970 and we can say that the idea still not come on ground level. But during a decade a photosensitive element discovery raise the active solar follower concept. ARCO (Atlantic Petroleum and the Richfield Oil Corporation) Solar initiated the production of solar panels since 1977 to reduce the overburden of energy on oil and put solution to energy crisis. From 1983 the big-scale production of solar trackers takes places in California (Carrizo Plains). ARCO hired the Carrizo Plains land (property) to developed and control 5.2 MW two complex dual- axis Sun follower photovoltaic plant. The power generated by these plants was vended to the network at $0.04 per KWh. But economical point of view this plant production failed and finally sold and disassembled. In 1980 closed loop optical controlled based Sun follower developed commercially is still going on.

In 1990s era the research completely concentrated on electro optical sensor and transducer for Sun following system. The basic sensors and transducers were photo-diode, photo-transistors and photo-conductor. Nonetheless, the concept of utilizing solar-cell to detect the radiance had done. Nevertheless the technology of that photo-cell was not established at that period. Furthermore, it cost was reasonably higher than other accessible transducer and sensors.

Since 1995 to now many researchers conducted their study on one and two axis Sun following system. Because of mechanical difficulties and circuitry complexity of two axis Sun follower, the researchers prime focus to one axis Sun follower. At that

time one axis follower use three photo sensors out of which two sensors used with comparator circuit to sense the position and remaining one to measure irradiance. Half-bridge driver circuit was utilizing for guiding the motion of motor. After developing the microcontroller and microprocessor, the circuit becomes smart controller. Two-axis following similarly utilize the identical technology and investigation on it began drastically by 2002. Frequently, photo-cells are substituting the conventional sensor by optical sensor, GPS, and Image sensor for Sun following. Our work is based on Soft computing, LDR, GPS and Image sensor.

2.2 Sun Energy

Solar or Sun energy power is devoted to the power hitched from solar light. The power from our star sun were assumed to be enormous and therefore the energy and power harnessing by the sun is targeted the foremost energy resource for forthcoming time. Visible radiant light and infrared radiation (IR) heat from the sun, is hitched by utilizing various methods like Sun IR heating, Sun photo-voltaic, Sun-thermal electric energy and Sun system design. Solar radiation intensity above Earth atmosphere is about 1380 Watt/m^2 called solar constant. But the solar energy radiation intensity received by Earth surface is 1000 Watt/m^2 as shown in Figure 2.1. The direct transformation of radiated photon energy into electric energy achieved because of that large scale solar power plant is establishing.

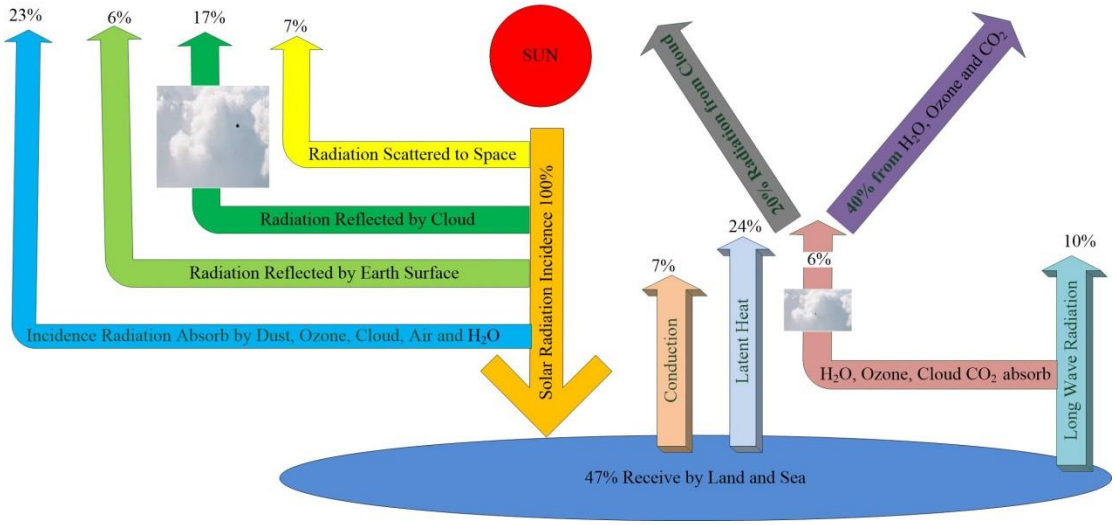

Figure 2.1 Available solar powers

In spite of this, it is significant to consider that Sun energy harvesting efficiency is still unsatisfactory. So research work is going on it to harness more or most possible power by plummeting different wastage. The Sun energy has gains compare to rest renewable or non-renewable energy resources. Most important point for it is that its maintenance cost is negligible except its initial installation cost which is high. It doesn't release heat and toxic gas or radioactive radiation and generate noiseless solar energy. So it's one of the best environmental friendly energy productions.

Sun energy is one of the consistent resources of power in the mountainous and remote region where electric spread via conducting wire is expensive or unbearable. PV module is utilized within remote region for electrification. Moreover in normal and metropolitan cities street lighting electrification through PV is popular. And most of Modern low power electric devices run on Sun PV. Likewise hybrid electric automobiles, house electricity and smart grid joined through PV module. Satellites and shuttles which sent to space for long duration have only solar energy as alternative. So researcher primarily focused through the solar power extensively.

2.3 Sun Pathway, Altitude and Azimuth angle

The sun shifts from one time to another and from one season to another because to the earth's periodic orientation on its axis and revolution around the Sun. This is the reason because of that it's necessary to relocate the tracker to trace varying position of sun for a specific moment. The paths of the Sun are indicated on a special chart named Sun Path Diagram [19] shown in Figure 2.2. It displays sun rise, Sun set, Sun path, elevation angle, solar time, daylight and azimuth angle.

Sun path diagrams are representations of the sun's path across the sky on a world flat map surface shown in Figure 2.3. They're used to swiftly and easily find the location of the sun at any time of day or year. In addition, the latitude has its own depiction of the sun's course. The sun comes from the east and sets towards the west. The largest disparity between the sunrise and sunset times is over 13:58 hours, which happens on 18 June 2021. The shortest day comes on 17 December 2021, with roughly 10:20 hours of daylight. The location of the sun at a given date at particular

time of the year can be easily determined using a sun path polar and Cartesian diagram. The Figure 2.4 show 12 month sun position of Greater Noida, India where experiment is performed. The given location Sunrise, sunset, dawn and dusk times is tabulated on Table 2.1 and expressed by Figure 2.5.

Figure 2.2: Sun trajectory diagram

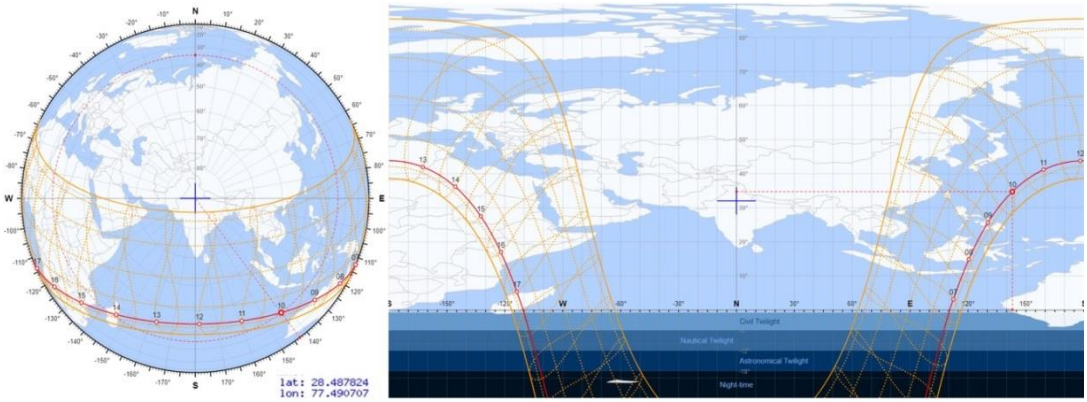

Figure 2.3 Sun Path Polar and Cartesian diagram in world map

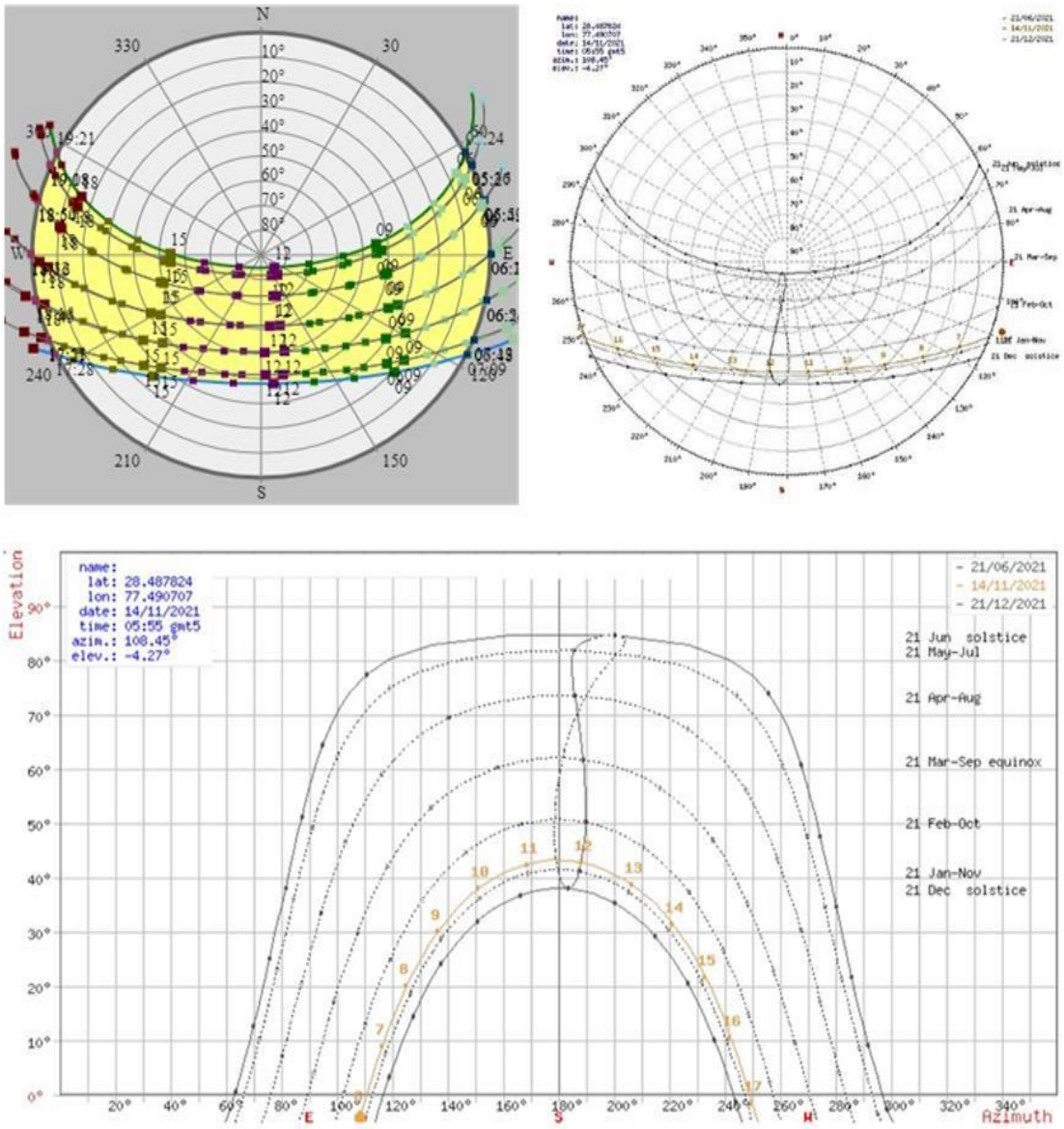

Figure 2.4 2021's 12 month Sun Path Polar & Cartesian diagram with latitude & longitude.

2.3.1 Azimuth Angle (Ĝ): The direction of the sun from the spectator is indicated as the angular displacement from the north point horizon to point at which a perpendicular circle fleeting through the sun transects the horizon shown in Figure 2.6.

2.3.2 Solar Altitude (Ʊ): The angle altitude of the sun analyzed from the horizontal. Upper part of the horizontal consider +ve and below is -ve.

2.3.3 Angle of Declination (®): The angle within the sun and vertical line directly above the equator is called angle of declination.

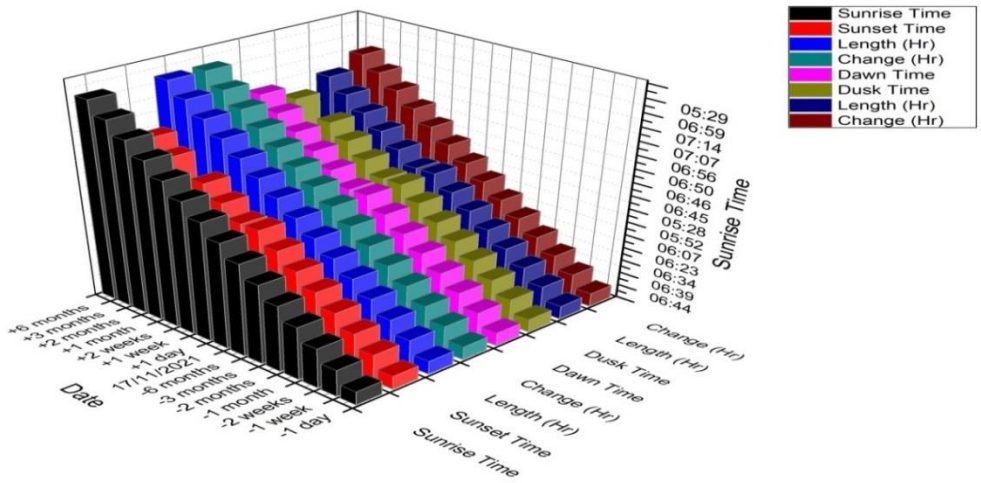

Figure 2.5 Graphical representations of dusk, sunrise, dawn and sunset times, length of day

Table2.1 Analysis of 2021 dusk, sunrise, dawn and sunset times, length of day

Date	SR	ST	L (Hr)	C (Hr)	DT	DU	L (Hr)	C (Hr)
-1 D	06:44	17:27	10:43	00:02 LN	06:19	17:52	11:33	00:02 LN
-1 WK	06:39	17:30	10:51	00:10 LN	06:15	17:54	11:39	00:08 LN
-2 WK	06:34	17:34	11:00	00:19 LN	06:10	17:59	11:49	00:18 LN
-1 MN	06:23	17:48	11:25	00:44 LN	05:59	18:12	12:13	00:42 LN
-2 MN	06:07	18:22	12:15	01:34 LN	05:43	18:46	13:03	01:32 LN
-3 MN	05:52	18:56	13:04	02:23 LN	05:28	19:21	13:53	02:22 LN
-6 MN	05:22	19:20	13:58	02:57 LT	05:03	19:32	14:29	02:58 LN
T	06:45	17:26	10:41	0	06:20	17:51	11:31	0
+1 D	06:46	17:26	10:40	00:01 ST	06:20	17:51	11:31	00:00 EL
+1 WK	06:50	17:24	10:34	00:07 ST	06:25	17:50	11:25	00:06 ST
+2 WK	06:56	17:23	10:27	00:14 ST	06:30	17:49	11:19	00:12 ST
+1 MN	07:07	17:27	10:20	00:21 SH	06:41	17:53	11:12	00:19 ST
+2 MN	07:14	17:47	10:33	00:08 ST	06:49	18:12	11:23	00:08 ST
+3 MN	06:59	18:11	11:12	00:31 LN	06:35	18:35	12:00	00:29 ST
+6 MN	05:29	19:06	13:37	02:56 LN	05:03	19:32	14:29	02:58 ST

MN, Month; WK, Week; D, Day; T, 17/11/2021; , Sunrise Time; ST, Sunset Time; DT, Dawn Time; DU, Dusk Time; L, Length; LN, Longer; ST, Shorter; SH, Shortest; LT, Longest; EL, Equal Length

2.3.4 The zenith Angle (j): Zenith angle is defined as the angle within the vertical line to the Earth plane and the sun. Zenith angle is complement of solar altitude as shown in Figure 2.6.

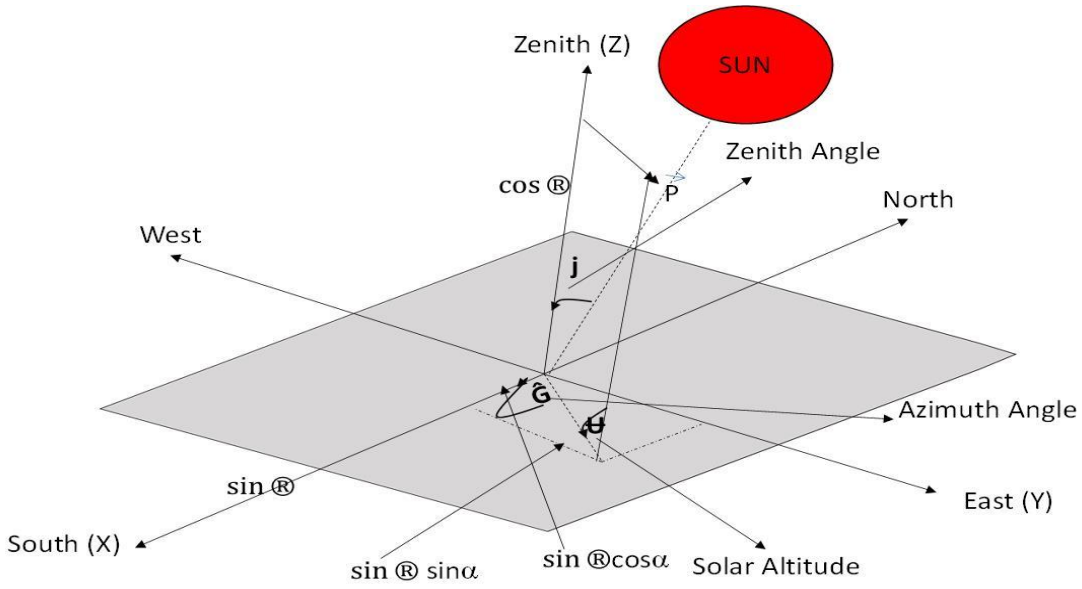

Figure 2.6 Azimuth and altitude angles

2.4 Solar Radiance

Measurement of the power density of solar radiation at particular place is called solar irradiance. It is instantaneous quantity having unit W/m^2. The intensity of solar radiation towards the earth is approximately 1367 W/m^2. The radiation transmitting through the earth atmosphere and reach at their surface and become 1000 W/m^2. It is significant to know that the solar cell output response affected by the definite range of radiation. Sun electromagnetic spectrum has different rage of wavelengths. But solar cell respond positively only visible spectrum from 390 nm to 700 nm. It doesn't respond to the ultraviolet (less than 390 nm). But the infrared light (greater 750 nm) is responsible for diminishing the solar cell efficiency because of heating effect of IR spectrum. So to achieve maximum solar irradiance the rays are directly incidence to solar panel. To focus the panel continuously towards sun a device called solar follower is used. Solar radiation in Grater Noida, U.P, India (latitude-28.4878^0 and longitude-77.490707^0) for year 2021 is given in Table 2.2 and expressed by Figure 2.7.

Table 2.2 Month wise realistic average daily solar insolation of 2021 (kWh/m²/day)

M	Jan	Feb	Mar	Apr	May	Jun	Jul	Aug	Sep	Oct	Nov	Dec
S	2.731	3.641	4.556	5.295	5.309	4.84	3.921	3.782	4.167	3.86	3.039	2.615

M, Month of 2021; S, Solar insolation by month (kWh/m²/day)

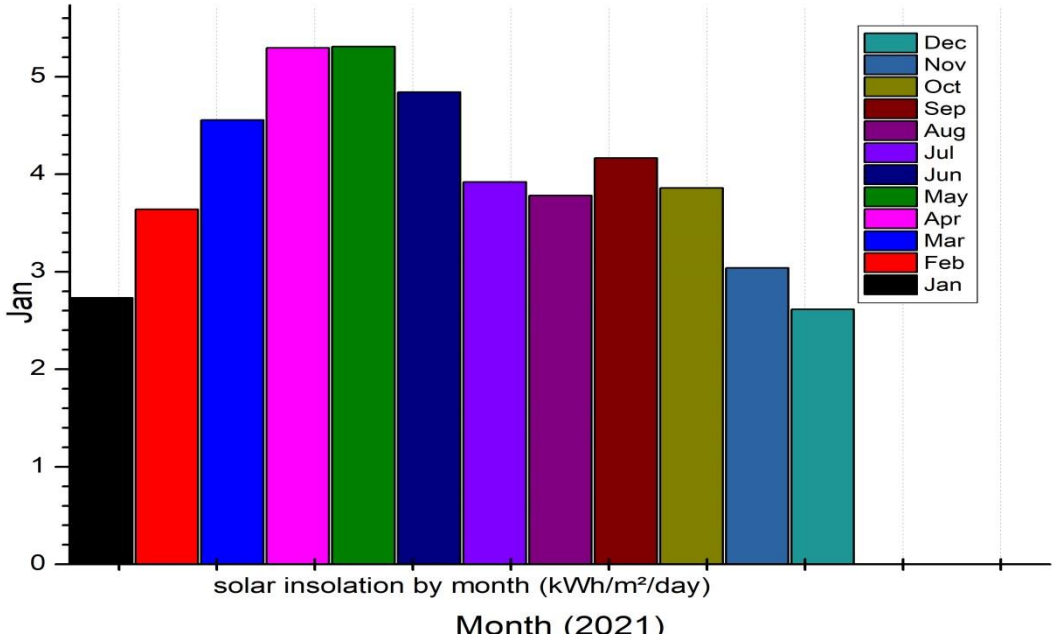

Figure 2.7 Month wise realistic average daily solar insolation

2.5 Sun follower

Sun tracking is a technique for capturing maximum solar power by following the Sun's path from Earth. The number of axis of orientation, control method, flexibility of rotation, and drivers given in Figure 2.8 are used to classify solar followers. Sun followers based on drivers are categorised as:

a) Passive Sun follower [20-25]
b) Semi Passive Sun follower [26-29]
c) Chronological Sun follower [30, 31]
d) Manual Sun follower [32]
e) Active Sun follower [33-39]

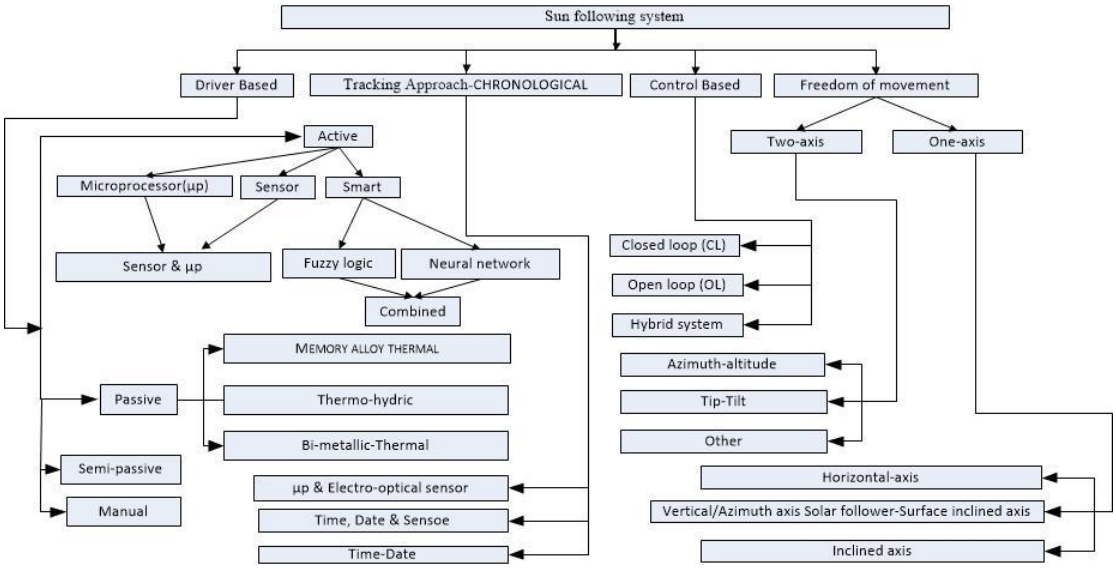

Figure 2.8 Classification of solar follower

2.6 Categories of Solar Follower on axis of rotation

Sun follower module is categorized by its degrees of freedom for movement. According to degrees of free rotation sun follower can be classify into two classes-

- One axis sun follower
- Two axis sun follower

2.6.1 One Axis Sun Follower: One axis sun follower tracks the motion of the sun only in horizontal or vertical direction as shown in Figure 2.9. Stated follower has only single axis of freedom for movement. Generally horizontal one axis sun follower utilized in Earth tropical areas wherever the days are short and the sun acquires high position at noon. On the other hand, one axis vertically solar follower where the days are very long and the region commonly situated at high altitude with low sun height.

2.6.2 Two Axis Solar Followers: This tracker has two orientation of free motion as shown in Figure 2.10. It can trace the sun vertically and horizontally both. Two axis sun followers universally used worldwide and assure highest fetching of Sun radiation. Two axis solar followers is complex in design compare to one axis solar follower but energy consumption is more. Though, for huge scale Sun energy generation two axis solar followers is more economical.

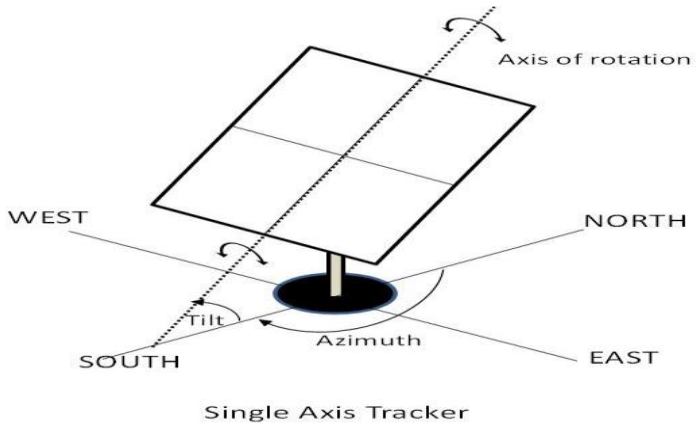

Figure 2.9 Single axis solar followers

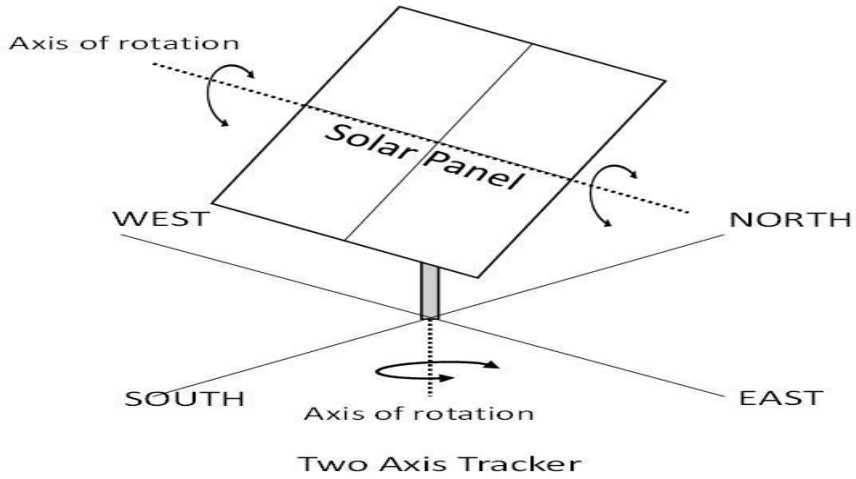

Figure 2.10 Two axis solar follower

2.7 Solar Following Methods based on Driver

Under this classification three methods are discussed.

- Active sun follower
- Passive sun follower
- Chronological sun follower

2.7.1 Active Sun Follower: The active Sun follower has a photo transducer with an electrical mechanism that regulates tracker movement by controlling the motor. A

LDR with a variable resistance [40] that varies on radiation incidence is a commonly used photo sensor. As a result of an electrical and electronics component, it is susceptible to environment and could be affected by lightning discharge. This device has limited reliability. It working based on the transducer, thus its tracer mechanism may hinder, causing serious issues and slowing down energy output. As a result, as shown in Figure 2.10, this system is constantly monitored.

2.7.2 Passive Sun Follower: To follow the Sun, a passive follower does not need an exterior power source. Figure 2.11 shows how these trackers utilise the energy generated by the Sun's thermal radiation. Despite its lower accuracy, this tracker is virtually inexpensive due to its low cost and eases of repair. This arrangement has an adjacent shock compensator that protects the follower from wind or other sources of rapid movement, as well as Sun follower orientation commanded by device counter weights [41].

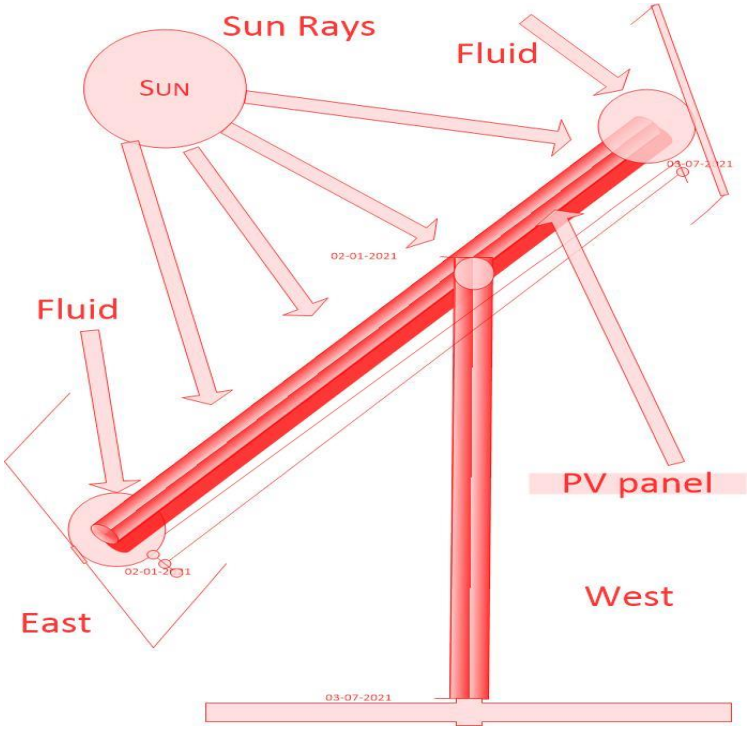

Figure 2.11 Passive solar trackers

2.7.3 Chronological Sun Follower: It is a time centered sun following system. The tracker is tracing at a constant speed all over the daytime meanwhile the sun is

passages through sky with constant rate of 15^0 /hour. The trajectory of the sun during the daytime is evaluated and fixed by the software program executed on the controller. It has advantage of high precision and can work in extremely harsh winter conditions at different latitudes to the equator [42].

Above discussed all three schemes are executed by using single and double axis solar following system. Installation, geographical location and requirement of solar energy decide the suitability of the method. In advance solar followers both the sensor and sensor less controller used collectively to raise the system output.

2.8 Parts of Sun Following System

A Sun follower has numerous basic parts [16]. The major parts are discussed below-

2.8.1 Solar Tracing Algorithm: Sun follower has open loop (OL) and closed loop (CL) controller equation. OL controller equation includes algorithm of altitude and azimuth angle based on astronomical equation. The Presence of clouds distorts the feedback signals in CL control system. Above said two techniques collectively used to maintain the stability between economic design and improved efficiency.

2.8.2 Controller of follower: The controller element performs the solar following algorithm for desired calculations. It also organizes the motion for tracking device. Microprocessor or microcontroller or a computer utilizing as control element and usually has instruction input and response output instrument for interconnection. In remote location automatic sun following is the best choice.

2.8.3 Driver and actuator Mechanism: The System changes the sun follower regarding the priority of control element. This may be either electronics or hydraulics. Electronics schemes use encoders and adjustable frequency drives or actuators to control the existing situation of the solar module and change to preferred situations. The drive device have mechanical parts like planetary gear, swivel drive, linear drive, motors, threaded spindle, linear actuator, worm gear and hydraulic cylinder.

2.8.4 Sensors: Sensors and transducer are utilized to trace location of the sun precisely. For OL system, optical transducer is applied for accurate control and

hardware fault analysis. Optical radiation sensing element comprises photoresist or, phototransistor, optical cell etc. The Sun power dependent electricity stations also utilize wind velocity, humidity, temperature, solar irradiance, pressure and additional essential physical quantity surveillance with sun follower.

2.9 Active tracker system with a single axis

Because it just has a one axis of orientation, it consumes a lesser amount of power than dual-axis module and has a lower circuitry complication.

Based on the Parabolic Trough Collector, Fabienne et al. [43] designed a one axis solar follower. The position of the Sun was computed using an algorithm at different periods and classified as a dynamic open loop (OL) actuator. To demonstrate angular following, a digital inclinometer is used. When compared to the acceptance angle, this approach delivers superior exactness for track inaccuracy, and their August 2012 seven testing day data is shown in Table 2.3 and graphically represented by Figure 2.12 with range of sun luminance (Gbn), least direct typical radiation (Hb), and wind velocity (u). In their tests, the authors found that the tracing error and tracing accuracy were $\pm 0.4^0$, $\pm 0.33^0$and 95%, respectively, and that their optical loss limit was just 0.32%.

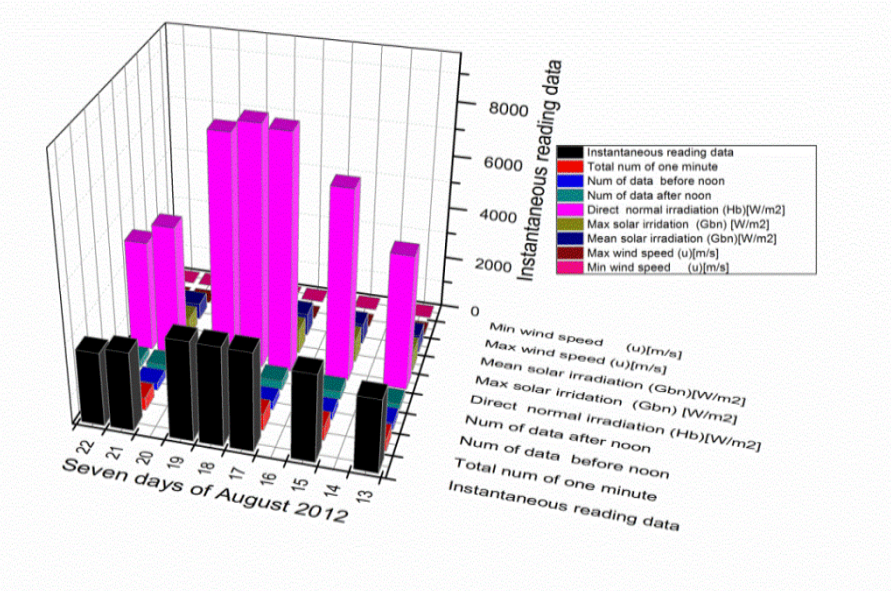

Figure 2.12 Test reading graph

Table 2.3 Test reading

SDA	IRD	TNM	NBN	NAN	DNI	MSI	MEI	MWS	MNWS
22	2779	463	216	248	4183	791	542	3.52	0.04
13	2767	461	272	190	5094	801	663	3.96	0.03
19	3748	624	281	344	8592	905	825	0.26	0.01
15	3298	549	254	296	7189	902	785	3.29	0.01
18	3732	621	280	342	9015	941	870	2.38	0.01
17	3716	619	278	342	8869	932	859	2.98	0.09
21	2982	496	275	222	4925	709	595	1.96	0.04
TOTAL	23,022	3833	1856	1984	47,867	–	–	–	–

SDA, Seven days of august 2012; IRD, Instantaneous reading data; TNM, Total num of one minute; NBN, Num of data before noon; NAN, Num of data after noon; DNI, Direct normal irradiation (Hb) [W/m. ¼; MSI, Max solar irradiation (Gbn) [W/m.]; MEI, Mean solar irradiation (Gbn) [W/m.];MWS, Max wind speed (u) [m/s]; MNWS, Min wind speed (u) [m/s]

Rahul and Subhadeep [44] investigate the use of concentrated solar power in small-Sun Belt locations. Concentrated solar power is a low-cost, high-capacity sustainable energy that is commonly employed in areas with high direct sun irradiation. The author conducts many critical analyses on lower DNI and concludes that the output is not as bad as it is with higher DNI (Direct Normal Irradiation). The capacity factor is 0.1952 $/kWh, 17.56%, and 32.50%, respectively, and this design reduces the LCOE and increases the efficiency of a system. In Table 2.4, a comparison has been made between solar thermal technologies with a large solar area and those with a smaller solar area.

The radiation influence on the sloped south-north single axis sun following was discussed by Zhimin et al. [45]. This tracker estimates the yearly engrossed radiation on a steady and sun following panels using a mathematical algorithm. In comparison to a dual-axis panel, the annual collectible radiation on south-north axis following panel was roughly 96%, according to their research. They also noted that a solar tracker isn't very beneficial in areas with poor solar resources. Figure 2.13 shows a graph that compares the optical outcome of two, inclined south-north one, and stable axis follower panels.

Table 2.4 Performance parameter in extreme DNI & least DNI value

NP		PEDNI		PLDNI	
	SPST	PSDNI	Measurement	PRDNI	OR
GPSE	Solar tower	2,717	28.72		20.38
	Parabolic	2,136	16		
WC	Parabolic	2248.17	2678.8		276.07
SE	Solar tower	2717	13.5		
	Solar tower	2012	38		17.56
	Parabolic	2248.17	21.3		
CGN	Parabolic	2248.17	94.2	1379.7 kWh/(m^2 a)	86.16
LC	Solar tower	2012	20		26.29
	Parabolic	2725	47.3		
LCE	Solar tower	1884	0.14		0.1952
	Parabolic	1884	0.15		
PCF	Solar tower	2012	24		
	Parabolic	2725	21		32.5
	Parabolic	2136	41		

NP, Normalized parameter; OR, Obtained reading; PRDNI, Present Reading DNI consideration; SPST, Solar power system technology; PSDNI, Prior studies DNI consider/(kWh(m^2a)$^{-1}$); PLDNI, Performance of system at least DNI; PEDNI, Performance of system at extreme DNI; PCF, Plant capability factor (%); SE, System efficiency (%); LC, Land claim/(MW km^{-2}.); WC, Water consumption/(L(MWh a)$^{-1}$.); CGN, Conversion of gross to net; GPSE, Gross conversion of plant solar to electricity; LCE, Levelized charge of energy/($ (kWh)$^{-1}$)

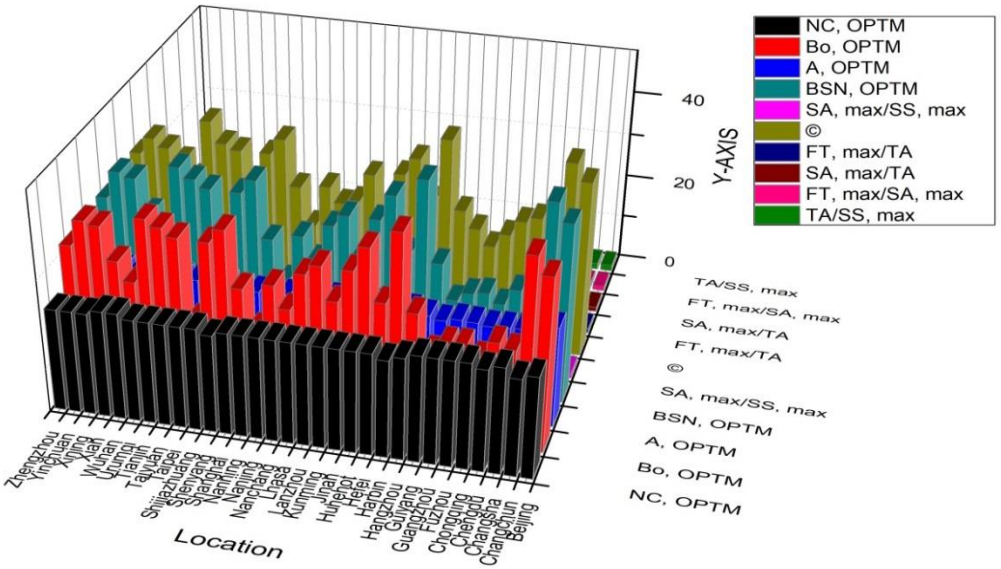

©, latitude; Bo, tilt-angle; BSN, tilt-angle of ISN-axis, Degree; OPTM, optimal value; ISN, inclined south-north single axis; SS, Yearly maximum amass Sun ray of stable solar array; SA, Yearly maximum amass Sun ray of single axis Sun tracker; TA, Yearly maximum amass Sun ray of two axis Sun tracker; FT, The ISN axis is four times annually tuned, the yearly amass radiation; NC OPTM, Tilt-angle modification date of an ISN-axis, days from the equinoctial point; A, OPTM; ISN-axis tilt-angle modification for each change

Figure 2.13 Dual axis, ISN axis, and stable axis optical outcome observations

Chang [46] investigated the outcome of an East-West rotated one-axis sun following module. A latitude and radiation for a distinct era are considered in the comparative analysis of the east west tracing module with a stable horizontal surface. The yearly improvements gained in a north south oriented one axis traced panel are substantially greater than those obtained in an east west allied one axis traced module, according to the survey. The incident radiation captured decreases as latitude increases, while the tracker radiation gain grows (equator=12% to arctic=143%). Figure 2.14 shows the apparent location of the Sun, which can be represented by a vector $\vec{P}$ given by equation 2.1.

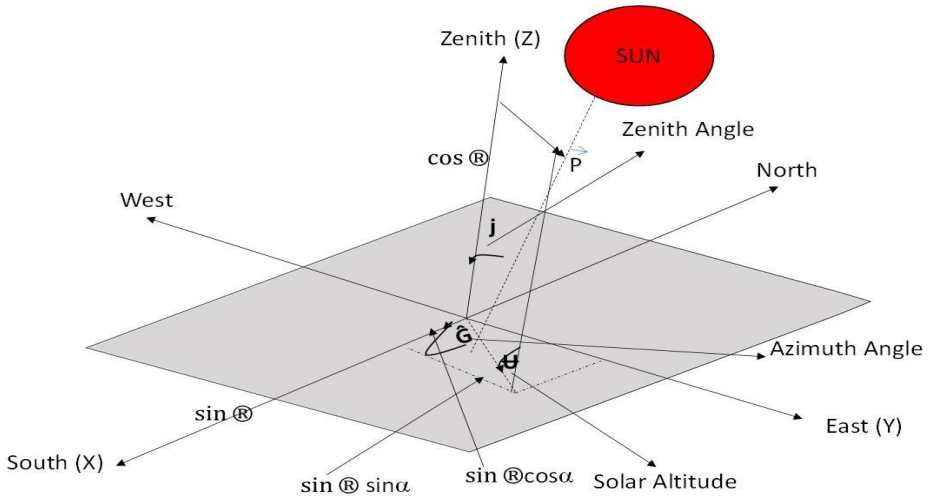

Figure 2.14 Apparent location of the Sun

$$\vec{P} = \sin j \cos \hat{G}\, X + \sin j \sin \hat{G}\, Y + \cos j\, Z \tag{2.1}$$

Where η represents the solar hour angle, which varies by 15^0 every hour and becomes 0^0 at solar noon, as illustrated in equations 3.2 and 3.3. In the morning and late afternoon, the W is -ve and +ve (for example, +300 at 2 PM and -450 at 9 AM).

$$\sin j = \sin ® \sin V + \cos ® \cos \delta \cos \eta \tag{3.2}$$

$$\cos \hat{G} = \frac{\left(\cos j \sin \hat{G} - \sin ®\right)}{\sin j \cos \hat{G}} \tag{3.3}$$

® represents the solar declination angle given in equation 3.4.

$$® = 23.45\ \sin\left(\frac{2\pi(284 + \mathrm{YSD})}{365.25}\right) \tag{3.4}$$

Solar amasser is a one-axis follower orientated East–West that circles solely in the south (or north) orientation around its axis of rotation. The amasser vector $\vec{M}$ and $\vec{N}$ are denoted by equations 3.5 and 3.6, respectively.

$$\vec{M} = \sin Б\, X + 0\, Y + \cos Б\, Z \tag{3.5}$$

$$\vec{N} = \sin(Б - 90)X + 0Y + \cos(Б - 90)Z \tag{3.6}$$

When vector $\vec{N}$ is vertical to $\vec{P}$, the system captures the most solar energy. When $\vec{P}.\vec{N}$= 0, the Sun tracking system angle oriented to focus the Sun can be determined using equation 3.7.

$$Б = \tan^{-1}(\tan j\ \cos \hat{G}) \tag{3.7}$$

The scalar product between $\vec{P}$ and $\vec{M}$, provided in equation 3.8, is used to solve the Qew.

$$\theta ew = \cos^{-1}\left(\sin j \cos \hat{G} \sin Б + \cos j \cos Б\right) \tag{3.8}$$

The entire Sun rays intercepted by the single axis tracker for a certain period of time may be solved by using equation 3.9, and the global radiation can be solved by using equation 3.10.

$$I_{GB} = \int G\left(1 + 0.33 \cos\left(\frac{2\pi \mathrm{YSD}}{365.25}\right)\cos(\theta ew)dt\right) \tag{3.9}$$

$$It = Ibb\ Rb + Idd\frac{(1 + \cos Б)}{2} + Ic\ \hat{Y}\frac{(1 - \cos Б)}{2} \tag{3.10}$$

The solar radiation of a clear sky on a horizontal plane is calculated using Equation 3.11.

$$Ic = Ibb + Idd \quad (3.11)$$

The two-positional daily monitoring PV modules were performed by Tomson [47]. His research discovered the best tracker for daily two-position tracking. According to the findings, daily two positional exposures provide better progress when compared to a stationary collector. -30° eastward deflection and +60° westward deflections were options for the most precise course. Table 2.5 and Figure 2.15 show the deflected collector parameters at X=± 30^0 bend angle, respectively.

Table 2.5 Parameters of the deflected collector

BO(Degree)	CO(Degree)	BX(Degree)	XE(Degree)	XW(Degree)
45	0	52	44	44
45	-15	52	59	29
45	-30	52	74	14
45	-45	52	89	-1

BO, initial tilt angle; CO, initial azimuth; BX, deflected surface slope angle; XE, azimuth angle of surface bent eastwards; XW= azimuth angle of surface bent westwards

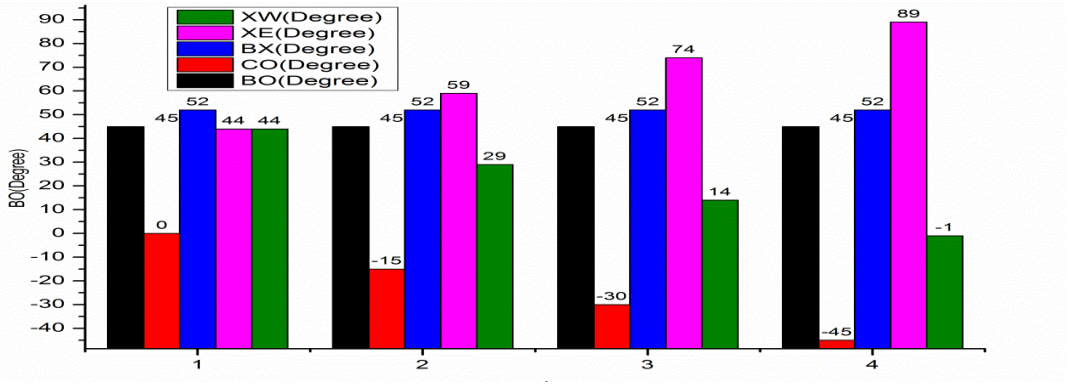

Figure 2.15 Parameters of the deflected collector

A one axis sun tracer and a fixed compound parabolic concentrator system are investigated by Grass et al. [48]. A magnetic device founded of an empty tube amasser and a converging mirror was proposed for a one-axis tracker. Radiation incidence efficiency has improved, according to the tracking system investigation. We've also discovered that minor tracking errors have noticeable consequences when the system's acceptance angle is low. Finally, the optical efficacy of a compound parabolic concentrator modal is 0.71, while the optical efficiency of a non-tracking type is just

0.69. In Table 2.6, the authors underline their observations on various irradiation systems and compared the results shown by graph in Figure 2.16.

Table 2.6 Optical irradiation systems % efficacy

Optical radiation systems	Efficacy (%)
Externally reflective CPC Collector	74
Parabolic trough collector	5
U-tube absorbers based CPC Collector	66

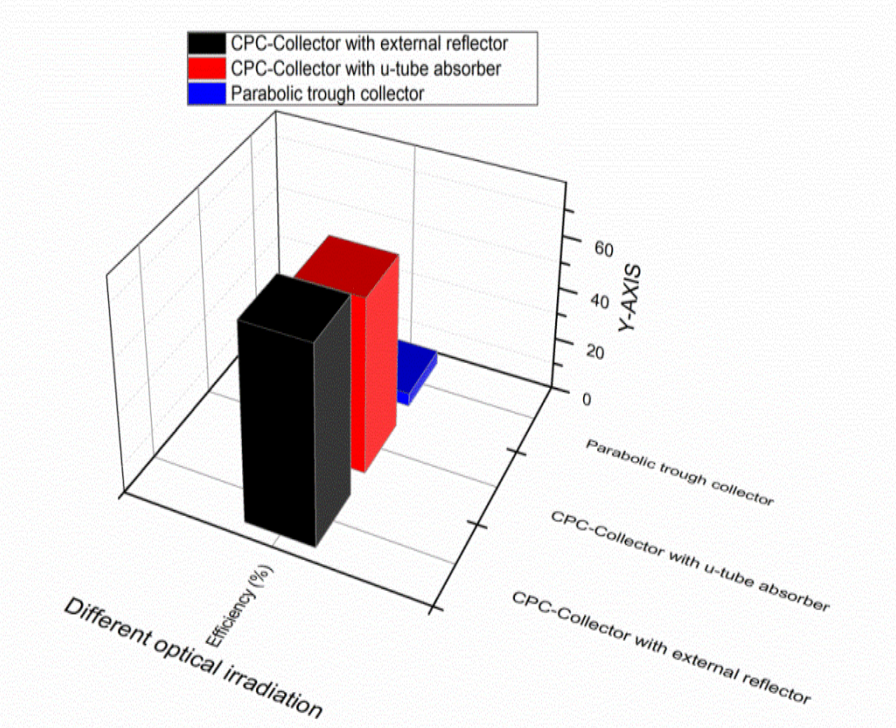

Figure 2.16 Irradiation efficiency

Bin et al. [49] developed an equation for calculating incident radiation by the 1-axis 3-step tracker of the azimuth system on a daily and hourly basis, and compared it to the incidence radiation engrossed by a stable panel plane. The two-axis 3-step azimuth follower is depicted in Figure 2.17. The angle of azimuth, interval of hour angle, and Solar time are described in Table 2.7, where ωst (south fronting morning or evening hour angle), ωtr (daylight hour angle at any slanting), and ωts (time of daylight hour angle at any slanting) are discussed (evening hour angle at any sloping).

Table 2.7 The three-step follower regulation parameter for azimuth

Solar Time	Azimuth Angle (Degree)	Interval of Hour Angle (Degree)
12-(1/15 | ωst |)	-(2/3) | ωst |	ωtr→ -(1/3) | ωst |
12+(1/45 | ωst |)	(2/3) | ωst |	(1/3) | ωst | →ωts
12-(1/45 | ωst |)	0	-(1/3) | ωst | → (1/3) | ωst |

The daily radiation (H"tt) produced by a 3-step following surface on the Sun azimuth angle is the sum of the Hbt1, Hbt2, and Hbt3 radiation over the course of a day. Equation 12 is used to determine daily radiation.

$$H"tt = Hbt1 + Hb2 + Hdh\frac{(1+\cos\beta)}{2} + Hth\,\rho\,\frac{(1-\cos\beta)}{2} \tag{12}$$

The daily radiation on the three-step following hour angle surface is the sum of the radiation in each individual time break, and may be computed using equation 13.

$$H"tt = Hbh\frac{3\cos\delta\sin\frac{1}{3}|\omega st|}{\frac{\pi}{180}|\omega s|\sin\delta\sin ©+\cos ©+\cos\delta\sin|\omega s|}+\left[\int_{-\omega s}^{\left[-\frac{1}{3}\right]\omega st} Edh\,d\omega + \int_{\frac{1}{3}\omega st}^{\omega s} Edh\,d\omega\right]\times$$
$$\left(\frac{1+\cos ©\,\cos\frac{2}{3}|\omega st|}{2}\right)+\left[\int_{-\frac{1}{3}\omega st}^{\left[\frac{1}{3}\right]\omega st} Edh\,d\omega\right]\times\left(\frac{1+\cos ©}{2}\right)+\left[\int_{-\omega s}^{\left[-\frac{1}{3}\right]\omega st} Eth\,d\omega +\right.$$
$$\left.\int_{\frac{1}{3}\omega st}^{\omega s} Eth\,d\omega\right]\times\rho\left(\frac{1-\cos ©\,\cos\frac{2}{3}|\omega st|}{2}\right)+\left[\int_{-\frac{1}{3}\omega st}^{\frac{1}{3}\omega st} Eth\,d\omega\right]\times\rho\left(\frac{1-\cos ©}{2}\right) \tag{13}$$

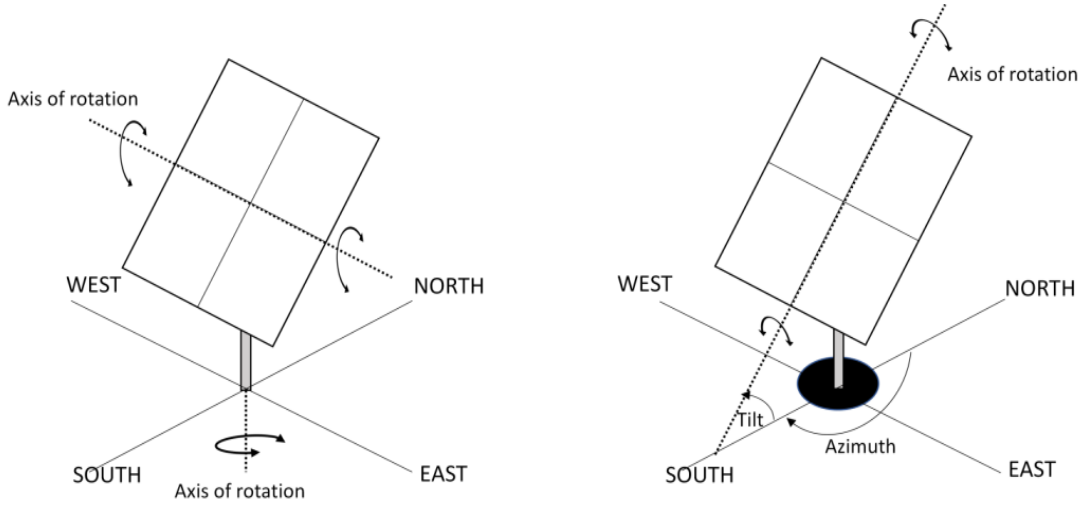

Figure 2.17 Three step tracking of azimuth angle

Table 2.8 Month wise power production

Year	Month name	AVG	TSR	RPV	PDS	PD
2010	March	11.21	348	23.1	22,783	28,044
2010	April	7.96	239	18.5	14,466	17,136
2010	May	10.41	323	22.6	20,464	25,082
2010	7 To 24 August	14.89	268	22	14427	17604
2010	September	14.42	433	25.8	26,930	33,867
2010	October	6.86	213	20.9	13,162	15,908
2010	November	6.53	196	21.7	12,041	14,654
2010	December	11.76	365	28	22,451	28,733
2011	January	3.32	103	21.3	6,911	8,386
2011	February	6.76	189	26.3	11,958	15,100
2011	March	5.16	160	24.4	10,067	12,527

PD, Power delivered 1- Angle- 3-Position photo voltaic (Wh); PDS, Power delivered stable photo voltaic (Wh); RPV, Rise of photo voltaic power delivered (E_{inc}), (%); TSR, Total Sun radiation in month (MJ/m^2); AVG, Average per day-total Sun radiation in month H_T (MJ/m^2 day)

A 3-angle single axis follower was designed by Huang et al. [50]. A direct current motor driver is required to move the PV mount, and a timer IC is required to trigger a DC motor at a variable angle. The PIC18F542 microcontroller is used to run the control algorithm, PV generating, and motion tracking function. The rise in month total power output from 1-angle 3-position Sun follower after photo voltaic is ranged between 18.5% and 28.0 %, as shown in Table 2.8 and Figure 2.18. From the first March 2010 to the thirty-first March 2011, overall power production increased by 23.6 %, which is close to the hypothetical estimate of Sun energy conversion to electricity (24.5%).

Chin et al. [51] developed a one-axis active solar follower with a constant load. PV panel, battery, two LDR, battery charger, servo-motor, constant load, and microcontroller make up this model. LDR detects the Sun's intensity. This LDR sends an instruction signal to the microcontroller, which moves the servomotor as shown in Figure 2.19. All components are powered by a lead acid battery, which creates energy that is stored via a charge controller. In comparison to a stable system, their practical observation resulted in a 20% increase in efficiency. Modeling the system under

constant load is done with the Matlb tool. The resulting result is similar to the model's Matlab simulation result. Because external disturbances like as wind loading and mechanical friction were not represented in the MATLAB Simulink model, the findings vary during the night time and noon. The Sun irradiance was measured using Light Dependent Resistor sensors (NORPS-12). The chosen resistor value should produce a voltage that is suitable for both bright and dark days. Table 2.9 shows the resistance measurement that was used, as well as a display analysis in Figure 2.20.

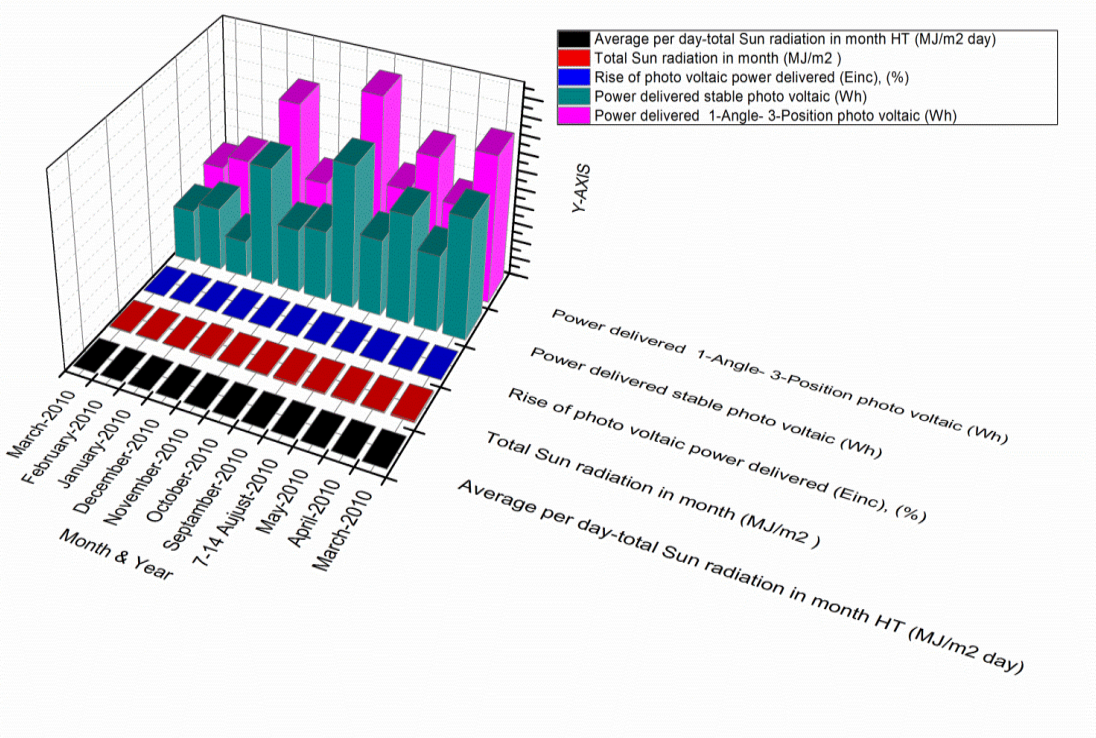

Figure 2.18 Sun radiation and power are analysed on a monthly basis

Table 2.9 LDR transducer voltage outcome

Resistance(Ω)	Sunny Day Voltage Output(V)	Cloudy Day Voltage Output(V)	Difference Voltage Output(V)
50	2.14	0.82	1.32
100	3.95	0.9	3.05
200	4.56	1.35	3.21
500	4.78	1.41	3.37
1000	5.02	1.9	3.12

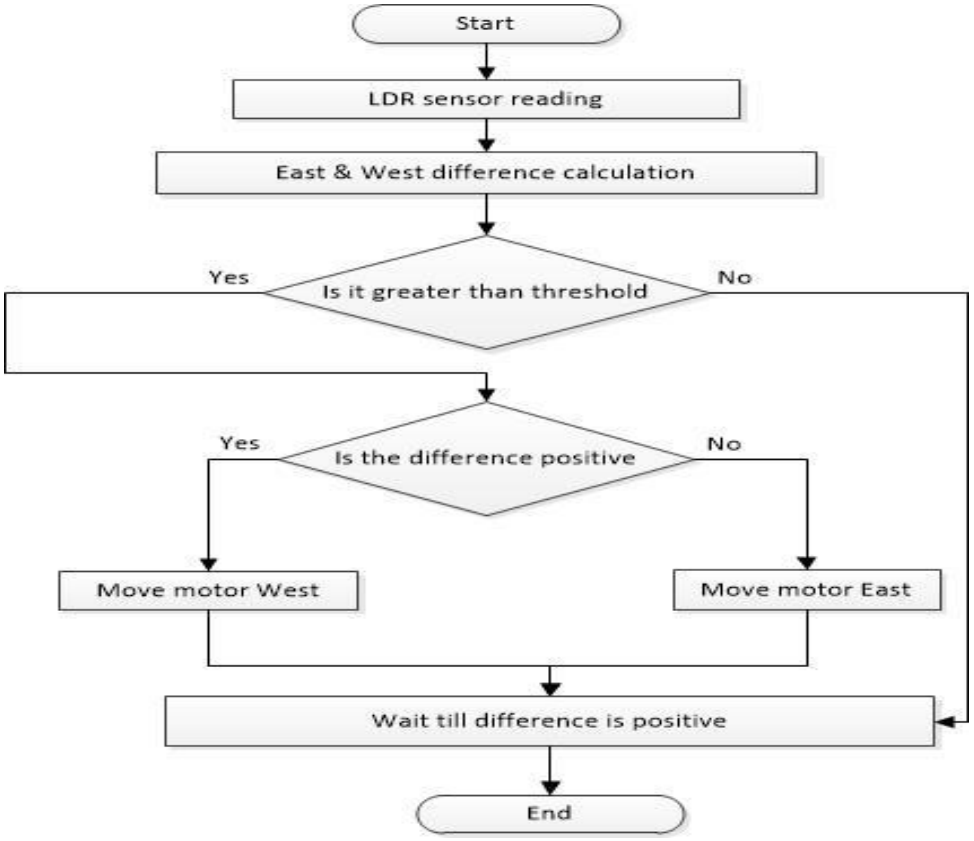

Figure 2.19 Flow chart of single axis tracer module

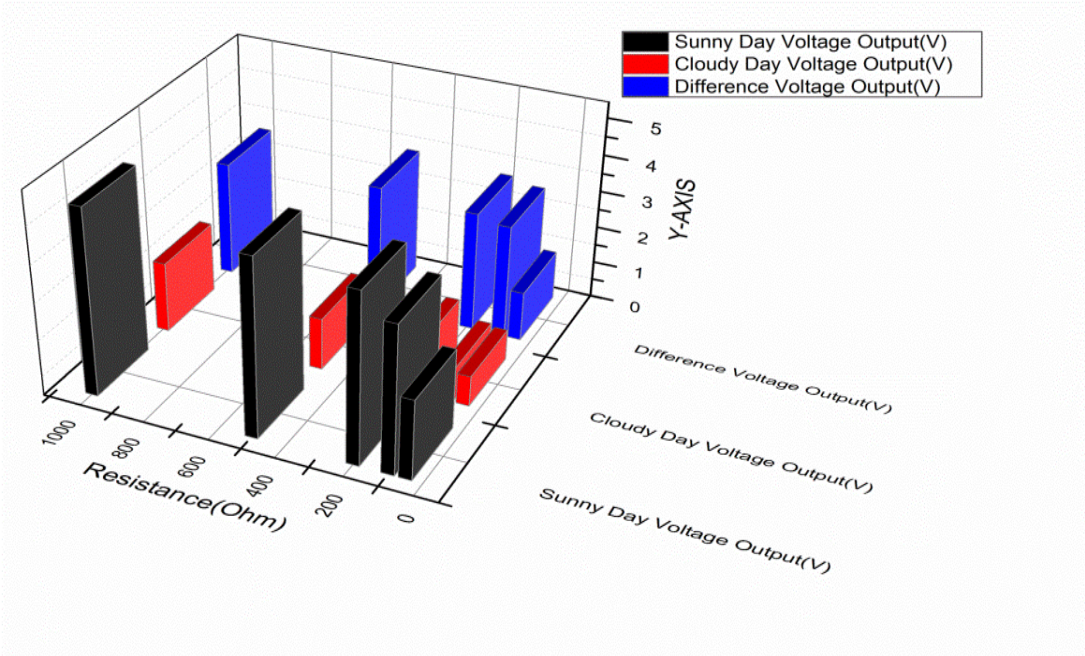

Figure 2.20 LDR transducer voltage outcomes

2.10 Two-axis Active tracker system

The horizontal and vertical orientations of the two-axis system are perpendicular to each other, as shown in Figure 2.21. The two-axis tracing system has greater precision and efficacy than the one-axis tracing system. When compared to one-axis systems, two-axis systems use more power and have a more complicated control system.

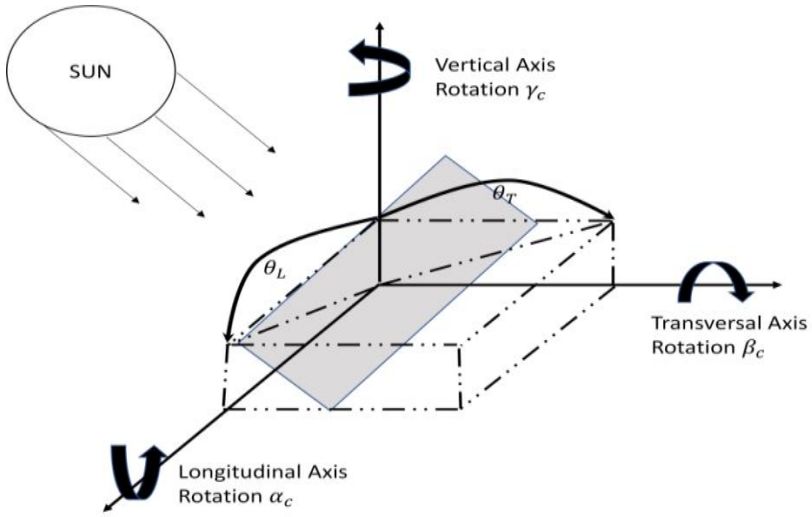

Figure 2.21 Rotation angles

Oner et al. [52] designed a decreasing timer mounting structure and correlated the response using two methods: a regular follower for a horizontal photovoltaic structure and a day-to-day regulation for a focused solar power system. In comparison to a fixed Photovoltaic mode, these two strategies result in increased power generation. In a standard tracking strategy, the tracker error drops to 0.15°. For tracking the Sun, they created a tracker using a microcontroller-controlled spherical motor. The spherical motor has the ability to move along both horizontal and vertical axis. Between 13 and 17 solar periods, they saw an approximately 3.5-volt increase in the system's output compared to a steady angled Photo Voltaic module.

M Rahimi et al. [53] discussed a hybrid two-axis solar and wind-follower system [29] that improves photovoltaic panel efficiency when compared to stable panel systems. The efficiency of the traditional approach was diminished due to the panel's heating. Nonetheless, the proposed system makes use of wind tracking to cool the PV panel and boost power generation. In comparison to a fixed tilting system, a standard

two-axis follower produces a 39.43% gain in energy. In comparison to a fixed mount system, the hybrid system gives a daily energy improvement of 49.83%. Table 2.10 compares the gain percent of fixed, tracking, and hybrid systems, with K2 and K3 representing percent gains over the E1 system. Figure 2.22 depicts the system gain comparison data graphically.

Table 2.10 Observation of fixed, following and hybrid PV system

T	E1	E2	E3	K2	K3
(7:35–11:25)	14.77	24.47	26.52	65.67366283	79.55314827
(11:25–15:15)	26.76	27.24	29.15	1.793721973	8.931240658
(15:15–19:05)	11.53	22.27	23.83	93.14830876	106.6782307
OGD	53.06	73.98	79.5	39.4270637	49.8303807

T, Time (hr : min); E1, Stable system energy in Wh; E2, Solar-following system energy in Wh; E3, PV & wind-Following system energy in Wh; K2, [(E2 - E1) / E1] *100 (%); K3, [(E3 - E1) / E1] *100 (%); OGD, Overall generation in a day

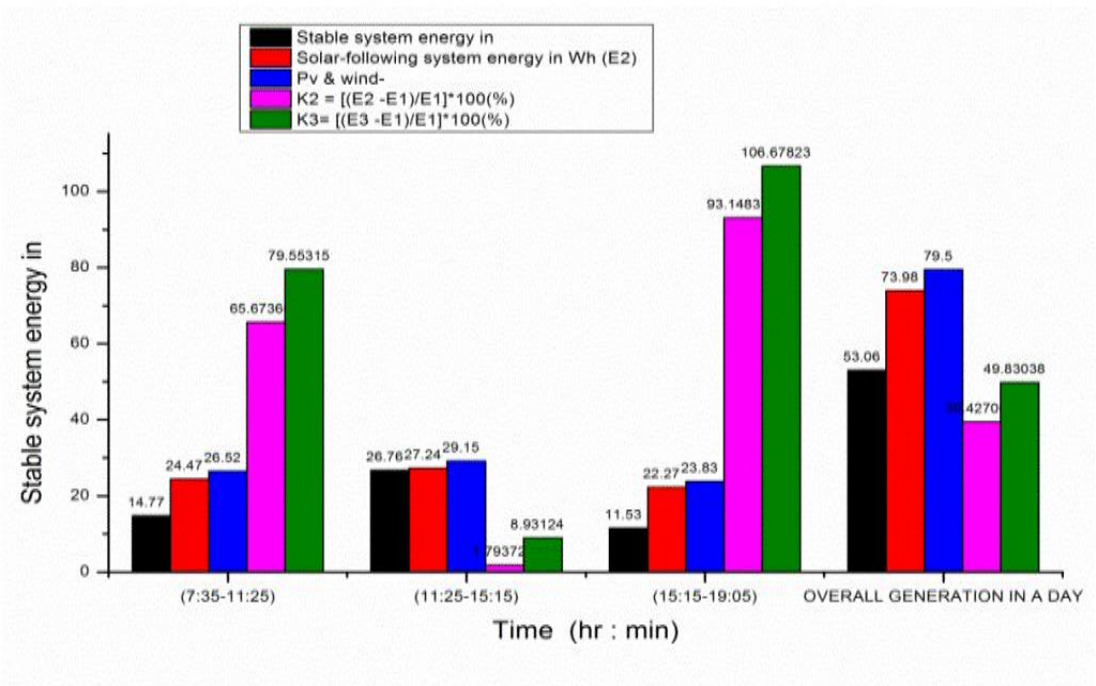

Figure 2.22 Comparison of maximum energy of fixed, tracking & hybrid system

Asif Khan and Nadeem Javaid [54] created a hybrid standalone system that utilises a fixed PV panel. For simulation of solar, wind turbine, and battery systems, a hybrid algorithm of TLBO and Jaya is employed in this standalone system. When comparing this JLBO approach to TLBO, it was discovered that JLBO had a lower

nominal total annual cost (TAC). TAC values of 34464, 43046, 50247, 60752, and 66542 USD are revealed by the economical solution at LPSPmax prices of 5%, 2%, 1%, 0.3%, and 0%, respectively. The worst performance, mean, SD , ranks of the schemes, and best performance over ten separate operations for the intended hybrid schemes at LPSPmax = 01 percent are shown in Table 2.11 and Figure 2.23.

Padmagirisan and Sankaranarayanan [55] developed a PV battery-powered HEV with two controller stages, the LLC and the HLC algorithms. This system, depicted in Figure 2.24, consists of a flat PV panel connected to a battery, which stores and delivers solar energy to a HEV. According to the limitations framed, LLC executes load regulation, battery charging, and the P&O MPPT algorithm, whereas HLC executes switching within several operating conductions such as high load, maximum charging, high battery current and minimum charging.

Table 2.11 Comparison table of proposed method

HS	Index	TLBO	GA	JAYA	JLBO
PVWTB	Mean (USD)	51 458	54 626	50 596	50 247
	SD (USD)	1 790.2	4 539.9	173.1658	0
	Best (USD)	50 268	50 247	50 268	50 247
	Worst (USD)	55 621	63 565	50 678	50 247
PVB	Mean (USD)	67 052	67 052	67 052	67 052
	SD (USD)	0	0	0	0
	Best (USD)	67 052	67 052	67 052	67 052
	Worst (USD)	67 052	67 052	67 052	67 052
WTB	Mean (USD)	138 250	138 250	138 250	138 250
	SD (USD)	0	0	0	0
	Best (USD)	138 250	138 250	138 250	138 250
	Worst (USD)	138 250	138 250	138 250	138 250
AR		85 586.67	86 642.67	85 299.33	85 183
FR		3	4	2	1

HS, Hybrid schemes; PVWTB, Photo Voltaic–Wind Turbine–Battery; PVB, Photo Voltaic–Battery; WTB, Wind Turbine–Battery; AR, Average Rank (USD); FR, Final Rank

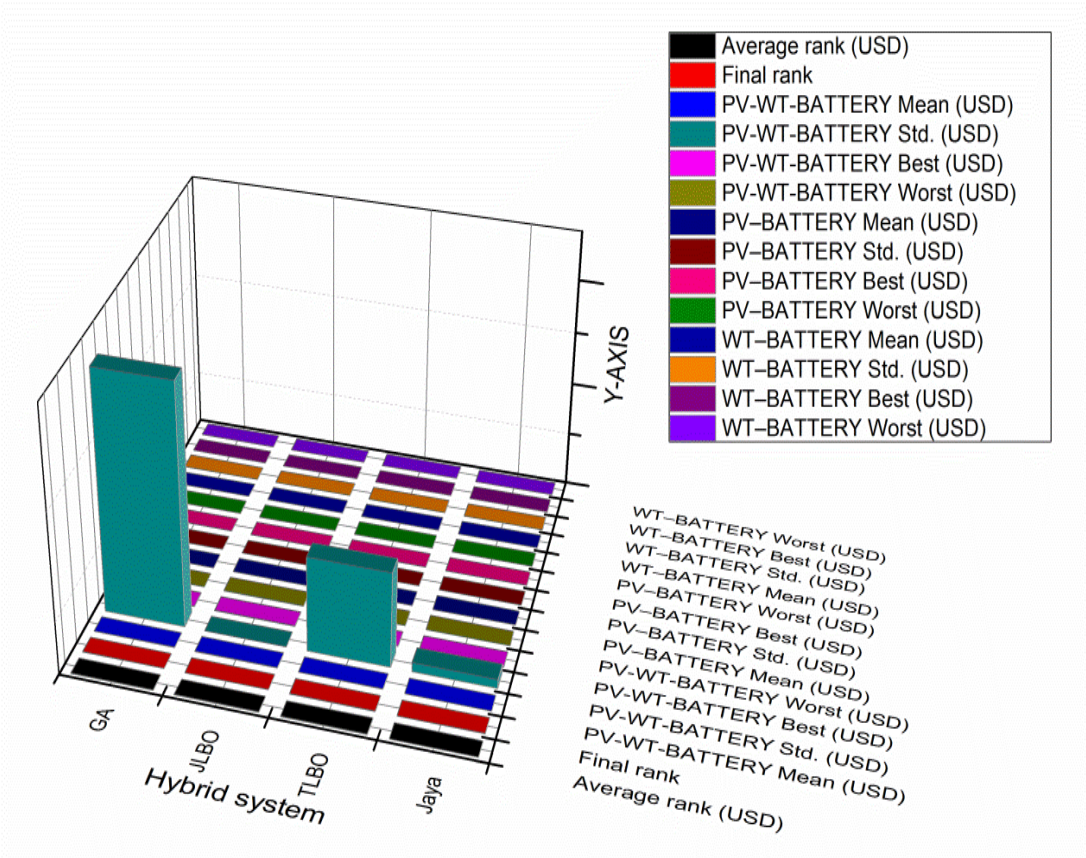

Figure 2.23 Proposed method analyses

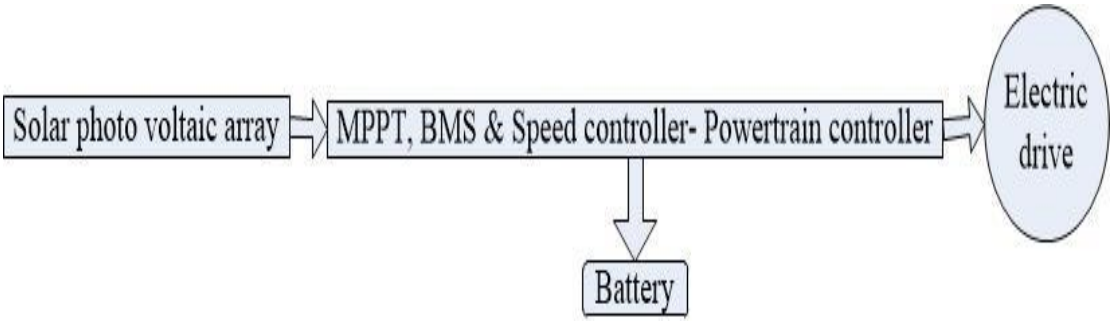

Figure 2.24 System diagram

Kanhaiya K. et al. [56] discuss a hybrid system that uses wind and a PV system to maximise power output. The primary system is a PV, while the secondary system is a wind energy system. Matlab is used to do the system analysis, which is based on standard data. Figure 2.25 shows the data analysis for a photovoltaic and wind hybrid system.

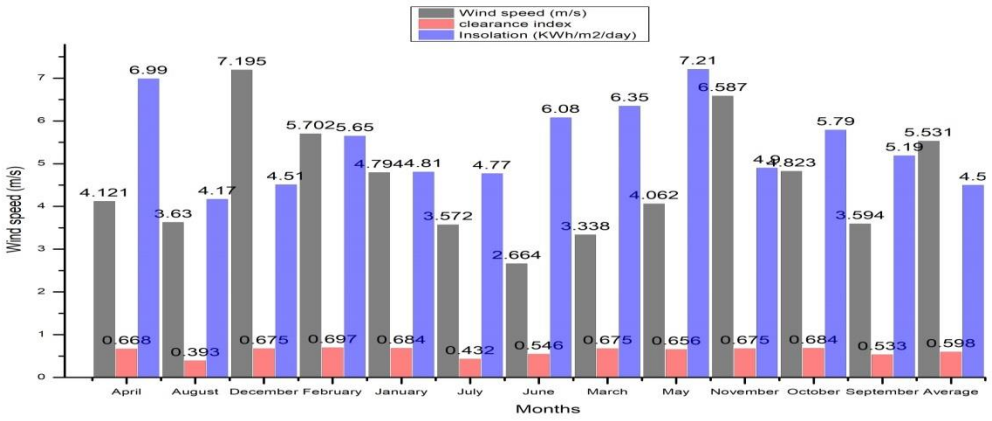

Figure 2.25 Hybrid system analyses

The best tracking approach for PV systems deployed at high elevations was devised by Quesada et al. [57]. The theoretical value of irradiation determined for a fixed panel in this method. It creates more power compare to a Sun tracker panel, according to the results. It was discovered that following the Sun is the best option only when the sky is clear or partly cloudy. Table 2.12 shows global hourly power production for June 11th, 2014 and expressed in Figure 2.26. The columns represent IC (internal solar radiation values per hour), IH (internal solar radiation on the horizontal plane), EDTS (internal solar energy generation per hour), EH (internal solar energy generation by horizontal PV module), and TA (thermal energy generation by horizontal PV module) (Tracking gain).

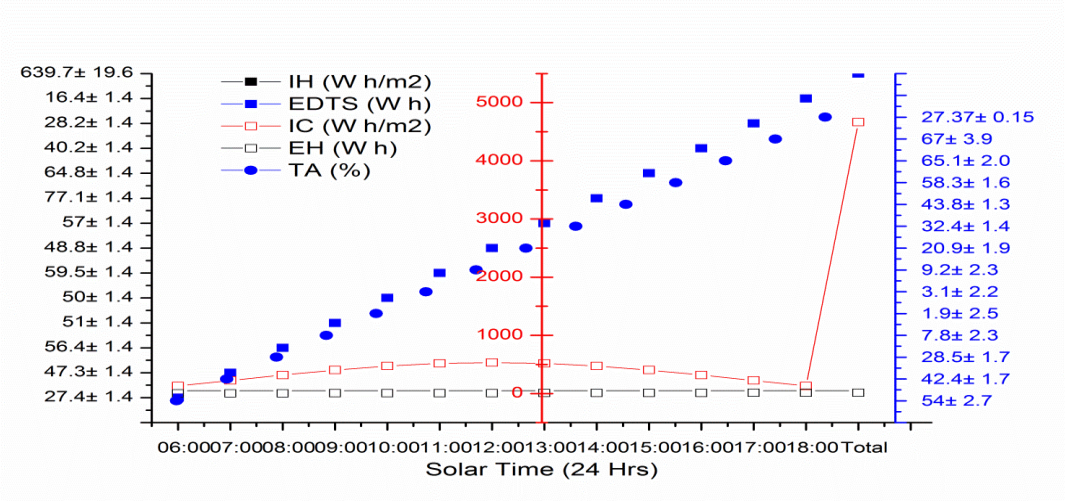

Figure 2.26 Advantage of tracking for global hourly energy output

Table 2.12 Tracking gains for global per hour energy generation on eleven June 2014 on solar time.

ST	IH (W h/m^2)	IC (W h/m^2)	TA (%)	EDTS (W h)	EH (W h)
06:00	27.4± 1.4	130.6	54± 2.7	0.147± 0.007	0.321± 0.010
07:00	47.3± 1.4	223.5	42.4± 1.7	0.069± 0.016	1.193± 0.023
08:00	56.4± 1.4	317.9	28.5± 1.7	1.364± 0.025	1.907± 0.031
09:00	51± 1.4	404	7.8± 2.3	1.46± 0.026	1.583± 0.027
10:00	50± 1.4	472.8	1.9± 2.5	1.444± 0.026	1.472± 0.026
11:00	59.5± 1.4	517.1	3.1± 2.2	2.008± 0.032	2.072± 0.033
12:00	48.8± 1.4	532.4	9.2± 2.3	1.375± 0.025	1.515± 0.026
13:00	57± 1.4	517.1	20.9± 1.9	1.621± 0.028	1.049± 0.033
14:00	77.1± 1.4	472.8	32.4± 1.4	2.44± 0.037	3.61± 0.05
15:00	64.8± 1.4	404	43.8± 1.3	1.379± 0.025	2.454± 0.037
16:00	40.2± 1.4	317.9	58.3± 1.6	0.364± 0.011	0.872± 0.019
17:00	28.2± 1.4	223.5	65.1± 2.0	0.131± 0.007	0.376± 0.012
18:00	16.4± 1.4	130.6	67± 3.9	0.0299± 0.0031	0.091± 0.005
Total	639.7± 19.6	4664.2	27.37± 0.15	12.42± 0.25	17.1± 0.31

ST, Solar Time (24 Hrs); IC, Per hour values of solar radiation; IH, Per hour radiation on the horizontal plane; EDTS, Per hour electrical energy generation by solar following; EH, electrical energy generation by horizontal PV module; TA, Tracking gain

Eldin et al. [58] devised a mathematical model for crystalline silicon PV solar tracker systems in order to assess their viability in hot and cold climates. They tested solar panels in Germany and Egypt under various climate (hot and cold) conditions to see how much energy they could save. They discovered that in warm regions, the average energy gain during tracking is 8.16 percent higher than a photovoltaic panel with less mobility. If the solar panel overheats, the tracker has a low energy gain. On a hot day, these trackers would capture the complete solar energy generation, but their high repair and maintenance costs make them unacceptable solutions in extreme heat. When a similar tracker was employed in Berlin with lower irradiance and temperature, it resulted in a 40 percent increase in energy over a fixed photovoltaic panel. Finally, the researchers discovered that tacking consumes 10% of energy and results in a total energy gain of roughly 30%. They realised that this concept is also consistent with the experimental findings. The tracking system showed an increase in energy from the PV

panel in Berlin and Stuttgart, Germany, whereas it showed a drop in energy from the PV panel in Cairo and Aswan, Egypt. As a result, a tracker is most effective in cold countries and less effective in Sunbelt countries.

According to Moharram et al. [59], the panel's output reduces by 0.5 percent with each increase in temperature. The efficiency of a crystalline silicon Photo Voltaic panel decreases due to warming. Table 14 and Figure 2.27 show the experimental arrangement that produced the highest power in 2011.

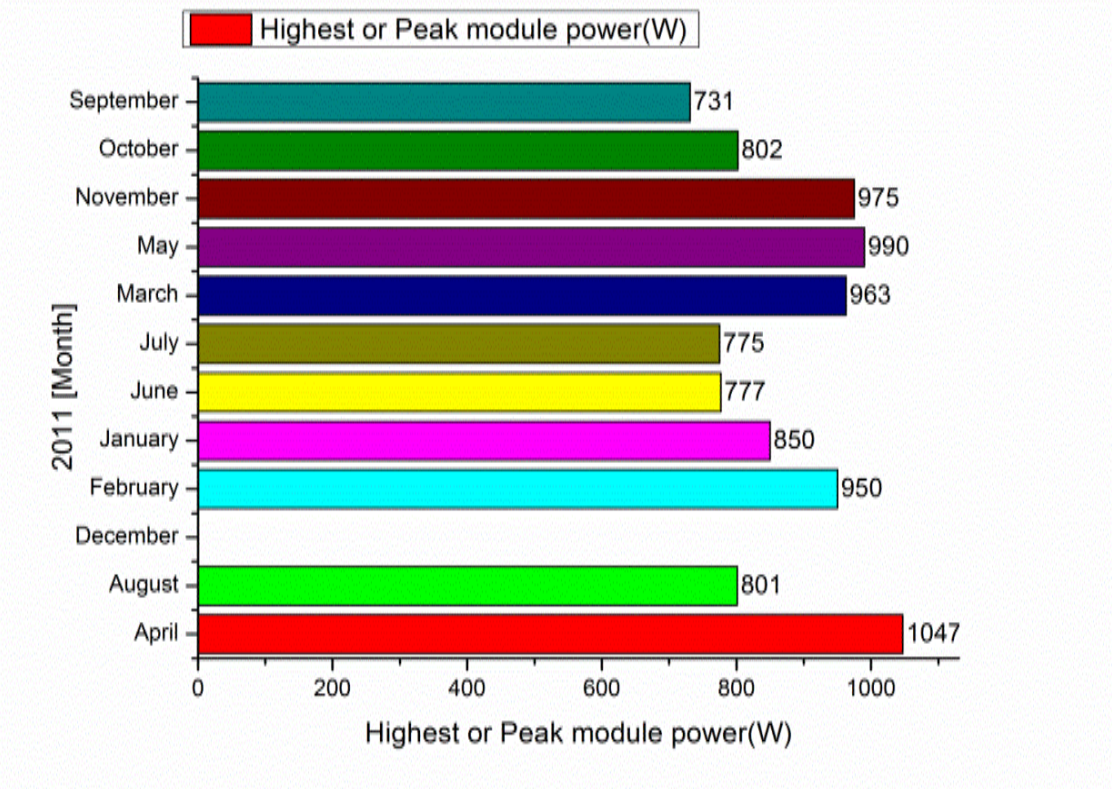

Figure 2.27 Peak power generation per month in 2011

The disadvantages of the following modes on a Sun-based multi-effect distillation plant were discussed by Mahdi et al. [60]. The system's two components are multi-effect distillation and solar fields. Solar heat is absorbed using a PTC loaded with heat transfer fluid. To evaluate the effective tracking technique to produce water and useful energy increase, a detailed study was conducted between North-South, East-West tracking, full tracking, and multi-effect distillation facilities. Table 2.13 shows the seasonal characteristic readings, and Figure 2.28 shows the analysis.

Table 2.13 Result analysis of formed water & valuable energy increase for four different session of a year

SC	RM	FD	VE	HD	MT	R	AC
	0.7904	196.119	248.127	182.441	Full Tracking	0.4552	430.848
	0.7896	195.917	248.12	182.437	Polar Axis	0.4547	430.838
SEP	0.7641	154.122	201.713	159.156	North-South	0.4268	361.104
	0.7776	175.972	226.303	171.492	East-West	0.4421	398.054
	0.7495	131.31	175.202	145.856	Fixed Angle	0.4087	321.267
	0.8007	214.769	268.235	192.529	Full Tracking	0.4658	461.063
	0.7867	191.094	242.897	179.817	Polar Axis	0.4518	422.989
SP	0.7982	210.431	263.648	190.227	North-South	0.4633	454.171
	0.7899	196.457	248.703	182.73	East-West	0.4551	431.714
	0.7872	191.925	243.799	180.27	Fixed Angle	0.4523	424.345
	0.7892	195.203	247.349	182.05	Full Tracking	0.4543	429.679
	0.7892	195.162	247.304	182.028	Polar Axis	0.4543	429.612
FEP	0.7628	152.154	199.461	158.026	North-South	0.4253	357.72
	0.7772	175.329	225.589	171.134	East-West	0.4417	396.982
	0.7482	129.306	172.83	144.665	Fixed Angle	0.407	317.702
	0.7665	157.946	206.071	161.342	Full Tracking	0.4296	367.652
	0.7554	140.416	185.893	151.219	Polar Axis	0.4163	337.332
WP	0.7093	72.446	102.142	109.202	North-South	0.3426	211.482
	0.7579	144.373	190.493	153.527	East-West	0.4194	344.243
	0.6932	50.518	72.88	94.522	Fixed Angle	0.3016	167.511

SC, Seasonal Characteristic; RM, Ratio(Formed Water/ Valuable Energy); FD, Formed WATER (Ton/h); VE, Valuable Energy (W/m^2); HD, Heat Dissipation (W/m^2); MT, Mode of Tracking; R, Ratio (Formed Water/ Acknowledged Radiation); AC, Acknowledged radiation (W/m^2); WP, Winter Peak; SEP, Spring Equinoctial Point; SP, Summer Peak; FEP, Fall Equinoctial Point

Roth et al. [61] create a Sun follower that is automatically closed-loop. A pyrheliometer detects the direct sun irradiation of a dual-axis module automatically. The Sun's picture is preserved in the centre of the four photo-detectors, which are arranged diagonally. On cloudy days, a software programme is used to determine or calculate the location of the Sun. For solar irradiation illustrated in Figure 2.29, this module is stable beyond 140 W/m^2.

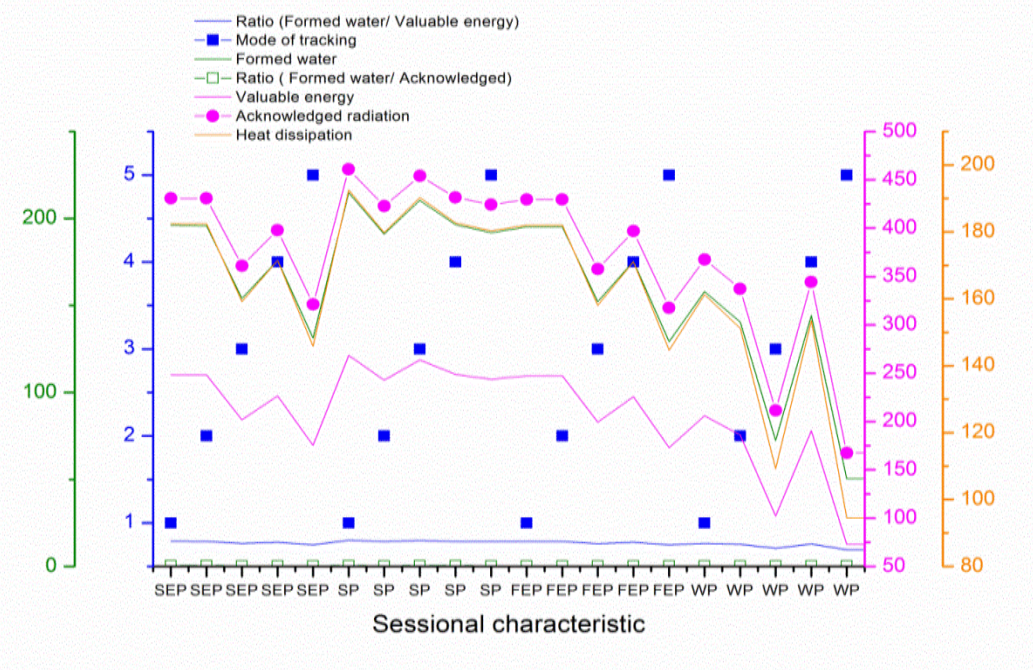

Figure 2.28 Graphical analyses of formed water & valuable energy increase for four different seasons

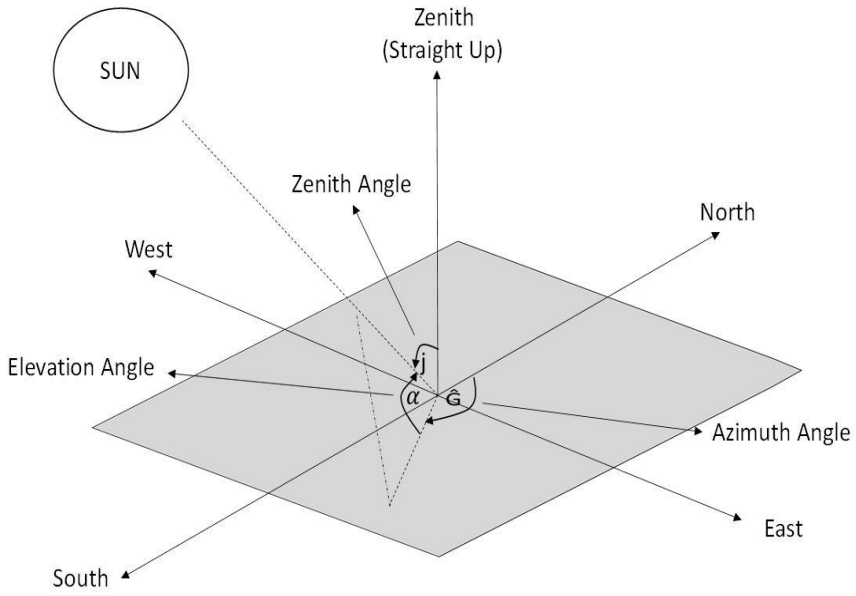

Figure 2.29 Dual-axis PV tracking surface

To increase energy production, Njoku [62] devised a two-axis solar follower model. When compared to one-axis and CPV solar following arrangements, the two-axis solar following arrangement produces the highest output (concentrated photovoltaic). The

output of a two-axis following system was about 25.2 percent higher than the production of a horizontal system. Figure 2.29 shows the dual-axis tracking system surface tracking around the zenith axes. Table 2.14 shows the maximum E/Pk (kWh/kWp) and DE/Pk (kWh/kWp) values for each season and year, as well as their visualisation in Figure 2.30.

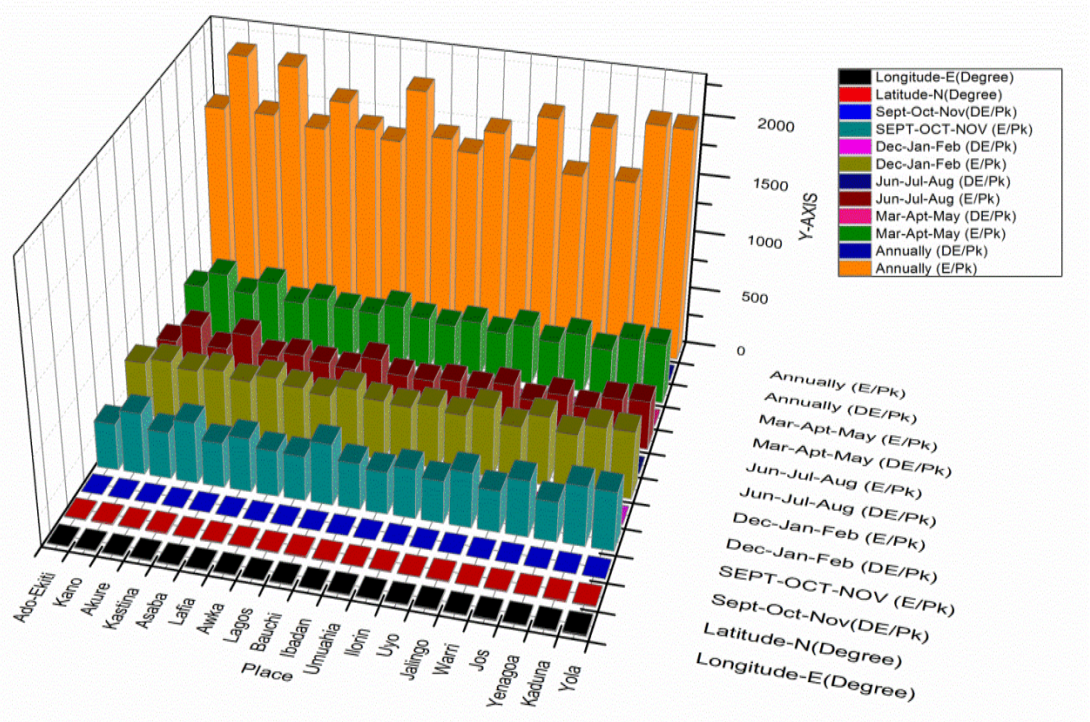

Figure 2.30 Quarterly and annually energy analysis

Yao et al. [63] created a fantastic declination clock motion mounting mechanism. It has two tracking systems: a daily adjustment tracking system and a regular tracking system. The standard technique keeps tracking mistakes below predetermined thresholds and enhances their attributes. A system implemented both the time and sensor control strategies. To reach an actual position, the Sun follower was also controlled by a local time. The tracker system's sensor provides feedback in order to fix the tracker's mistakes. Because flat PV systems do not require high accuracy, they use the daily adjustment technique. At midday, the angle of declination is adjusted once a day to ensure that the solar radiation beams are directed perpendicularly to the Photovoltaic panel (12:00). The second axis changes by 0.5° every two minutes until the finish time, with a tracking error of less than 0.5^{0}.

Table 2.14 Monthly and Early analysis E/Pk and DE/Pk of two axis following PV module at prominent urban locations of Nigeria

Place	LE	LN	SON		DJF		JJA		MAM		A	
			DP	EP	DP	EP	DP	EP	DP	EP	DP	EP
Yola	12.46	9.23	0.3432	499.4	0.4759	570.5	0.2062	416.2	0.2641	515.1	0.3245	2001
Kaduna	7.44	10.52	0.3573	508.4	0.4932	573.3	0.1904	399.2	0.2651	523.6	0.3295	2005
Yenagoa	6.33	5.03	0.2046	337.1	0.3586	475.3	0.1374	289.1	0.205	400.4	0.235	1502
Jos	8.88	9.93	0.3334	477.3	0.4848	588.4	0.174	365.5	0.255	500.1	0.3193	1931
Warri	5.75	5.52	0.2184	352	0.3547	470	0.1259	277.8	0.2053	401.4	0.2349	1501
Jalingo	11.37	8.9	0.32	471.8	0.4729	594.2	0.1904	382.3	0.2597	507	0.3172	1955
Uyo	7.92	5.02	0.2186	357.1	0.3694	492.9	0.1585	314.5	0.2126	413.1	0.247	1578
Ilorin	4.55	8.5	0.289	422.7	0.4391	534.8	0.166	344	0.2442	476.6	0.2907	1778
Umuahia	7.48	5.53	0.2186	357.1	0.3694	492.9	0.1585	314.5	0.2126	413.1	0.247	1578
Ibadan	3.92	7.4	0.2589	392.6	0.4065	508.6	0.1571	325.3	0.2273	443.7	0.269	1670
Bauchi	9.84	10.32	0.3622	520.9	0.4927	575.1	0.2113	435.4	0.2636	515.2	0.3334	2047
Lagos	3.4	6.45	0.2398	378	0.3734	480.8	0.1514	313.8	0.2163	422.5	0.2512	1595
Awka	7.07	6.21	0.248	387.8	0.3973	514.9	0.1692	334.4	0.2231	433.1	0.2659	1670
Lafia	8.5	8.4	0.31	455	0.45	566	0.18	366	0.24	482	0.30	18

	2	9	08	.5	79	.1	02	.5	7		51	70
Asaba	6.73	6.22	0.2422	378.5	0.388	499.9	0.1591	321.3	0.2162	421.2	0.2581	1621
Kastina	7.52	12.25	0.3768	517.6	0.5148	558.6	0.2225	475.9	0.2862	566.7	0.3456	2119
Akure	5.2	7.25	0.2629	396.1	0.4166	523.4	0.1561	324.1	0.2261	441.3	0.2732	1685
Kano	8.52	12	0.3821	525.4	0.5203	568	0.2279	486.4	0.2918	578.2	0.3509	2158
Ado-Ekiti	5.25	7.62	0.2629	396.1	0.4166	523.4	0.1561	324.1	0.2261	441.3	0.2732	1685

LE, Longitude E (Degree; LN, Latitude N (Degree); SON, Sept-Oct-Nov; DJF, Dec-Jan-Feb; JJA, Jun-Jul-Aug; MAM, Mar-Apt-May; A, Annually; DP, DE/Pk; EP, E/Pk

The combined approach of the photoelectric and time-based active solar tracker was developed by Zhang et al. [64]. The tracker's four photo sensors were utilised to estimate weather conditions. Photoelectric and other daytime tracking techniques were utilised on a sunny day. A stepper motor is utilised in a tracking system that rotates at a fixed angle at a predetermined time interval. When a solar panel touches the limit switch at sunset, the tracking comes to a halt, and it is then reset for the next day. This research also looks at the mechanical features of the breeze, such as movement and blockage. The average energy efficiency of a tracker is around 36% higher than that of a fixed mode over the course of a year. However, the installation latitude had an effect on the yearly average energy efficiency, according to their findings. Within 90° and 85° latitudes, energy absorption was negligible, making tracking impossible.

A dual-axis active Sun follower system was discussed by Chaowanan et al. [65], and the system was refereed for relative learning. In comparison to the fixed panel configuration, the investigation response says that the planned follower structure boosts output by 44.89 percent on average. Nowadays, terrestrial location is used to obtain steady horizontal-plate insertion with a predetermined orientation. As a result, the system output power produced decreases dramatically as solar radiation changes during the day and the seasons change throughout the year. To get around this, they constructed a structure for a low-cost, two-axis solar follower system. The devotee

technique is implemented as a CL-loop active controlled system with light dependent resistor sensors as input. As shown in Figure 2.31, the model based on a DLD (computerised reasoning structure) of the sensors is linked to a pseudo-azimuthally moving around the east-west and north-south pivots. The four LDRs in the logic judgement truth table, one, two, three, or four, represent the four directions in Table 2.15.

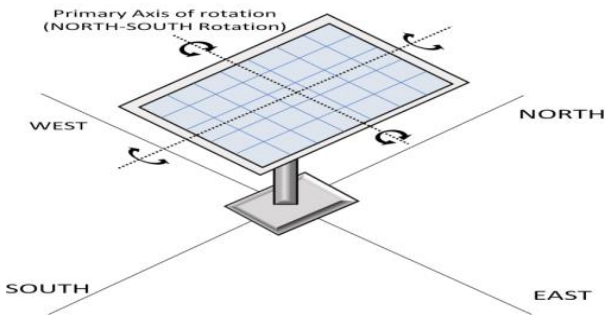

Figure 2.31 System axes of rotation

Table 2.15 4-LDR truth table with Sunlight Direction

TT	LDRI				FA		SA	
	LDR1	LDR2	LDR3	LDR4	E-W	W-E	N-S	S-N
1D	1	0	0	0	1	0	0	1
1D	0	1	0	0	1	0	1	0
1D	0	0	1	0	0	1	0	1
1D	0	0	0	1	0	1	1	0
2D	1	1	0	0	1	0	0	0
2D	0	0	1	1	0	1	0	0
2D	1	0	1	0	0	0	0	1
2D	0	1	0	1	0	0	1	0
3D	0	1	1	1	0	1	1	1
3D	1	0	1	1	0	1	0	0
3D	1	1	0	1	1	0	1	1
3D	1	1	1	0	1	0	0	
4D	1	1	1	1	0	0	0	0

LDRI, Light Dependent Resistor Inputs; E-W, East-West; W-E, West-East; N-S, North-South; S-N, South-North; FA, First Axis; SA, Second Axis; TT, Truth Table

Table 2.16 Findings of Solar position calculator and proposed Sun following algorithm

OB	ST	09:00	10:00	11:00	12:00	13:00	14:00	15:00	16:00
SC	SHA	-52.36	-37.36	-22.36	-7.35	7.65	22.65	37.66	52.66
	SD	2.85	2.85	2.85	2.85	2.85	2.85	2.85	2.85
	SAA	35.59	48.76	60.68	69.02	68.94	60.50	48.55	35.37
	AZA	-76.56	-66.83	-50.88	-20.92	21.71	51.37	67.17	76.85
	SNT	6:24	6:24	6:24	6:24	6:24	6:24	6:24	6:24
	STT	18:34	18:34	18:34	18:34	18:34	18:34	18:34	18:34
OS	SHA	-52.45	-37.45	-22.45	-7.45	7.54	22.54	37.54	52.54
	SD	2.34	2.34	2.34	2.34	2.34	2.34	2.34	2.34
	SAA	35.35	48.47	60.31	68.55	68.52	60.24	48.38	35.26
	AZA	-76.13	-66.32	-50.32	-20.72	20.97	50.46	66.40	76.18
	SNT	6:29	6:29	6:29	6:29	6:29	6:29	6:29	6:29
	STT	18:38	18:38	18:38	18:38	18:38	18:38	18:38	18:38

OB, Observation By; SC, Solpos Calculator; OS, Our System ; ST, Solar Time ; SHA, The Sun's Hour Angle ; SD, The Sun's Declination ; SAA, The Sun Altitude Angle ; AZA, Azimuth Angle; SNT, Sunrise Time ; STT, Sunset Time

Table 2.17 Relative error between the designed system & SOLPOS calculator

	ST	09:00	10:00	11:00	12:00	13:00	14:00	15:00	16:00	MSD
Relative Error	SHA	0.09	0.09	0.09	0.1	0.11	0.11	0.12	0.12	0.00014
	SD	0.51	0.51	0.51	0.51	0.51	0.51	0.51	0.51	0
	SAA	0.24	0.29	0.37	0.47	0.42	0.26	0.17	0.11	0.01339
	AZA	0.43	0.51	0.56	0.2	0.74	0.91	0.77	0.66	0.37258
	SRT	5	5	5	5	5	5	5	5	0
	SN	4	4	4	4	4	4	4	4	0

ST, Solar Time; SHA, The Sun's Hour Angle; SD, The Sun's Declination; SAA, The Sun Altitude Angle; AZA, Azimuth Angle; SRT, Sunrise Time; SN, Sunset Time

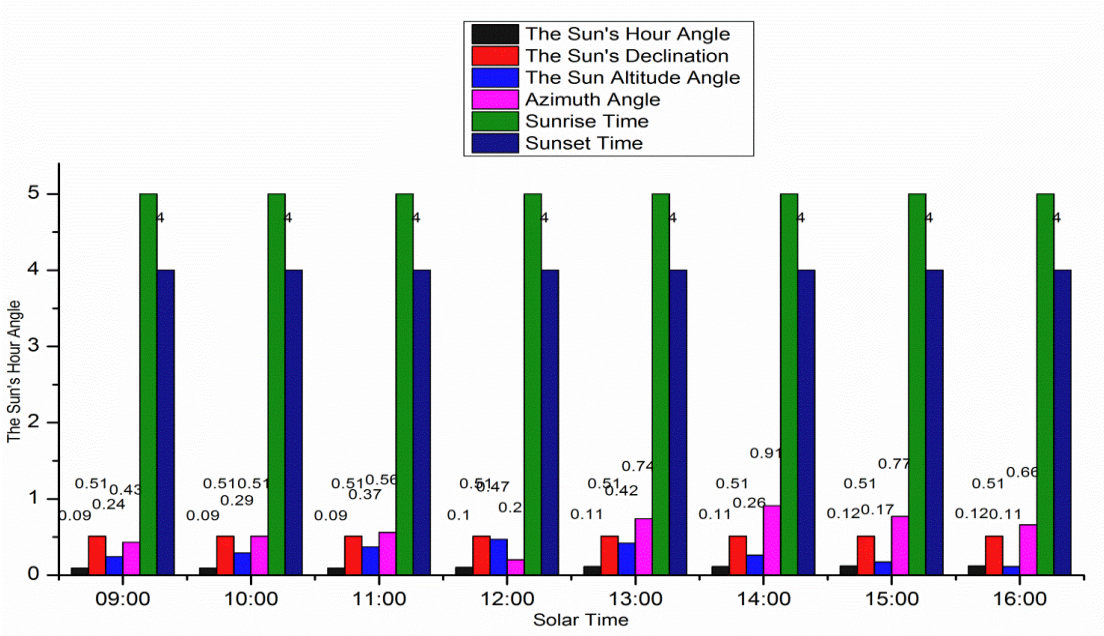

Figure 2.32 Graphical representation of Relative error of the designed system & SOLPOS calculator

2.11 Maximum power point tracking (MPPT)

The MPPT algorithm [67-70] is used to determine a panel's peak power point, which increases the generation of photovoltaic panels. Many researchers have developed PV MPPT strategies to boost the output of photovoltaic modules.

Ramli et al. [71] looked at how different maximum power point approaches in solar modules affected normal and partial shadowing under various scenarios. This article also discusses how different AI strategies can improve the output of a PV system, as well as how researchers have concentrated more on partial shading in recent years.

Z Meixia et al. [71] created a distributed MPPT system for optimising PV system output. In this research, a comparison of centralised and distributed maximum power point tracking is made. In comparison to CMPPT, the DMPPT technique proved to be more useful in partial shading. A distributed MPPT module solves the problem of battery mismatch in centralised MPPT. Within the organisational capacity of CMPPT, the batteries automatically interact with each other. Distributed MPPT mismatch

problems are decreased by 50% of the producing capacity. They discovered that the distributed maximum power point tracking yields 96.54 percent efficiency at a 10% power point (i.e. 30 Watt). However, DMPPT's greatest efficiency was 98.41%, which is higher than European efficiency and the current equalisation scheme. Overall efficiency was limited to 77.31 percent in the end. It was evident from the trial and the results that efficiency was extremely low, and that distributed maximum power point tracking may enhance production efficiency. Table 2.18 shows the efficiency of DMPPT.

Kheldoun et al. [73] devised a 99.602 percent efficient MPPT algorithm based on the GSO method in both static and dynamic conditions. This strategy worked in a fast-changing and partially shaded environment. The proposed approach uses multiplications and additions/subtractions. As a result, the convergence is quick, and the minimum power point is only reached after seven steps. As a result, it is favoured over other MPPT algorithms. When Photovoltaic arrived at MPP, it was operating at a constant voltage with no oscillations. The performance of the suggested approach is compared to that of the other methods listed in Table 2.19.

Table 2.18 Efficiency checks of DMPPT non-shadow and shadow condition

S. No	Output Voltage 0f DMPPT(V)		
	Shaded(2,9)	Shaded(9)	Un-shaded
1	45.1	40.6	35.94
2	55.5	49.8	44.3
3	0	40.9	36.31
4	0	0	44.7
5	45.2	40.7	36.09
6	56.1	50.4	44.8
7	45.6	41	36.35
8	55.8	50.1	44.9
9	45.7	41	36.45
10	55.5	49.8	44.3
Generated Power Efficiency (%)	77.2	77.31	78.46
Current output(A)	2.13	3.46	3.98
Voltage output(V)	404.5	404.3	404.14
Power output(W)	1266.09	1406.96	1608.48

Table 2.19 Outcome of various MPPT systems

Evolution Factors	APO	HCF	ST	CPO
Direct Duty Control	Affirmative	Affirmative	Nope	Nope
Tracing Technique	FLC25	FLC16	GSO	P&O
Efficiency (%)	99.98	99.68	99.43	98.83
SA	HC	Moderate	Very Simple	Very Simple
Power Error (Watt)	Negligible	0.643	1.143	2.343
Sensor	V, I	V, I	V, I	V, I
PG	200.1	199.5	199	197.8
Robustness	Affirmative	Affirmative	Affirmative	Affirmative
Response Time (Sec)	0.04	0.055	0.025	0.069

CPO, Conventional Perturbation & Observation; APO, Adaptive Perturbation & Observation FLC; HCF, Hill Climbing FLC; V, Voltage; I, Current; FLC25, FLC with 25 rules; FLC16, FLC with 16 rules; HC, High Complexity; SA, Simplicity of Algorithm; ST, Suggested Technique; PG, Power Generation(Watt)

J Ahmed and Z Salam [74] used a Perturbation and Observation MPPT technique that has been enhanced. This method is capable of reducing steady-state oscillations, which will improve tracking efficiency.

H. Brahmi and R.D. et al [75] proposed a strategy for determining the peak point of power on an online platform. As a result, the data can be simply analysed, and efficiency may be increased.

N. Kahoul, M. Houabes, and A.N. et al. [76] developed an alternate simulator for PV modules in hasty disparity situations that is more successful than MPPT. This simulator has a much shorter repose time than a standard MPPT. It was created using the ISIS Proteus programme and a 16F876A microcontroller.

N. Rakesh and T.V. Madhavaram et al. [77] devised a new method based on magic square that organises the positioning of PV modules that are shaded. As a result, the output power is higher than with typical positioning.

The Su- Do- Ku technique was used by P. S. Rao et al. [78] to introduce a new configuration strategy. Under partial shadowing, they were able to reduce line losses by increasing output power.

To alleviate the fractional darkening of TJSE, Ahmed Fathy et al. [79] proposed a robust GMPPT employing the MRFO algorithm. Increased competency triple-junction photovoltaic cells (TFSC) have gotten a lot of attention in concentrated photovoltaic approaches, although the amount of energy produced by TJSC-based entities has been reduced under fractional shading conditions. As a result, the author presents a novel global MPPT based primarily on current computer science and mathematical optimization strategies for Manta ray foraging optimization in this research note (MRFO). Seven topologies of triple junction photovoltaic module depicted in Fig 27.

For one year, Eke and Santurk [80] studied a two-axis Sun follower and a horizontal position photovoltaic system. On the same latitude, the two-axis PV tracker generates 30.79 percent more than the tilt angle fixed system. The suggested system's monthly analysis is compared to the stable system's data, which is graphically shown in Fig 28.

Bentaher et al. [81] used the LDR sensor to create a solar follower model. The angle between two LDRs can be optimised to improve system precision. This solar tracking system yields good results. Figure 29 shows the sensor's shape and the edge of an incidence.

Nadia AL-Rousan et al. [82] developed novel adaptive neuro-fuzzy inference-based smart solar follower control systems. By correctly forecasting an appropriate lean and inclination angle, ANFIS was successfully used to manage Sun follower systems. The simulation's output was fairly accurate. Their goal was to create and implement effective one- and two-axis solar follower control algorithms in order to improve the performance of solar follower systems by accurately forecasting the Sun's passage throughout the sky and reducing inaccuracy, resulting in increased energy generation. Table 2.20 lists the data and MES for one and two axis (tilt and orientation) systems.

Table 2.20 MSE (mean square error) & Prediction rate of proposed model

S. No	Single Axis(SA)		Two Axis-Orientation		Two Axis-Tilt	
	Mean Square Error	Prediction Rate (%)	Mean Square Error	Prediction Rate (%)	Mean Square Error	Prediction Rate (%)
1	0.30×10^{-2}	37.91	0.080×10^{-2}	58.82	0.290×10^{-2}	83.01
2	1.60×10^{-6}	100	1.520×10^{-4}	100	6.580×10^{-6}	100
3	0.03×10^{-2}	82.35	0.230×10^{-2}	93.46	0.070×10^{-2}	98.04

Bio-inspection optimization [83] based MPPT, which is an advanced squirrel search strategy, was developed by D Fares et al (ISSA). When compared to the traditional SSA method, this strategy reduces tracking time by 50%. The suggested ISSA technique was compared to GA and PSO during GMPP tracking and found to have faster convergence and reduced power oscillation. The GMMP tracking experiment yielded a 99.48 percent average efficiency and a 0.66 second tracking time.

Imran Pervez et al. devised a revolutionary player algorithm [84] to find the best operating position for a PV module to provide the most electricity. This method's performance is compared to particle swarm and a modified version of the Jaya algorithm.

Mostefa Kermadi et al. provide a literature that aids the performance of direct and indirect [85] methods for tracking MPPT of PV systems under varied environmental circumstances. The authors also confirm that the direct technique produces a considerable amount of steady state oscillation because the direct method produces more power loss than the indirect way. When this indirect method is added to it, the steady state oscillation is reduced.

The MPPT control approach is compared in Table 2.21 based on many parameters such as Technique, CP, AOD, CT, PVD, TMPPT, CS, IC, Sensor, and

efficiency.

Table 2.21 Table comparing various MPPT techniques

MPPTM	S	AD	CT	TMPPT	PVD	IC	CP	EFF	CS
ASVPS [74]	IR	A	DCB	Yes	No	Low	DC	99.72%	Fast
PBGMPPT [56]	V & I	A	DCB	Yes	No	Low	DC	High	Fast
ANN-PSO [75]	IR & T	A	DCB	Yes	Yes	N/A	DC	97%	N/A
HMMP [57]	I & V	D	DCB	Yes	No	N/A	DC	High	Fast
GMPPT [76]	IR	A	DCB	Yes	No	N/A	DC	99.43%	Fast
NRMPPT [63]	IR & V	A	N/A	Yes	Yes	N/A	N/A	High	Slow
GA-CS [77]	V & I	A	DCB	Yes	Yes	High	DC	SSE-99.95% & TSE-94.02%	Fast
ADE-OPPT [78]	V & I	D	DCB	Yes	No	High	DC	NS-99.7%, 30% S-99.45% & 50% S-98.34%	N/A

ASVPS, MPPT-Auto scaling variable perturbation–size MPP tracking algorithm; PBGMPPT, Pollination based Global Maximum Power Point; ANN-PSO, Artificial neural network-particle swarm optimization approach; HMMP, Hybrid Maximum Power Point; GMPPT, Hybrid global maximum power point tracking; NRMPPT, Newton-Raphson MPPT; GA-CS, Genetic algorithm and cuckoo search; ADE-OPPT, Adaptive differential evolution algorithm- based optimum power point tracking; DC, Duty cycle; AD, Analog or Digital; A, Analog; D, Digital; DCB, DC-DC boost converter; IR, Irradiance; V, Voltage; I, Current; T, Temperature; SSE, Steady state efficiency; TSE, Transient state efficiencies; NS, No shading; S, Shading; EFF, Efficiency; s, Sensor

2.12 Comparison of various solar follower on the basis of Tracker type, control strategy, algorithm and control type

Active, Passive, Fixed panel & Chronological tracker control strategy, algorithm, control type, circuit with their limitation discussed in Table 2.22.

Table 2.22 Solar tracker control strategies

TT	Limitation	CS	Control algorithm	Motor used	Circuit	Type of control
CSDA	Regular tracking consume excess power - useless tracking on cloudy weather.	GPS based	Astronomical Equation	YES	GPS data used to set Azimuth & altitude	time-based controlling system
PAS	Not used for concentrated PV system and have less accuracy.	MC	N/A	NO	Material differential expansion	Mechanical movement of actuator
ASD	Excess power consumption and accuracy reduce in cloudy day	CLC	ON-OFF, PID, PI, Fuzzy logic, Sliding mode, PID-FLC, NN, Adaptive SMC, IMC-PID, Neuro-Fuzzy logic, Cascade, Linear quadratic regulator, Machine learning & robust control.	YES	Complex circuit using different sensor	Classical & Modern Control
ASD	Excess power consumption and accuracy reduce in cloudy day	OLC	ON-OFF, PID, PI, Fuzzy logic, Sliding mode, PID-FLC, Adaptive & ANFSI	YES	Complex circuit using different sensor	Classical & Modern Control

ASD	Excess power consumption and accuracy reduce in cloudy day	HLC	ON-OFF, PID, PI, Fuzzy logic, Adaptive, Distributed, Bayesian network & Logic based Supervisor	YES	Complex circuit using different sensor	Classical & Modern Control
FP	Fixed incidence radiation can be optimize	DMCT	N/A	NO	Simple circuit with Optimization control technique	Different MPPT technique compared on Table 9 with their control strategy

ASD, Active single & dual axis; CSDA, Chronological Single & Dual Axis; PAS, Passive; MC, Mechanical Control; DMCT, Different MPPT control technique; OLC, Open Loop Control; CLC, Close Loop Control; HLC, Hybrid Loop control; TT, Tracker Type; CS, Control Strategy

More solar tracker (ST) review papers are discussed in Table 2.23 [23, 32, 86-119], which state their tracking mode, type, method, and ultimate observation.

Table 2.23 Recent studied solar tracker data

Ref.	Year	Authors	Observation	ST-Type & ST-Method	ST-Mode
[23]	2018	Sendhil Kr. Nataraja n et al.	Short ckt current improve by 86% compare to conventional PV panel.	Altitude and Azimuth-Dual	Active
[32]	2020	Susant Kr. Sahu et al.	It extracts power from sun as heat and electricity by tracking.	Dual axis-Dual	Manual
[86]	2020	Carlos D. et al.	Yearly % rise in insolation collection 3.3%, 7.1%, 2.9%	Horizontal (TBO)-Single, Tilt (TBO)-Single, Dual (TBO)-Dual	Active
[87]	2019	C. Kas-burg, and S. Frizzo	Accurately forecast the electricity Production capability and efficient tracking position updating.	Artificial recurrent neural network architecture-Dual	Active

[88]	2015	Jun Wu. Et al.	Minimise the driving torque of driver which complicity and power loss of system.	Parallel mechanism- Dual	Active
[89]	2020	Stéfano Frizzo et al.	Forecasting of power production and tracking position.	Azimuth, ARNN LSTM- Dual	Active
[90]	2012	M. and Abdul	poly-crystalline PV panel have better output in Malaysian hot-humid climate than Mono and Amorphous PV	Horizontal- Single	Chronol ogical
[91]	2014	Choi et al	Test Commercially floating PV system's durability and stability in water with 100 kW and 500 kW power generations.	Azimuth- Single	Manual , Active
[92]	2016	Wu et al.	Simulation study of 600 MW parabolic concentrator based solar aided coal-fired power generation (SACPG).	horizontal & tilt tracking- Single & Dual	Active
[93]	2016	Hong et al.	Electricity generation and Sun shading function problem solved by smart photo- voltaic blind (SPB).	Altitude and Azimuth- Dual	Active
[94]	2016	Vijaya lakshmi et al.	Output generation of PV is more in dual compare to single axis module.	Azimuth and altitude- Single & Dual	Active

[95]	2016	Bhaskar and Yuvaraj	GSM controlled electric vehicle. GSM powered by solar tracker.	Azimuth and altitude-Dual	Active
[96]	2015	Sallaberry et al.	Use IAM analysis technique On tracking & solve collector data to reduce long term optical losses.	N–S tracking, Fixed tilt concentrator-Single	Active
[97]	2015	Parmar et al.	PV tracker using Zomework principle and improve 25% more electrical output compare to fixed panel.	Vertical-Single	Passive
[98]	2015	Lazaroiu et al.	Observed 12% to 20% more energy generated by tracker compare to fixed panel.	Fixed panel & Polar-Single	Active
[99]	2017	H. Fathabadi	Find that tracking error reduces to 0.11^0 & solar energy seizing efficiency- in- crease from 28.8% to 43.6% based on the season.	Azimuth and altitude-Dual	Passive
[100]	2019	Silvana Ayala et al.	Observed 7% to 9% gain in energy by bifacial & 11% rear irradiation gain.	bifacial modules-Single	Active
[101]	2020	Armand A. et al.	Dust Mitigation	Single-axis-Single	Active
[102]	2020	Krishnas A et al.	Develops least cost two axis tracker for remote irradiation measurements.	Azimuth & tilt-Dual	Active

[103]	2016	D Zhao et al.	Reduce orientation installation error and tracking error (<4 m rad).	Single-axis-Single	Active
[104]	2016	H Fathabadi	High precise tracker decreases tracing error.	Azimuth and altitude-Dual	Active
[105]	2016	J Parthipan et al.	One axis Improve 20% energy where as two axis improve greater than 40% energy.	Single, Dual	Active
[106]	2016	Kumar N et al.	Proposed system output rise by 15-20% compare to fixed one and also remove common error produce in system.	Horizontal-Single	Active
[107]	2016	Avarand	Improve the accuracy.	Azimuth-Single	Active
[108]	2015	Li et al.	Early efficiency of heat for azimuth tracking fixed mirror solar collector reach to 61% of operating temperature.	Azimuth tracking-Single	Active
[109]	2015	Hussain and Lee	Produce maximum electrical & thermal output.	Dual	Active
[110]	2015	Patel et al.	Rise per unit area of solar collection.	Azimuth-Single	Active
[111]	2015	Das et al.	Improve power output by 19.73% compare to fixed system.	Azimuth-Elevation-Dual	Active
[112]	2018	A. K. Saymbetov et al.	UA improve solar energy by 27-32% whereas BA improves 35-40%.	Uniaxial (UA) and Biaxial (BA)-Single & Dual	Active & Passive

[113]	2020	M. Kh. Safaraliev et al.	Annually Dual tracker produces 30% more energy than stable one. And in autumn Dual produce 80% more energy than stable. All result experiment done in Tajikistan	Single & Dual axis-Single & Dual	Active
[114]	2014	Yougesh w singh & Vishwa mitra	Proposed system generates energy gain of 43.6% compare to stable system.	Dual axis-Dual	Active
[115]	2015	J. P. Reges et al.	Sun detecting rate is 96%.	Single axis-Single	Active
[116]	2014	Bashar K et al.	Azimuth and altitude angle error reduce.	Azimuth and altitude-Dual-Dual	Active
[117]	2017	Shahrokh A. et al.	Increase the output of residential solar panel.	Azimuth-Dual	Manual
[118]	2019	Ahmad Fazlizan et al.	49%, 35% & 46% energy improvement in unclear, sunny day & intermittent condition respectively.	Dual axis-Dual	MLD-Active
[119]	2015	Seung Jin et al.	Solar conversion to electricity efficiency reaches to 21%	Dual axis + CPV –Dual + CPV	Active

Study of different sun tracker papers are tabulated in the comparison Table 2.24.

Table 2.24 Sun followers different parameter Comparing table

S. No	TT	SC	IC	TB	DF	CSN	AC	EIN	PEG	TE	PE
1	PAS	LC	LCO	R	1	N	Low	No	25% compared to FP	0.43	Lowest
2	FP	MTP	LT ASA or ADA	NT	N	N	MT P	No	—	—	51.65 %
3	ASA	LT ADA	MT FA	R	1	Y	HT FP	0.4 to 0.5% of energy generated 0.5% of energy	22 to 56%	0.14	67.65 %
4	ADA	MT ASA	MT ASA	R	2	Y	HT ASA	0.4 to 0.5% of energy generated	22 to 56%	0.12	70%
5	CAL	MT AP	MT ASA & ADA	AE	1 or 2	Y	HT ADA	LT ASA & ADA	8.5% com-pare to FP	0.1	LT ASA & ADA
6	OLC	LT CL	LT CL	R	1 or 2	Y	HT CAL	Most	28.50%	0.14	60%
7	CLC	LT H	MT OL	R	1 or 2	Y	HT OL	Most	33%	0.134	HT OL
8	H	MC	Most cost	R	1 or 2	Y	Highest	Most	23.30%	0.12	95 to 97 %

TT, Tracker Type; PAS, Passive; SC, System complexity; IC, Installation cost; TB, Tracking based on; DF, Degree of freedom; CSN, control system need; AC, Accuracy; EIN, Energy intake; PEG, Power/Energy gain; TE, Tracking error; PE, Panel efficiency; FP, Fixed Panel; ASA, Active-Single axis; ADA, Active-Dual axis; CAL, Chronological; AP, Active & Passive; AE, Astronomical equations; OLC, Open Loop control; CLC, Close Loop control: N, No; Y, Yes; R, Radiation; NT, No Tracking; LT, Less Than; MT, More Than; P, Passive; H, Hybrid; MC, Most Complex; LC, least complex; LCO, Least Cost; HT, Higher Than; LOT, Lower Than

The solar tracker market is expected to grow to 9.30 billion USD in 2019 and 49.21 billion USD by 2026, according to the artical. In contrast to passive and chronological trackers, active trackers are more often employed, according to our findings. Aside from issues like maintenance, obstacles and lightning discharge, active trackers that

use both axis tracking are able to improve the efficacy of a solar system and also providing reliable and efficient energy dispersal and collection. Furthermore, as compared to a steady horizontal system, the review paper achieves a 22 percent to 56 percent increase in energy gain. The results show that incorporating a tracking module into a solar system increases power generation by a significant amount. We highlight a few key conclusions based on this review transcript:

- Passive Tracker is rarely use and does not need outside power to operate.
- A 2, 3, or 4 point one or two axis active solar followers enters the scene to lower the amount of power consumed by a continuous active solar tracker.
- With the use of an appropriate control system, single or double axis sun followers generate energy gains of 22 to 56 percent.
- Because of the minimal tracking error, sensor and microprocessor-based control schemes are commonly utilised in solar trackers.
- A recently designed Sun tracker provides weather forecasting capabilities as well as water and wind cooling for PV systems.
- 76.42 percent of research confirms in active tracker, and 7.55 percent of studies are chronological.
- 42.57 percent of studies were carried on a one axis, whereas 41.57 percent were delivered and existing on two axes.
- The following tracking types were used in the study: polar tracking (4.44%), azimuth (10%), and azimuth and altitude (16.67%). 16.67 percent vertically, and 16.67 percent horizontally.

On above said conclusion we recommend that-:

Because of its considerable energy gain (56%) and best panel efficiency (76%), the active solar tracker outperforms conventional trackers. However, if the goal of the tracker is to have the least amount of tracking error, the chronological tracker is the ideal option (0.10^0). The two axis is the best choice out of stable, single-axis, and the

double-axis energy improvement is largest (56 percent) adding tracing inaccuracy is the smallest (00.11^0). So, in terms of energy improvement and tracing error, two axis sun tracking with optimum control is the best choice.

CHAPTER 3

HARDWARE, ELECTRICAL, ELECTRONICS AND SOFTWARE DESCRIPTION

3.1 Overview

The Sun following system has two sections according to which it is discussed further:

1. Hardware section-
   - Mechanical hardware
   - Electrical and Electronics
2. Software section

The hardware section constitute the mechanical structure of solar tracker and electrical and electronics deal with electrical and electronics parts. This section is combination of both these parts which contain solar panel, DC motor, mechanical structure, Raspberry PI 4B, GPS, image sensor, light dependant resistor (LDR), Arduino Uno, personal computer and power supply. Software section is the heart of tracker system which control and instructs the hardware section to focus the solar panel toward the centroid of the Sun. The Sun following system methodology is brief as follow:

First the Sun following solar panel is guided by the GPS to its initial place where it focuses directly to sun centroid. After the initial position grabs the Raspberry PI use Image sensor to find, is there a cloud? If yes, than Image processing is implemented to the taken image to find quadrate of the sun and this result is compared with LDR output response to set panel at minimum tracker error position. Then the Raspberry PI instruct to the motor driver to set panel. These steps follow regularly at interval of twenty minutes.

3.2 Hardware Design

The hardware design further divided into two parts named as mechanical and electrical hardware shown in Figure 3.1.

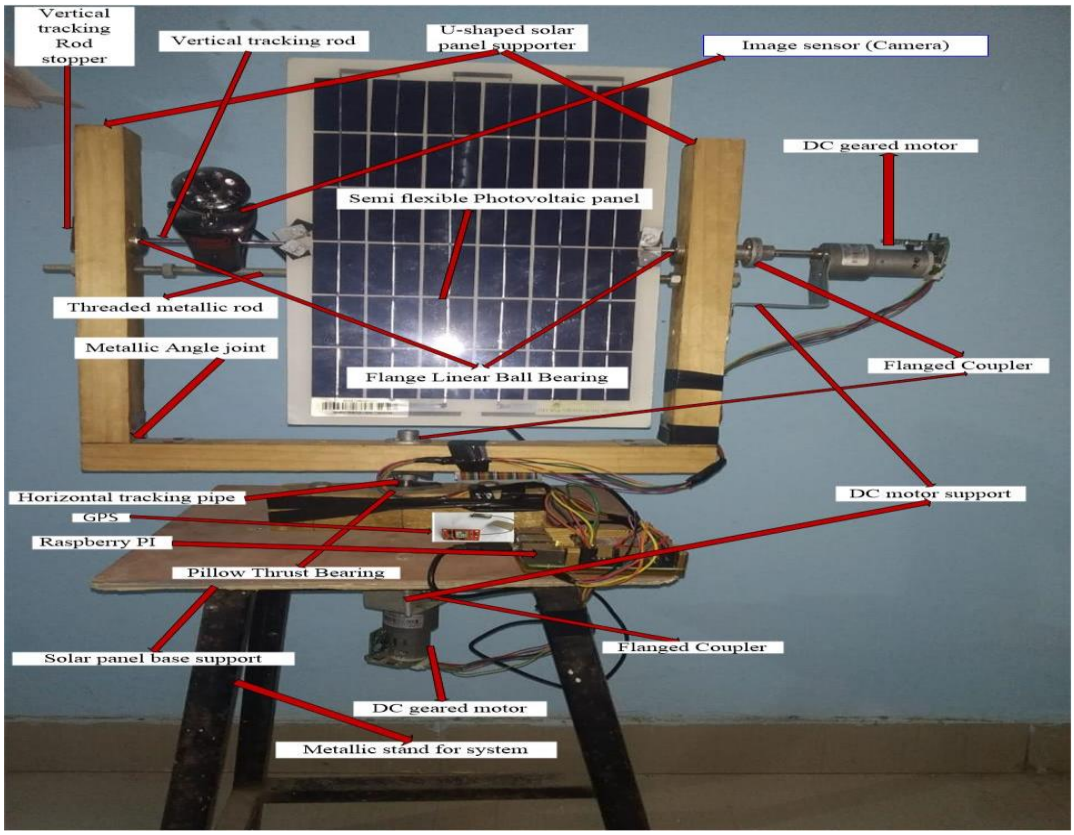

Figure 3.1 Solar Tracker design

3.2.1 Mechanical Hardware: Mechanical system having various parts like:

- U-shaped solar panel supporter
- Solar panel base support
- Metallic stand for system
- Threaded metallic rod
- Vertical tracking rod
- Horizontal tracking pipe
- Metallic L joint
- Vertical tracking Rod stopper
- Motor support
- Flange Linear Ball Bearing
- Flanged Coupler
- Pillow Thrust Bearing
- Angular support for DC motor

3.2.1.1 Rectangular U-shaped Solar Panel Supporter: This U-shaped solar panel supporter is made up of wood as shown in Figure 3.2. The wood has property that they are bad conductor of heat and because of that they do not radiate too much heat

towards solar panel. This actually does not produce heating effect to panel which reduces their efficiency. Its vertical wood piece dimension is 320mm length, 40mm breath and 30mm thickness. And its horizontal wood piece dimension is 390mm in length, 30mm breath and 30mm in thickness.

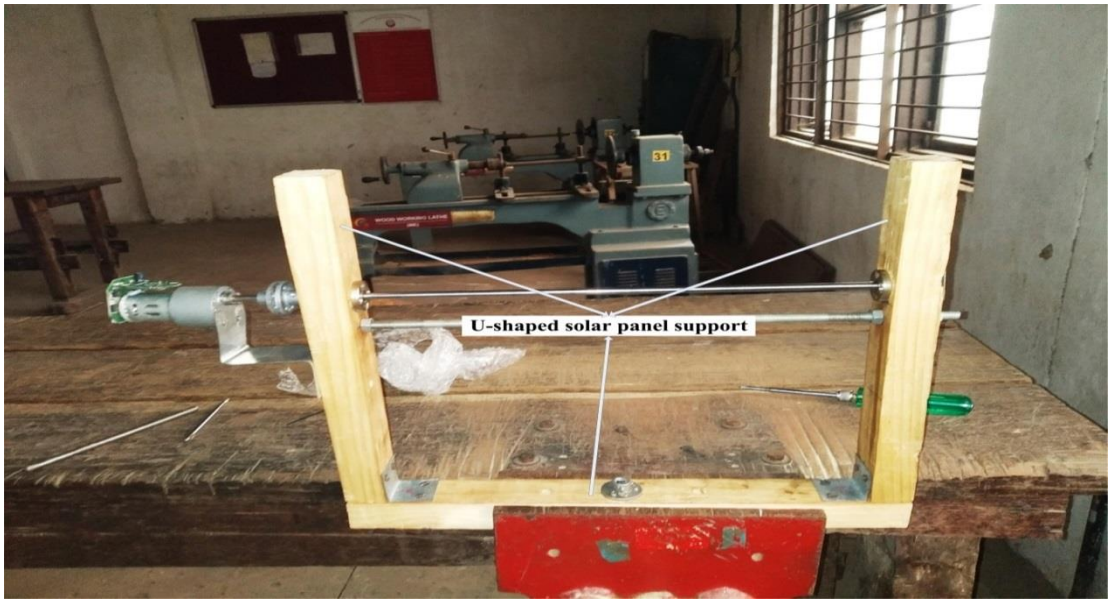

Figure 3.2 U-shaped solar panel supports

3.2.1.2 Solar Panel base Support: It is made of wood as shown in Figure 3.3. Its length, breath and thickness are 300mm, 300mm and 5mm respectively. The whole upper part of solar panel is supported by the base which is tied with Flanged Coupler and Pillow Thrust Bearing.

Figure 3.3 Panel base supports

3.2.1.3 Metallic Stand for System: The support given to the base of tracker by metallic stand shown in Figure 3.4. It has four legs angular in shape to hold ground to give stability to the tracker. Its length, Breadth and thickness are respectively 580mm, 20mm and 20mm.

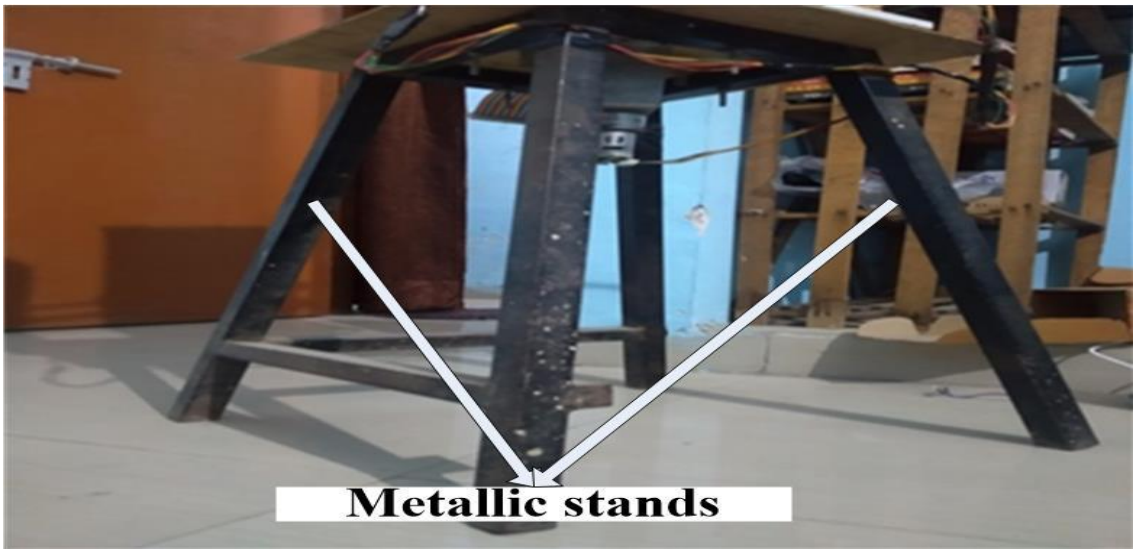

Figure 3.4 Metallic stands for system

3.2.1.4 Threaded Metallic Rod: It is connected between two vertical cuboid shaped woods as shown in Figure 3.5. It actually holds the U-shaped frame stable within which a solar panel is suspended. Its length is 420mm and diameter is 8mm.

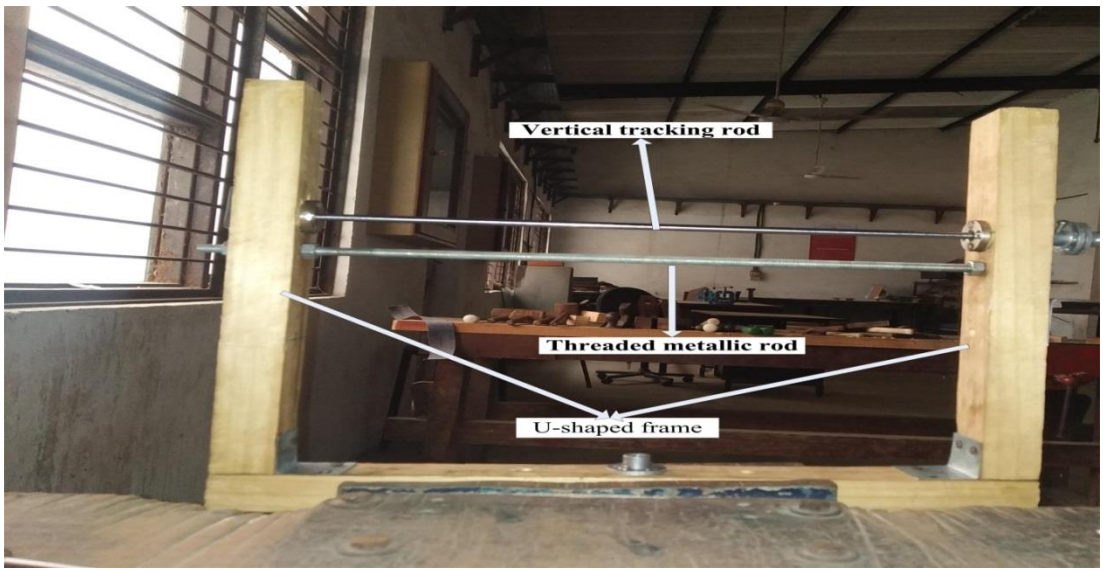

Figure 3.5 Threaded metallic rod

3.2.1.5 Vertical Tracking Rod: The solar panel is attached with vertical metallic rod through which it can do vertical movement along the axis shown in Figure 3.5. It has

6mm of diameter and 400mm of length. This rod is connected between the vertical arm supports through Flange Linear Ball Bearing.

3.2.1.6 Horizontal Tracking Pipe: The horizontal aluminium pipe connected to horizontal motor through Flanged Coupler shown in Figure 3.6. The pipe passes through Pillow Thrust Bearing to connect U-shaped wood frame through Flanged Coupler. Thus the horizontal taking motor passes their motion to Solar panel. Its length, internal diameter, external diameter and thickness are 80mm, 6mm, 8mm and 2mm respectively.

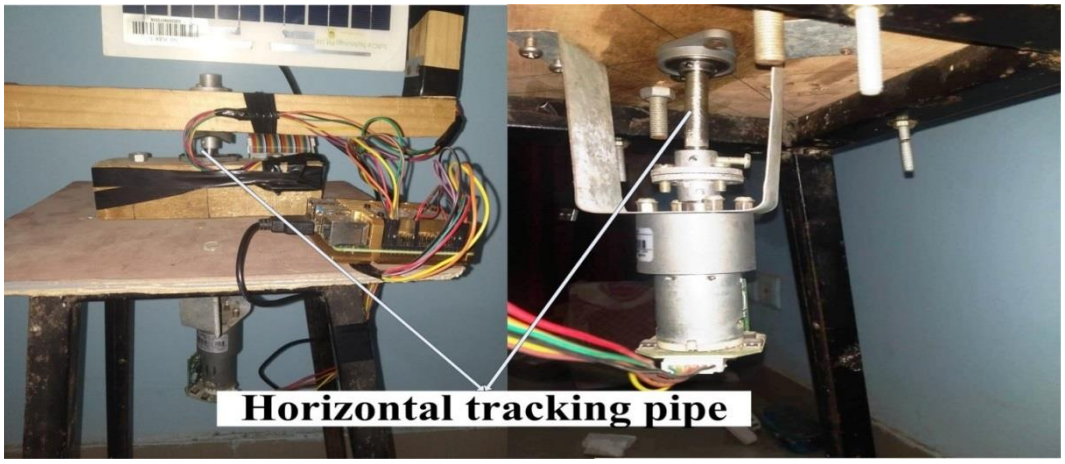

Figure 3.6 Horizontal tracking pipe

3.2.1.7 Metallic L Joint: This is a tin sheet have given angular shape in order to connect wood vertical and horizontal piece as shown in Figure 3.7. This will strength whole panel support frame. Its length is 60 mm and is turn to support horizontal and vertical arm having 30mm each. Its breath and thickness are 30 mm and 2 mm respectively.

Figure 3.7 Metallic L joint

3.2.1.8 Vertical Tracking Rod stopper: It is a metallic sheet connected at outer side of vertical wood peace in order to stop the vertical rod to move out shown in Figure 3.8. Its length, breath and thickness are 65 mm, 30 mm and 2 mm respectively.

Figure 3.8 Vertical tracking Rod stopper

3.2.1.9 DC Motor Support: It is a sheet metal piece to connect motor with their respected connected rod or pipe as shown in Figure 3.9. Vertical motion motor connected with L shape sheet and horizontal motion motor by U-shape sheet.

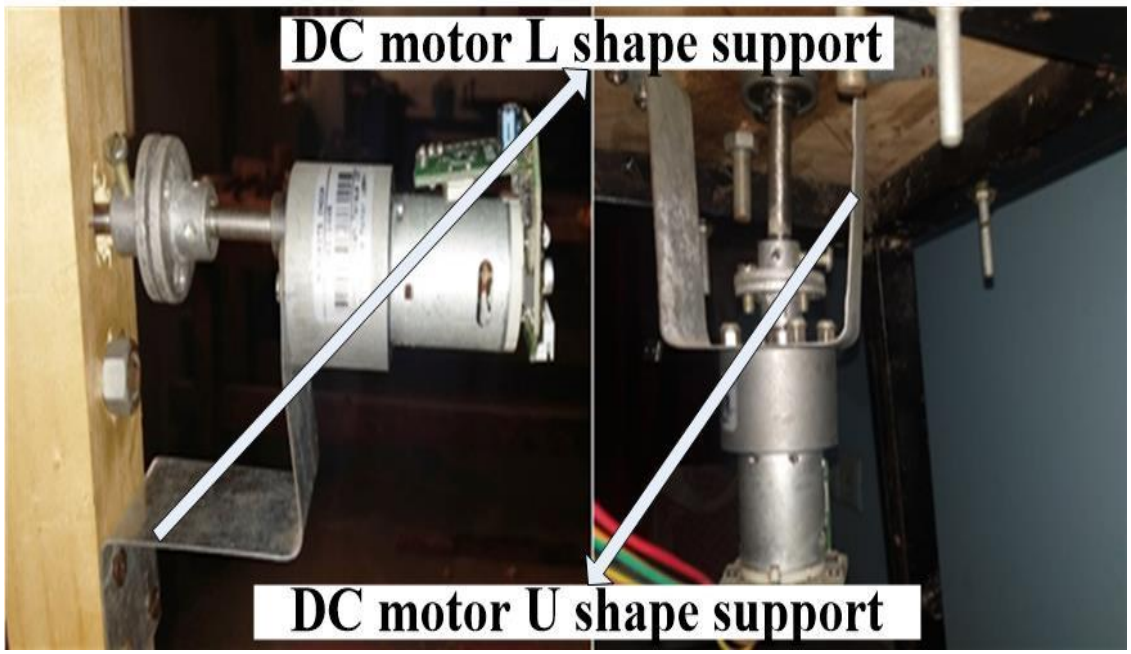

Figure 3.9 DC motor L & U shape support

3.2.1.10 Flange Linear Ball Bearing - Flange Linear Ball Bearing is connected both inner side of vertical wood piece to support vertical tracking rod as shown in Figure 3.10. This rod attaches solar panel with it. This rod is free to move along vertical direction through Flange Linear Ball Bearing. The dimension of Flange Linear Ball Bearing is given below in Table 3.1.

Table 3.1 Dimension of Flange Linear Ball Bearing

Model No	Ball Rows	Internal Bore Diameter		Outer Diameter		Length		Flange Diameter	
		Dr	Tolerance	D	Tolerance	L	V	D_1	Tolerance
LMF6	4	6mm	0-0.009	12mm	0-0.011	19mm	0-0.2	28mm	0-0.2

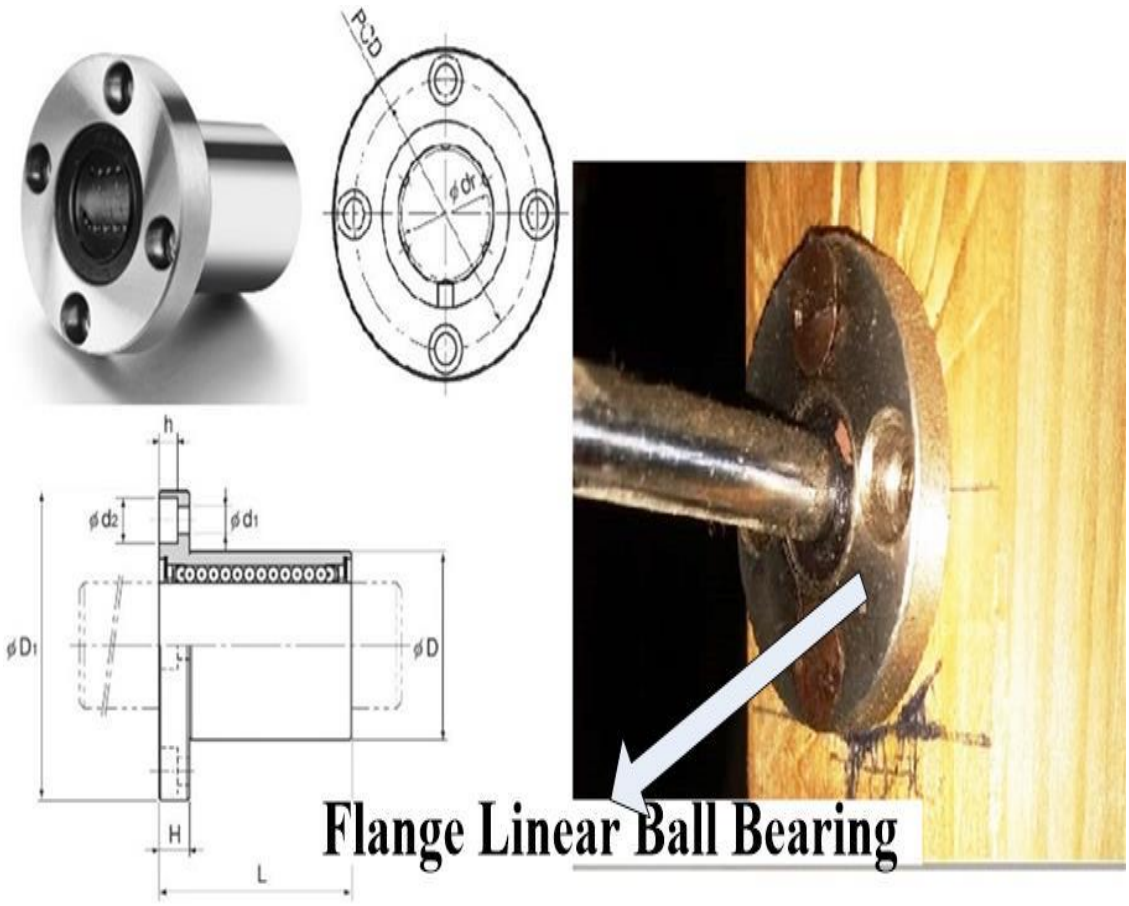

Figure 3.10 Flanges Linear Ball Bearing

3.2.1.11 Flanged Coupler: It is a coupler which is use to couple the two medium at a single junction shown in Figure 3.11. Here in my hardware the vertical rod connected with vertical motion motor with Flanged Coupler. Also horizontal motor connected

with the horizontal tracker pipe through Flanged Coupler similarly wood U-shaped structure connected with base through Flanged Coupler. The Specification and dimension of Flanged Coupler shown in Figure 3.12.

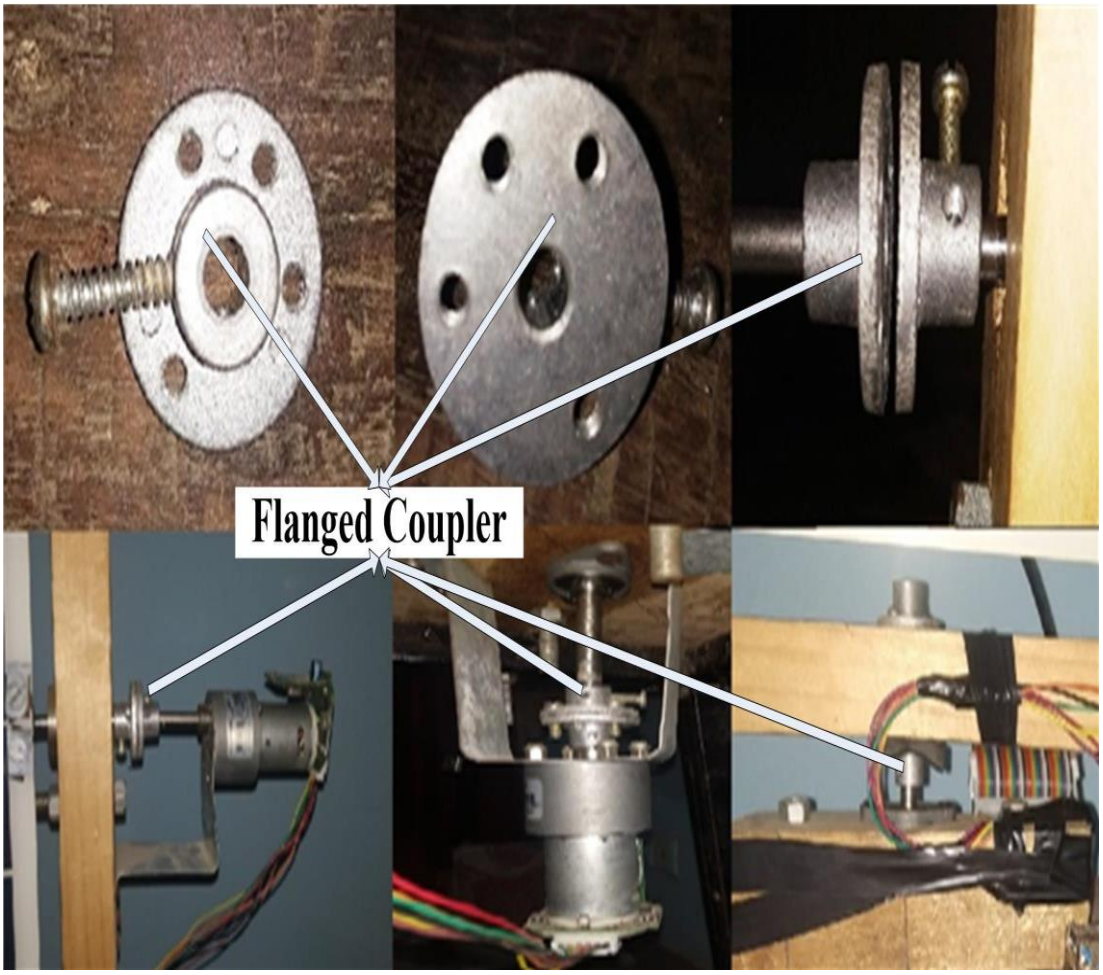

Figure 3.11 Flanged Coupler

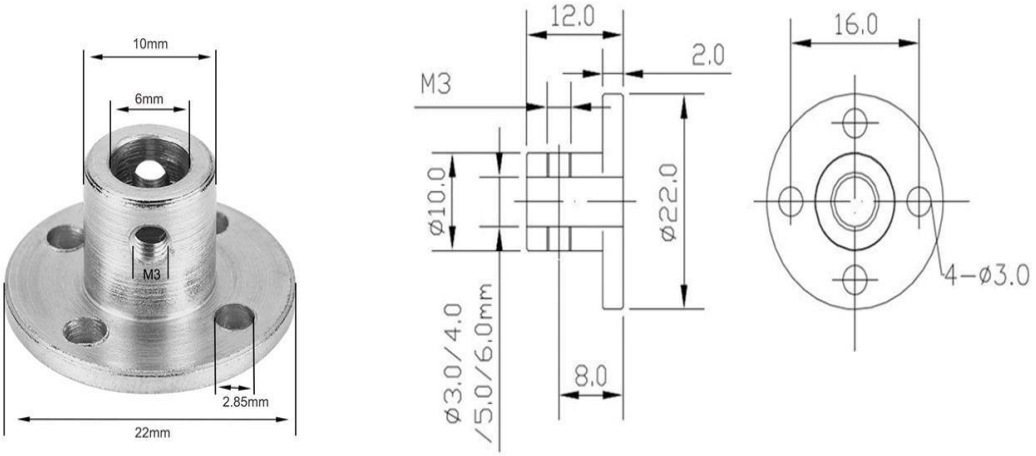

Figure 3.12 Flanged Coupler dimension

3.2.1.12 Pillow Thrust Bearing: It is a type of bearing which put all the tracker weight or thrust on it. It hangs on base support, so force disperses on base and the horizontal motion rod pass through it as shown in Figure 3.13.

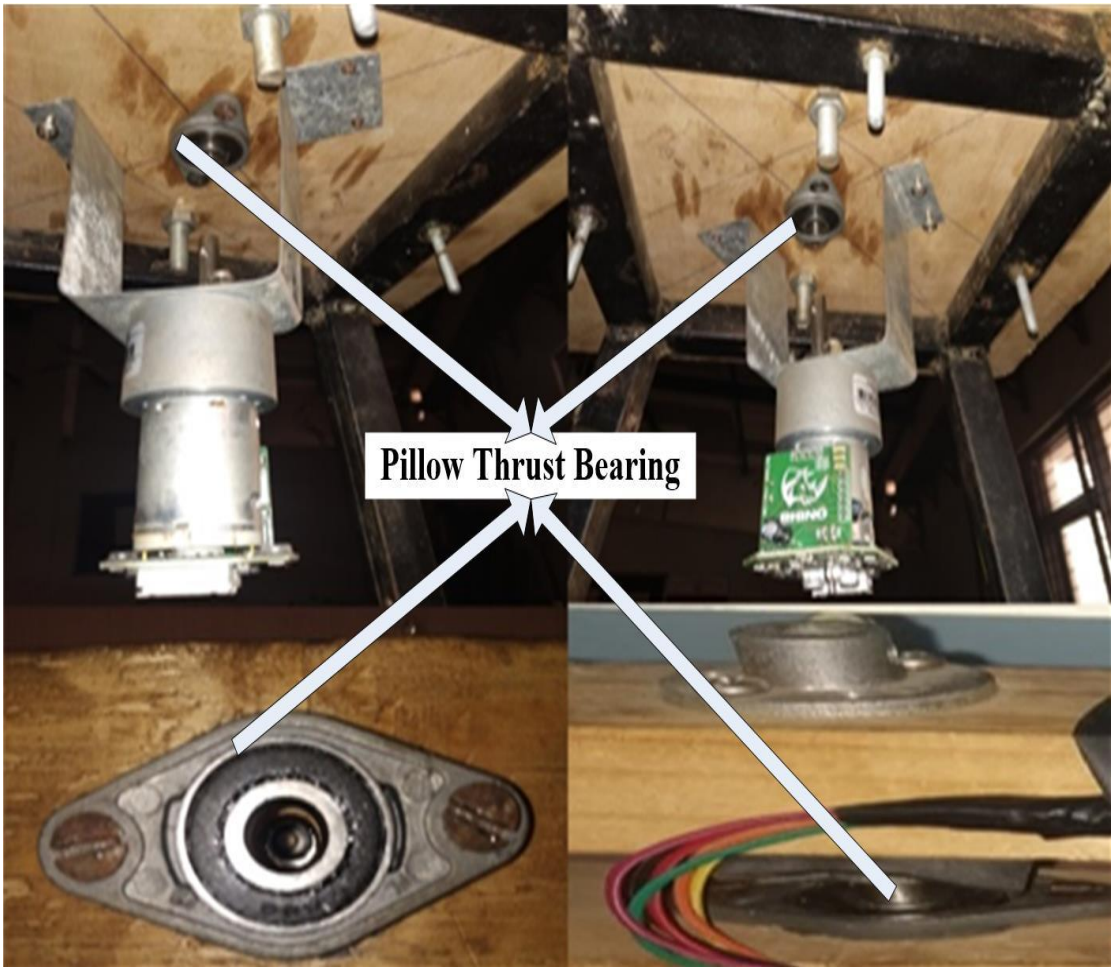

Figure 3.13 Pillow Thrust Bearing

The specification diagram is shown in Figure 3.14 where feature is described.

Features:

- Model KFL08
- Made of Zinc Alloy

Specifications:

- Inner Diameter: 8 mm.
- Height: 13mm.
- Length: 48mm.
- Width: 27mm.
- Weight : Approx 30 gms

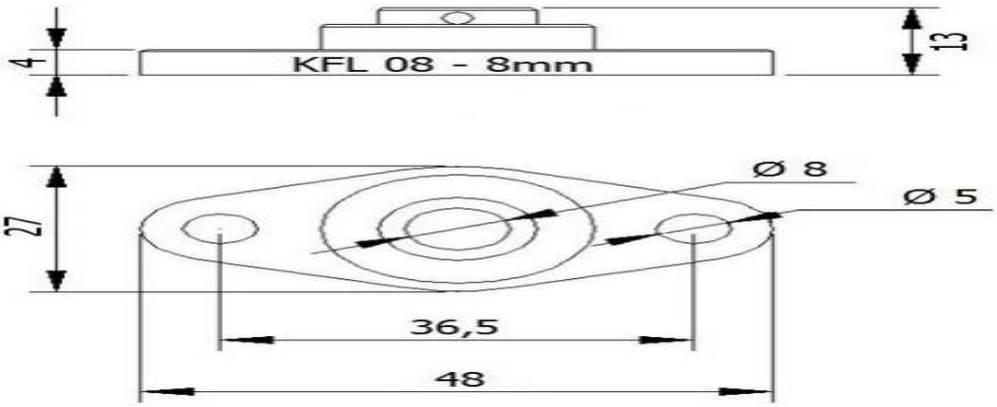

Figure 3.14 Specification of Pillow Thrust Bearing

3.2.2 Electrical –Electronics Hardware: Electrical system having various parts like:

- DC geared motor & driver
- Image sensor
- GPS
- LDR
- Raspberry PI
- Arduino Uno
- Semi flexible Photovoltaic panel
- Voltage regulator
- Personal computer

3.2.2.1 DC Geared motor & Driver: In this project high torque 10 RPM DC motor is used whose technical and physical specification is given in table. Gear and driver connected permanently with this motor as shown in Figure 3.15. The specification of high torque DC motor where given in Table 3.2.

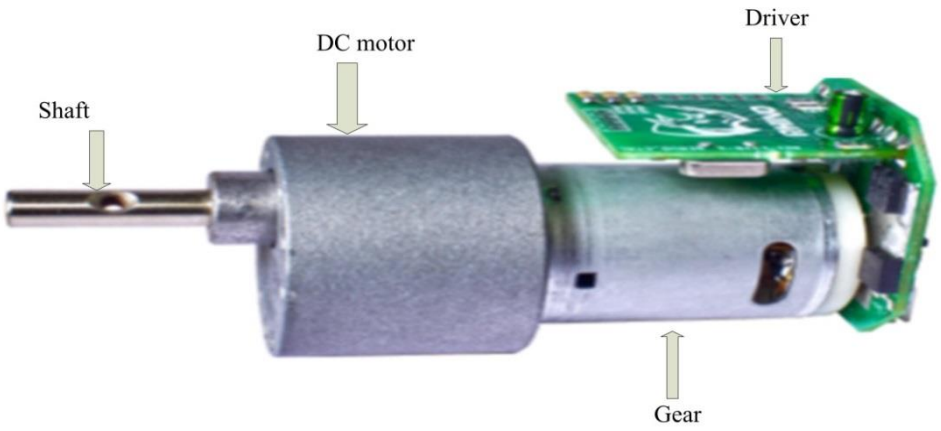

Figure 3.15 DC geared motor & driver

Table 3.2 Specification of high torque DC motor

Physical Specification		
Characteristic	Value	Units
Motor Torque	1	Kg cm
Gear ratio	0.166666667	--
Motor speed	10	RPM
Operating Voltage	12	Volt DC
Dimension(L*W*H)	110 * 50 * 55	Mm* mm* mm
Weight	180	Gms

Technical Specification				
Characteristic	Description	Maximum	Minimum	Unit
Supply Voltage	BTW B+ and GND	13	11	V DC
Current	No load to Stalled condition	7	0.5	Ampere
I/p high voltage	With respect to GND	6	4	V DC
I/P low voltage	With respect to GND	1	0	V DC
UART Baud Rate	For UART interface	9600	-	Bps
12C Clock freq.	For 12C interface	200	10	KGz
Ambient Temp.	Operating Temp	70	0	Celsius
Humidity	-	95%	0	-
Analog I/P voltage	For Analog voltage interface	5	0	V DC
PPM Pulse width	For PPM signal interface	2400	600	Uses

Driver Pin-Out			
Characteristic	Description	Name	Colour
Terminal 1	GND connected to –Ve of supply of battery	GND	Black
Terminal 2	12 C clock/PPM I/P signal/Analog voltage I/P	SCL/PPM/Analog	Brown
Terminal 3	12 C data/Analog I/P sense	SDA/Analog Sense	Red
Terminal 4	UART data transmit	UART TXD	Orange
Terminal 5	UART data Receiver	UART RXD	Yellow
Terminal 6	Connected +Ve of supply or battery	V+	Green

3.2.2.2 Image Sensor or Camera: ESP32S is a prevailing, universal WiFi BLE MCU section applied on small power transducer systems to the best challenging jobs such as encoding of voice, streaming of music, visual surveillance and decoding of MP3. Here we are using ESP-32S camera to track sun. Top and side view of EPS-32S shown in Figure 3.16.

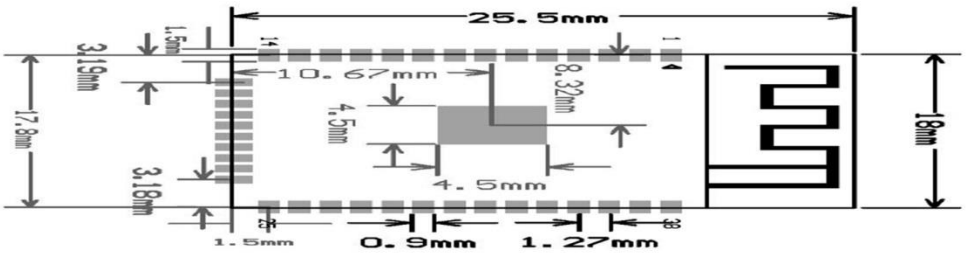

Figure 3.16 Top and side view of EPS-32S camera

The Specifications, dimension and Pin diagram of EPS-32S where given in Table 3.3 Table 3.4and Table 3.5.

Table 3.3 Specifications of EPS-32S

Categories	Items	Values
Wi-Fi	Protocols of Wi-Fi	802.11 b / 802.11g / 802.11n / 802.11d / 802.11e / 802.11i / 802.11k / 802.11r
	Wi-Fi range of Frequency	02.4 to 02.5GHz
Bluetooth	Protocols of Bluetooth	Bluetooth(v4.2)
	Bluetooth Radio signal	NZIF98 dB m sensitivity- receiver C-1, C-2 and C-2 transmitter(where C is class) Adaptive Frequency Hopping (AFH)
	Bluetooth Audio signal	Sub Band Codec & Continuously variable slope delta modulation
Hardware	Interfaces	IR, Motor PWM, SD card, SDIO, UART, SPI, , I2C, I2S, LED PWM, I2C LNA pre-amplifier , DAC, GPIO, capacitive touch sensor, ADC,
	Working voltage	3.0 to 3.6V
	Working current	Average value: 80Ma
	Range of working temperature	-40° to 125°
	Range of Ambient temperature	Common temperature
	Package size	14.3mm*24.8mm*3mm
Software	Mode of Wi-Fi	Station/soft AP + station /P2P
	Securities	WPS/WPA2-Enterprise//WPA2
	Encryptions	SHA/RSA/AES/ECC
	Upgrade Firmware	Download from UART / Over-The-Air –through network / Through host it can be write and download
	Expansion of Software	Cloud Server Development / software development kit

Table 3.4 EPS32S dimensions

Length stretch	Breadth	Altitude	Size of PAD (Bottom)	Pitch of Pin	Height of Shielding	Thickness of PCB
1.8cm	2.55cm	.28 ± .01 cm	.045 cm x .09 cm	0.127cm	0.2 cm	0.08 ± 0.01 cm

Table 3.5 Pin Descriptions

S. No	Function	Pin Name
1	Grounds	GND
2	Supply of Power	3V3
3	Enable signal of chip (Active high)	EN
4	RTC-GPIO0, GPI36, ADC-H, SENSOR-VP, ADC1-CH0,	SENSOR_VP
5	RTC-GPIO3, ADC1-CH3, SENSOR-VN, ADC-H, GPI39,	SENSOR_VN
6	RTC-GPIO4, ADC1-CH6, GPI34	IO34
7	RTC-GPIO5, ADC1-CH7, GPI35	IO35
8	RTC-GPIO9, TOUCH9, XTAL-32K-P , ADC1-CH4	IO32
9	RTC-GPIO8, XTAL-32K-N, TOUCH8,ADC1-CH5	IO33
10	EMAC-RXD0, DAC-1, RTC-GPIO6, ADC2-CH8, GPIO25,	IO25
11	EMAC-RXD1, DAC-2, RTC-GPIO7, ADC2-CH9, GPIO26,	IO26
12	EMAC-RX-DV, ADC2-CH7, RTC-GPIO17, TOUCH7	IO27
13	GPIO-0	IO0
14	GPIO-1	TXDO
15	GPIO-2	IO2
16	GPIO-3	RXD0
17	GPIO-4	IO4
18	GPIO-5	IO5
19	GPIO-6	SCK/CLK
20	GPIO-7	SDO/SD0
21	GPIO-8	SDI/SD1
22	GPIO-9	SHD/SD2
23	GPIO-10	SHD/SD3
24	GPIO-11	SCS/CMD
25	GPIO-12	IO12
26	GPIO-13	IO13
27	GPIO-14	IO14
28	GPIO-15	IO15
29	GPIO-16	IO16
30	GPIO-17	IO17
31	GPIO-18	IO18
32	GPIO-19	IO19
33	GPIO-20	NC
34	GPIO-21	IO21
35	GPIO-22	IO22
36	GPIO-23	IO23
37	Ground	GND

3.2.2.3 Global Positioning System: The NEO-6 segment is a part of individual Global Positioning System having great performance u-blox six placing engine. NEO-6 is a flexible and of low cost receivers offers copious connectivity possibilities in a miniature 16 mm * 12.2 mm * 2.4 mm set. The construction design, consumption of power and selection of memory mark the NEO-6 unit perfect for cell functioned mobile devices with limited constraints.

The NEO-6M Global Positioning system has antenna & fabricated in EEPROM. It is friendly by using many flying control panels fabricated to work with a Global Positioning System.

Technical Specifications:

- GY-GPS6MV2-Model
- Battery for backup
- Power Supply Range: 3 V to 5 V
- Ceramic antenna (Size-12*12mm)
- 9600 bps- Baud rate
- EEPROM save the configuration of data during power off
- LED used as signal indicator
- 23mm * 30mm module size
- Mounting Hole Diameter: 3 mm
- 20mm cable

Output Pin:

1. 5V or 3.3V - VCC (Voltage Common Collector)
2. Ground -GND
3. MCU.RX - TXD
4. MCU.TX - RXD

3.2.2.4 Light Dependant Resistor: Conductors have a huge amount of loose electrons that can move within influence of a voltage gradient. Bad conductor having a huge resistance with scanty loose electrons make them bad conductor of electricity.

A Light Dependant Resistor or optical-resistor is prepared from semiconductor material with great impedance shown in Figure 3.17. It has a huge resistance because of less amount of free electron. And most of electrons are locked within crystal lattice and stopped to move and responsible for high resistance.

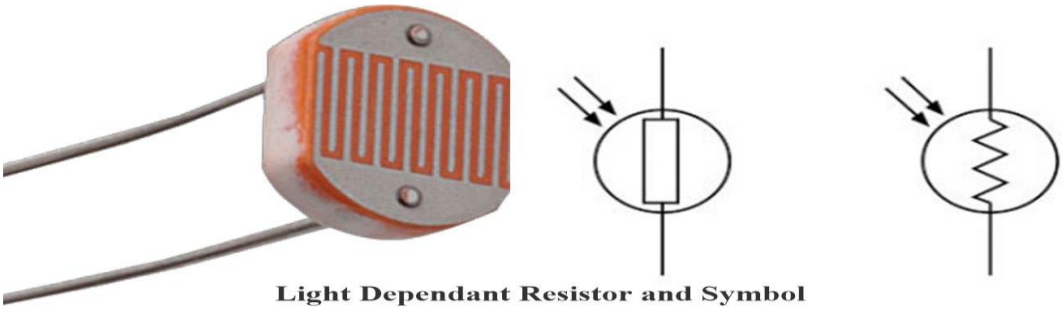

Figure 3.17 Light Dependant Resistor and symbol

When the Sun light incident on the semiconductor due to which photons are soaked by the lattice structure is transfer to the electrons. This absorbed energy by electron shifts the electron energy level higher and break them to free from the lattice structure and start conducting electricity. The above said reason results in the reduction of electric resistance of the semiconductor and light dependent resistor (LDR).The specification of LDR.

Table 3.6 Specification of LDR

Light Dependant Resistor (LDR) Specifications	
Parameter	Values
Dark resistance after 5 sec	0.25MΩ
Dissipation Maximum power	200Mw
Dark resistance after 1 sec	0.03MΩ
Maximum voltage @ 0 lux	200V
Typ. resistance @ 100lux	0.7kΩ
Wavelength at Peak	600nm
Maximum. resistance @ 10lux	4.5kΩ
Minimum. resistance @ 10lux	1.8kΩ

Features

- Spectral response is wide
- Cost is low
- Range of ambient temperature is wide.

3.2.2.5 Raspberry PI: The Raspberry Pi is a one board computer panel with reasonable cost, reliable size, with friendly design make them popular. The newest model of the Raspberry Pi 4 Model B are powerful, high processing efficiency, enrich video response and flexible in peripheral connection, however sustaining the same

least cost and compact size existing on previous models. The Raspberry Pi 4B is used in this project having some attracting features, like USB-3.0 ports, Type-C-power connection and Ethernet, and 4K video response monitor. It is just like the best mini Personal Computer for watching, listening and video surveillance.

Hardware configuration:

- Quad core-64-bit ARM- 1.5GHz
- HDMI display output (4Kp60)
- LPDDR4 RAM 4, 2 and 1 Gigabyte
- 3D Graphics
- H.265 & H.264 hardware decode

Interfaces:

- 1 SD Card
- Wireless LAN -802.11 b / 802.11g / 802.11n / 802.11a / 802.11c
- Bluetooth BLE -5.0
- USB2 ports-2
- Micro-HDMI -2
- USB3 ports-2
- Gigabit Ethernet port
- Raspberry Pi display port
- Raspberry Pi camera port
- 28 users GPIO
- UART-6
- I2C-6
- SPI-5
- SDIO interface-1
- DPI (Parallel RGB Display)-1
- PCM-1
- PWM channels-2
- GPCLK outputs-3

Electrical Specification:

Power Requirements: It uses USB-C power supply of 5V at 3A. If connected downstream USB devices uses supply less than 500mA, a 5V, 2.5A.

Interface

GPIO: The Raspberry Pi 4B uses 28 BCM2711 GPIOs having standard 40-pin header and computable with all back dated Pi version shown in Figure 3.18.

GPIO Pin Assignments: GPIO pins can be used (multiplexed) into many other manners supported by devoted peripheral blocks like UART, SPI and I2C.

Figure 3.18 Pin diagram of Raspberry Pi 4B

- Display Parallel Interface: A RGB DPI interface is provided to the GPIOs and can support 24-bit parallel interface with secondary display.
- SDIO Interface: The Raspberry Pi 4B has inbuilt Secure Digital card socket which backings 1.8V, DDR50 mode.
- Camera and Display Interfaces: The Raspberry Pi 4B has two lane MIPI CSI Camera and one Raspberry Pi two lane MIPI DSI Display connector.
- USB: The Raspberry Pi 4B has two USB2 and two USB3 type-A sockets.
- HDMI: The Raspberry Pi 4B has two micro-HDMI ports which backing CEC and HDMI 2.0 with resolutions up to 4Kp60.
- Audio and TV Out: The Raspberry Pi 4B backings CD-quality audio output and composite TV-output via a four ring TRS 'A/V' jack.
- Thermal and Temperature Range: The suggested ambient effective temperature range varies within 0 to 50 degrees Celsius. To control thermal output- At light load Raspberry Pi 4B diminishes the voltage and Central processing unit clock speed and at high load voltage and speed are increased.

3.2.2.6 Arduino/Genuino Uno: It's an ATmega328P-based microcontroller board. Figure 3.19 shows that it features 14 digital input/output pins (six of which can be used as PWM outputs), six analogue inputs, a 16 MHz quartz crystal, a USB

connection, a power jack, an ICSP header, and a reset button. It comes with everything you'll need to get started with the microcontroller; simply plug it into a computer with a USB cable or power it with an AC-to-DC adapter or battery. You can experiment with your UNO without fear of making a mistake; in the worst-case situation, you can replace the chip for a few rupees and start over. Table 3.7 lists its technical specifications.

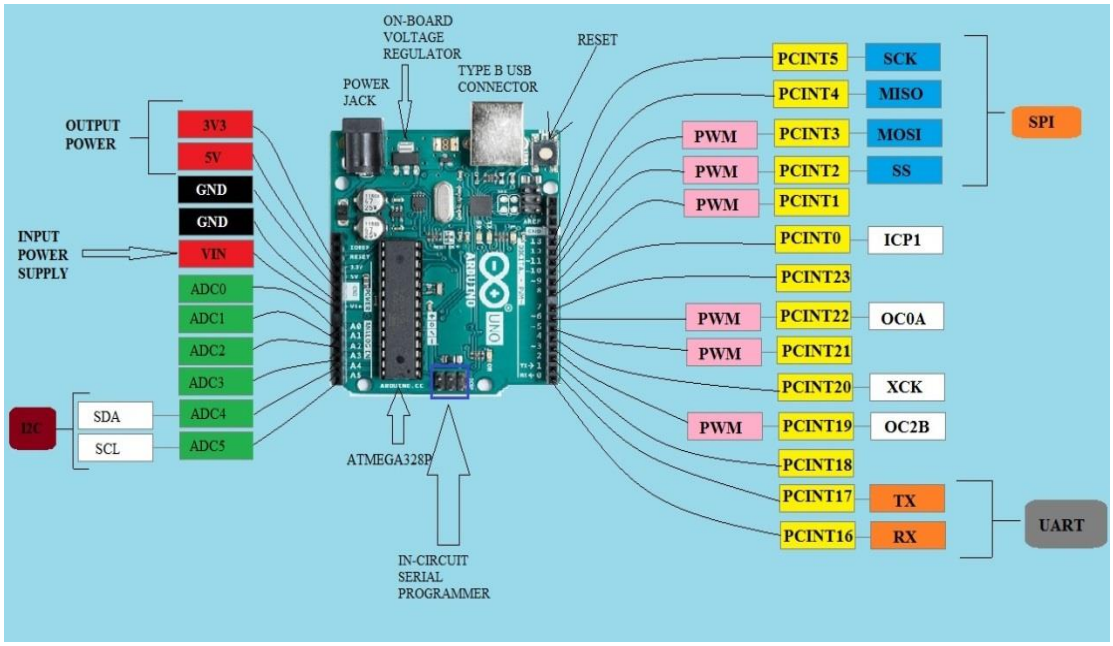

Figure 3.19 Arduino/Genuino Uno Pin configurations

Table 3.7 Technical specification

S. No.	Parts	Specification
1	Microcontroller	ATmega328P
2	Weight	25 g
3	PWM Digital I/O Pins	6
4	Digital I/O Pins	14 (of which 6 provide PWM output)
5	Analog Input Pins	6
6	Operating Voltage	5V
7	DC Current per I/O Pin	20 mA
8	Input Voltage	7-12V
9	SRAM	2 KB (ATmega328P)
10	Input Voltage (limit)	6-20V
11	Clock Speed	16 MHz
12	LED_BUILTIN	13
13	DC Current for 3.3V Pin	50 mA
14	EEPROM	1 KB (ATmega328P)
15	Length	68.6 mm
16	Width	53.4 mm
17	Flash Memory	32 KB - 0.5 KB used by boot loader.

3.2.2.7 Semi Flexible Solar Panel: Thin-film (TF) and crystalline-silicon (CS) are the two different types of flexible solar panels. The TF solar modules are the maximum flexible than CS. The flexibility of the panels means a multipurpose use in numerous settings charging various energy sources or individual devices. This panel is assured to provide unpolluted, Sun power with the benefits of placing on bent, rough and oblique surfaces area. The use of different manufacturing material is the main variance between bendable sun panels and fixed sun panels. The flexible sun panels are prepared from much thinner silicon wafers than the norm. Extreme-thin layers of photo-voltaic material are coated on a glass base, malleable or metal. The sudden increase in utilization of lightweight panel is because of modern advancements in PV technology, versatility in structure, lightness and obviously the, flexibility shown in Figure 3.20. In this project a semi flexible solar panel is used shown in Figure x and whose specification is stated below.

Technical Data:

Max Power: 10Watts

Max Power Voltage: 22V

Max Power Current: 0.6A

Open Circuit Voltage: 18V

Short Circuit Current: 0.56A

Tolerance: ± 5%

Weight: 0.27kg

Dimension: 345*240*2.75 mm

Figure 3.20 Semi-flexible Polycrystalline solar panel

3.2.2.8 Voltage Regulator Power Supply: The LM7805 voltage regulator receives a variable voltage at its input pin from the photovoltaic panels and provides a constant 5 voltage at its output pin and dissipate the difference as heat as shown in Figure 3.21. The regulated voltage is used to supply the control board VVC pin.

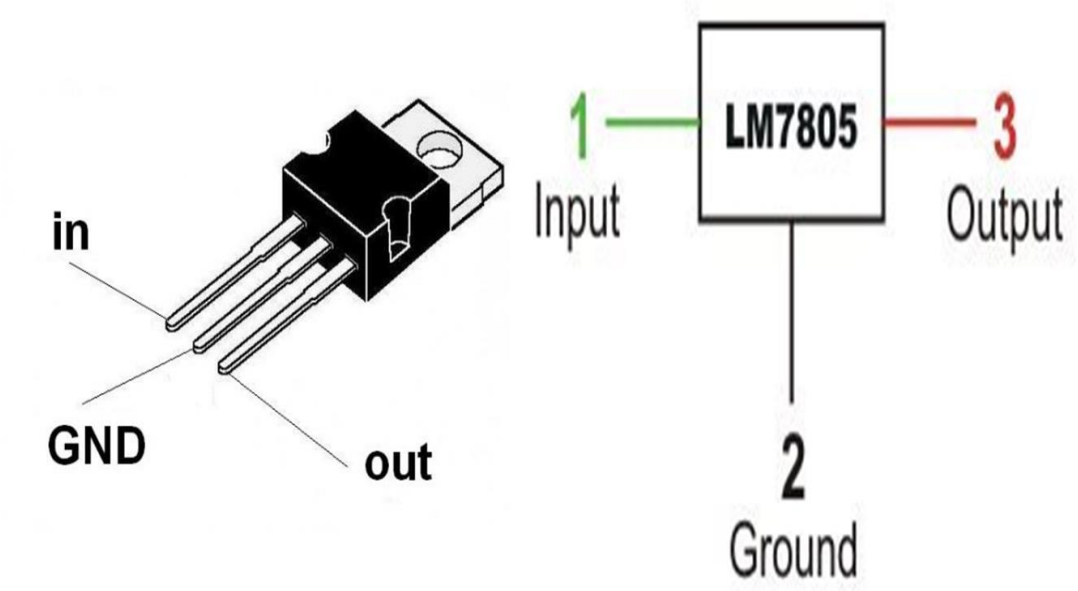

Figure 3.21 LM7805 voltage regulator Pin diagram

3.2.2.9 Personal Computer: Acer Aspire 7 Core i5 10th Gen Specifications of Processor and Memory Features shown in Table 3.8.

Table 3.8 Specification of personal computer

S. No.	Personal Computer Parts	Specification
1	Model Number	A715-75G-50TA/ A715-75G-41G
2	System Architecture	64
3	RAM Type	DDR4
4	Processor Generation	10th Gen
5	Part Number	NH.Q97SI.001
6	Processor Name	Core i5
7	Series	Aspire 7
8	Dedicated Graphic Memory Capacity	4 GB
9	Dedicated Graphic Memory Type	GDDR6
10	Operating System	Windows 10 Home
11	SSD Capacity	512 GB
12	Clock Speed	2.4 GHz with Turbo Boost Upto 5 GHz
13	Processor Brand	Intel
14	RAM	32 GB
15	OS Architecture	64 bit
16	Graphic Processor	NVIDIA GeForce GTX 1650

3.3 Software

- **Python software**
- **Arduino Software (IDE)**
- **MATLAB Simulink**

3.3.1 Python Software: The Python programming language is used to code the project. Python is a programming language with a wide range of applications. Many of its features assist functional and aspect-oriented programming (for example, Meta programming and Meta objects (magic methods). Many of its features support functional programming and aspect-oriented programming, as well as object-oriented programming and structured programming. Extensions support a wide range of paradigms, including design by contract and logic programming. Python maintains memory via dynamic typing, reference counting, and a garbage collector that detects cycles. [63] Late binding (dynamic name resolution) binds method and variable names while the programme is running.

3.3.2 Arduino Software (IDE): Writing code and uploading it to the board is simple with the open-source Arduino Software (IDE). Any Arduino board can be used with this software.

3.3.3 MATLAB: MatLab is a computer language that engineers and scientists use to study and build systems and products that change the world. MATLAB is built around the MATLAB language, a matrix-based language that provides for the most natural expression of computer mathematics. In our project we use MATLAB code and simulation for image processing operation, simulation of hybrid system and also in other system.

3.4 Costing of Hardware

Table 3.9 Cost lists of items used to make hardware

Item Name	Quantity	Specification	Single piece cost (INR)	total cost
U-shaped solar panel supporter	1		200	200
Solar panel base support	1		50	50
Metallic Angle joint	2		10	10
DC motor support	2		10	10
Angular support for DC motor	2		10	10
Metallic stand for system	1		10	100
Vertical tracking Rod stopper	1		10	10
Threaded metallic rod	1	8mm, 500mm	200	200
Vertical tracking rod	1	6mm, 50mm	200	200
Horizontal tracking pipe	1	6mm,500mm	200	200
Flange Linear Ball Bearing	2	6mm	70	140
Flanged Coupler	6	6mm	40	240
Pillow Thrust Bearing	1	6mm	120	120
DC geared motor & driver	2	10 RPM	750	1500
Image sensor-camera	1	2MP	650	650
GPS	1	NEO-6M	800	800
LDR	4		10	40
Raspberry PI	1	4B	6500	6500
Arduino/Genuino Uno	1	Uno	600	600
Semi flexible Photovoltaic panel	1	10 Watt	875	875
HDMI cable	1	1.5m	250	250
C-type power cable	1	1.5m	700	700
HDMI converter	1	Cable	100	100
Memory card and slot	1	32 GB	400	400
Voltage regulator power supply	1	LM7805	300	300
Total Cost	37			14205

CHAPTER 4
MODELLING AND SIMULATION OF HYBRID SYSTEM

4.1 Introduction

The simulation, modelling, and design of a hybrid power generating system based on non-conventional (renewable) wind turbine energy and solar photovoltaic dependable sources is provided in this paper. The principal system is a solar electric generator that consists of six models that are connected in series based on expected P&O and is connected to an MPPT controller and AC/DC converter. The system is linked to a Permanent Magnet Synchronous Generator. The major goal of this project is to connect systems so that they can create the most power for single auxiliary phase loads, as well as solar PV generators and wind turbine systems for simulation using Simulink/MATLAB. The hybrid power system is planned for efficiency, stability, reliability, and model, according to the results of this simulation. For maximum voltage generation, use a renewable energy source such as a wind turbine or solar PV.

Renewable energy sources play a vital and fundamental role in electrical systems, and photovoltaic solar energy is being used at an unprecedented rate. Photovoltaic panels and electrical inverters are used to generate solar energy. The output power provided by solar panels in nature is discontinuous and fluctuates depending on irradiance, panel ageing, temperature, varied orientations, and other factors [120].

A solar photovoltaic system is more environmentally benign and financially effective in numerous implementations, particularly in rural locations. This work develops and reveals the fundamental combination of the photovoltaic array, as well as the significantly different output characteristics of the solar photovoltaic array in various conditions, such as temperature, irradiance, and several other internal resistances, in order to demonstrate the different impacts of the parallel and series photovoltaic arrays. This article [121] discusses a MATLAB model of a solar cell based on the Shockley diode's equation. The comparison of single and double diode solar photovoltaic cell models was also studied. This work has built a feature model of a solar cell with filters and inverters in general. A hybrid electric system combines two or more non-conventional energy sources. There are several advantages: it is more efficient than separate productivity, mobility, energy source reliability, and cost.

Furthermore, there are few environmental and economic gains that may be accomplished by increasing or decreasing production costs.

4.1.1 Principle of Operation: When a photovoltaic cell is exposed to sunlight, current is generated and a pair of electron holes is formed, while photovoltaic cell equipment captures photons with energy greater than the band gap of the material. When external circuits are connected to the cell, these generate photons and carriers that eliminate the cell's internal electrical fields and aid in the current flow.

4.1.2 Photovoltaic Cell Corresponding Circuits: A photovoltaic cell can be represented by two types of diodes and an established equivalent circuit, as shown in Figure 4.1.

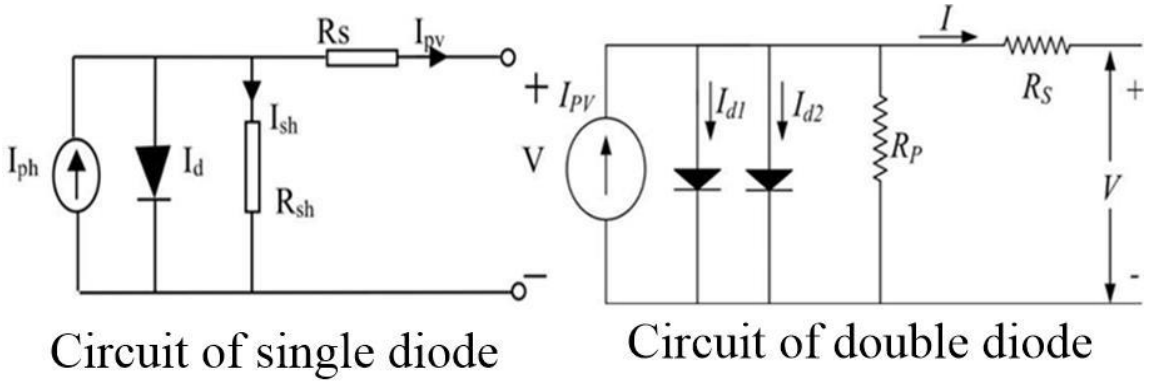

Figure 4.1 Circuit of single and double diode

When sunlight strikes a photovoltaic cell, it generates a direct current that varies considerably with photovoltaic radiation, and the model might be improved by including shunt resistances R_P and series R_S effects. R_S is used to account for internal losses and voltage decreases caused by current flow, while R_P represents current leakage to the surface when diodes are reversed [122-125].

4.1.3 Comparison of double and single diodes models: The impact of free electron and pair of photon recombination is reflected in every double diode model. However, it increases the number of equations and undefined parameters in an attempt to make simulations more sophisticated and precise than the single diode model. Because of the mathematical calculations and the number of iterations, there are less mathematical errors in the single.

4.2 Photovoltaic Cell

It's a semiconductor device that absorbs and converts photon energy as it approaches that of sunshine. Determining the parameter associated with cell temperature in a perfect solar cell

model is quite difficult.

On the other side, steady state oscillation around the MPP is produced by increasing the size of permutation radiation intensity such as R_{Sh}, and R_S. The current of a short circuit I_{SC}, the voltage of an open circuit V_{OC}, the maximum power point voltage V_M, the maximum power point current I_M, and the maximum power point P_M are all observable conceptual characteristics provided by solar array manufacturers.

$$I = I_{PV} - I_{d1} - I_{d2} - \frac{(V + IR_S)}{R_P} \tag{4.1}$$

R_P and R_S, on the other hand, are the parallel and series resistances, respectively. Despite of the fact that V_T is the diode's thermal voltage. I_{PV} is the current created by lights.

$$I_{PV} = \left[[I_{PV-STC} + K_1(t - T)] \frac{G}{G_{STC}} \right] \tag{4.2}$$

The standard test setting is irradiance G=1000 W/ m^2 and temperature t=298 k (25^0C). The function Object typically delivers variable K1, which is the I_{SC} coefficient. [126] specifies the saturation current of a diode.

$$I_{d1} = I_{d2} = \frac{I_{SC-STC}\ K_1(t - T_{STC})}{exp\left(\frac{\left(V_{OC-STC}K_V(T - T_{STC})\right)}{V_T}\right) - 1} \tag{4.3}$$

Equation (4.3) represent the short circuit current is $I_{SC\text{-}STC}$, and the open circuit voltage is $V_{OC\text{-}STC}$ in typical test conditions (STC). The temperature factor of a voltage is indicated by K_V.

4.3 Perturb and Observe (P&O) Method

The cark Perturb & Observe method is extensively used because to its ease of implementation, as shown in the picture below. It's a steady gradient of observation and perturbation until the operative point combines at the MPP. The P&O algorithm estimates the time to method to maximum power point by equating the voltage and power of time (K) with the model at a time (K-1). If the power modification is positive, the solar panel's power conversion is accomplished by a modest voltage perturbation; in the analogous pathway, the voltage perturbation is constant. Negative delta power, on the other hand, indicates that the

maximum power point is far away, and the perturbation is reduced to trace the maximum power point. Table 4.1 contains the abstract for the cark P&O. As a result, tiny perturbations are used to check the complete P-V curve in order to find the greatest power point. Numerous academics have predicted that mutations in the P&O algorithm will overpower the steady state oscillations and response displayed in Figure 4.2.

Table 4.I: Scheme of the P&O Algorithm

Power Change	Perturbation	Resultant Perturbation
-ve	-ve	+ve
+ve	+ve	+ve
-ve	+ve	-ve
+ve	-ve	-ve

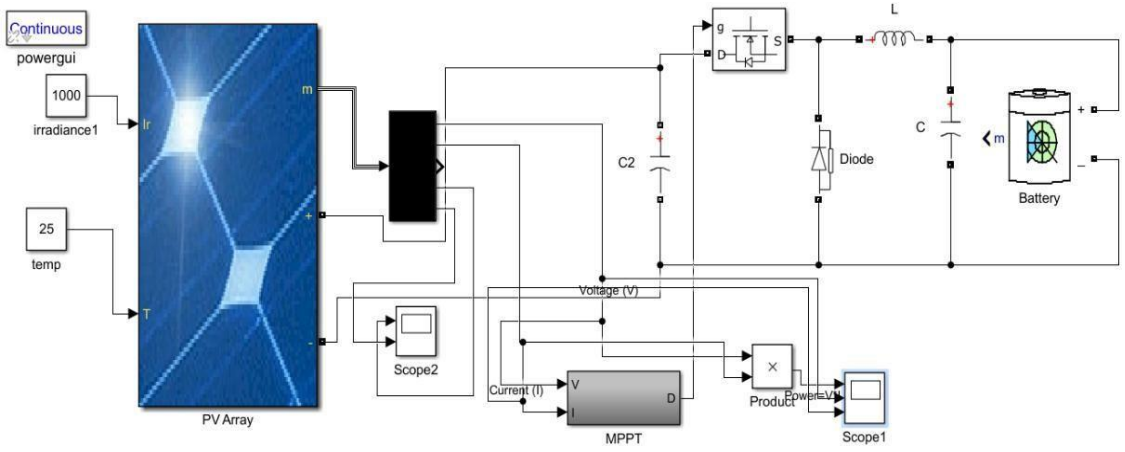

Figure 4.2 Solar PV model simulations in Simulink

4.4 Predictive PO Based MPP Tracker

An adaptive filter is one that regulates its carriage task by itself, as expressed by an optimization method. Digital filters are also adaptive filters (AF) that do digital signal processing (DSP) and alter their actions based on the incoming signals to the filter, due to the complexity of the optimization methods. A non-adaptive filter has static filter factors due to compare (that jointly custom the transfer functions).

4.4.1 An Adaptive FIR Filter execution by using the least mean squares (LMS) Algorithm: LMS procedures are a session of adaptive filter applied to simulate a preferred filter by defining the filter factors that narrate to creating the LMS of the error signal.

4.4.2 Least Mean Square (LMS) Algorithm: The adaptive filter is a versatile and

effective instrument for analyzing signals for people of all ages. For example, let F be the length of the adaptive filter. The arrangement gives output signal y (n) for input vector x (n), as shown in the following equation.

$$y(n) = x(n)\,Tw(n) = w(n)Tx(n) \tag{4.4}$$

The following equation specifies the weight updated vector for the LMS algorithm.

$$w\,(n\ +1)\ =\ w(n)\ +\ \mu\,x(n)\,e(n) \tag{4.5}$$

Figure 4.3 depicts the entire PV system that has become operational; with the MPPT block employing the PREDICTIVE-PO based tracking approach. Figure 4.3 depicts a complete photovoltaic system optimized for efficient MPPT tracking. The voltages and currents cannot be fed directly to the energy storage units or appliances due to variations in irradiance and temperature; instead, they must be fed to the controller device, which tracks the maximum power for the available voltage and current in such a way that an energy storage unit consisting of an inductance and capacitance circuit holds the extra power for a period of time when there is extra power generation from the previous cycle and donates the power when it is no longer needed. A MOSFET/IGBT switch connected to the LC circuit via the MPPT control unit sets the on-off timing.

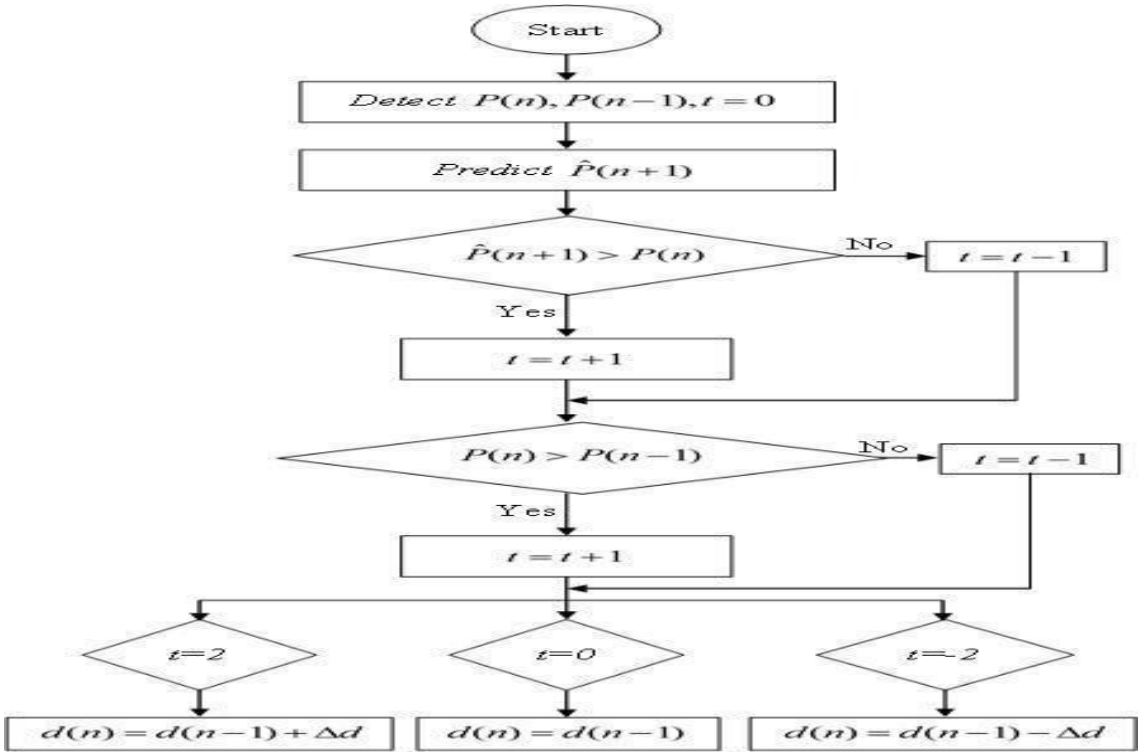

Figure 4.3 Flowchart of MPPT algorithm based on LMS predictive power

The LC circuit and switch are part of a buck booster system that converts DC to DC. Only current and prior readings were used in the existing perturb-observe algorithm, with no consideration of optimum future power values. Predictive power is induced in the projected methodology, which is optimized using the least mean square algorithm to preserve the optimal maximum point of power. The prediction power [127] displayed in Figure 4.4 is P (n+1) in the flowchart above.

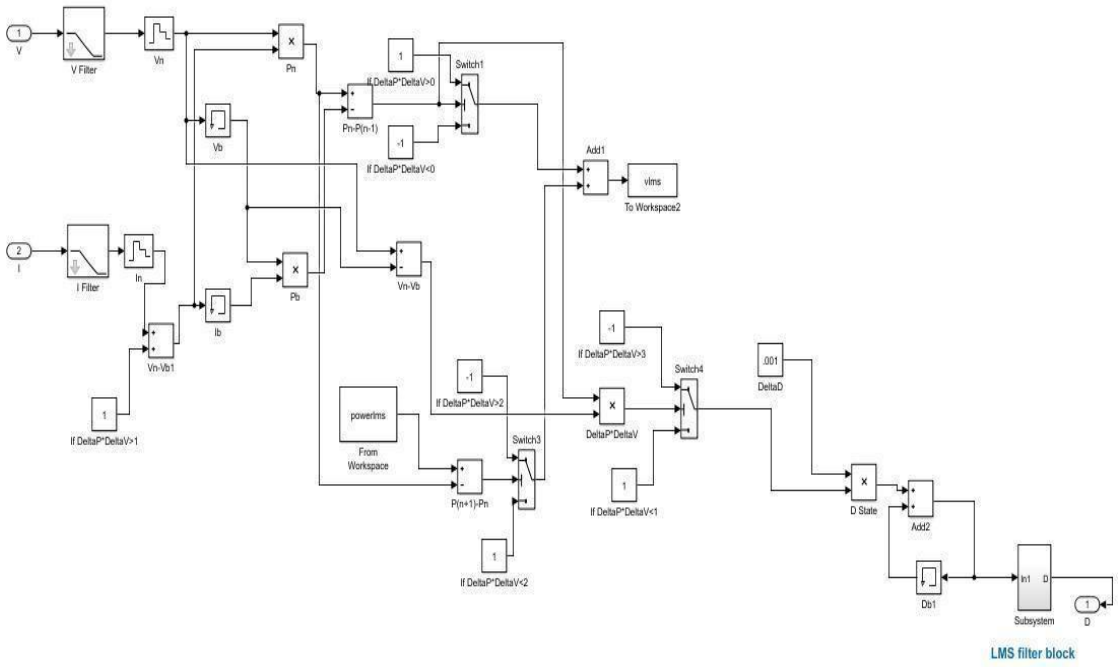

Figure 4.4 Flowchart implementation of MPPT algorithm based on LMS based predictive power

4.5 Results of SPV Simulations

The simulation of 30 series modules and 15 parallel modules yielded the following result. The following are the attributes that are used in modules. Open circuit voltage (V_{OC}) is 42 volts, short circuit current (I_{SC}) is 29.7 amps; maximum power point voltage (V_{MP}) is 36 volts, maximum power point current (I_{MP}) is 27.7 amps, and cells per module are 10. Figure 4.5 shows the current-voltage and Power - Voltage curve for a functional module in optimum condition. Figure 4.6 depicts solar power waveforms using the normal PO method and the upgraded Predictive-PO approach. At 1000 W/m^2 at a temperature of 25^o, the proposed MPP Tracking algorithm was tested.

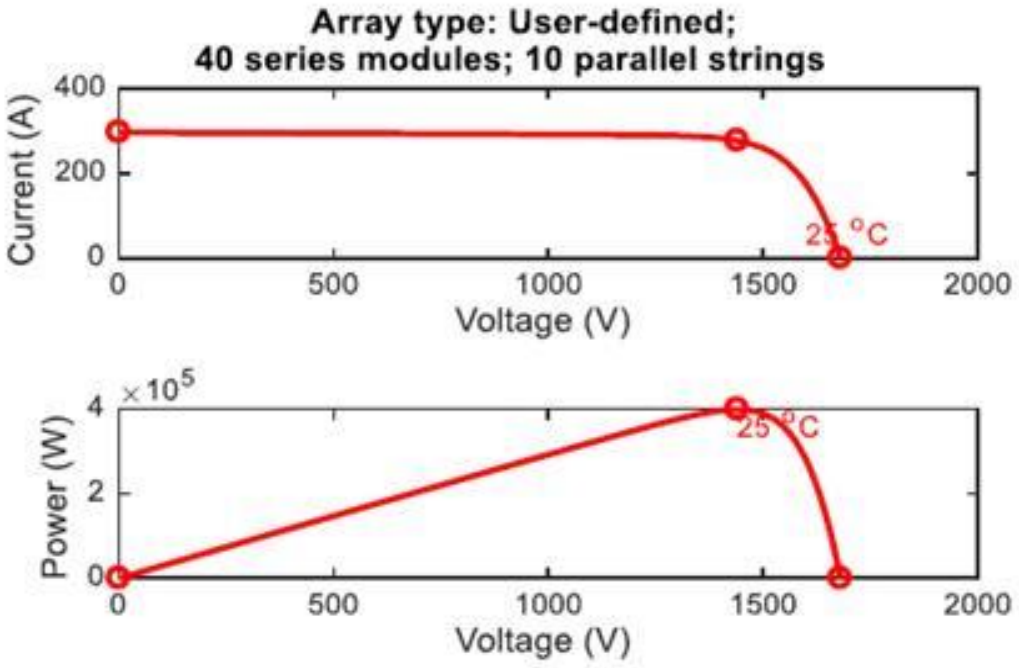

Figure 4.5 IV-PV plots of array in optimum conditions

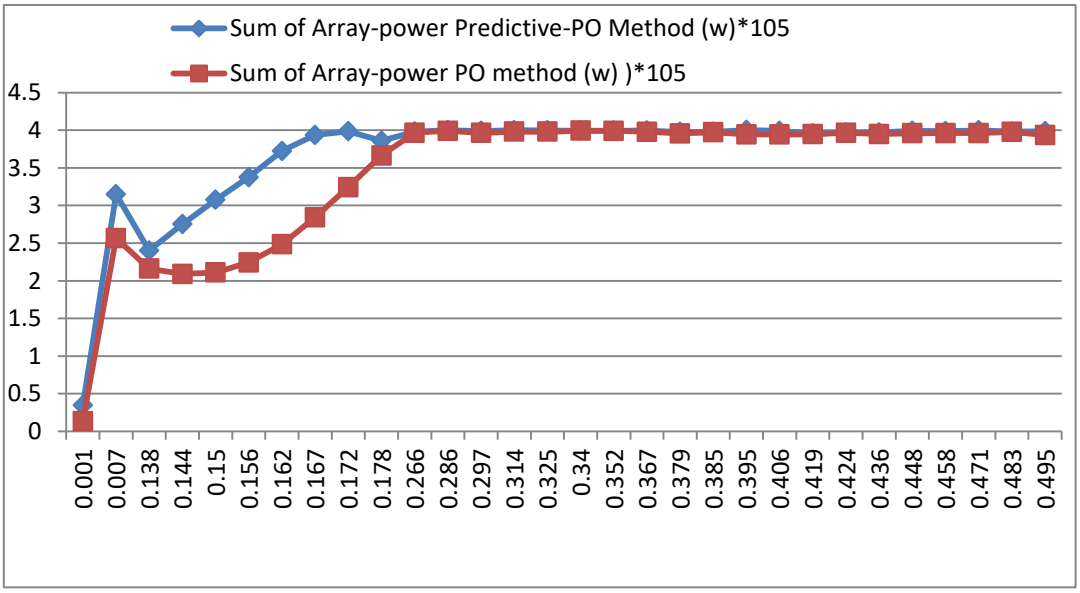

Figure 4.6 Comparison of power output

Table 4.2 shows the power values obtained using two different compare methods [128]. The specified method reaches the greatest position significantly sooner than prior PO methods. In this experiment, a buck-booster DC-DC converter is used for conversion, and a MOSFET switch is used to turn on and off the energy storage circuit. It is also discovered that the proposed approach has the least fluctuation variance and reaches higher stability in peak value sooner than the PO method.

Table 4.2: Analysis of Array-power Predictive-PO Method and Array-power PO method

Time in sec	Array-power Predictive-PO Method (w)*10^5	Array-power PO method (w))*10^5
0.001	0.3454412	0.1348961
0.007	3.148676	2.56783
0.138	2.401896	2.160324
0.144	2.75178	2.091705
0.15	3.076002	2.109727
0.156	3.374525	2.244176
0.162	3.723589	2.48507
0.167	3.936695	2.84275
0.172	3.985329	3.243486
0.178	3.859299	3.663758
0.266	3.979981	3.964967
0.286	3.99966	3.990856
0.297	3.988756	3.964305
0.314	3.999921	3.980359
0.325	3.998522	3.980254
0.34	3.993838	3.993378
0.352	3.994139	3.992309
0.367	3.996013	3.97805
0.379	3.977473	3.957534
0.385	3.979642	3.972263
0.395	4.001416	3.943966
0.406	3.990422	3.943331
0.419	3.954703	3.946502
0.424	3.968741	3.964913
0.436	3.969882	3.948922
0.448	3.990388	3.959257
0.458	3.988104	3.961834
0.471	3.997269	3.961564
0.483	3.983383	3.977512
0.495	3.984729	3.936324

4.6 Wind Turbine Modeling

Wind energy is a renewable and environmentally acceptable form of electricity. It is a renewable energy source that, when combined with a wind energy producing system, can meet the future need for electrical power. It turns the kinetic energy of the wind into mechanical energy, which is then used to create electricity. The magnitude of mechanical energy is determined by the wind speed and the density of the air [129 - 131].

Equation (4.6) gives the wind power generated by wind turbines (Pm):

$$\text{Pm} = \frac{1}{2} C_P(\lambda, ¥) € \text{A} w^3 \quad (4.6)$$

Where:

w = Wind speed (m/sec)

€ = Density of Air (Kg/m^3)

A = Turbine blades area (m^3)

C_P = Turbine performance coefficient

¥ = Angle of blade pitch (degree)

λ = Rotor blade tip velocity ratio to wind velocity

C_P is the coefficient of fraction of kinetic energy which is converted into useful mechanical power by wind turbines; it depends on the ratio of Tip velocity (λ). The wind turbine torque is given by the equation:

$$Tm = \frac{1}{2} € \text{A} C_p \left(\frac{w}{\lambda}\right) \quad (4.7)$$

Figure 4.7 shows the ideal power curve of a wind turbine, which is used to calculate the distinct regions of operation at different wind speeds, such as rated wind speed, cut in wind speed, and cut out wind speed.

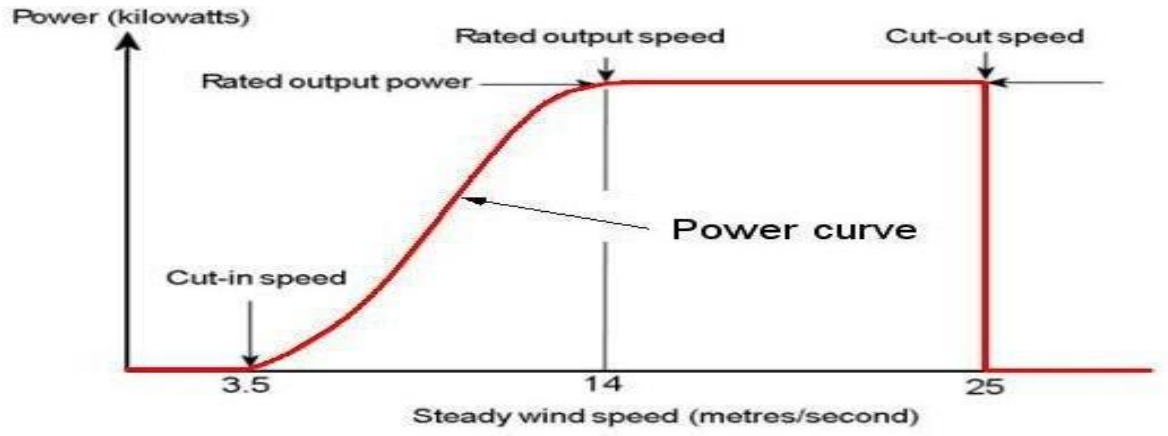

Figure 4.7 Typical wind turbine power output with steady wind speed

Figure 4.8 depicts the use of Simulink/MATLAB to combine a wind system and PMSG generators. The PMSG turbine for wind power generation has been accurately simulated, and the DC and AC outputs are depicted in Figure 4.9 as voltage waveforms.

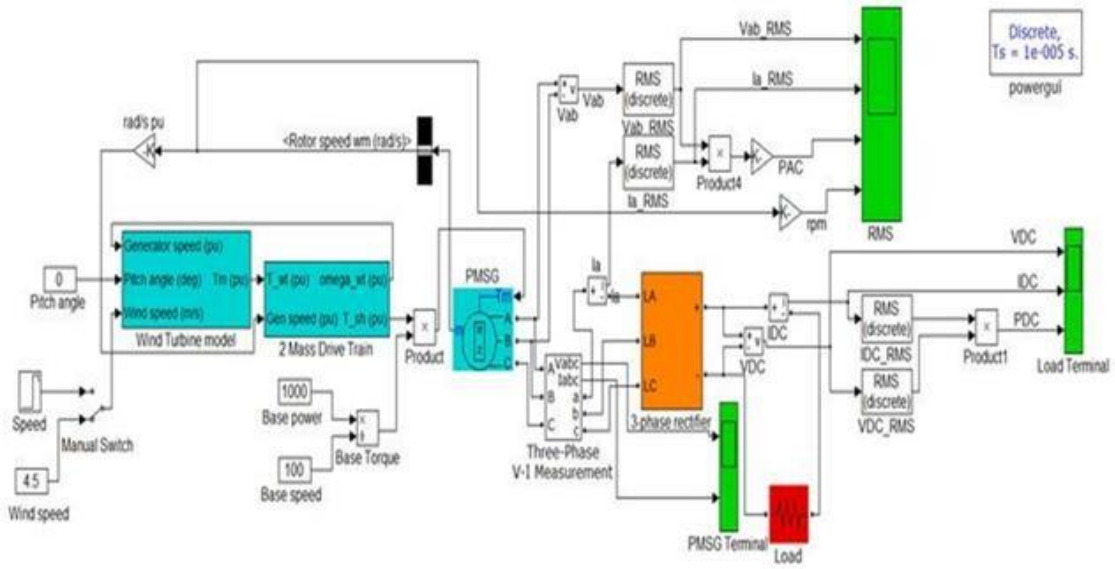

Figure 4.8 Wind turbine model simulations in Simulink

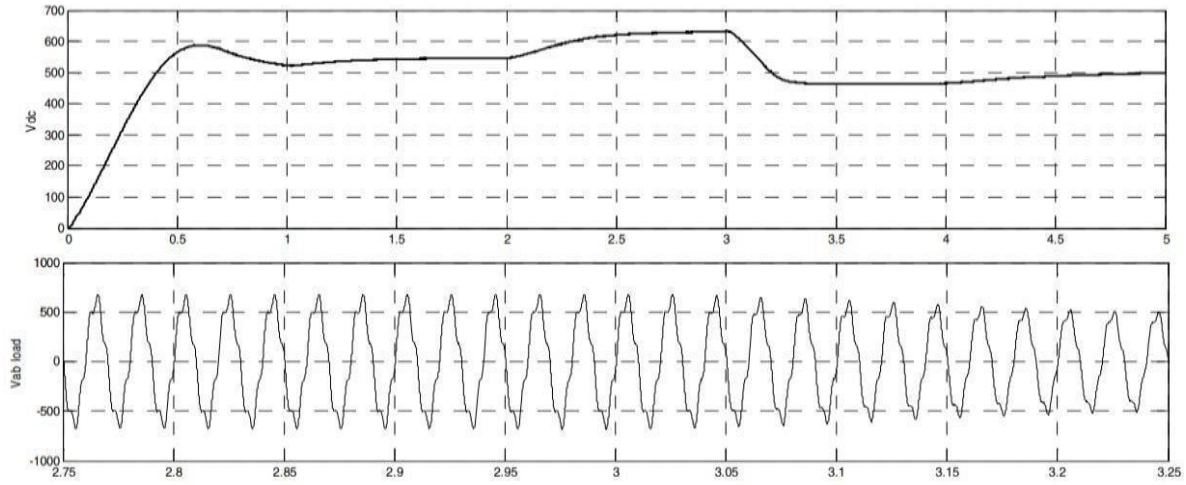

Figure 4.9 DC and AC voltage PMSG under different wind speed

4.7 Grid Connected Hybrid Power System Simulation and Modeling

The hybrid power system is made up of two non-conventional energy sources: a solar photovoltaic and a wind turbine system, as shown in FIGURE 4.10. In addition, the hybrid power system can handle single-phase AC loads.

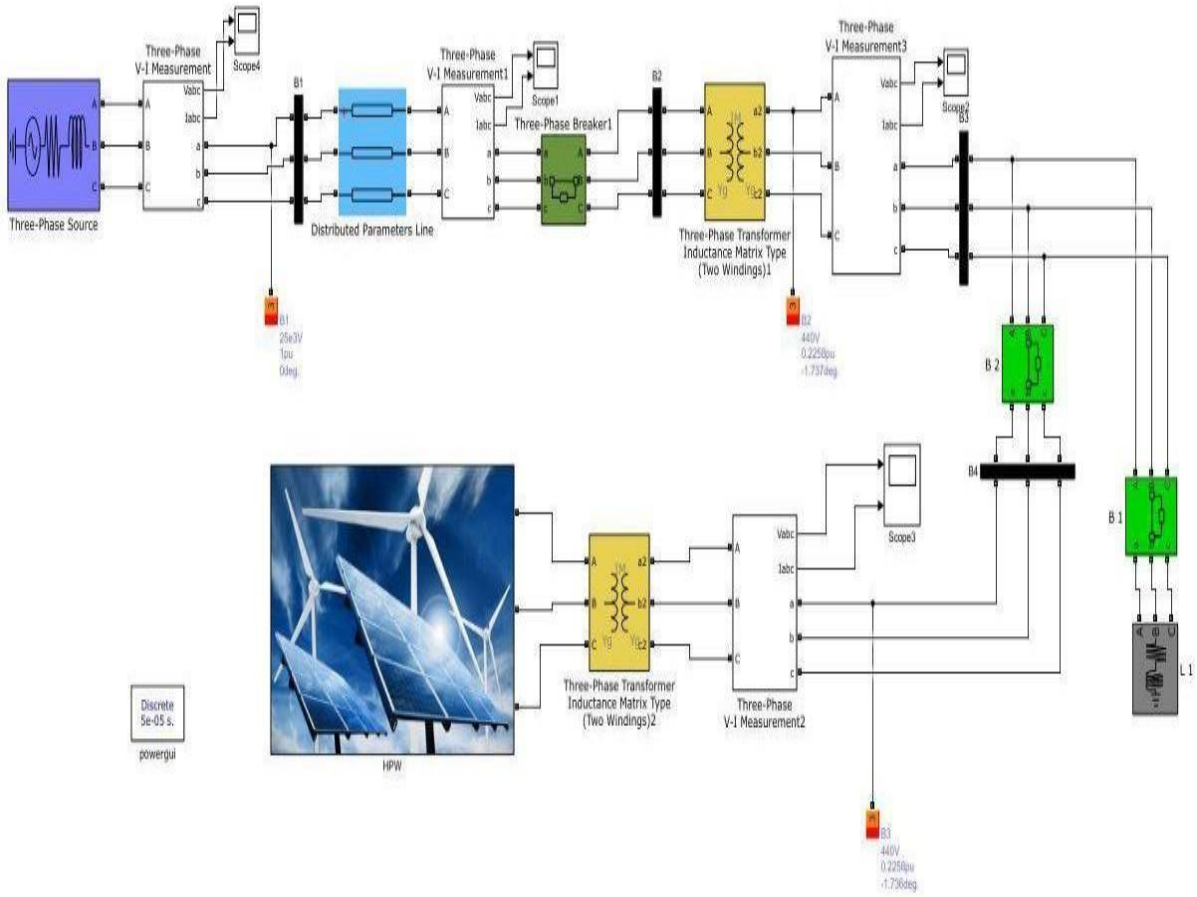

Figure 4.10 Wind and Solar photovoltaic hybrid power system

Figure 4.11 depicts the voltage waveform of a wind turbine and a solar photovoltaic system that uses the predictive – P&O MPPT technique.

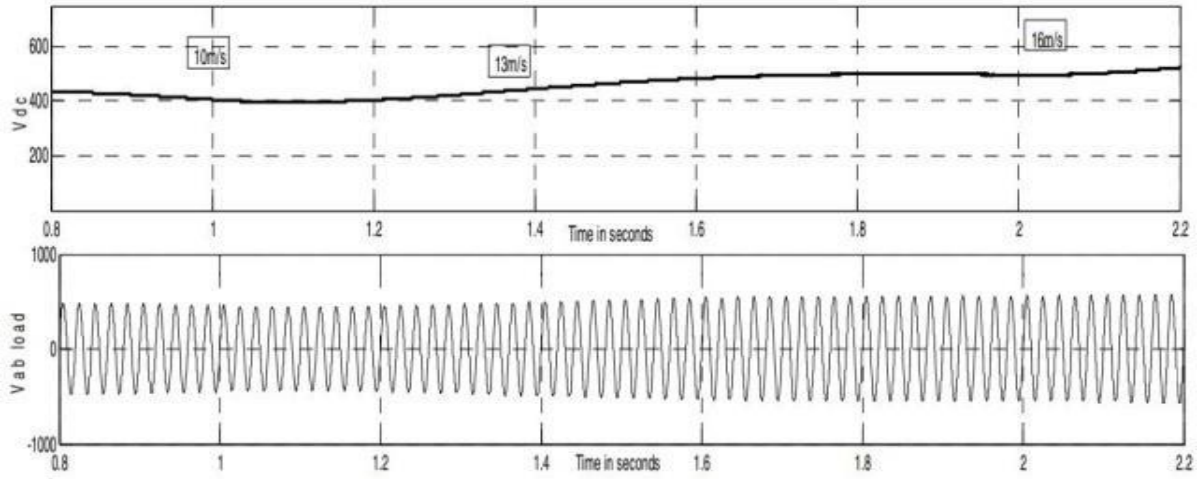

Figure 4.11 Output for both wind speed and solar

4.8 Conclusion

The major goal of this article is to demonstrate the efficiency, dependability, and maximum power generation of a hybrid power system by integrating a wind turbine system with a solar photovoltaic system. This system was then prepared and modeled alone for comparison of the volatile and power variation, and then linked using Simulink/MATLAB. The efficiency of the plant hybrid power system is proved by simulation effects in order to create maximum power for damp summer weather in various countries that are attempting to employ non-conventional energy sources. The use of MATLAB/ Simulink is used to implement the solar photovoltaic model's power generation. In the description of Simulink execution of the Solar Photovoltaic Model, there are five parameters.

CHAPTER 5

SOFT COMPUTING BASED SOLAR FOLLOWER USING RASPBERRY PI 4B

5.1 Introduction

The proposed work deal with image based solar tracker utilizing raspberry pi 4B. The system works fine with a webcam supporting the digital image processing within the raspberry pi model 4B board which manages to arrest the Sun's Image during hazy days due to cloud. India is the country that acquires Sunlight all-round the year. Sunlight can be utilized as substitute energy to fossil fuels or hydroelectricity for the generation of electricity. There are numerous methods which are available to expand the harvesting of solar energy but few are expensive and others can't provide accurate position of the Sun during hazy Sunlight. Raspberry Pi is the foremost board which is used to replace the CPU (central processing unit) to develop and process the Sun image. The two servo motors consisting of tilt & pan are helping to position the web camera to track the position of the Sun. The system provides easy execution of Sun follower with the ability to find the centroid of the Sun on sky picture. Raspberry board then sends the instruction to the driver and it rotates in line with the trajectory of the Sun. The result state that tracking error reduced on haze or cloudy day with the use of raspberry pi model 4B.

Sun energy is an easy available renewable energy and it can be harnessed persistently and steadily, generally in the nations where the Sunlight available all through the year. There are various type of solar harvesting system currently used [132, 57]. It is anticipated that the worldwide energy accumulation by PV will reach nearly 4670 GWp [133] and installed capacity (4.67 TWp) by 2050, because of that price of power could be minimized in the Sun-belt nations. In order to produce Sun energy coherently, Sun trackers can be utilized to assure the concentrated gathering of solar energy by tracking the trajectory of the Sun. The IRNEA [134] 2020 report on Solar energy generated electricity of world and India is showing continuously given in Figure 5.1.

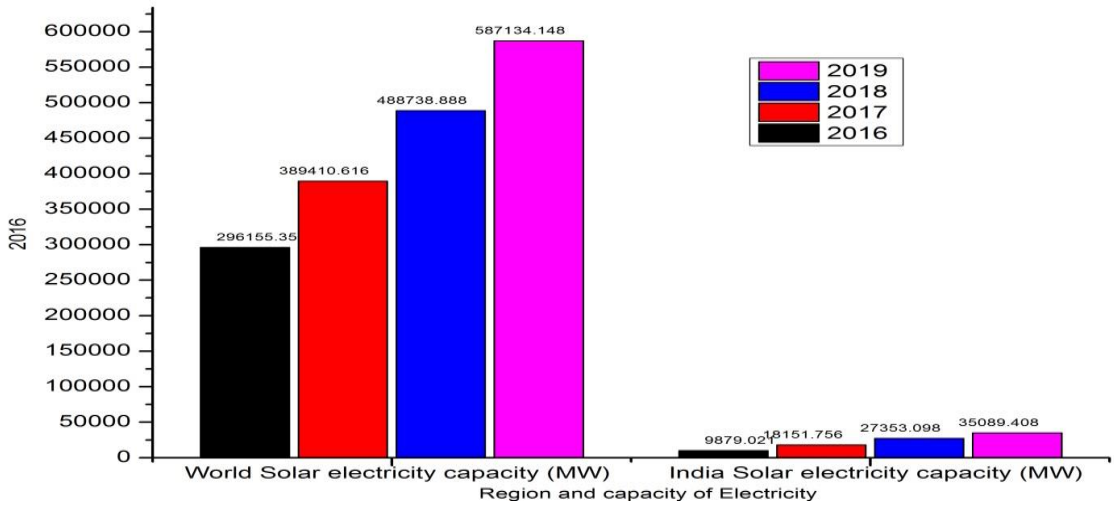

Figure 5.1 World and India electricity generation by solar energy

Sun follower in the recent study & research utilize transducer like photodiodes and photo-transistors [135]. These sensors track down the position of the Sun based on the Sunlight intensity. The drawbacks of these types of trackers are that they are highly responsiveness to climate change like humidity, heat and worst weather situation [136]. Many other solar tracker use an intricate control systems and complex circuitry [137] which replace the problem of high sensitivity & reduce demanding price.

In order to remove the hitches referred above, a DIP based Sun follower has been made in modern era. Exceedingly accurate Sun following system using budget web camera was designed, which used to trace the Sun trajectory and deduce its location with tracing precision of 0.1° without getting effected by weather conditions. Also, an image-based Sun tracking sensor and tracing controller consisting of image processing algorithm [138-141] initiated solar image tracing model. This system is able to deal the issue of unstable tracing when the weather is cloudy and accomplish tracing precision of 0.1°. It proves the possibility of tracking the Sun with the use of image processing techniques which motivates the analysis shown in the work [142].

The proposed work introduces a Sun tracing system with the use of DIP algorithms as the main components and the price can be minimized with the help of a web camera as a substitute of a costly camera. The DIP processing is done within Raspberry Pi (RP) board. The RP was designed in the United Kingdom by Raspberry Pi foundation. It is an

integrated board computer whose leading objective was to upgrade the education of fundamentals of computers in educational institutions. It consists of two main models and both of them are alike excluding the model B, it contains an Ethernet, 2 USB (Universal Serial Bus) ports and 1 GB synchronous DRAM can work on a operating system. In this project we have used RP Model 4B.

5.2 Methodology

5.2.1 Design & Operation of Hardware: The solar tracker system diagram shown in Figure 5.2 and hardware layout consists of a RP board, servo motors and finally a web camera shown in Figure 5.3. The Raspberry Pi (RP) is the primary board that operates the images and controls the servo motor. The web camera catches the pictures from the sky and sends it to the RP board through the camera port. The sky image is processed to find out Sun picture and their centroid co-ordinate. The servo motors are attached to RP board through General Purpose Input/output port. After tracing down the exact solar position, Raspberry Pi rotates the servo motors, either pan or tilts or both if necessary. Sometimes both tilt & pan are necessary to adjust so that the Sun will be placed exactly at the centroid of the sky image.

If the Sun is not recognized in pictures, RP board will continue to rotate the servo motors till the Sun discover. If the Sun is positioned at the centroid of the picture, the RP board sends the message to driver motor to remain at their current position for next ten minutes.

5.2.2 Processing of Image: As image is captured from webcam, it's a 24- bits coloured image and later converted into an 8-bits gray-scale image to permit the efficient processing of the sky image. The processing of image [143] uses OpenCV module. The OpenCV coding, converts twenty –four bits coloured image into eight bits coloured image. Than eight bit coloured image is converted to gray image by OpenCV code then finally gray-scale picture is converted into binary picture [144] which is threshold to recognize the circle or curved shape of the Sun as shown in Figure 5.4.

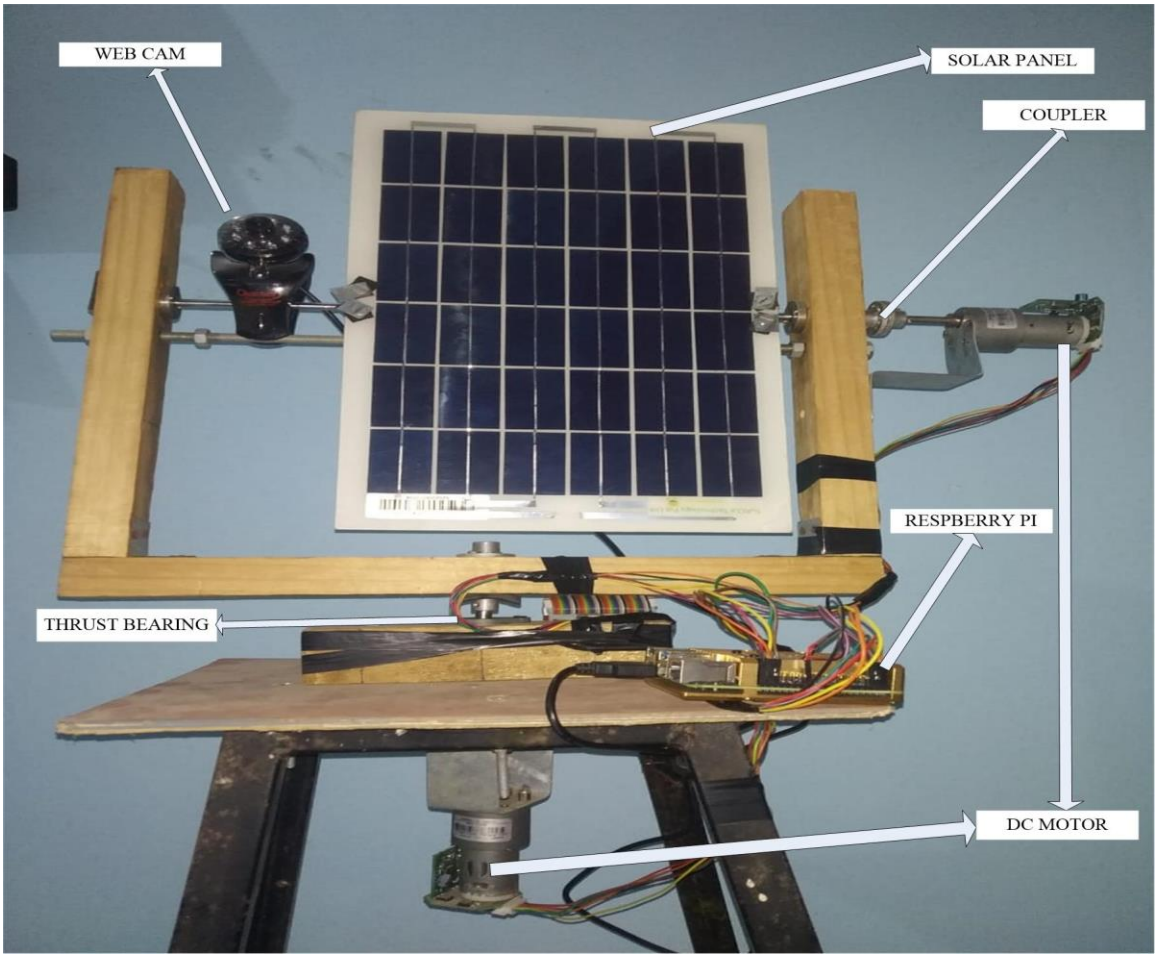

Figure 5.2 Solar tracker system diagrams

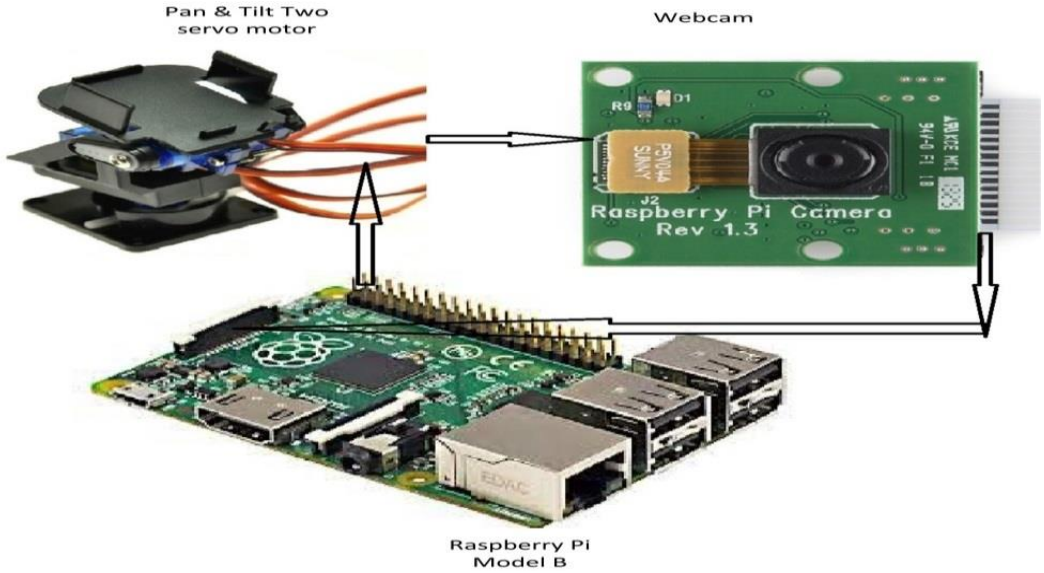

Figure 5.3 Design of DIP Solar trackers

Figure 5.4 Processed Images

Adaptive Thresholding is an excellent method for transforming the gray image to binary image and in addition to this, the thresholding provides an easy and convenient way to separate background pixels (usually set to black) from those corresponding to the target objects (usually set to white). The source image is the first parameter in adaptive thresholding. The maximum nonzero value allotted to pixel for which the situation is fulfilled. In adaptive method the adaptive Gaussian thresholding [145] algorithm were used. There are two types of adaptive methods-

Adaptive mean thresholding: The threshold value is the mean of the neighbourhood area minus the constant C.

Adaptive Gaussian thresholding: The threshold value is a Gaussian-weighted sum of the neighbourhood values minus the constant C. By using thresholding we separate Sun from image taken by web cam as shown in Figure 5.5.

Figure 5.5 Adaptive Gaussian Thresholding

Hough transformation is used to recognize the shape of the Sun where the circle figure is shorted because of Sun circular shape from the source image; it can be 8-bits image in binary format. The work deal HOUGH-GRADIEN method where dp (Inverse Ratio of Accumulator Resolution) is given by equation 5.1.

$$dp = \left(\frac{Accumulator\ resolution}{Image\ resolution}\right)^{-1} \tag{5.1}$$

Assume that *dp =1*, then

$$Accumulator\ resolution = Source\ image\ resolution$$

Assume that *dp =2*, then

$$\text{Accumulator resolution} = \frac{1}{2}(\text{source image})$$

Criterion 1 along with Criterion 2, the first along with the second, the particular method is to set up. The lowest level radius called the minimum radius of the circle, which is used for purposes of the identification. The maximum radius of the circle also used for purposes of identification.

5.2.3 Motor control: Servomotors control depends on pulse width modulation signal via RP board. Pulse width modulation indicators can be managed using Sun's placement in the photograph. Figure 5.6 show the flow chart which represent technique to recognizing the coordinates of Sun by identifying the Shape of the Sun.

When the Sun is not identified in the picture, since the webcam's face away from the Sun, the Raspberry Pi arbitrarily deliver pulse width modulation signal to the servo driver. The process will go till the Sun is recognized in the images. When the Sun is recognized, the RP board will have to analyse its orientation and proceed further to control pan as well as tilt of driver. When the Sun is in the right / left side of the pan tilt control, the RP board sends a command to the pan-tilt control in order to set the location of the Sun at the centre of Image. Figure 5.7 represent the pan and tilt of the Sun in the image. In given Figure 5.7(a) is a real RGB image and rest 5.7(b), 5.7(c) and 5.7(d) represent the right traced, left traced and centre traced threshold scanned image respectively. If the traced tilt and pan is not at centroid than Raspberry board will

generate the pulse width signal to change the pan-motor towards the pan line to come near the Sun centroid. The similar action occurs for tilt motor. When Sun comes exact at the centre of the picture shown in Figure 5.7(d), RP board will send the same pulse width modulation signal continued for twenty minutes.

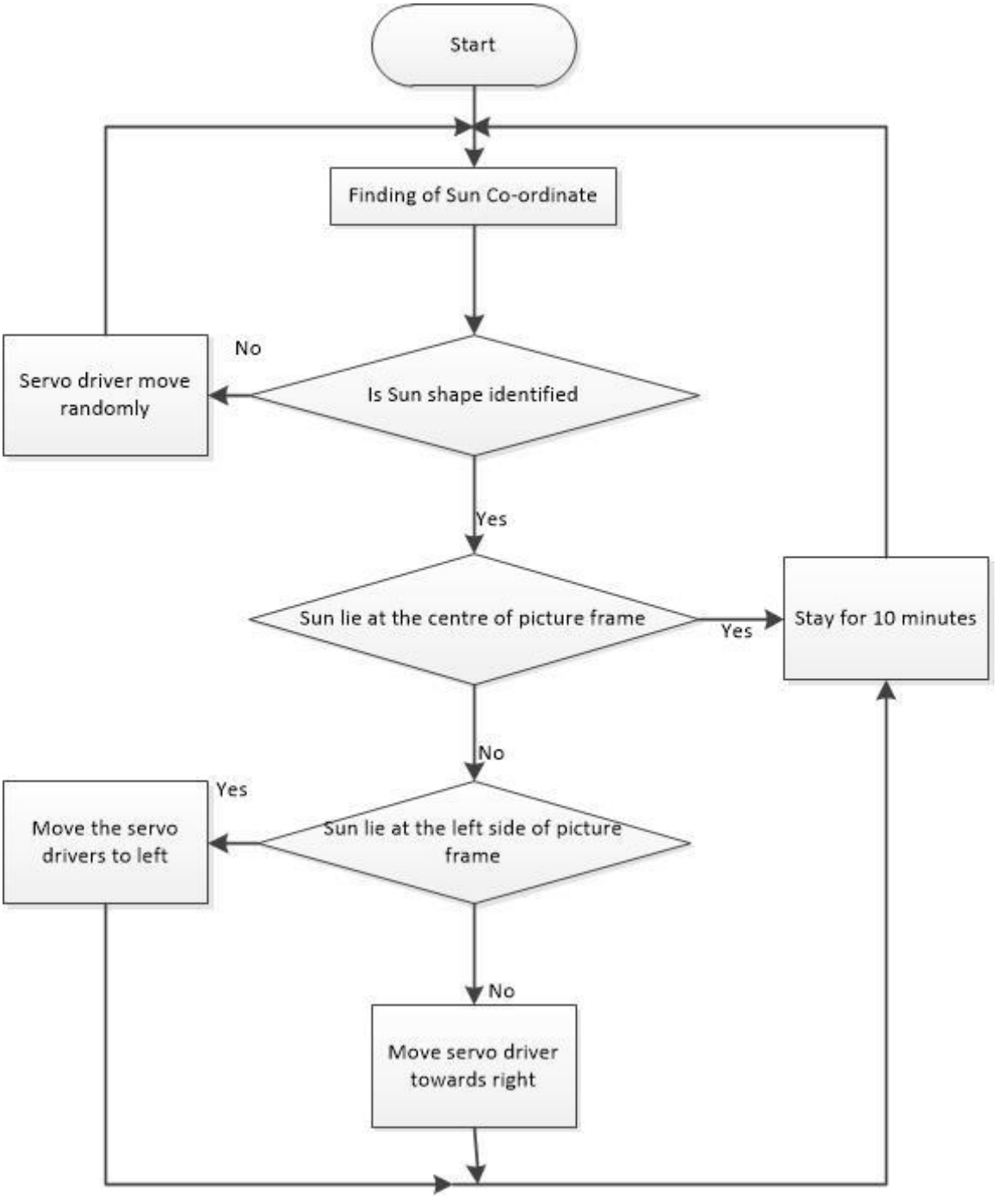

Figure 5.6 Flow chart of motor driver movement

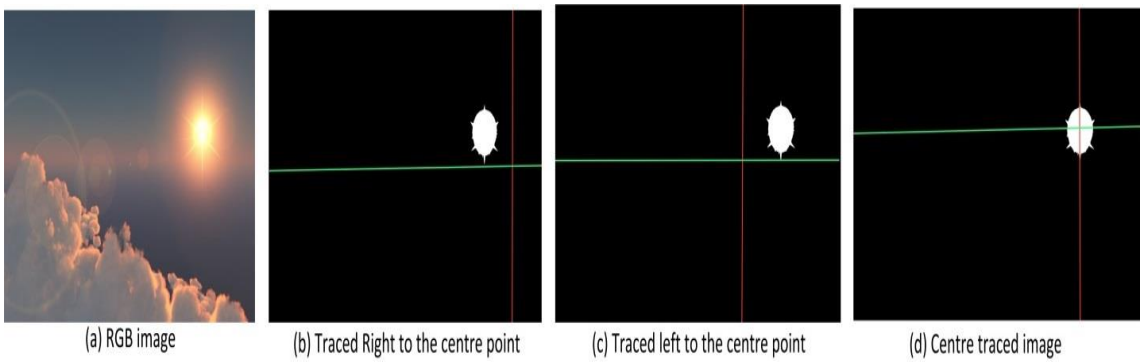

Figure 5.7 Control of tilt & pan

5.2.4 Control of PWM: GPIO control and PWM library are the two methods to control PWM in servo motor. The sleep time is controlled in order to transfer PWM signal to driver. Sleep time is a delay time which is regularly sends to driver shown in Figure 5.8. The time 'a' lie within 1ms to 2 ms (millisecond) depends on the orientation require to face web camera towards the Sun. The co-relation of time 'a' & 'b' stated as b = (-a) + 20ms, where 'b' is in ms.

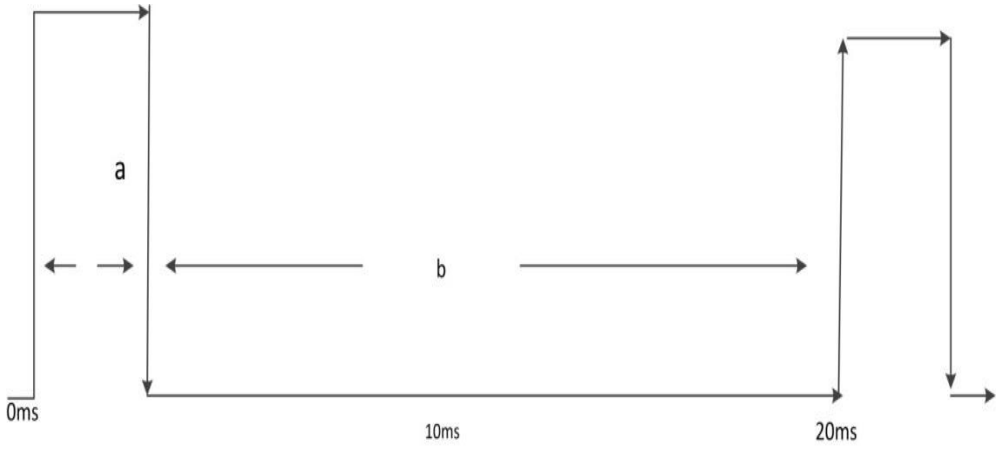

Figure 5.8 Time 'a' & 'b' relation in millisecond

5.3Results and Performance

5.3.1 Hardware: GPIO Port 22 & 23 is connected to pan signal of PWM and servo motor & these servo motor powered by Pi board itself shown in Figure 5.9. Raspberry Pi camera is directly connected to the camera port in Raspberry Pi board. It can be transmit to personal computer through USB.

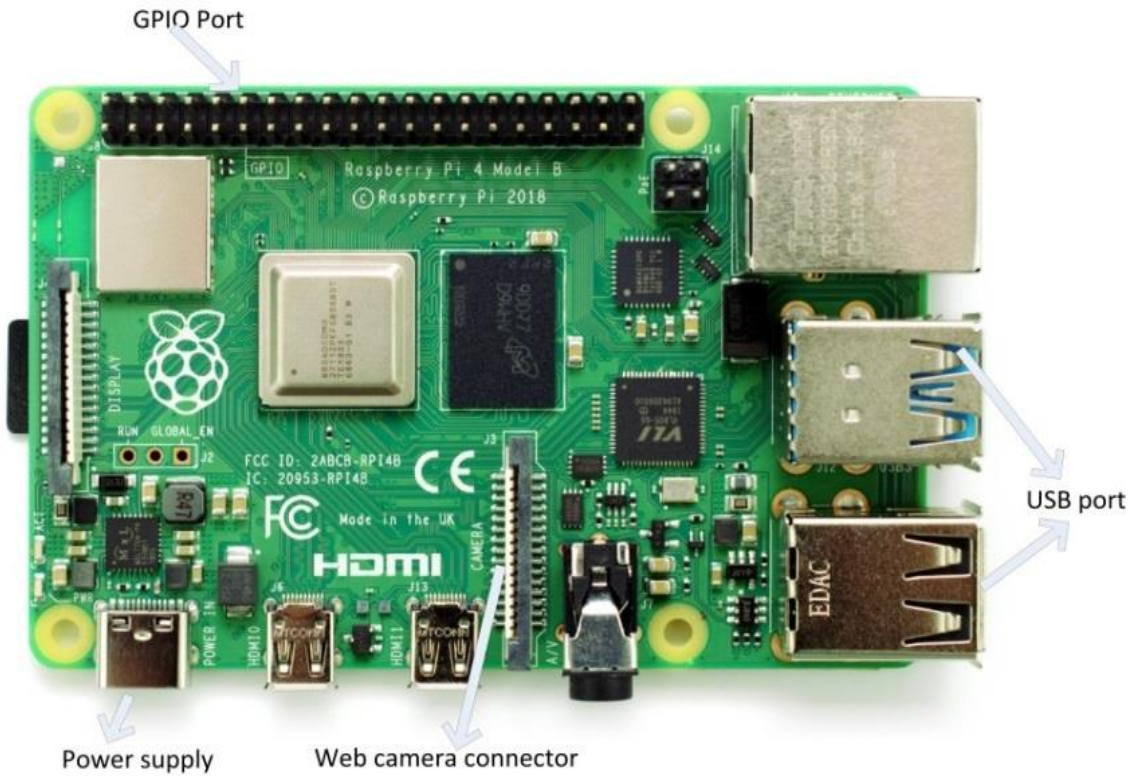

Figure 5.9 Raspberry Pi B4 board

5.3.2 Processing of Image: The pixel range of web camera is 2048 × 1536 and it has 3.15 mega pixel images. It also has dual light emitting diode (LED) flash and auto focus. The given Figure 5.10 is taken by web camera at noon and one hour after the rain and their Gray and binary conversion shown. We can clearly observe that Sun is not clearly visible because of clouds. We put this image under image processing and it can be seen in Figure 5.11 that the Sun's circumference or boundary and centre is being detected.

Fig. 5.10 Image processing

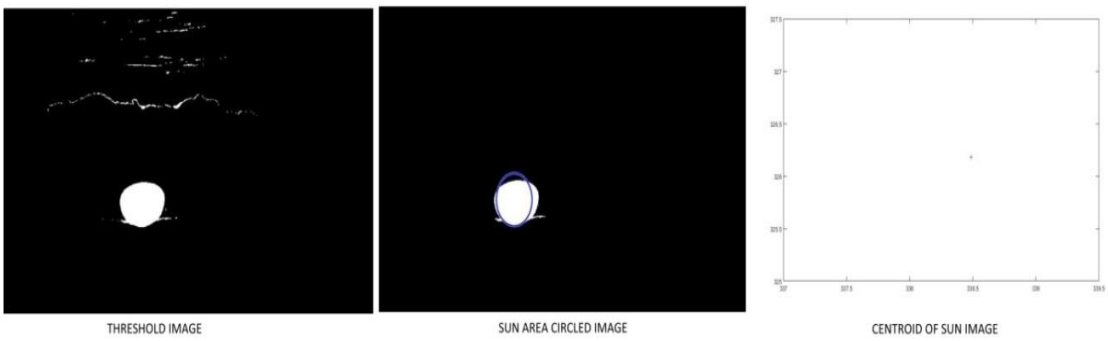

Fig. 5.11 Sun boundary and centre detection

The red and green lines show pan and tilt servo motor respectively assuming both are perpendicular to each other. The servo motor moves the webcam towards the centre of Sun with the help of Image centre shown in Figure 5.12.

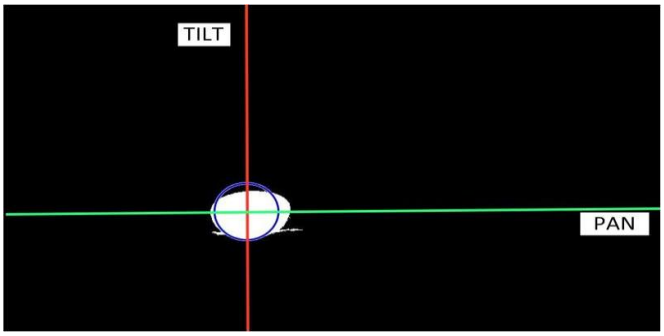

Figure 5.12 Traced Image

The degree of rotation is requiring reducing so the pan servo motor lines cross the centre, than the Sun is located. At 90 degrees, the Raspberry Pi send PWM signal of 1.49 ms, as shown in Table 1. According to this, when the pulse width signal directed to the driver is lower, which is 1.28 ms, the orientation will be equal to 70 degrees. The same is repeated with tilt of servo motor.

Line of tilt should pass the blue circle which is present slightly left to the circle hence rotation degree of the servos should be reduced. The tilt lines are at degree 90 so now lines are hence decreased to 750 and the signal has taken 1.32ms. Various images data were given in Table 5.1. The observed results represented in Figure 5.13 where Image and Sun centre coincide and pan & tilt line cross each other at image centre.

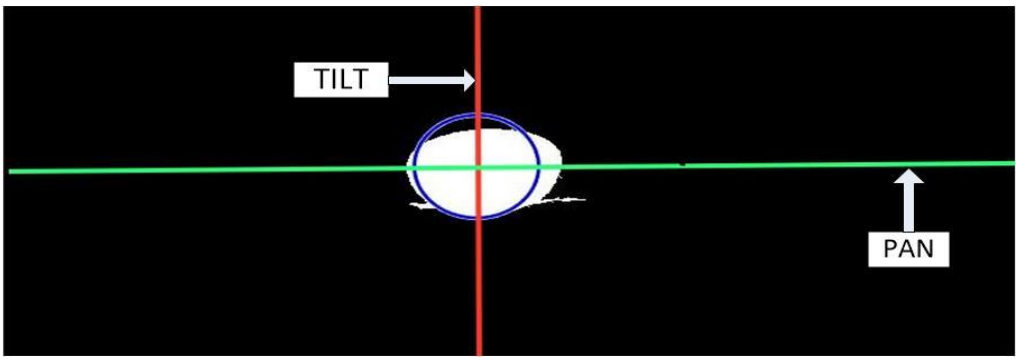

Fig. 5.13 Centroid of Sun located

Table 5.1 Time L and K relation with the degree of rotation of the motor

Picture	L (ms)	K (ms)	Rotation(Degree)
1	0.56	19.48	0
2	1.03	19.01	40
3	1.49	18.55	80
4	1.96	18.08	120
5	2.42	17.62	160
6	3.78	16.26	180

In given Table 1 high signal of the PWM which given to drivers to calculate the rotation degree of motor shown in Figure 5.14.

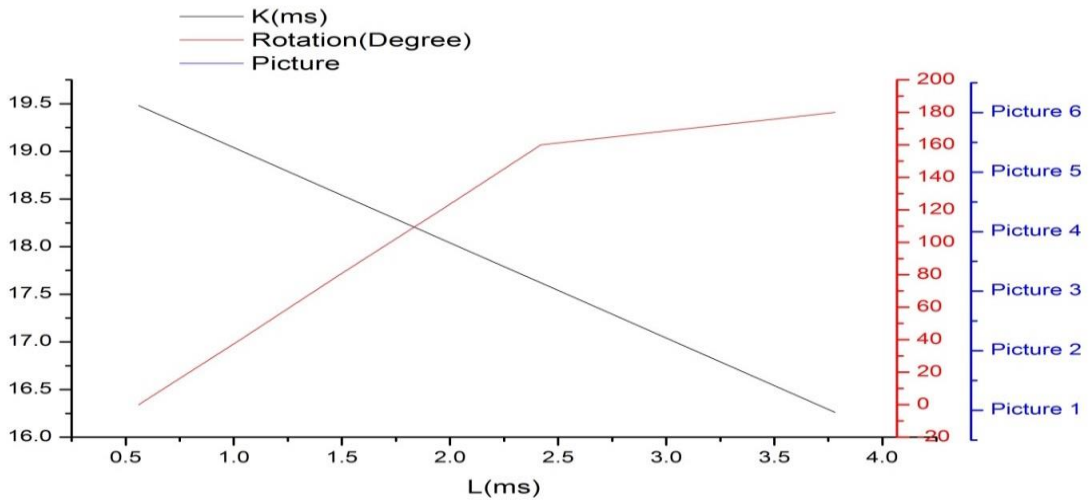

Figure 5.14 Result analysis

5.4 Conclusion

The proposed work based on solar tracking by the raspberry pi 4 B board systems. The system consist of webcam with image processing by raspberry pie board which is effective and works very well in tracking the Suns position during the cloudy days. This has effectively increased the efficiency of the solar power output. The system has the capability to track and to find the centroid of the Sun by the Sun's picture which initiates the motors to rotate according to the position of the Sun. The Sun following system using photo-diode or photo-transistors presents drawbacks due to changing weather and environment effect. To upgrade this work in future the system needs an optimistic approach by doing proper adjustment and a more efficient algorithm to cope up with the real time operation on ground level.

CHAPTER 6
VISION BASED SOLAR TRACKING SYSTEM FOR EFFICIENT ENERGY HARVESTING

6.1 Introduction

Electricity is a vital source of energy for a rapidly rising population, and its consumption is hazardous to the environment. This reason is harmful to the environment, so immediate action is needed to address the issues that have arisen as a result of the development of solar energy. If we utilize a solar follower, we can maximize the production of solar energy. The main component of solar panels is a microcontroller with an LDR sensor setup that is used to track the sun. However, due to the poor sensitivity of LDR sensors, they are less effective in tracking the sun. With the use of both LDR sensors and image processing, we propose a way for tracking the sun more effectively. This type of mechanism can follow the sun using image processing software that combines the sensor results with the processed sun image to operate the solar panel. Thousands of solar panels in solar power facilities can be controlled using a combination of software and hardware.

The development of a nation is dependent on energy, but because energy is becoming increasingly scarce, a vast amount of energy will be required to build a nation, and this energy can only be obtained from non-renewable sources. Fossil fuels account for over 85% of all energy production. Fossil fuels are scarce and a major contributor to global warming [146]. That is why we suggest this project, which provides a long-term power source to help us save our planet and address the energy crisis and pollution problem. Solar energy is a great source of energy that is both environmentally friendly and cost-effective as a backup supply of energy.

Solar photovoltaic modules are the most efficient technique to collect and convert solar energy into electricity. A solar panel can be made out of a variety of different materials. When we utilize a Si panel, it is 24.5 percent [147] more efficient than a standard solar panel. A solar tracker is a system that allows solar panels to monitor the sun in order to maximize electricity efficiency [148]. The main goal of the system is to implement a DIP & LDR based solar tracking system with

simultaneous sensors using the programming language. As a result, as compared to a stationary system, it can improve the effectiveness of a sun panel tracking system [35].

6.2 Photovoltaic Development & Performance

This tracking system is proposed to maximise the output power of solar panels. The highest power was obtained during the tracking of the sun during the sunshine hour, and the characteristics of current vs voltage and power vs voltage [149] of photovoltaic cell are shown in Figure 6.1.

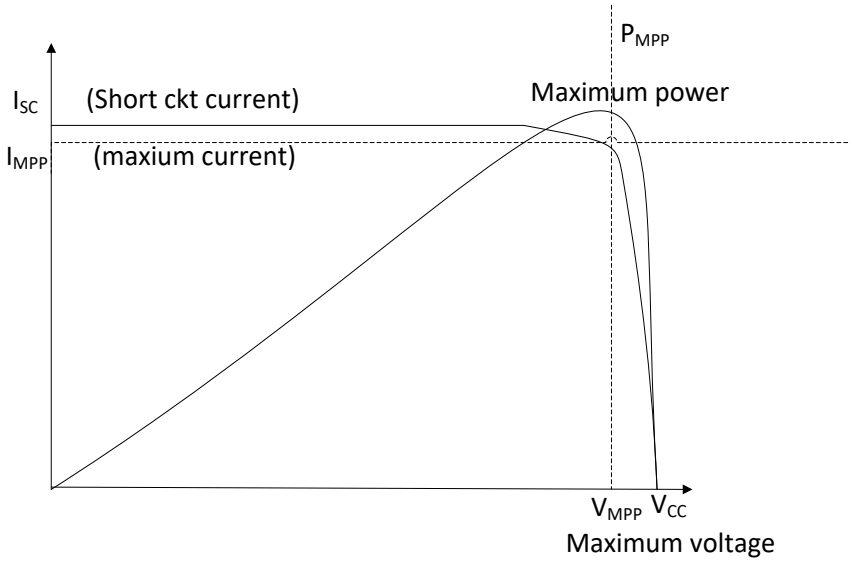

Figure 6.1 Photo Voltaic responses Isc-V and P-V

Many MPPT algorithms have been created by researchers to boost the power output of solar panels. When compared to a fixed panel, a sun follower can improve the performance of a sun tracker by 22% to 56 %.

The azimuth and altitude changes with respect to the Sun azimuth and altitude point are obtained using the Sun direction tracing method. The sun azimuth and height [150] at any position can be computed using an astronomical equation. Equations 6.1 and 6.2 can be used to calculate the azimuth of the Sun and the height point [151].

Where,

© = latitude angle

® = Declination angle

η=Solar hour angle

$$\sin È = \sin © \sin ® + \cos È \cos ® \cos \eta \quad (6.1)$$

$$\sin Â = \frac{\cos ® \sin \eta}{\cos È} \quad (6.2)$$

Declination angle is calculated by equation 6.3.

$$® = 23.45^0 \sin \frac{360^0(284 + d)}{365} \quad (6.3)$$

Where,

d=date

And Sun hour angle calculated by equation 6.4.

$$\eta = (ß + E)x15 + ψ - 300^0 \quad (6.4)$$

Where,

þ= local longitude

ß= Beijing time

E=Jet lag

(Â, È)= Sun location

At time t_a, the sun's current location is ($Ât_a$, $Èt_a$). After T_a seconds, Â & È becomes ($Ât_a + T_a$, $Èt_a + T_a$) and the new position is given by $ΔÂ = Ât_a + T_a - Ât_a$ $ΔÈ = Èt_a + T_a - Èt_a$. The panel can be rotated ΔÂ & ΔÈ in the horizontal and vertical directions respectively. The direction of the Sun can be explored using this method.

6.3 Projected System

Figure 6.2 depicts the system's block diagram, in which the LDR [57] sensor outputs to the microcontroller, and the camera captures the Sun picture to determine the Sun centre coordinate (A_C, B_C) using the image processing [145] algorithm. Finally, the motor driver is supplied the refined azimuth and altitude, which causes the solar panel to focus directly towards the Sun's centre, resulting in improved performance output.

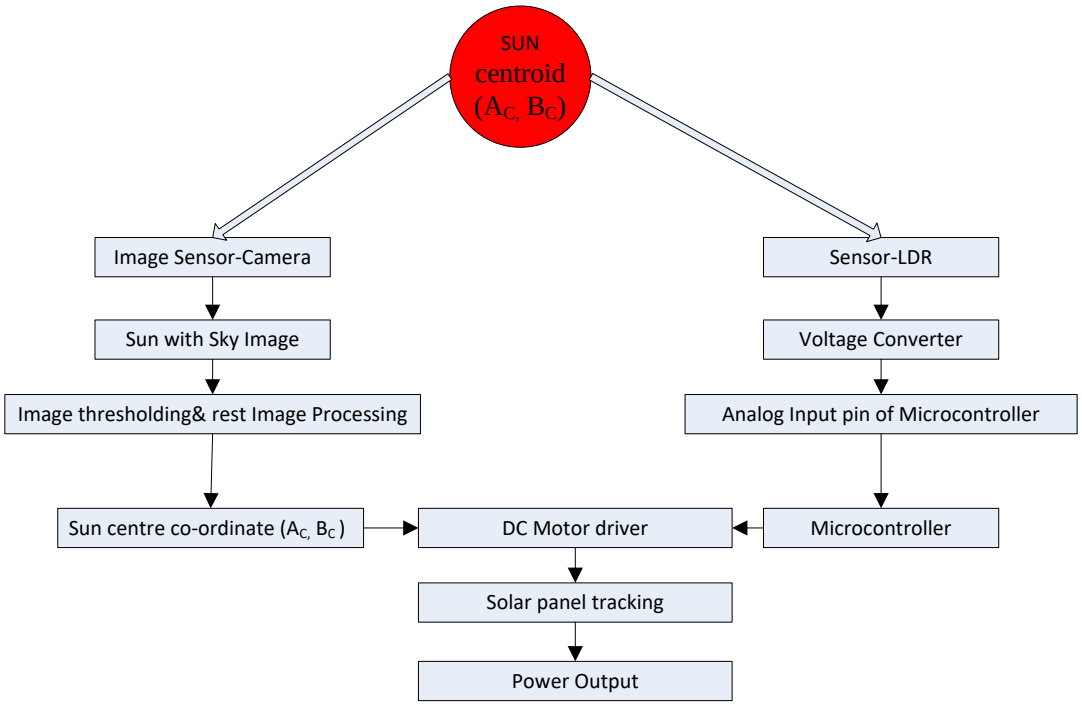

Figure 6.2 System block diagram

6.4 Design of Hardware

Two servo motors, four LDR sensors, and an Arduino UNO make up the system. As pre-processing, the LDR sensor [152] detects the intensity of solar light, and the Arduino UNO controls the panel's orientation [153]. Figure 6.3 shows a circuit design for an LDR-based tracker.

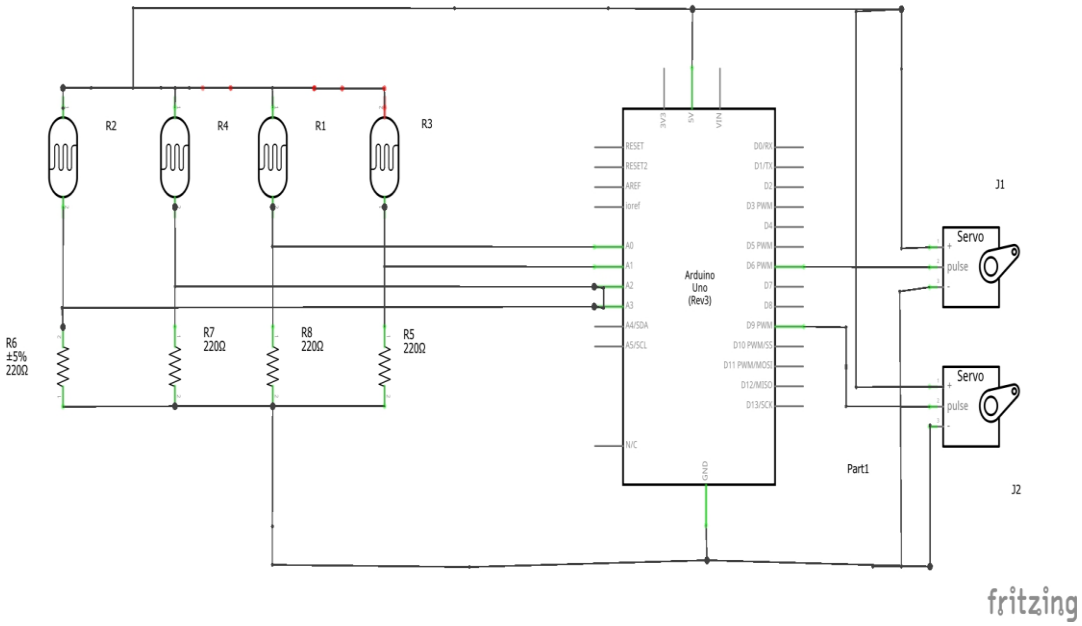

Figure 6.3 System Circuit diagram

Fritzing software is used to create the PCB (Printed Circuit Board) and simulate the project shown in Figure 6.4. Figure 6.5 shows the Arduino Uno board, 4 LDR, connecting resistance, two DC motors, and their connections to the Arduino board.

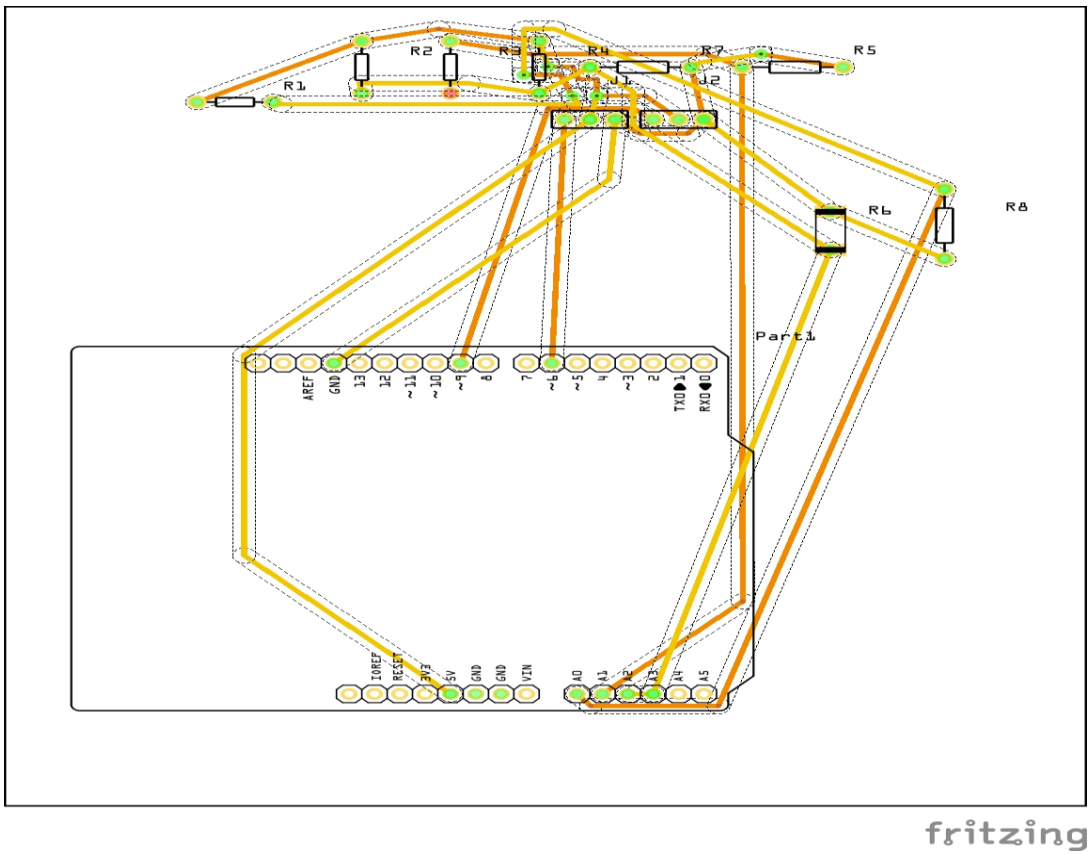

Figure 6.4 System PCB design

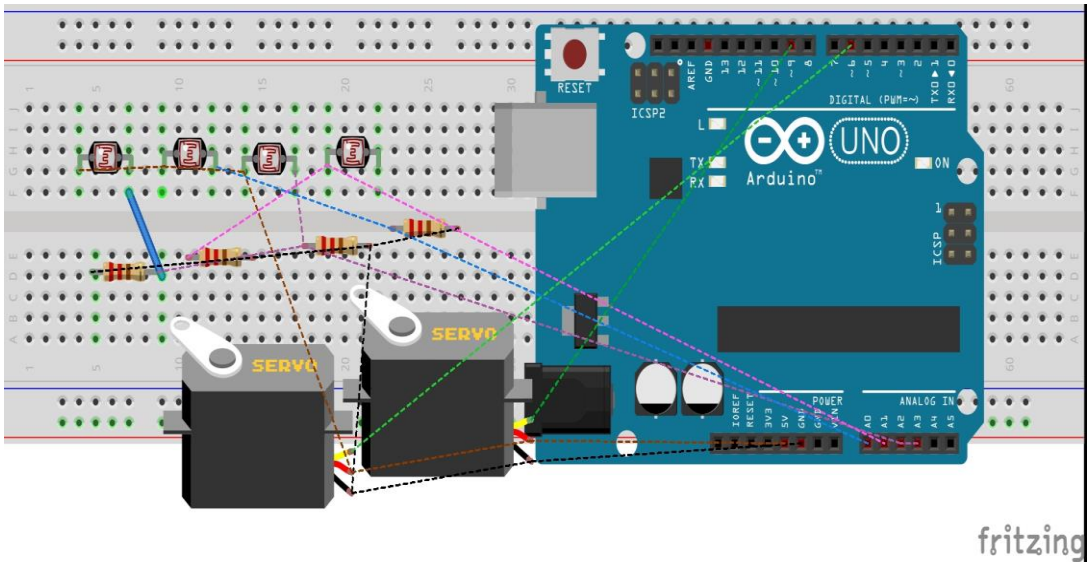

Figure 6.5 Circuit connection diagram

The above given hardware component list for the system shown in Table 6.1.

Table 6.1 Assembly List

Label	Part type	Properties
J1	Basic Servo	12 volt ,10RPM
J2	Basic Servo	12 volt ,10RPM
Part1	Arduino Uno (Rev3)	type Arduino UNO (Rev3)
R1,R2,R3 & R4	Photocell (LDR)	dark 300 kOhms@ 10 seconds; package THT; resistance@ luminance 16 kOhms@ 10 lux
R5,R7 & R8	220Ω Resistor	bands 4; pin spacing 400 mil; package THT; resistance 220Ω; tolerance ±5%
R6	220Ω Resistor	package 2512 [SMD]; resistance 220Ω; tolerance ±5%

6.5 Methodology

The proposed system tracked in two stages. The first stage employs an LDR sensor, while the second stage employs a corrected measure tracker based on image sensor tracking. Initially, the solar tracker uses an LDR sensor to track the Sun's intensity and adjusts the panel accordingly. Because of partial shade and out of track conditions, there may be errors in this tracking. The second tracking approach, known as picture tracking, eliminates this issue. To get a Sun image, image tracker uses a camera near the panel that takes a photo of the Sun with the sky as the threshold. This sun image [154] is used to compute the circumference, from which the centroid (AC, BC) of the sun is calculated using various image processing algorithms. The estimated centroid will tell the second track driver to move the panel straight towards the Sun's centre. As a result, this two-stage tracking improves the sun follower's tracking accuracy [155].

6.6 Intensity Sensor Tracking

The resistance value of LDR decreases as the intensity of the solar light increases in this tracking, reaching nearly a mega ohm [156] after the sun light is fully gone. As illustrated in Figure 6.6, we modify the LDRs so that when one side of the LDR focuses Sun, the other side of the LDR remains dark. Increased current flow to operate drives can be achieved by lowering resistance. Because the sun's location alters the strength of light incident on the panel, the four LDR receive varied proportions of light, resulting in vertical and horizontal motion.

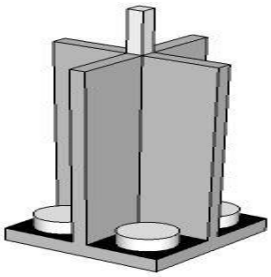

Figure 6.6 LDR shadow principal

6.7 Image Sensor tracking

In this part, the various image processing steps used to follow the sun's course were detailed.

6.7.1 Image Processing: Figure 6.7 shows how the suggested mode calculates the Sun centroid co-ordinate [157] utilising an image processing (IP) technique and various Sun following phases.

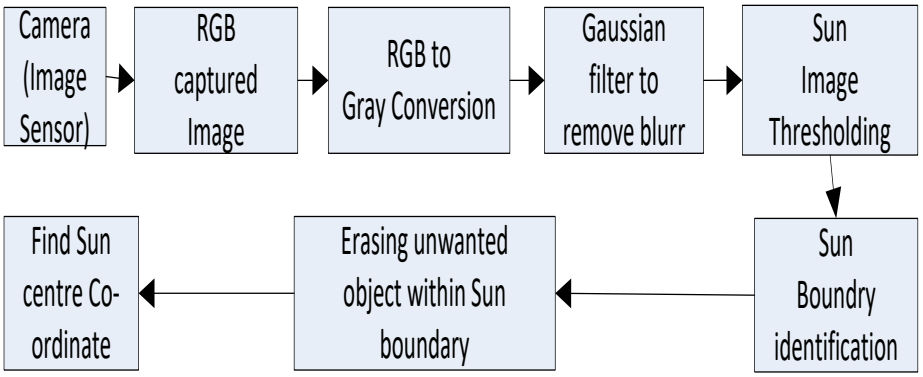

Figure 6.7 Steps in Image processing

6.7.2 Image conversion and noise reduction: The RGB image captured by the camera is transformed to grey scale, which decreases algorithm complexity and processing time. The converted image has contrast starch, and the image is noise-free thanks to the Gaussian filter [158]. Figure 6.8 depicts an RGB and Gray picture.

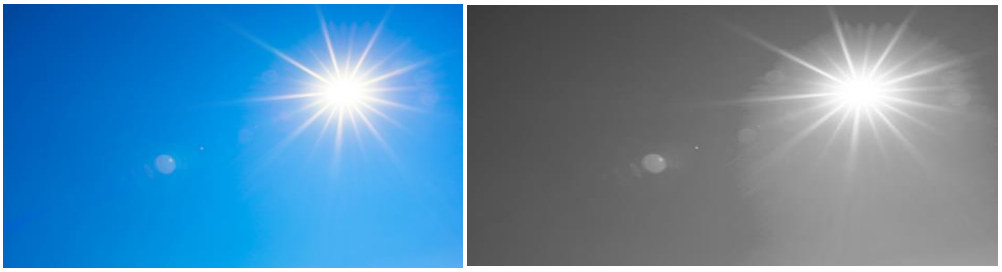

Figure 6.8 Sun RGB & Gray image

6.7.3 Sun identification [146]: The cloud is represented by a bright spot in the grey image. On the grey image displayed in Figure 6.9, these spots were removed using binary thresholding. Unwanted dots in the image were removed by locating the largest contours.

Figure 6.9 Binary thresholding of Gray image

6.7.4 Estimation of Sun following trajectory: The Sun's border is segmented [147], and the centroid of each segment is computed using the centroid formula. The image centre is determined as well, and the Image and Sun centres [141] are compared to determine the exact Sun centre co-ordinate, which tells the driver [159] to track the Sun.

6.8 Result of Different Scheme of Solar Tracker

Table 6.2 shows the proposed approach, based on LDR and fixed panel follower to capture a single day reading for 17 hours of sunlight. Figure 6.10 shows a comparison of power generation from fixed, LDR, and suggested modals. The proposed system generating more power compares to the rest other two models. Figure 6.11 shows a graphical representation of the short circuit current for all three systems, and it was shown that the I_{SC} is the same across the modes. In figure 6.12, the V_{OC} of all of the above-mentioned models is calculated and examined, and it is noted that the V_{OC} of LDR and IP-based systems is higher than that of Fixed and LDR systems. The results demonstrate that LDR and IP-based trackers create more power than the other two schemes, as illustrated in Figure 6.13, which shows their combined parameter analysis.

Table 6.2 Result of different Scheme of solar tracker

Variable	LDR & IP based Solar follower			LDR based Solar follower			Fixed Panel		
Solar Time	P_{OUT} (W)	I_{SC} (A	V_{OC} (V)	P_{OUT} (W)	I_{SC} (A)	V_{OC} (V)	P_{OUT} (W)	I_{SC} (A)	V_{OC} (V)
07:00	1.35	0.078	17.3	1.23	0.072	17.10	0.92	0.059	15.7
08:00	2.32	0.123	18.9	1.75	0.099	17.70	1.39	0.088	15.8
09:00	2.73	0.144	19.0	2.53	0.140	18.10	1.91	0.117	16.3
10:00	3.43	0.172	19.9	2.83	0.154	18.40	2.46	0.137	18.0
11:00	4.13	0.201	20.5	3.53	0.185	19.10	2.96	0.162	18.3
12:00	4.96	0.246	20.2	4.89	0.245	20.00	4.57	0.241	19.0
13:00	4.83	0.245	19.7	4.74	0.244	19.40	4.64	0.242	19.2
14:00	4.75	0.250	19.0	4.32	0.236	18.30	3.85	0.214	18.0
15:00	3.81	0.202	18.9	3.26	0.188	17.30	2.75	0.172	16.0
16:00	1.75	0.094	18.7	1.24	0.073	17.00	0.97	0.063	15.3
17:00	1.30	0.073	17.7	1.11	0.067	16.50	0.77	0.055	14.1

- In comparison to LDR, the efficiency of LDR & IP is 12.50%.
- In comparison to SS, LDR & IP have 30.05% efficiency.

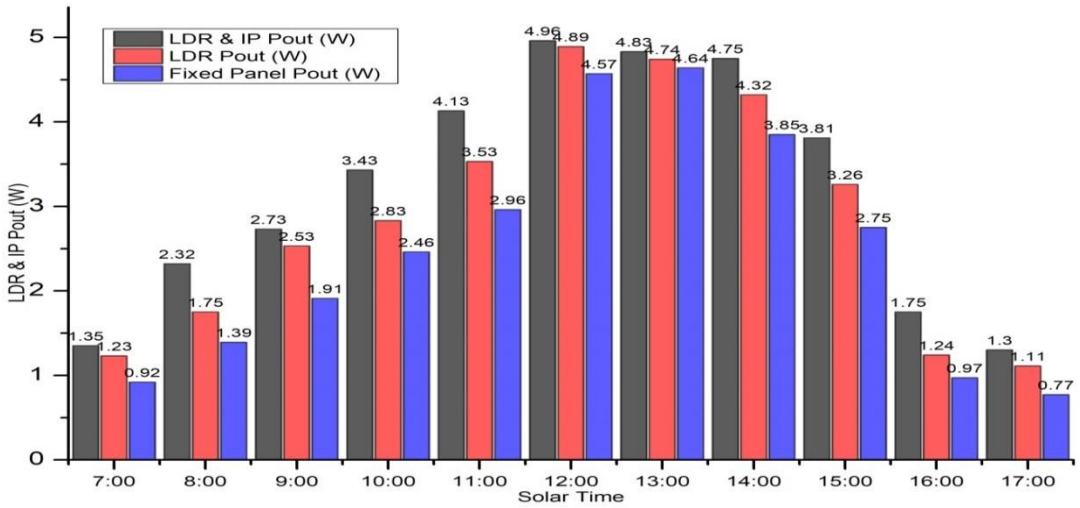

Figure 6.10 Power comparisons of all three systems

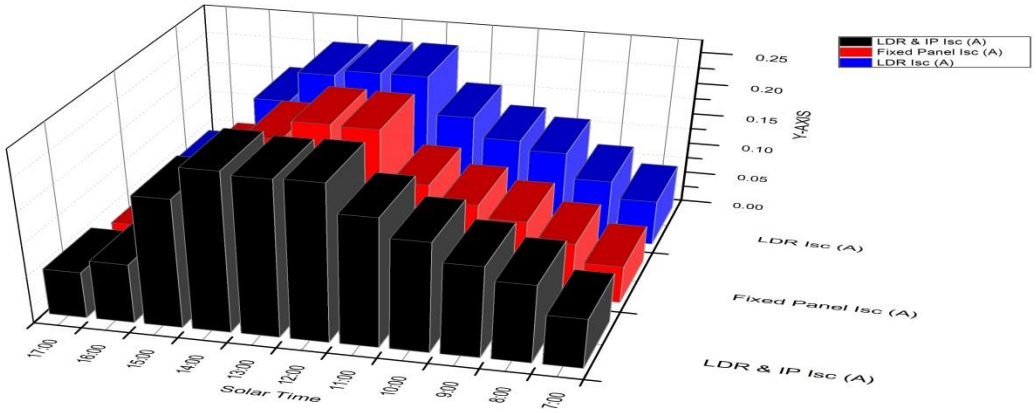

Figure 6.11 Short circuit current comparisons of all three systems

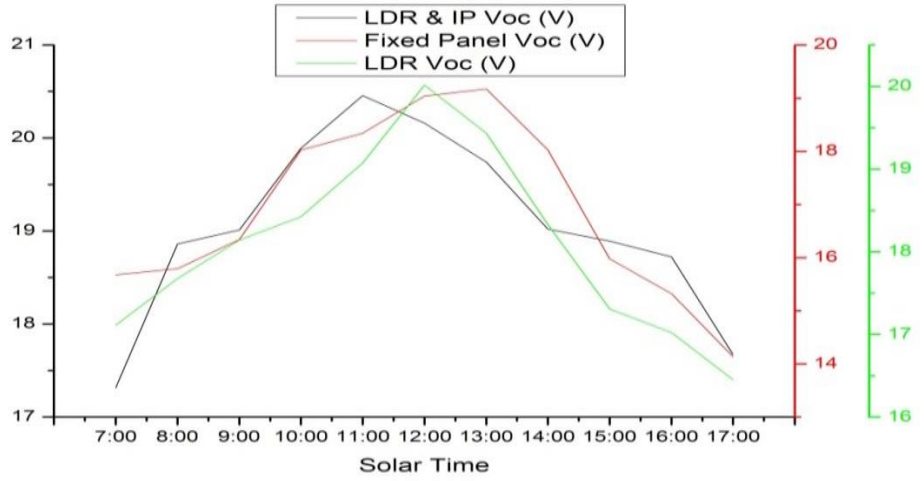

Figure 6.12 Open circuit voltage comparison of all three systems

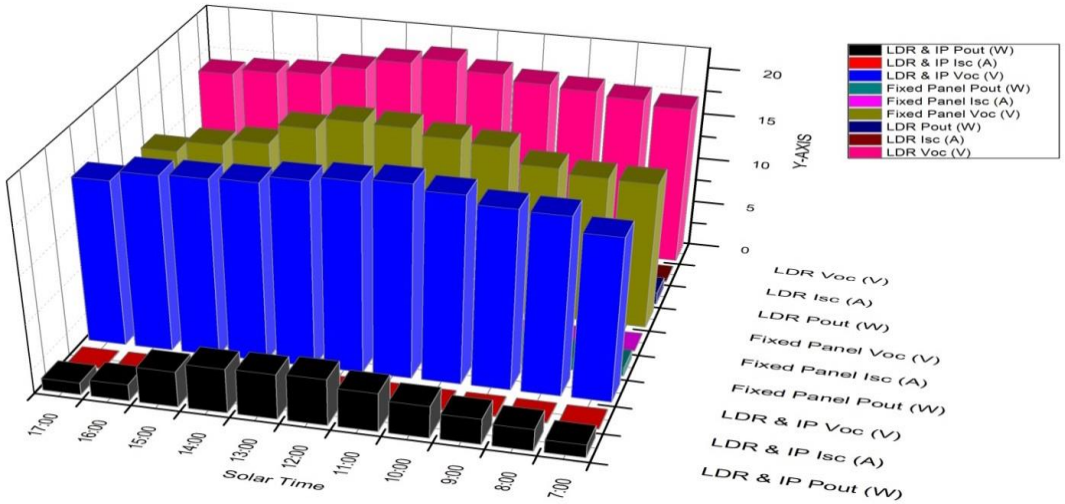

Figure 6.13 Power, I_{SC} & V_{OC} analysis of all three systems

6.9 Conclusion

After examining the full scheme, we discovered that the LDR and IP-based solar trackers produce the best results compared to the other two. When only a few panels need to be tracked, LDR is the best option; however, when hundreds or thousands of panels need to be tracked, IP & LDR is the most cost-effective option. If we utilise a higher resolution camera, the solar panel's efficiency will increase. With the use of a PLC, thousands of solar panel trackers in a power plant may be controlled via IP and LDR. The energy generated by the solar panels will be used to power all of the system's passive components (Microcontroller, Servomotor etc.).

CHAPTER 7

WORKING ANALYSIS OF STABLE, LDR BASED AND GPS BASED TWO AXIS SYSTEM ON VARIOUS WEATHER CONDITIONS

7.1 Introduction

In given work energy harvesting assessments were piloted between a Static base PV arrangement and a two orientation Sun follower module with 10 watt solar panels. The Global positioning centred Sun follower arrangement was designed to confirm highest possible power production from the solar radiation. The GPS-based two-orientation sun following system was able to capture sunlight intensity from 6:00 to 19:00 solar time by following the sun's movement across the sky during the day. The engrossed power of the sun follower module using GPS was more than that of the LDR based two axis follower and static base panel, with the energy generated for two days by 10 watt panel on sun shine, hazy or cloudy and rainy day at 147.4Wh, 83.9Wh and 42.87Wh, respectively. The average amount of energy produced by the two axis-GPS sun following system was 4.021754Wh/day in 2021, which was 45.85% more than the average energy produced from the static base PV system.

Renewable energy sources like solar, biogas, wind etc. are among the most promising technological development in the advanced world. The demand for renewable energy sources is growing, while traditional fossil fuel energy is rapidly decreasing [2]. The annual change in production of renewable energy for different country is shown in Figure 7.1 [3].

Solar PV energy systems have advantage over other renewable energy because of their easy installation; maintenance and specially India have nearly 245 days of clear sky annually. The annual change in solar energy generation for China, France, Germany, USA, India and Australia is compare in Figure 7.2 [4].

Solar energy, obtained from the sun’s radiation, is a clean energy source with no CO_2 emissions. A photovoltaic (PV) system can reduce carbon emissions by using sustainable energy sources, thereby substituting the use of fossil fuels [160]. Due to growing fuel prices and an electrical shortage, the usage of solar energy is rapidly

increasing. Sunlight is among the most promising future energy sources since it is both clean and inexhaustible. Photovoltaic cells are used to convert solar radiation into useful electricity. Large amount of energy is available within the core of the sun, and a

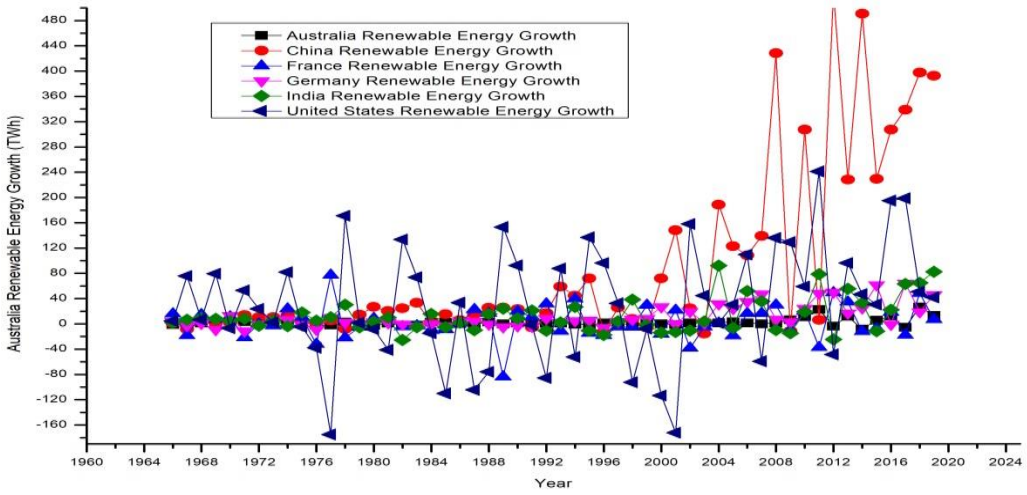

Figure 7.1 Renewable energy Annual changes in production

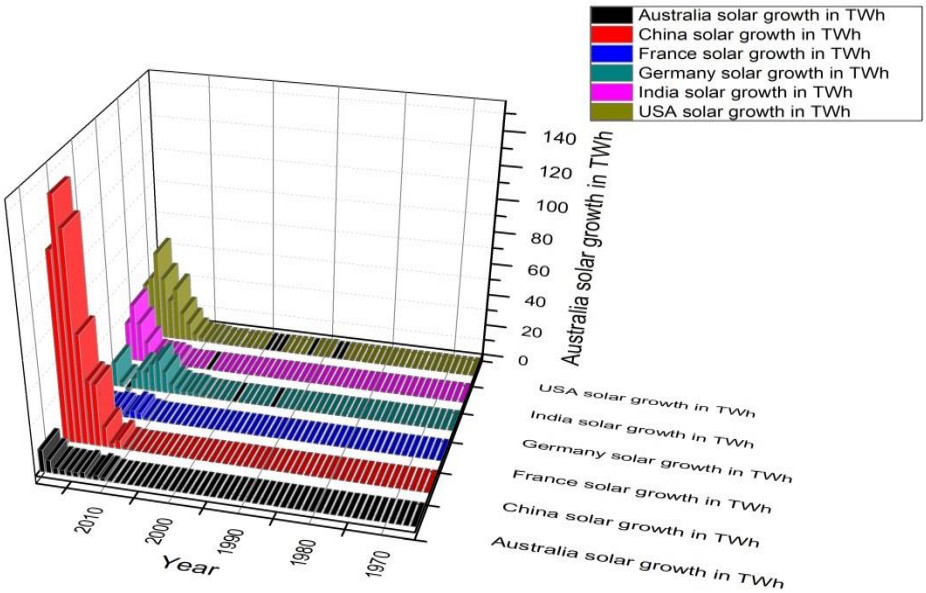

Figure 7.2 Solar energy generation Annual changes

solar tracking system in which the solar panel [143] is being positioned in perpendicular angle to the sunlight during day time, can be used to follow the path of the sun to obtain maximum power from it. Besides from the solar panel's alignment, solar system energy efficiency is directly influenced by brightness, the duration of time the panel is exposed to the sun, its geographic region, and the local climate.

Photovoltaic panels output is influenced not only by sun irradiation power, climate conditions, and ambient temperature, but also by the angle at which solar radiation strikes the PV panel [161]. To maximise energy harvest, a solar module focus perpendicular to the solar radiation. Additionally, because the sun passages crossways the sky throughout the year, a solar module must be capable to trace the sun's position [140].

Various solar harvesting systems described here on which hybrid system [57] having fixed panel and wind system is used to achieve maximum power. Here solar panel is primary and wind energy is secondary system. A one-axis sun following system (OASFS) [162] employing a low power regardless of motor speed. Their findings revealed that the OASFS had a low energy harvest because it could not monitor the sun when it moved in different directions. It could only travel in one direction: horizontally shown in Figure 7.3. The fundamental disadvantage of the one-axis following system is that it can only follow the sun as it moves across the sky on a daily basis, not as it moves across the sky on an annual basis. The following system's efficiency is also much diminished during cloudy days due to its rotation around only one axis

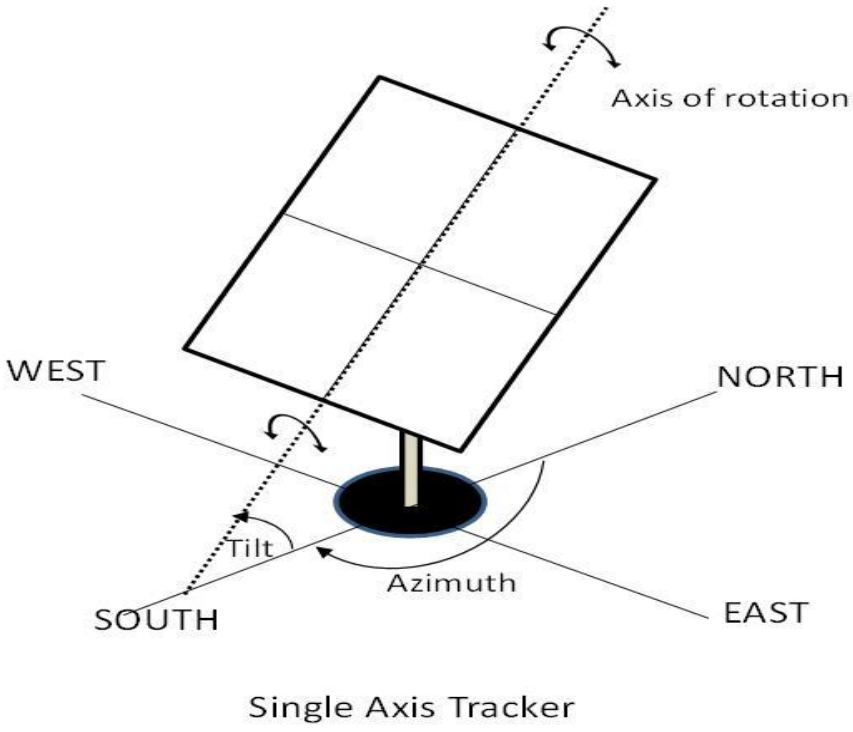

Figure 7.3 One axis sun following system

A two-axis sun following system (TASFS) is a technique that rotates two pivot points to track the sun in two different axes [133, 163]. Similarly found that employing a light sensor for a two-axis following system (TASFS_LDR) resulted in improved gathered energy, but the results were impacted by dust in poor conditions or dark clouds in the sky. A two-axis sun following system is a form of solar tracker that has two degree of free rotary axes that allow it to always align the PV panels and aim directly towards the sun panel. With the use of a microcontroller [164] the two-axis sun following system intelligently monitors the sun and captures maximum solar power. The quantity of power generated by a solar module is measured by the amount of radiation that reaches the panel and at what direction the radiation hits it [165] as shown in Figure 7.4.

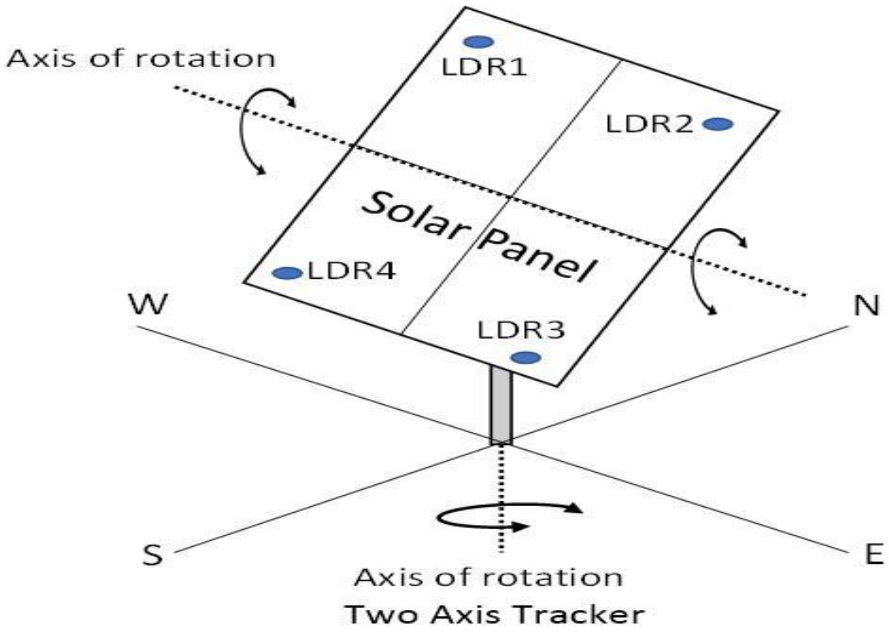

Figure 7.4 Two axis sun following system

An Image processing [145] and Soft computing [146, 166] base two axis sun follower system is also developed to enhance the power generation which is greater than that of conventional two axis solar follower. In image processing different steps like Gabor feature extraction [167], Histogram equalization [159], Wavelet transform [163, 147] is used after getting image of sun from camera and then centroid of sun is calculated to instruct both drivers to locate the solar panel exact towards the sun as shown in Figure 7.5.

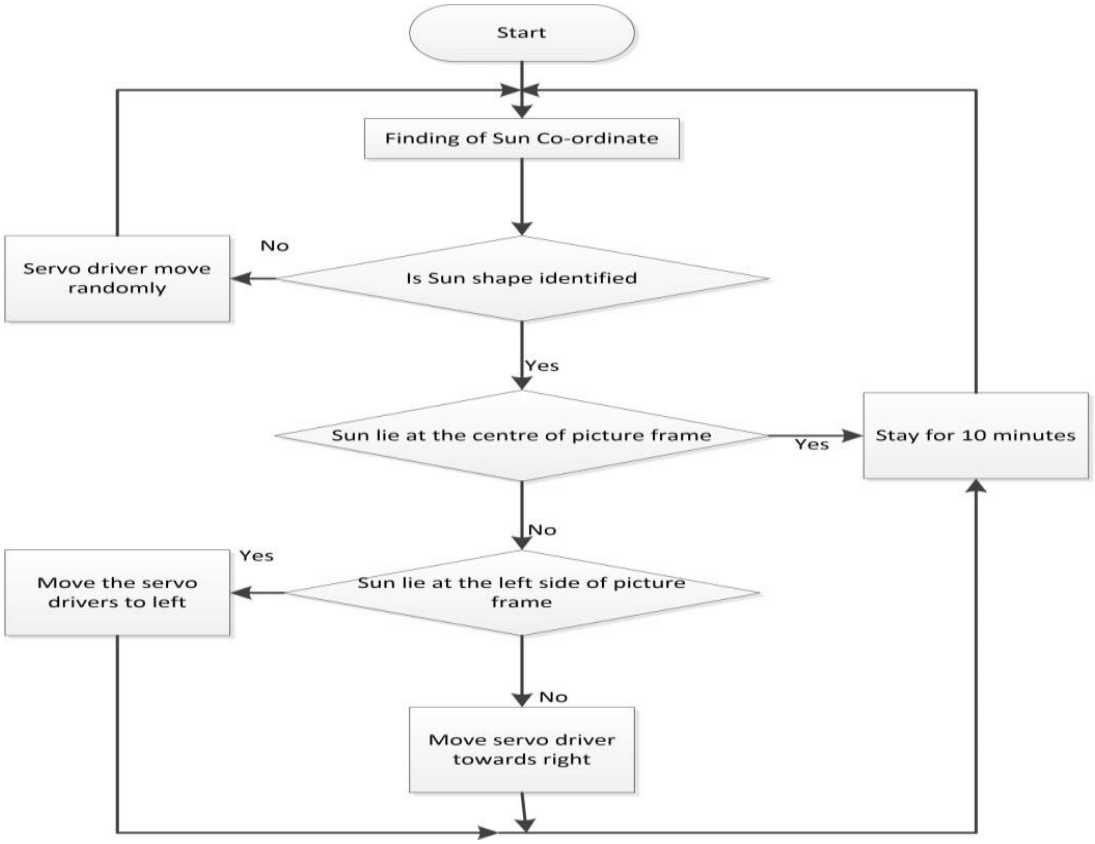

Figure 7.5 Image Processing based solar tracker

The volume of sun radiation that strikes on a panel is determined by solar irradiance (W/m^2). It is the most important factor to find Photovoltaic panel's efficiency. The amount of sun energy absorbed by Solar panel is dependent on the amount of solar irradiation absorbed. The Solar panel are always pointing the sun, ensuring that the optimum solar irradiance is turned into electric power during the day. As a result, the cloudy weather and electric discharge drawback is removed and as compared to a static system (SS) and TASFS_LDR, adopting GPS-based two axis follower (TASFS_GPS) can yield significant gains. With a fixed panel, there is just a small window of opportunity during the day when the panel is producing maximum output. Because they are only set at one angle, these PV systems are inefficient. This inefficiency can be reduced by constructing a GPS-based sun follower system that intelligently adjusts its orientation in response to the sun's motion. All detectors, along with the GPS device, were included in the microcontroller, and the power received using this approach was determined to be greater than the power collected using the conventional Photovoltaic systems. However, the system had the same issue as others in that the following system had to be manually positioned towards true-north to

enhance power production. Tilting and radiation detectors are used in the active sun following modules, which are located at different positions throughout the monitor to calculate the exact sun's location. Thanks to advancements in GPS and sensor technology, this is achieved by tilting the solar panel by utilising motors.

The primary goal of this study is to increase the production of Photovoltaic panels. By increasing the angle of incidence of solar energy on the PV array, this can be accomplished. A digital compass sensor, a real-time clock, and a GPS module are used in this following system to determine the position of the sun even when it is clouded. As a result, a two-axis sun follower system with GPS was created to ensure that the solar panel system stayed on course to generate maximum output.

7.2 Methodology

Three solar photovoltaic systems were built and examined on cloud day, sunshine day and rain session. The study calculated the monthly energy yields of the three systems (SS, TASFS_LDR and TASFS_GPS) as well as the averages of the three weather patterns for two days. The solar follower is a combination of an electromechanical system and the algorithm that controls it.

7.2.1 Geometrical Drawing: The sun's location in the sky is known to shift hourly and daily. As a result, two angles, the altitude angle and the azimuth angle, are used to determine the precise position of the sun in the sky, as illustrated in Figure 7.6. The altitude angle is well-defined as the angle measured perpendicular to the horizontal plane from the viewer's horizon to the sun. The azimuth angle, on the other hand, is observed clockwise from true north to the horizon point exactly beneath the sun. The azimuth and altitude angles are critical for tracking the sun effectively [168]. The design incorporates two linear motors. One is attached to the vertical edge for azimuth tracing that can revolve 360 degrees, while the other is attached to the horizontal for altitude tilt tracing from 0 to 90 degrees.

Sun path diagrams are representations of the sun's path across the sky on a flat surface. They're used to swiftly and easily determine the position of the sun at any time of day or year. In addition, the latitude has its own depiction of the sun's course. The sun rises from the east and sets to the west. The largest disparity between the

sunrise and sunset times is over 13:58 hours, which happens on 18 June 2021. The shortest day comes on 17 December 2021, with roughly 10:20 hours of daylight. The position of the sun at a given time and date of the year can be easily determined using a sun path polar and Cartesian diagram. The Figure 7.7 show 12 month sun position of Greater Noida, India where experiment is performed. The given location Sunrise sunset, dawn and dusk times is tabulated on Table 7.1 and analyse in Figure 7.8.

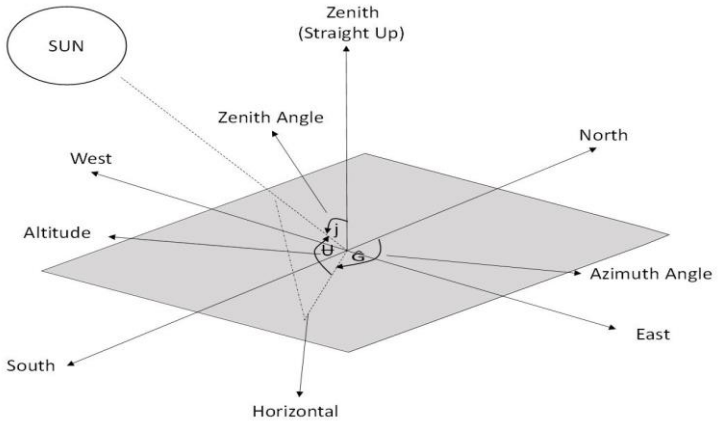

Figure 7.6 Altitude angle and the Azimuth angle

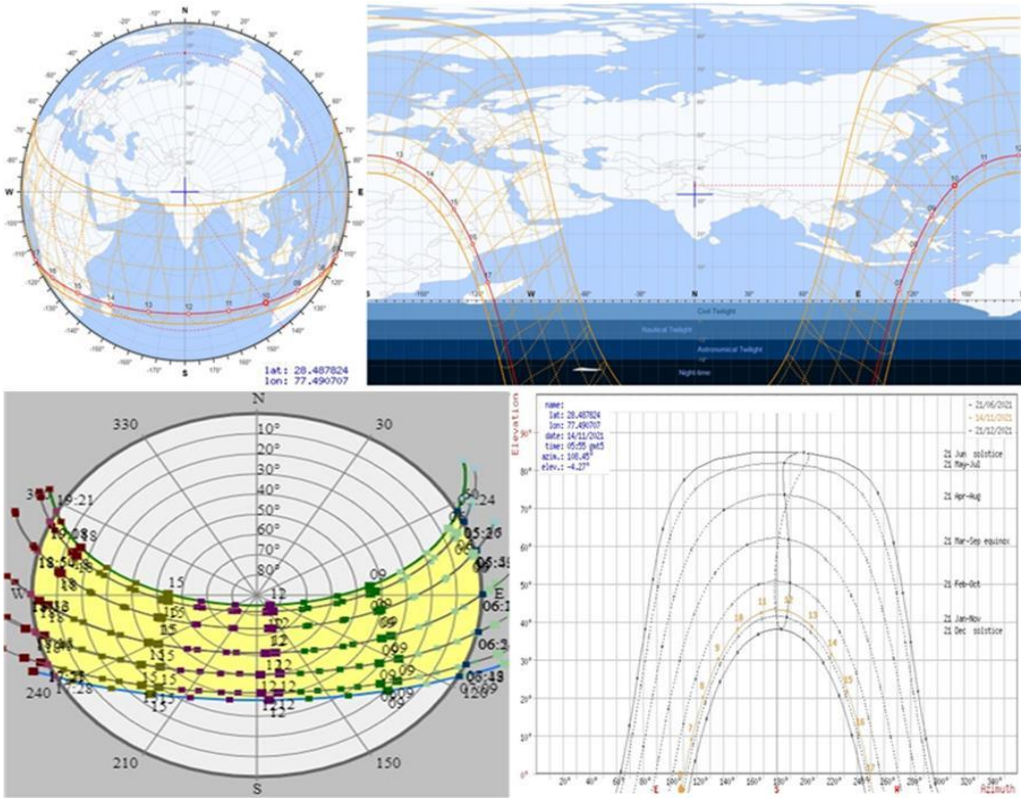

Figure 7.7 Sun Path Polar and Cartesian diagram for 12 month of 2021 with latitude and longitude

Table 7.1 Analysis of 2021 Sunrise, sunset, dawn and dusk times, Length of day

Date	SR	ST	L (Hr)	C (Hr)	DT	DU	L (Hr)	C (Hr)
-1 D	06:44	17:27	10:43	00:02 LN	06:19	17:52	11:33	00:02 LN
-1 WK	06:39	17:30	10:51	00:10 LN	06:15	17:54	11:39	00:08 LN
-2 WK	06:34	17:34	11:00	00:19 LN	06:10	17:59	11:49	00:18 LN
-1 MN	06:23	17:48	11:25	00:44 LN	05:59	18:12	12:13	00:42 LN
-2 MN	06:07	18:22	12:15	01:34 LN	05:43	18:46	13:03	01:32 LN
-3 MN	05:52	18:56	13:04	02:23 LN	05:28	19:21	13:53	02:22 LN
-6 MN	05:22	19:20	13:58	02:57 LT	05:03	19:32	14:29	02:58 LN
T	06:45	17:26	10:41	0	06:20	17:51	11:31	0
+1 D	06:46	17:26	10:40	00:01 ST	06:20	17:51	11:31	00:00 EL
+1 WK	06:50	17:24	10:34	00:07 ST	06:25	17:50	11:25	00:06 ST
+2 WK	06:56	17:23	10:27	00:14 ST	06:30	17:49	11:19	00:12 ST
+1 MN	07:07	17:27	10:20	00:21 SH	06:41	17:53	11:12	00:19 ST
+2 MN	07:14	17:47	10:33	00:08 ST	06:49	18:12	11:23	00:08 ST
+3 MN	06:59	18:11	11:12	00:31 LN	06:35	18:35	12:00	00:29 ST
+6 MN	05:29	19:06	13:37	02:56 LN	05:03	19:32	14:29	02:58 ST

MN, Month; WK, Week; D, Day; T, 17/11/2021; , Sunrise Time; ST, Sunset Time; DT, Dawn Time; DU, Dusk Time; L, Length; LN, Longer; ST, Shorter; SH, Shortest; LT, Longest; EL, Equal Length

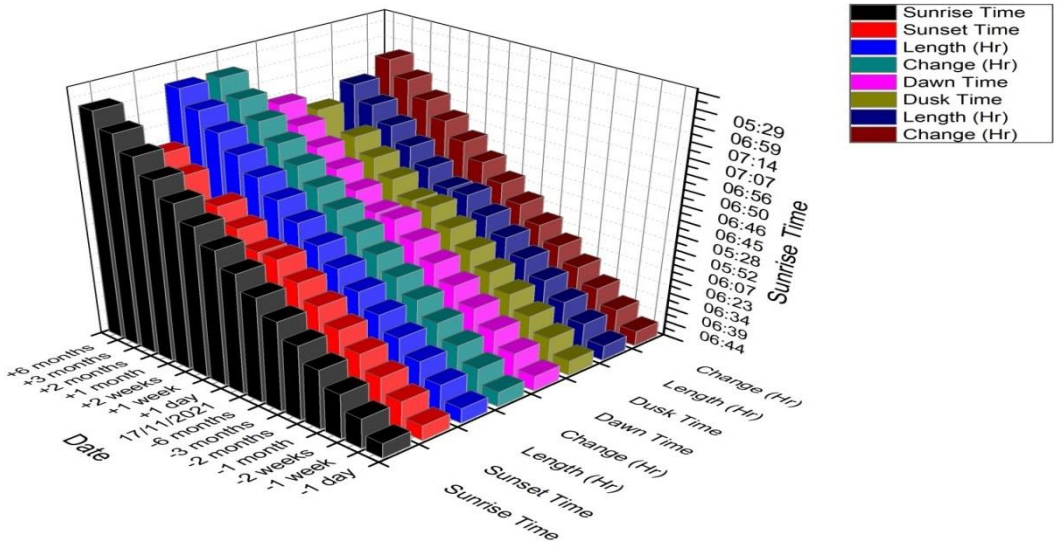

Figure 7.8 Sunrise, sunset, dawn and dusk times, Length of day

7.2.2 Hardware description: The Figure 7.9 shows a schematic diagram of the GPS-based two-axis sun follower's control scheme. The controller is designed to provide an appropriate command to the electromechanical system with the aim of optimize the solar cell's energy yield. The sun follower module is made up of transducer and a Raspberry Pi controller that regulate driver to move the solar array vertically and horizontally while keeping the sun's radiation aligned with the solar panel.

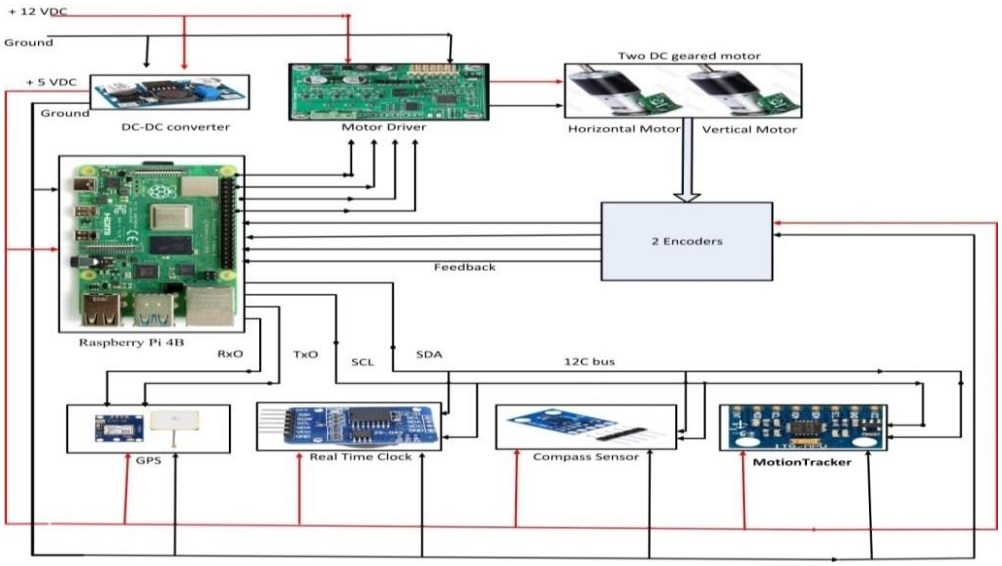

Figure 7.9 Schematic diagram of the control system of the solar tracker

A DC to DC converter converts the voltage from the 12 V DC battery source to 5V DC, which powers the Raspberry Pi, RTC module, Driver module, encoders, and transducer. The GPS module received 3.3 VDC from the Raspberry Pi's +3.3VDC pin and GRD pin, as well as 5 VDC from the DC/DC converter module. Furthermore, the GPS module is connected to the Raspberry Pi's TX0 and RX0 pins. The Raspberry Pi uses the I2C bus to receive signals from the two sensors. The RTC module is connected to the I2C bus's SCL and SDA pins. The Raspberry Pi's pins 9, 10, 11, and 12 send a signal to the driver module. For the azimuth and elevation motion of the sun follower, the feedback inputs from the two encoders were delivered to Raspberry Pi via pins 16, 17, 18, and 19. The vertical and horizontal motors are controlled by the 12V driver module.

The Raspberry Pi 4B, which serves as the system's main controller, controls the solar PV movement. Its purpose is to meet the procedure requirement and create the databank needed to track the sun's course. The Raspberry Pi is connected to the GPS module, which transmits the necessary signals to the system on a regular basis. Furthermore, a compass and tilt sensor module communicate with the microcontroller through the I2C protocol. The compass transducer detects the earth's magnetic field and delivers a measure that serves as a solar follower feedback signal. Figure 7.10 depicts the design's architectural system.

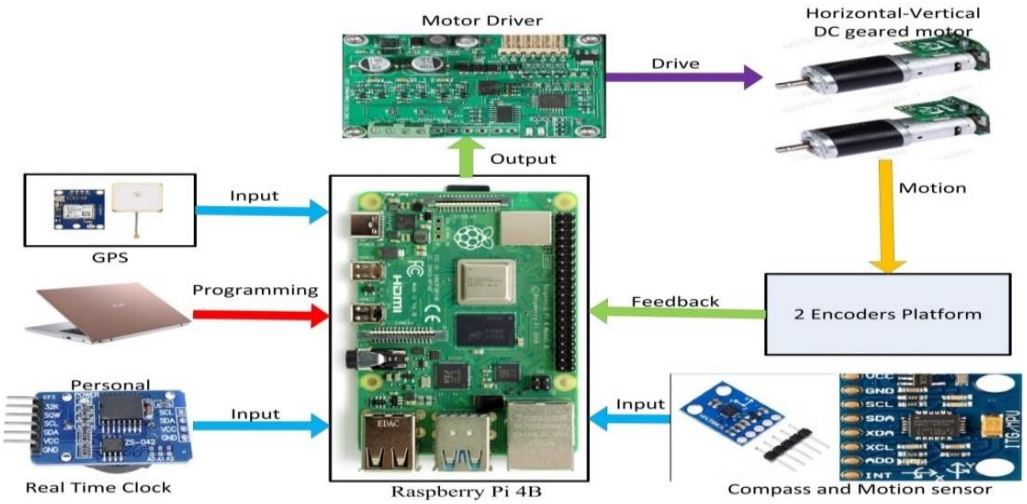

Figure 7.10 System architecture of the GPS Two axis solar Follower

7.3 Experimental Setup

Two photovoltaic solar systems were built and tested. PV systems are solar-powered devices that generate electricity straight from the sun [169]. Both the two-axis sun following system and the permanent mount Photovoltaic has their solar panel mounts to absorb sunlight. In addition, the solar tracker was outfitted with GPS, sensors, and motors to precisely follow the sun's azimuth and elevation angles, optimising sunshine exposure. Furthermore, the algorithm took into account the global location, season, and environment, as well as comparing the power efficiency of the produced sun following system to that of a stable system in the same place and environment.

7.3.1 Fixed Mount and Two Axis sun following System: It is required for the sun's rays to fall vertically on the solar panels [170]. As the non-tracking array or static mount system was slanted at an inclination angle of 23.01^0, facing north. 28^0 34' 48"N 77^0 19' 47.999E was the location of the solar tracker illustrated with Polar and Cartesian diagram shown previously in Figure 7.5. In order to monitor the sun, the solar tracker panels were constructed with a tilted angle ranging from 0 to 50 degrees. The linear actuator adjusts the angle of the solar panel rack by pushing and pulling it up and down shown in Figure 7.11. The design ensured that the linear actuator's length was precise.

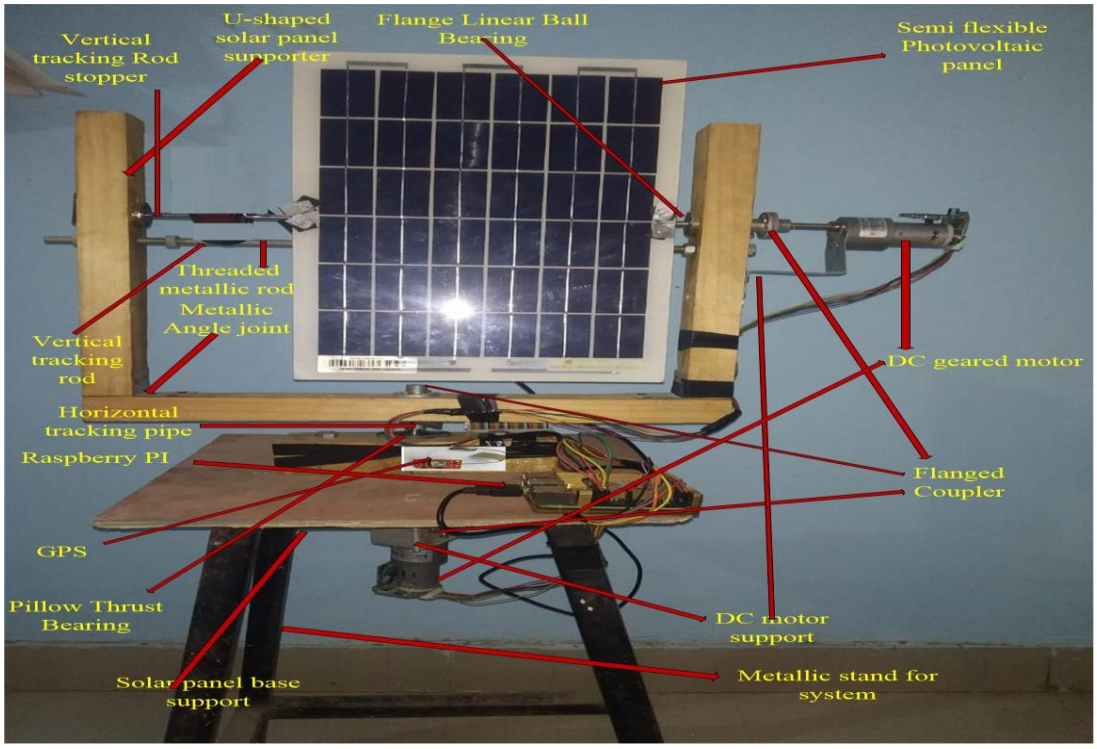

Figure 7.11 10 watt two-axis sun follower using GPS

In terms of energy producing capabilities and output, comparisons were done between the installed fixed system and the tracking system. The theoretical values of altitude and azimuth angles derived from sun-earth relationships are converted into digital commands for driving DC motors to the corresponding position, according to Yuan et al. [171]. GPS may be used to obtain the current time as well as the solar tracking system's latitude and longitude positions. In the azimuth and elevation angles, the panel moves around two degrees of freedom at the same time.

7.3.2 Algorithm of the Control System: Figure 7.12 depicts the system control programming algorithm. Latitude, longitude, and time, which may be obtained through the solar tracker's GPS, are used as inputs to the algorithm for estimating planetary positions. This algorithm was applied using an investigational based employing a three position control scheme, which was found to be efficient, in which a sun following algorithm for control of the PV module motion was designed. For energy generating performance measurement, a 30-minute loop was programmed in the microcontroller from 6:00 to 19:00 solar time. This loop represented the program's service mode in the control unit, which was detailed in the program's algorithm.

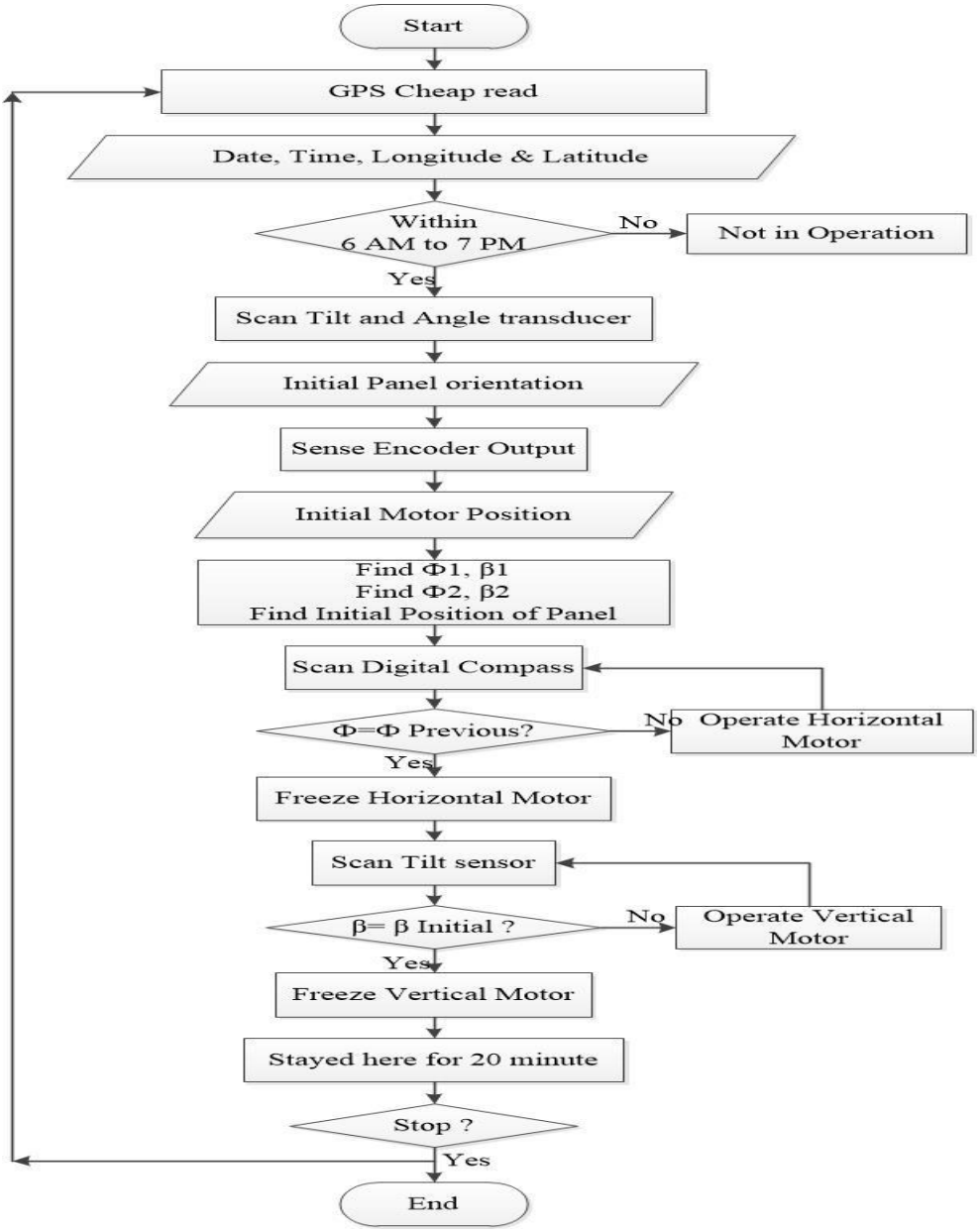

Figure 7.12 Control strategy flow chart

7.3.3 Astronomical Equation for GPS: The GPS determine latitude, time and longitude, which are utilized to determine the Sun's azimuth angle and zenith angle. The GPS practices an astronomical equation [191] to determine and estimate the Sun-following system's trajectory. The angle of declination (®) and the Equation of time (TQ) are the two primary astronomical equations employed here. Equation 7.1 estimates the fractional year (**Ω**) in radians.

$$\Omega = \frac{2\Pi}{365}\left[(YSD - 1) + \frac{(Hr - 12)}{24}\right] \tag{7.1}$$

Where, Hr stands for hour, while YSD stands for Year Day. In leap years, the number 366 is substituted for the number 365 in equation 7.1.

Equation of Time (TQ in minute) and Sun declination angle (® in radian) are calculated using fractional years (Ω) and equations 7.2 and 7.3 correspondingly.

$$TQ = 229.18(0.000075 + 0.001868\cos\Omega - 0.032077\sin\Omega - 0.014615\cos 2\Omega - 0.040849\sin 2\Omega \quad (7.2)$$

$$® = 0.006918 - 0.399912\cos\Omega + 0.070257\sin\Omega - 0.006758\cos 2\Omega + 0.000907\sin 2\Omega \quad (7.3)$$

Equation 7.4 calculates the offset time (OT) in minutes.

$$OT = TQ + 4 \times longitude - 60 \times Zonal\ Time \quad (7.4)$$

Where,

Standard time of India (IT) = Zonal time having time offset of UTC+05:30.
Equation 7.5 is used to calculate true solar time (ST).

$$ST = H \times 60 + \mathrm{MN} + (\mathrm{SC}\backslash 60) + \mathrm{OT} \quad (7.5)$$

Where,

H – 0 to 23 hours
MN – 0 to 59 minutes
SC – 0 to 59 seconds
η – Sun Hour angle (degree)
© = Angle of Latitude

Equation 7.6 is used to calculate the hour angle.

$$\eta = \left(\frac{ST}{4}\right) - 180 \quad (7.6)$$

Equation 7.7 is used to compute the sun zenith angle (j) using η, latitude, and ®.

$$\cos j = \sin © \sin ® + \cos © \cos ® \cos\eta \quad (7.7)$$

Equation 7.8 gives the sun azimuth angle (Ĝ, in degrees clockwise from north).

$$\cos(180 - \hat{G}) = \frac{\sin © \cos j - \sin ®}{\cos © \sin j} \quad (7.8)$$

7.4 Results and Discussions

All of the trials were carried out at Greater Noida City, India (28^0 34' 48"N 77^0 19' 47.999E). The amount of energy engrossed was found to be highest in the months of May to July, and then began to decline in the months of August to December, before rising again in January. During these three seasons, the solar tracker and fixed systems behaved differently.

Based on the values displayed in the solar tracking system's power inverter, the values were tabulated and graphs were created. On the specific month, the absorbed energy during sunny, overcast, and rainy days was tallied for six days. Experiments with the TASFS_GPS were conducted on overcast days (August 3 & 4, 2021), rainy days (June 6 & 7, 2021), and sunny days (May 26 & 27, 2021), and the findings were compared to the results from the TASFS_LDR and SS. During the experiment, the average energy produced by TASFS_GPS, TASFS_LDR and SS were recorded from 6:00 to 19:00 solar time. The actual readings were taken and recorded in a 20-minute interval, as reflected in Table 7.2.

The high and low energies were formed as a result of the season's bright, overcast, and wet days, which were accompanied by heavy, day-long clouds. The solar charge controller display screen was used to track and tabulate monthly energy yields. The highest and minimum monthly energies produced as a consequence of tabulation and analysis are summarised in Table 7.3 and expressed by Figure 7.13. The TASFS-GPS system produced more absorbed energy than the TASFS_LDR and SS type arrangement, according to the average energy values. The GPS solar tracker's energy collection was calculated to be 45.85 % higher than SS and 14.93% greater than TASFS_LDR. The tracking error of TASFS_GPS and TASFS_LDR are 0.10% and 0.11% respectively.

Table 7.2 Summary of the two days' average energy generated in Sunshine, Cloudy and Rainy day by SS, TASFS_LDR and TASFS-GPS

Solar Time	Average values of 2 Sunshine days			Average values of 2 Cloudy days			Average values of 2 Rainy days		
	TASFS-GPS (Wh)	TASFS_LDR (Wh)	SS (Wh)	TASFS-GPS (Wh)	TASFS_LDR (Wh)	SS (Wh)	TASFS-GPS (Wh)	TASFS_LDR (Wh)	SS (Wh)
06:00	1.6	1.2	0.7	0.7	0.5	0.1	0.6	0.4	0.1
06:30	1.9	1.5	1.1	1.4	1.1	0.2	1	0.8	0.2
07:00	2.7	2.2	1.3	2.3	2	0.3	1.3	1.1	0.22
07:30	3.8	3.5	1.7	2.9	2.5	0.4	1.7	1.3	0.44
08:00	4.7	4.2	2.5	3.6	3.1	0.6	2	1.7	0.8
08:30	6.9	6.2	3.6	3.9	3.3	1.7	2.4	1.9	1.2
09:00	7.2	7.1	4.6	4.2	4	2.5	2.6	2.2	1.4
09:30	8.2	8	5.8	4.4	4.1	3	2.7	2.4	1.9
10:00	8.8	8.3	7.4	4.6	4.2	3.2	2.8	2.6	2.2
10:30	8.9	8.6	8.4	4.8	4.4	3.8	2.4	2.35	2.3
11:00	9.2	9	9.1	4.9	4.6	4.2	2.3	2.25	2.22
11:30	9.3	9.2	9.2	5.1	4.8	4.3	2.2	2.17	2.12
12:00 Noon	9.4	9.3	9.3	5.2	4.9	4.2	2.2	2.19	2.17
12:30	9.6	9.4	9.2	5.3	5	4.1	2.3	2.18	2.12
13:00	9.5	9.3	9.1	5.2	4.8	3.8	2.4	2	2.03
13:30	9.1	8.9	8.8	4.8	4.3	3.5	2.2	1.9	1.8
14:00	8.1	7.5	7.3	4.3	4.1	3	1.9	1.6	1.6
14:30	6.9	6.4	5.4	3.7	3.4	2.3	1.7	1.4	1.3
15:00	5.6	5.1	3.9	3	2.6	1.8	1.5	1.3	1.1
15:30	4.3	4	2.7	2.4	2.1	1.7	1.4	1.1	1
16:00	3.3	3.1	1.7	2.1	1.9	1.5	1.2	0.9	0.8
16:30	2.7	2.2	1.1	1.8	1.6	0.9	0.9	0.6	0.5
17:00	2	1.5	0.8	1.5	1.3	0.7	0.6	0.5	0.3
17:30	1.3	1.1	0.6	0.9	0.4	0.5	0.3	0.2	0.1
18:00	0.9	0.5	0.4	0.4	0.2	0.3	0.1	0.09	0.04
18:30	0.8	0.4	0.3	0.3	0.1	0.2	0.09	0.06	0.03
19:00	0.7	0.2	0.3	0.2	0.8	0.1	0.08	0.05	0.02
Total Energy Generated	147.4	137.9	116.3	83.9	76.1	52.9	42.87	37.24	30.01

Table 7.3 Average energy generated in 2021 by the two systems

System Type	Month of Maximum Energy Produced (Wh)	Month of Minimum Energy Produced (Wh)	Sum of Energy produced in year 2021 (Wh)	Average Energy per day (Wh)	Tracking Error (%)
TASFS_GPS	147.4	42.87	1447.83144	4.021754	0.10
TASFS_LDR	137.9	37.24	1260.07668	3.500213	0.11
SS	116.3	30.01	992.71476	2.757541	-

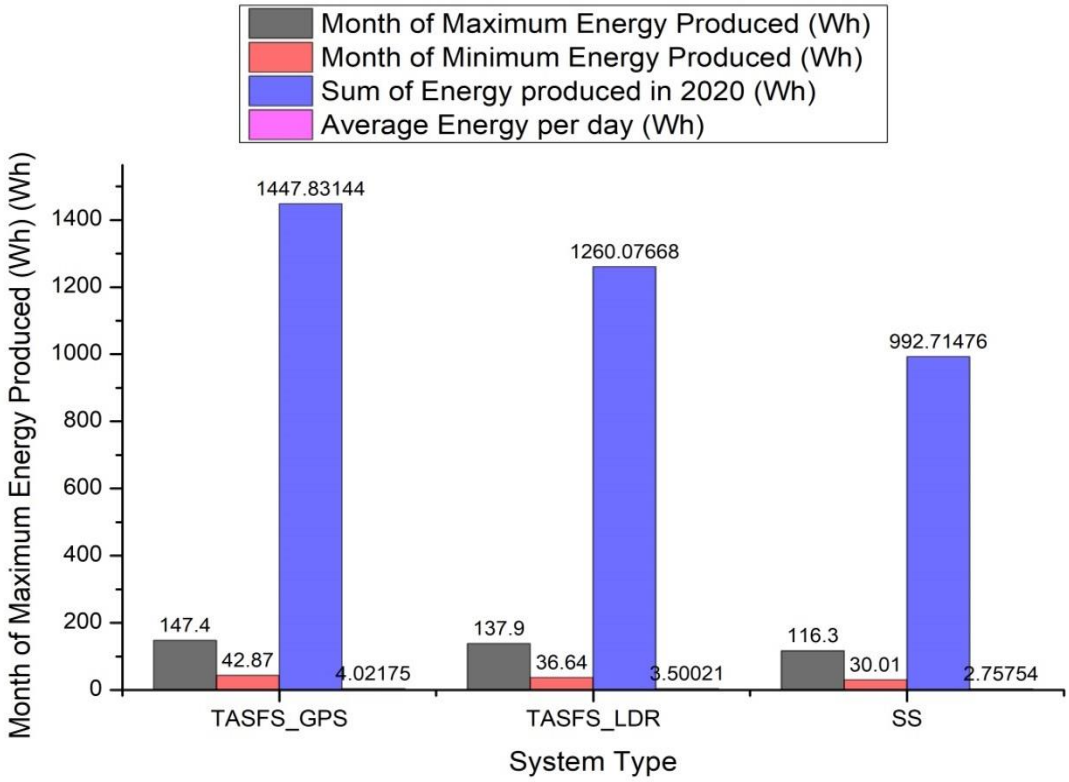

Figure 7.13 System comparison graph

Equation 9 gives the average panel output efficiency.

$$n_{Avg} = \frac{\sum(P_Y - P_X)}{P_X} \times 100 \quad (9)$$

Where,

P_1-The SS panel's power output

P_2 – The TASFS_LDR panel's output

P_3-The SFS-GPS panel's Power output

So the TASFS-GPS power output efficiency is greater than SS is given by equation 10, where, $\Sigma P_Y = \Sigma P_3$ and $\Sigma P_{X=} \Sigma P_1$.

$$n_{Avg(TASFS\_GPS-SS)} = \frac{4.021754 - 2.757541}{2.757541} \times 100 = 45.85\% \quad (10)$$

TASFS-GPS power output efficiency is greater than TASFS-LDR is given by equation 11, where, $\Sigma P_Y = \Sigma P_3$ and $\Sigma P_{X=} \Sigma P_2$.

$$n_{Avg(TASFS\_GPS-TASFS\_LDR)} = \frac{4.021754 - 3.500213}{3.500213} \times 100 = 14.93\% \quad (11)$$

TASFS-LDR power output efficiency is greater than SS is given by equation 12, where, $\Sigma P_Y = \Sigma P_2$ and $\Sigma P_{X=} \Sigma P_1$.

$$n_{Avg(TASFS\_LDR-SS)} = \frac{3.500213 - 2.757541}{2.757541} \times 100 = 26.93\% \quad (12)$$

The comparison result of above system efficiency equation is expressed by Figure 7.14.

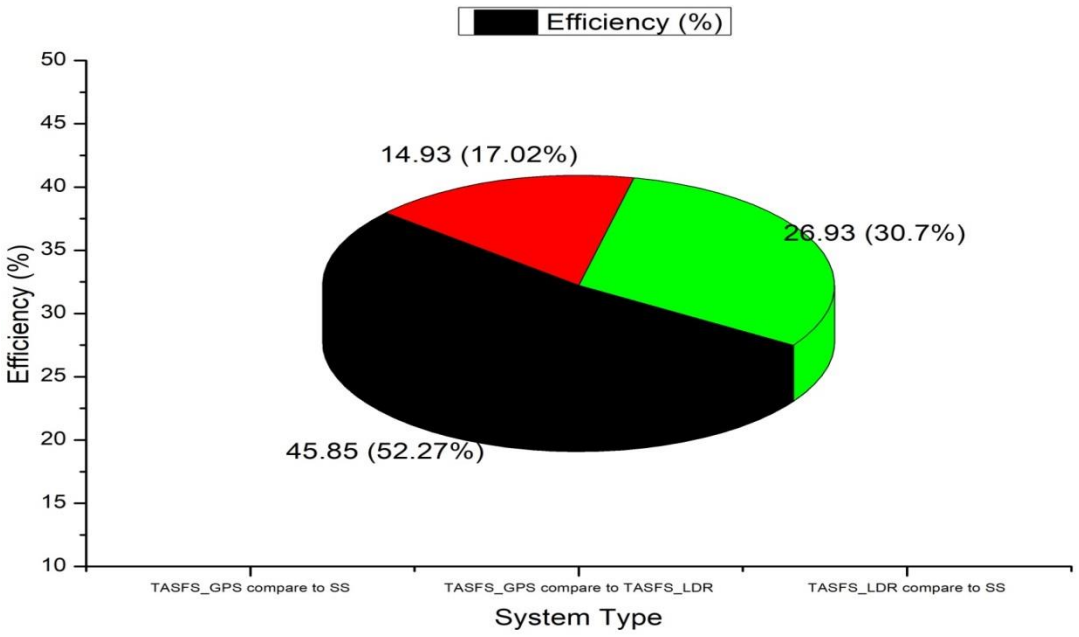

Figure 7.14 Output efficiency of three systems

7.4.1 Solar Energy Produced on Sunny Days: While all solar systems produced more energy on sunny days, the TASFS_GPS harvested more solar energy from 9:30 to 14:30 solar time, due to the system capacity to correctly catch the sun's energy

through its solar tracker. When the sun was at a 90-degree angle and the sunlight angle was the same for the three solar systems, the TASFS_GPS were nearly equal to the TASFS_LDR and SS from 11:30 a.m. to 12:00 noon. Due to its capacity to track the sun as it travelled from east to west with minimum tracking error, TASFS_GPS regularly captured more energy than TASFS_LDR and SS in the afternoon. When considering a tracking system, the most critical thing to consider is energy gain.

When compared to a stationary system, the energy gain refers to the increase in energy generated by the sun following system. The SFS was designed in such a way that it can capture solar energy from all angles. On sunny days, Figure 7.15 displays TASFS_GPS (May 26 & 27, 2021) exceptional solar energy trapping capabilities.

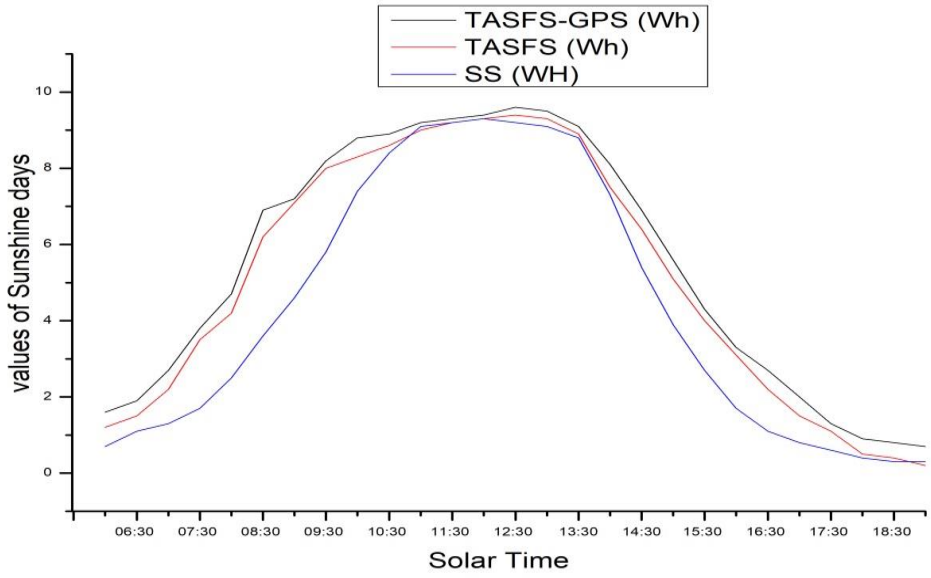

Figure 7.15 Average energies produced by the TASTS_GPS, TASFS_LDR and SS during two sunny days

7.4.2 Solar Energy Produced on Cloudy Days: Figure 7.16 reveals significant differences in energy harvesting within the TASFS_GPS, TASFS_LDR and the SS on cloudy days (August 3 & 4, 2021), with the SFS obtaining more energy. There was no oscillation in the energy obtained because the tracking was done in real time.

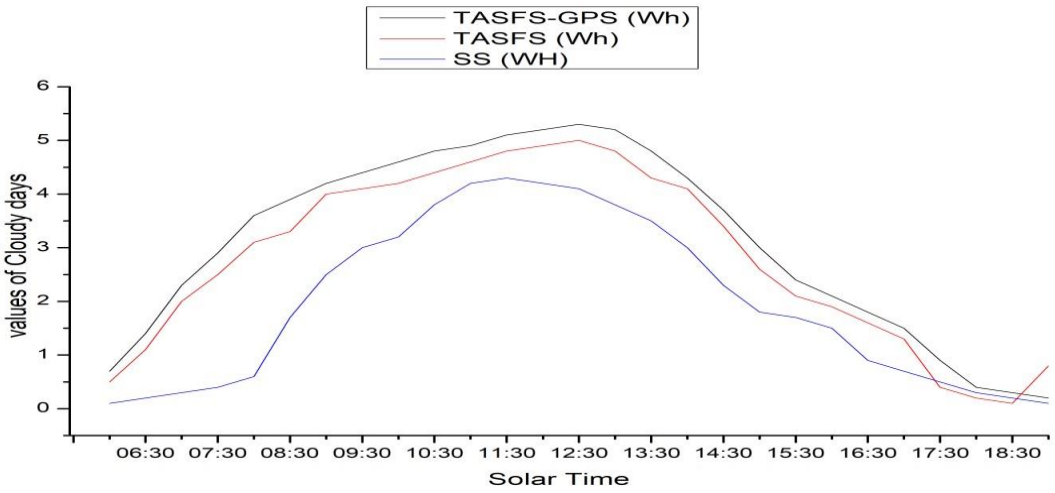

Figure 7.16 Average energy generated by the TASFS_GPS, TASFS_LDR and SS during the two cloudy days

3.4.3 Solar Energy Produced on Rainy Days: The data on energy harvested during wet days (June 6 & 7, 2021) from 6:00 to 19:00 solar time, when the sun rose swiftly in the morning, shows that the TASFS_GPS values are substantially bigger than the TASFS_LDR and SS values, as shown in Figure 7.17.

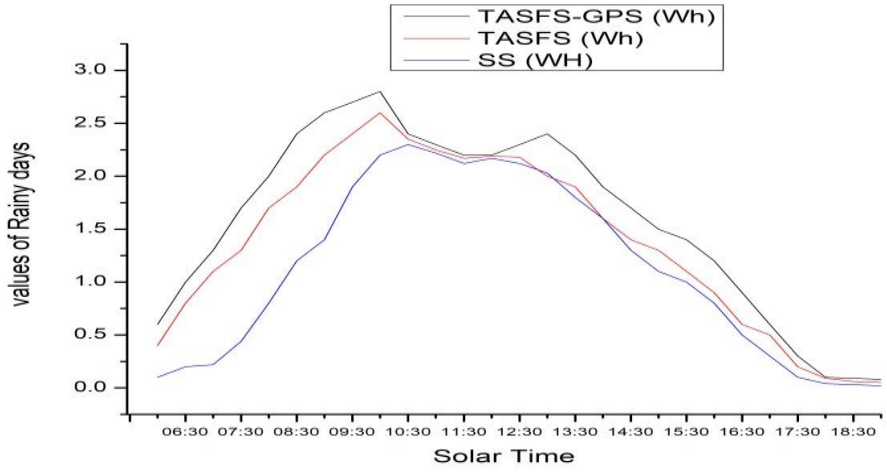

Figure 7.17 Average energy generated by the TASTS_GPS, TASFS_LDR and SS on the two rainy days

The TASFS_GPS absorbed more energy than the TASFS_LDR and SS solar system, even during wet days. The TASFS_GPS was only nearly equal to the TASFS_LDR and SS from 11:30 a.m. Figure 7.18 compares total energy production under three different weather conditions.

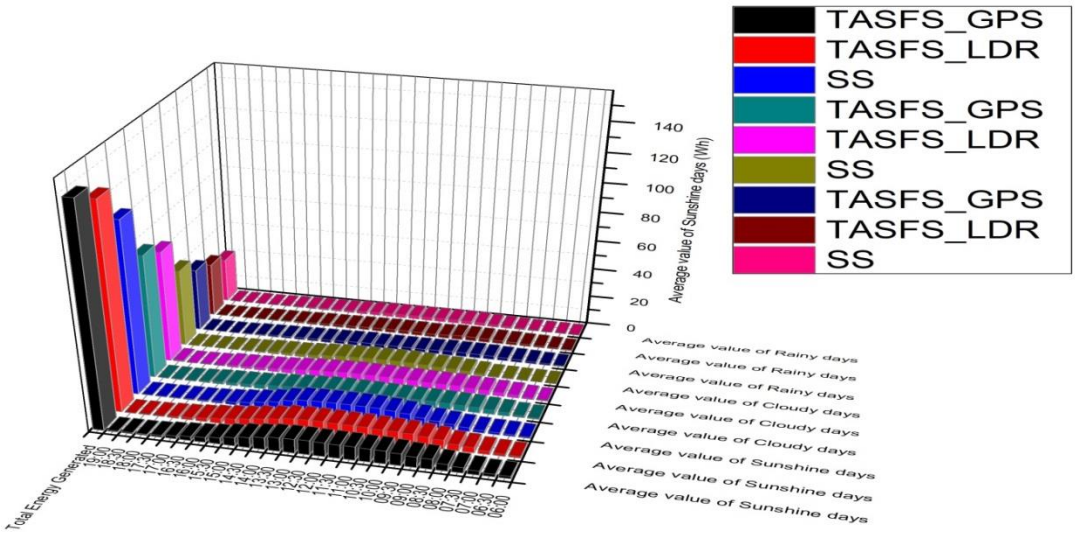

Figure 7.18 Comparison of the energies generated from the TASFS_GPS, TASFS_LDR and SS on different weather conditions

7.5 Conclusion

Even on cloudy days, the two-axis sun following with GPS delivered better energy yield than the SS and TASFS_LDR. The energy yield of the two-axis sun following was more than 45.85% higher than the fixed mount system and 14.93% more than TASFS_LDR. The tracking error of TASFS_GPS and TASFS_LDR is 0.10 and 0.11 respectively. The most crucial element to consider when evaluating a solar tracking system is its energy yield. The use of lightweight materials for the building of the GPS solar tracker is another area of research that can be pursued to improve the GPS solar tracker. Furthermore, more research into the use of artificial intelligence approaches to regulate the GPS location of the PV panel for the solar tracker and PV panel, employing flexible monocrystalline materials, can be done.

CHAPTER 8

SOFT COMPUTING & IOT BASED SOLAR TRACKER

8.1 Introduction

The importance of solar energy is to increase the efficiency of the Solar Panel by using a primitive solar tracking system. Using the global positioning system (GPS), artificial neural networks (ANN), and image processing (IP), we proposed a solar positioning system. The sun's azimuth angle is calculated by global positioning system data, which includes latitude, date, longitude, and time. The IP is utilised a sun image, from which the centre quadrate of the sun image conference is determined, and then the centroid of the sun is compared to the GPS quadrate to choose the best tracking point. Weather conditions and situations are monitored using AI decision-making and IP algorithms. Experimental effects are used to analyse and establish the offered advance adaption, which might then be stored on the cloud carrier's memory for systematisation. When compared to a stable system and a conventional two-axis solar following system, the proposed method improves power gain by 59.21 % and 10.32 %, respectively. The azimuth angle error of the IoT-based Two-axis solar following system is lowered by 0.20 degree due to the reduced tracking error.

Inadequate electricity supply and rapid urbanisation around the world have forced people to look for alternative methods of energy production. Energy from the sun is one of the most widely used and constant sources of energy because it is abundant and could potentially replace other fuels such as fossil [172]. Because solar output varies with changes in location, site selection is one of the most important considerations for a power plant that harnesses solar energy [173].

Renewable energy expansion has successfully captured worldwide interest in the energy production industry these days. The three main elements that contribute to their relevance are the continued rapid consumption of global non-renewable resources, the finite nature of fossil fuel reserves, and the need to regulate pollution. India has a great potential of 245 days of clear and sunny sky, thus we may simply reduce our reliance on fossil fuels. Solar energy in the country is predicted to be around 750 GWp [145] by the National Institute of Solar Energy and the Ministry of

New and Renewable Energy at the highest level. India, on the other hand, recently achieved a grid-connected solar energy capacity of 36.62 GW through October 31, 2020 [174].

Solar PV systems are an essential source of energy that can create clean energy. Solar trackers have become a popular addition to solar PV systems. Because of its capacity to track the sun's changing location in the sky, photovoltaic dual axis module can gain 25 to 45 % more energy [175]. Despite the rise in system cost, this increment is sufficient to make a profitable proposition. PV panels with trackers follow the movement of the sun. These trackers must change their orientation in response to the sun's location in order to capture more energy [176]. The concentrated solar frameworks don't generate energy until they're precisely aligned with the Sun [177].

The scale of the framework, electric rates, land limits, government incentives, scope, and climate all play a role in deciding on a sun-based tracker. Sun-based trackers with a single hub rotate one pivot in a single direction. Flat, vertical, shifting, and polar adjusted single-pivot trackers are among the various types of single-pivot trackers. Because they may move in two different orientations, double hub trackers always point towards the sun. These sun trackers add in obtaining the increased solar directed energy [150].

There are also a few methods for powering solar-powered trackers. Trackers [178] are latent or passive move from a packed gas liquid to one side or the other. Direct dynamic solar oriented trackers are prepared by engines and equipment using methods for a regulator that reacts to the sun's location.

Regardless, there are a few flaws with solar-powered trackers. Adding a sun-oriented global positioning system [179] means more hardware, moving parts, and cog wheels, all of which will demand routine maintenance and repair or replacement of broken parts.

Mohaimin et al. [180] constructed a low-power PV system and compared their findings based on external or self-power. According to the author, a two-axis self-powered system saves 18% compared to a two-axis system with external power. Low internal powered two-axis PV systems consume over 82.5% of energy while producing only 10 %. In the case of single-axis, consumption is 31.7 %, while

production is only 5 to 9 %. As a result, low-power PV panels should be avoided in order to maximise power generation. Chan and Zalani [181] create a sensor-free two-axis solar follower using an Arduino microcontroller.

The work's major goal is to put up a monitoring system that uses the most cost-effective and precise solar coordinates possible for optimal efficiency. Concentrated photovoltaic (CPV) panels are more efficient than regular PV [182] panels because they use optics to concentrate a large amount of sunlight on the photovoltaic panel to create more power. Based on camera-captured photos, the design and performance of the solar positioning system are suggested. Using DIP and a GPS [183] and artificial neural network, such photos were used to calculate the sun azimuth angle. These characteristics are supplied to the microcontroller via IoT [184] in order to obtain the exact location of the sun coordinate for maximum energy. The proposed method can lessen the reliance on LDR tracking, which is easily impacted by electric discharge caused by bad weather. Image-based tracking [185] and ANN-based weather forecasting [186] were also used to refine a solution for cloudy weather.

8.2 Objective of the Work

The following is the main idea of the paper: the system uses GPS [141], ANN [187], and DIP [188] to handle the following problems that commonly occur in solar trackers:

- Solar tracking system with DIP-based feed-forward.
- AI predicts solar module production more accurately than the DIP method, which approximates tracking control.
- The panel's output is continuously monitored via IoT.
- A cost-effective solution is provided.

8.3 Research Methodology

The Arduino board is a microcontroller that runs on the IDE software. It is a central processor and a 32-bit Intel Pentium-class system that is based on a chip. Its mainframe is built on an Intel architecture that is intended to run hardware. With Arduino shields made for Uno R3, all software must be pin-adaptable. The Arduino board is designed to aid shields that run on 3.3V or 5V.

As a result, a digital sensor and GPS are used to collect real-time information about the sun, and an Arduino Uno is used to support cloud computing with Wi-Fi supporting mini PCIs slots. It will flow into an IoT-based solar monitoring system, allowing all of the sensors to be readily connected. The MPPT-based technique using LDR sensors is stored in "Thingspeak" virtual storage, and this information is used to record sun images at various time portals during the day. Internet protocol methods, artificial intelligence approaches, and the equipment application software required for monitoring and managing the panels for optimal effectiveness and affordability were chosen as tools for this project. A vision camera that rotates with the help of a servo motor system monitors the sun in real time. With the help of live GPS coordinates, you can see the azimuth angle, latitude, longitude, and altitude. The readings and algorithm obtained will be used in conjunction with IoT and a microcontroller to automate sun tracking.

8.3.1 Materials and Methods: The tracking system is made up of DIP, ANN, GPS, and AI machines that the operating system uses to track and gain energy. The image sensors that operate the servo motors assembly depicted in Figures 8.1 and Figure 8.2 conduct the tracking. The height of the panels to track the sun is determined by the azimuth angle. Figure 8.3 shows how to transform an RGB image of the sun into a grey image. We don't consider the RGB image in our work because its DIP will take longer to process due to its three co-ordinates or RGB image. The grey image is made up of two co-ordinates that are represented digitally as 0 or 1. When compared to RGB images, the DIP time for grey images is shorter.

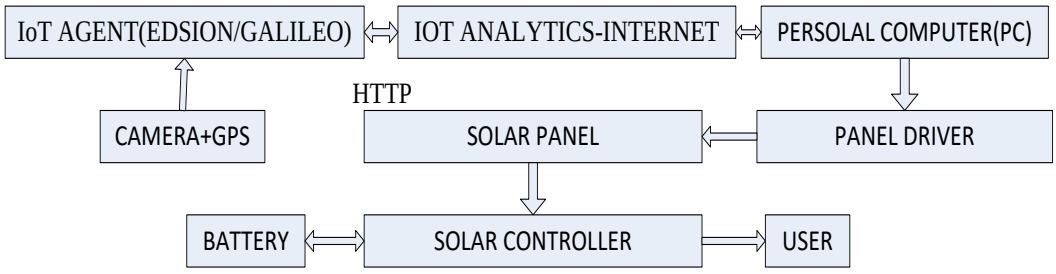

Figure 8.1 Solar Following System process using IOT

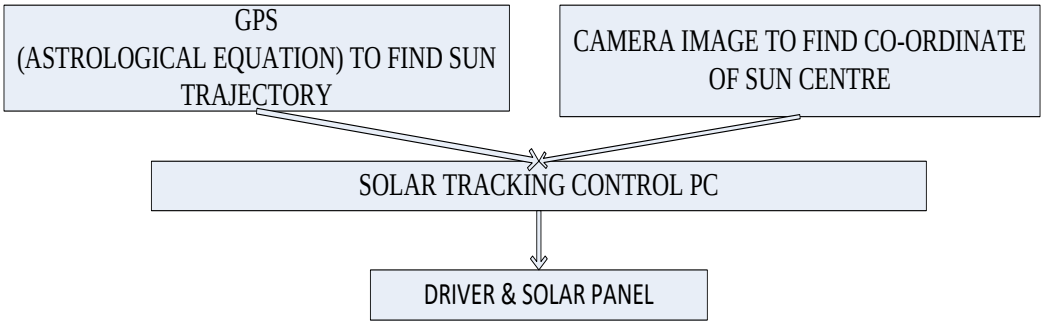

Figure 8.2 Sun Image Acquisition Based on IoT Solar Following System

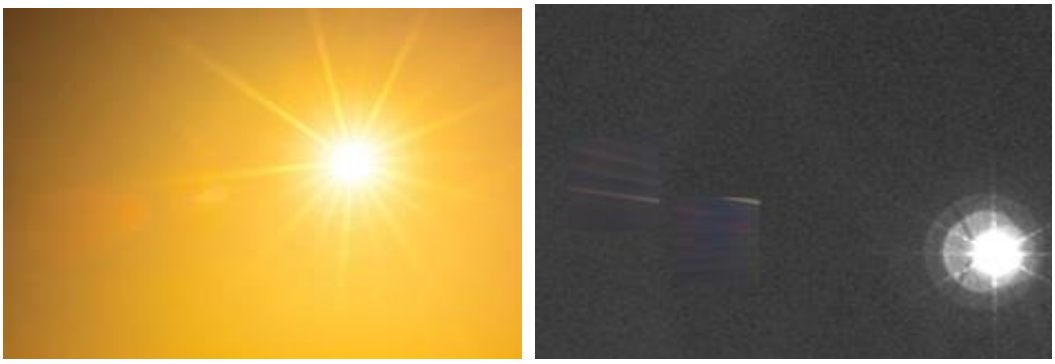

Figure 8.3 Normal & their gray scale sun image by IoT based solar follower DIP techniques

Image processing can be defined as a method of performing operations on a photograph in order to produce a accurate image data or extract useful information from it. It's a signal process in which the input is a picture and the output is picture information.

8.3.2 Digital Image processing: DIP processes digital photos using a digital computer and the appropriate algorithm. It allows a wide range of methods to be used as input data, and it prevents problems like noise and distortion from occurring throughout the process. DIP approaches have been developed and are thriving in order to optimize the machine. The DIP control techniques are used on the sun picture to help track the sun. Accurate and precise tracking is a basic need. It is concerned with picture conversion, acquisition, and processing. Preprocessing, feature extraction [159], and data transformation selection are the steps of the technique. For the sake of classification and recognition, this will be processed more easily and constructively.

Pre-processing - Pre-processing is a well-known term for operations involving images at the lowest level of abstraction, with intensity images as both input and output. Preprocessing creates image data with acceptable distortions suppressed. It enhances some image qualities that are important for further processing and analysis. Cropping, filtering, intensity-adjustment, histogram-equalization [189], brightness thresholding, cleaning regions of a binary image, and detecting edges are examples of pre-processing procedures.

Picture smoothing filters - Image smoothing decreases image noise [190]. It is a key picture enhancement method that reduces noise from the image. As a result, performing within spatial co-ordinate and frequency is an essential feature of image-processing software. The Gaussian, median, mean, maximum, minimum, non-local means, percentile, and rank filters are all included. These can be used to minimise image noise, but they must be used with caution to avoid altering crucial information in the image. Smoothing filters, both linear and non-linear, are used to remove blurring from images. Sobel, directional mask, and prewitt are examples of other filters.

8.3.3 Wavelet Transformation: Edge is the principle of high frequency detail in a digital image. Noise is removed ineffectively by conventional filters, so it is necessary to eliminate the noise without affecting the edges. The Wavelet program identifies the appropriate frequency range based on the indicator's oneness. The spectrum is then converted to a frequency band, which amplifies the decision. The Wavelet Transform reduces visual noise. It examines de-noising as hard and soft thresholding based on orthogonal Wavelet Transform [147] and operates on various scales. A wavelet transform in MatLab is used to demise the image's edge spotting and noise suppression.

8.3.4 GPS System

The GPS system, which stands for global positioning system, can determine longitude, time, and latitude positions, which are then used to calculate the sun's zenith and azimuth angles. The GPS uses an astronomical equation [191] to determine and estimate the Sun-following system's trajectory. The declination angle (®) and the time equation are the two primary astronomical equations

employed here (TQ). The fractional year (Ω) is calculated in radians using the equation (8.1).

$$\Omega = \frac{2\Pi}{365}\left[(\mathrm{YSD} - 1) + \frac{(\mathrm{hR} - 12)}{24}\right] \tag{8.1}$$

YSD stands for Year Day. In leap years, the number 366 is used instead of 365 shown in equation (8.1). Time equation (TQ in minute) and angle of Sun declination (® in radian) are calculated using fractional years (Ω) as indicated in (8.2) and (8.3), respectively.

$$\mathrm{TQ} = 229.18(0.000075 + 0.001868\cos\Omega - 0.032077\sin\Omega - 0.014615\cos 2\Omega - 0.040849\sin 2\Omega \tag{8.2}$$

$$® = 0.006918 - 0.399912\cos\Omega + 0.070257\sin\Omega - 0.006758\cos 2\Omega + 0.000907\sin 2\Omega \tag{8.3}$$

The offset time (OFT) calculated in minutes given by equation 8.4.

$$\mathrm{OT} = \mathrm{TEQ} + 4 \times \mathrm{longitude} - 60 \times \mathrm{Zonal\ Time} \tag{8.4}$$

Where Indian Standard time (IST) = Zonal time having time offset of UTC +05:30. True Solar time (ST) is derived by (8.5).

$$\mathrm{ST} = \mathrm{H} \times 60 + \mathrm{MN} + (\mathrm{SC}\backslash 60) + \mathrm{OFT} \tag{8.5}$$

Where H – 0 to 23 hour, IN – 0 to 59 minute, SC – 0 to 59 second, η - Hour angle (degree) of Sun & © = Latitude angle. Hour angle is estimated by (8.6).

$$\eta = \left(\frac{\mathrm{ST}}{4}\right) - 180 \tag{8.6}$$

Sun zenith angle (j) is calculated by using η, latitude & ® represented by (8.7).

$$\cos \mathrm{j} = \sin © \sin ® + \cos © \cos ® \cos \eta \tag{8.7}$$

Sun azimuth angle (Ĝ, degree clockwise from north) is given by (8.8).

$$\cos(180 - \hat{G}) = \frac{\sin © \cos j - \sin ®}{\cos © \sin j} \quad (8.8)$$

8.3.5 Artificial Intelligent (AI) Classification Technique: Figure 8.4 shows a multilayer perceptron with input, hidden, and output layers in a neural network diagram. Predictable vector values (X1...Xp) and a bias of 0.1 are used in the input layer, which normalise within a -1 to 1 span given to each hidden layer node. A transfer function is given the weight, and the result is hj. The output layer nodes receive the hidden layer outputs, which are multiplied by a weight, and the resulting weights are added together to produce the output vj at the outer layer. 'y' is the neural network's real value.

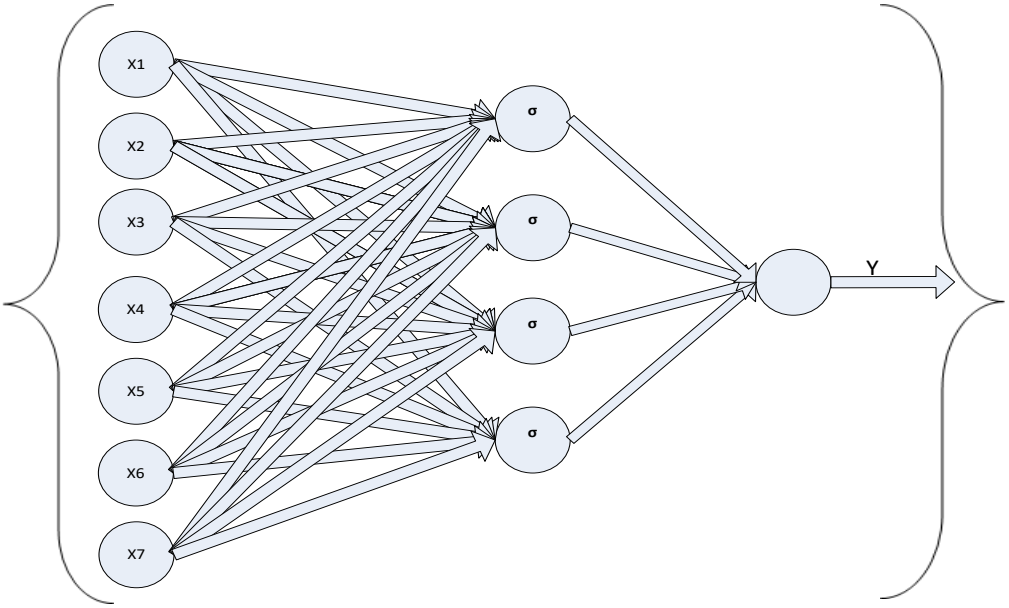

Figure 8.4 Multilayer perceptron Structure

8.4 Results and Discussion

The suggested project uses an ANN approach to calculate the maximum power from a photovoltaic panel, which is then simulated using the MATLAB tool. The MPPT algorithm is utilized by the ANN to develop and generate maximum power. With the usage of ANN-based MPPT, system efficiency improves and tracking time decreases. Through the Internet of Things platform, a tracking algorithm has been added to Thingspeak cloud, which may be worn in smart home applications. This technique can forecast weather conditions such as

sunny, rainy, and cloudy. In a solar photovoltaic system, an IOT-based algorithm is used to launch the maximum power yield of the solar panels and to maintain the highest photovoltaic energy translation during partially shadowed conditions. More specifically, the internet of things reduces the repetitive effort of visiting sites and repeatedly recording performance data, allowing for better control of isolated areas and more efficient and quick troubleshooting and repairs. DIP is a method for performing different image processing operations on an image, such as de-noising, feature extraction, filtering, contrast stretch, and presenting the output as the most informative image or the image's features in frequency form, so that an ANN may analyze the image properly. Pre-processing, augmentation, and feature extraction are the three core DIP stages.

8.4.1 Histogram Investigation: The histogram gives us a broad picture of the image's pixel intensity value and the frequency with which it occurs. The histogram improves the image contrast so that the image intensity is practically uniform. Figure 8.5 shows a histogram for sunny days, indicating that the rate of high intensity (255) occurrence is highest when compared to wet or cloudy days. Table 8.1 lists the retrieved features from various photographs of the sun.

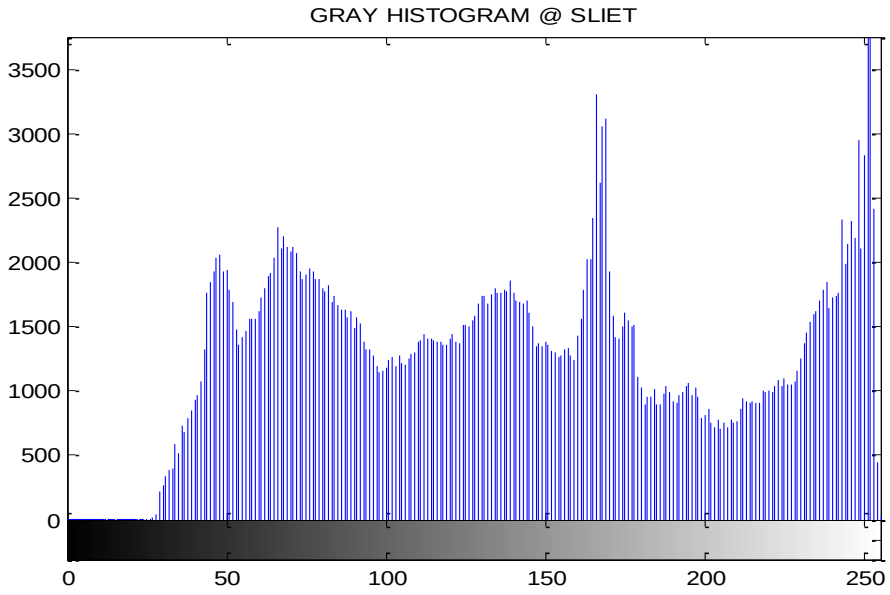

Figure 8.5 Histogram of Sun image

Table 8.1 Sun Image Extracted Feature

S. No.	Width	Max	Mean
1	70	255	111.49
2	69	255	106.835
3	68	255	106.835

8.4.2 Classification using ANN: The maximum power conclusion of a back propagation artificial neural network (BPN) classification is depicted in Figures 8.6 and Figure 8.7, and the processed parameters of the ANN are recorded in Table 8.2. The sun azimuth angle is precisely around the desired value. In comparison to the estimated result, the BPN power output increased by 15% and the azimuth angle inaccuracy was reduced to 0.20 degree. In comparison to a steady solar system, the overall power gain increased by 59.21%.

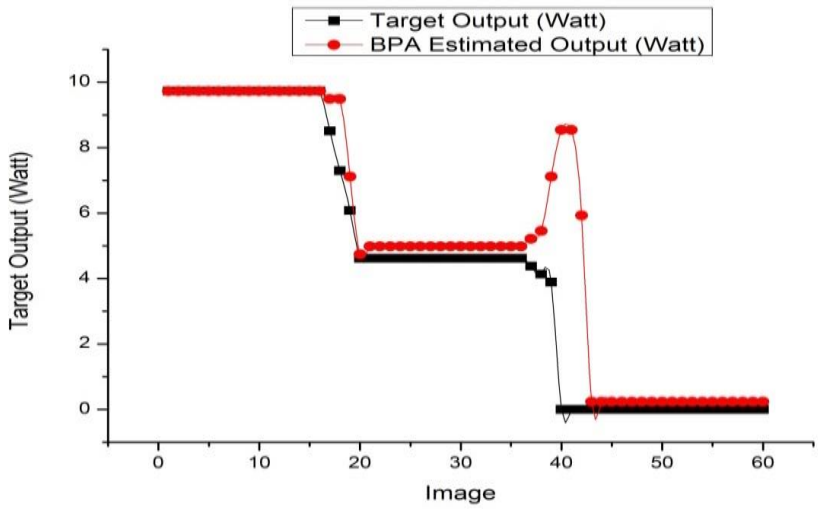

Figure 8.6 Power output comparison of IOT sun following system

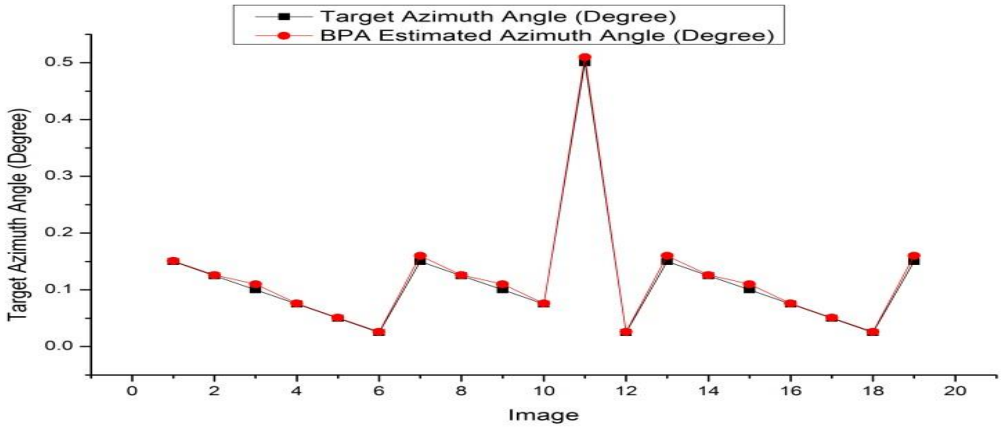

Figure 8.7 Azimuth angle of solar following system

Table 8.2 Parameter of Artificial Neural Network

S. No.	Characteristic of ANN	Value
1	Total number of input layer nodes	7
2	Total number of hidden layer nodes	4
3	Hidden layer activation function	Sigmoid
4	Total number of output layer nodes	1
5	Output layer activation function	Sigmoid
6	Total number of iterations	204
7	Factor of learning	0.8
8	MSE (Mean Squared Error)	0.0197

8.4.3 Digital Sensor: The camera uses a digital sensor to communicate between the sun's location and binary information in the image. So the feature is extracted from the camera image, and the ANN goes on to discover the exact co-ordinate of the sun centre, after which the motor driver is instructed to track the sun centre quadrate. The A_0 connector connects the sensor to the Arduino board.

8.4.4 Experimental Observation: Table 8.3 shows the experimental observation analysis of a 10-watt SS, a TASF, and an IoT-based TASF, with a graphical representation in Figure 8.8.

The average panel output efficiency is calculated by equation (9). Where, P1- Stable panel power output, P2- TASF's power output and P3-Power generated by an IoT-based TASF.

$$n_{Avg} = \frac{\sum(P_X - P_y)}{P_y} \times 100 \tag{8.9}$$

So compare to stable system (SS) the increased efficiency of IoT based TASF is given by (10) where $\Sigma P_Y = \Sigma P_3$ and $\Sigma P_X = \Sigma P_1$.

$$n_{Avg(IoT-SS)} = \frac{(4.06 - 2.55)}{2.55} \times 100 = 59.21\% \tag{8.10}$$

Respect to TASF, IoT TASF increased efficiency is given by (11) where $\Sigma P_Y = \Sigma P_3$ and $\Sigma P_X = \Sigma P_2$.

$$n_{Avg(IoT-TASF)} = \frac{(4.06 - 3.68)}{3.68} \times 100 = 10.32\% \quad (8.11)$$

Table 8.3 Experimental observation of 10 watt SS, TASF and IoT based TASF

R	SV	SC	SP	TAV	TAC	TAP	IV	IC	IP
1	0.031	0	0	0.0318	0	0	0.0319	0	0
2	1.031	0.49	0.50519	0.4134	0.018	0.007441	0.4147	0.0198	0.008211
3	3.131	0.051	0.159681	3.975	0.09	0.35775	3.9875	0.099	0.394763
4	3.472	0.102	0.354144	4.611	0.18	0.82998	4.6255	0.198	0.915849
5	3.782	0.119	0.450058	5.7876	0.162	0.937591	5.8058	0.1782	1.034594
6	11.532	0.2924	3.3719568	12.6564	0.351	4.442396	12.6962	0.3861	4.902003
7	16.647	0.425	7.074975	17.62038	0.495	8.722088	17.67579	0.5445	9.624468
8	17.05	0.4709	8.028845	17.649	0.4986	8.799791	17.7045	0.54846	9.71021
9	16.74	0.4471	7.484454	17.6172	0.5004	8.815647	17.6726	0.55044	9.727706
10	13.113	0.3179	4.1686227	17.6172	0.5004	8.815647	17.6726	0.55044	9.727706
11	5.363	0.255	1.367565	14.7552	0.342	5.046278	14.8016	0.3762	5.568362
12	1.8383	0.068	0.1250044	5.9466	0.162	0.963349	5.9653	0.1782	1.063016
13	0.031	0	0	1.8126	0.054	0.09788	1.8183	0.0594	0.108007
AV	7.212408	0.233715	2.54542276	9.268722	0.257954	3.67968	9.297868	0.283749	4.060376

R, Readings; SV, SS-Voltage (V); SC, SS-Current (A); SP, SS-Power (W); TAV, TASF-Voltage (V); TAC, TASF-Current (A); TAP, TASF-Power (W); IV, IoT TASF-Voltage (V); IC, IoT TASF-Current (A); IP, IoT TASF-Power (W); AV, Average value

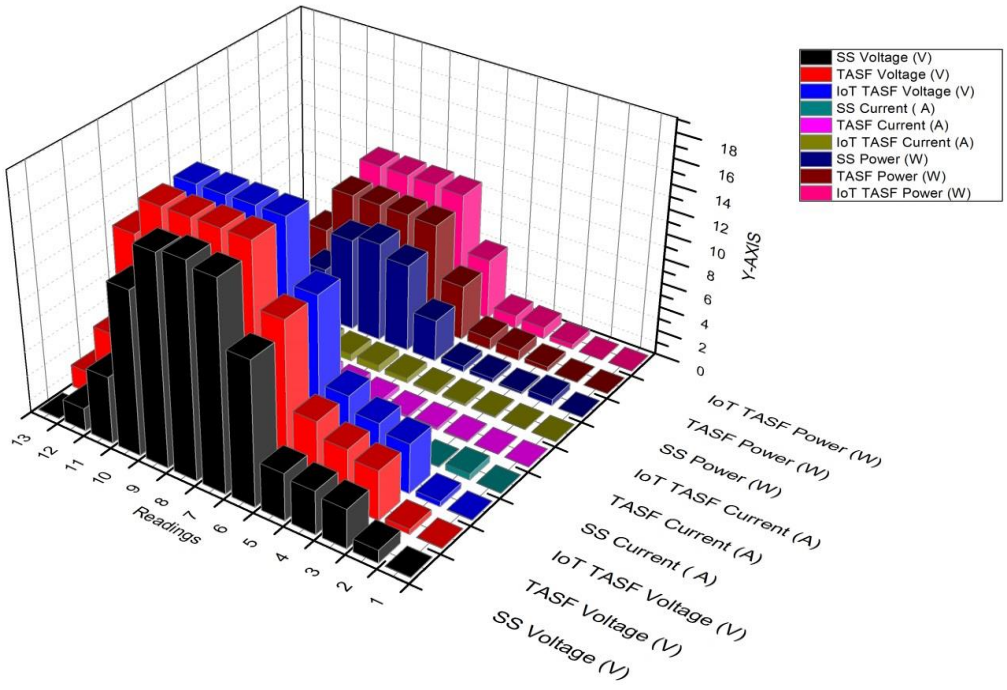

Figure 8.8 Comparison SS, TASF and IoT TASF parameter

8.5 Conclusion

It is effectively re-enacted a modernised method of dealing with constructing a scholarly classifier to investigate and control the following capacity of the sunlight-based board. When synchronised with other conventional classifiers, the back propagation (BPA) classifier is lively. The proposed innovation had the ability to summon all of the photographs of the sun at different tendencies with precision whose values are individually, according to the goal fulfilment for the planned classifier. As a result of the image analysis, a smart feed forward controller for tracking the sun's position in terms of azimuth point is now possible. Furthermore, electricity generation is mainly reliant on high light generation intercity. As a result, the output power is estimated using information from the sun's image. When compared to SS and 10.32 % when compared to TASF, the GPS plus ANN-DIP system reduced azimuth angle error by 0.20° and increased efficiency by about 59.21 %. The main goal of this investigation is to identify the unfavourable weather conditions that drive people to age during shady and windy days. Because of the Internet of Things, it is now possible to monitor output remotely. This technology (GPS+DIP+BPN+IOT) will be useful

in solar farming in the future, where a single online system or computer can handle a large number of solar trackers, lowering the cost of each PV panel tracking systems. In order to maximise yield, this automation technique sets numerous quantitative restrictions for the sun's location.

CHAPTER 9

RESULTS AND DISCUSSION

Results of the research work carried out during the Ph.D. discussed in previous chapters, is summarized in following sub-sections:

9.1 Modelling and Simulation Result of Hybrid System

PV modelling result- The simulation of 40 succession modules and 10 parallel modules yielded the following result. The following are the attributes that are used in modules. V_{OC} is 42 volts, I_{SC} is 29.7 amps; VMP is 36 volts, IMP) is 27.7 amps, and a cell per module is 10. Figure 4.5 shows the current voltage -PV curve for a functional module in optimum condition. Figure 4.6 depicts PV power waveforms based on the normal PO technique and the upgraded Predictive-PO approach. At 1000 W/m^2 at a temperature of 25^{o}C, the proposed MPP Tracking algorithm was tested.

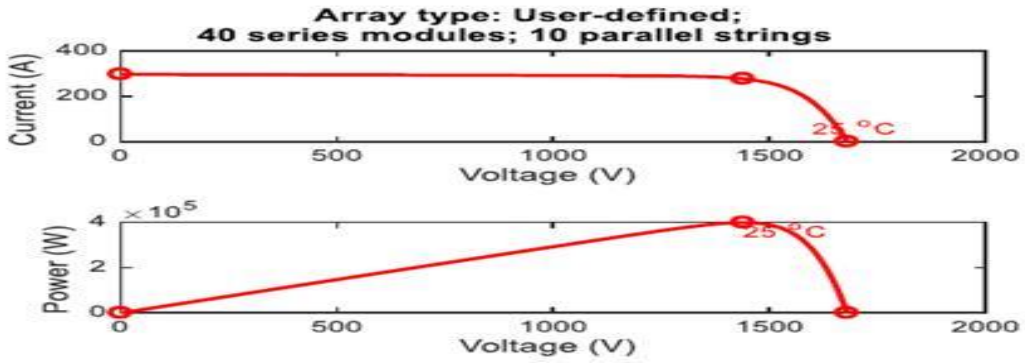

Figure 4.5 IV-PV plots of array in optimum conditions

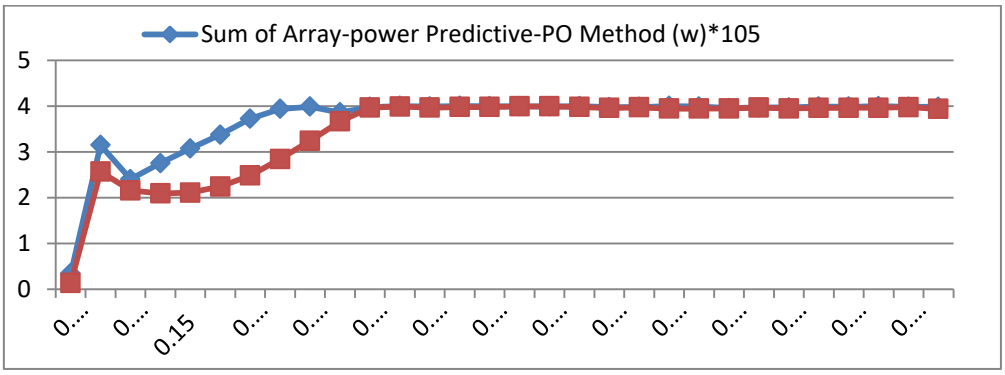

Figure 4.6 Comparison of power output

The ideal power wave shapee of a wind turbine, as shown in Figure 4.7, is utlize to regulate the distinct regions of processes at various wind speeds, such as rated wind speed and cut in wind speed.

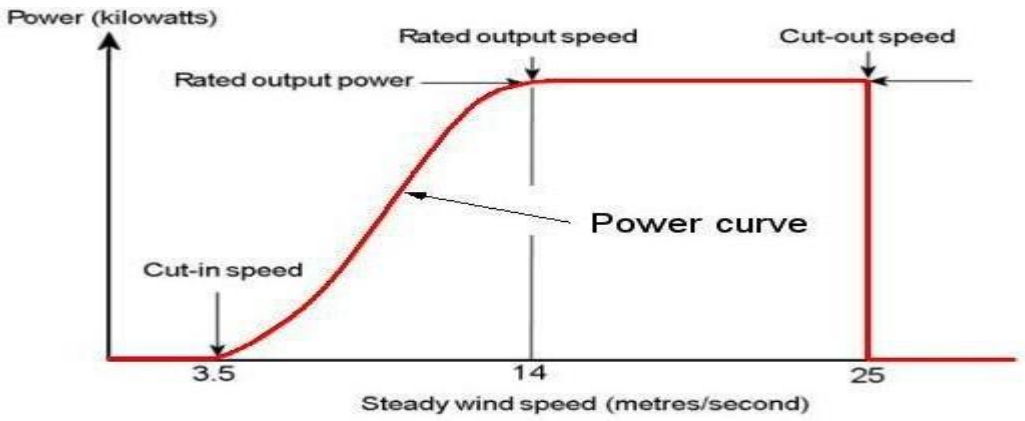

Figure 4.7 Typical wind turbine power output with steady wind speed

The Permanent magnet synchronous generator turbine for wind energy generation has been accurately simulated, and their AC and DC outputs are depicted in Figure 4.9 as voltage waveforms.

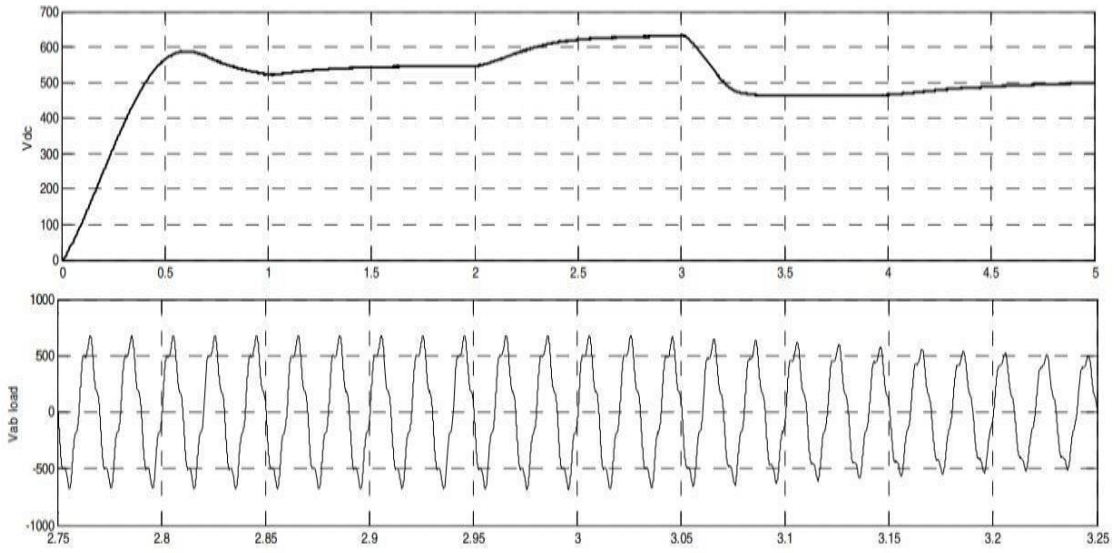

Figure 4.9 DC and AC voltage PMSG under different wind speed

The simulation and modeling of a grid-linked hybrid power system yielded the following: The hybrid power module is made up of two renewable energy resources: a PV system and a wind turbine system. In addition, the hybrid power module can handle single phase AC loads. In Figure 4.11, the voltage wave shape of a wind

turbine and a PV system based on the predictive Perturb and Observe MPPT mathod is shown.

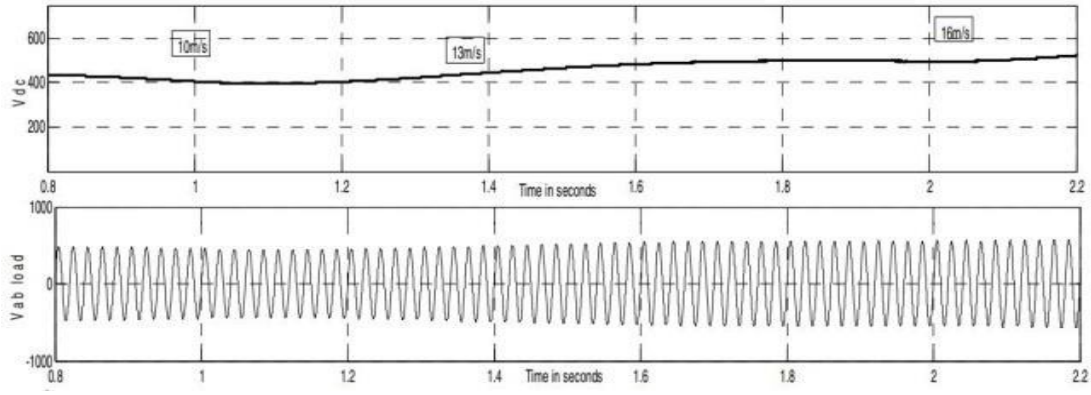

Figure 4.11 Output for both wind speed and solar

The major goal of this work is to prove the efficacy, dependability, and maximum power production of a hybrid power module by integrating a wind turbine with a PV system. This system was then prepared and modeled alone for comparison of the volatile and power variation, and then linked using Simulink. The efficacy of the hybrid power system is proved by simulation outcome so as to create increased power for damp summer weather in many countries that are attempting to employ renewable energy sources. The use of MATLAB/ Simulink is used to implement the solar photovoltaic model's power generation.

9.2 Soft Computing Based Solar Follower Using Raspberry Pi 4b

GPIO Port 22 & 23 is connected to pan signal of PWM and servo motor & these servo motor powered by Pi board itself. Raspberry Pi camera is directly connected to the camera port in Raspberry Pi board. It can be transmit to personal computer through USB.

Processing of Image - The pixel range of web camera is 2048 × 1536 and it has 3.15 mega pixel images. It also has dual LED flash and auto focus.

The given Figure 5.10 is taken by web camera at noon and one hour after the rain and their Gray and binary conversion shown. We can clearly observe that Sun is not clearly visible because of clouds. We put this image under image processing and it can be seen in Figure 5.11 that the Sun’s circumference or boundary and centre is being detected.

Figure 5.10 Image processing

Figure 5.11 Sun boundary and centre detection

The red and green lines show pan and tilt servo motor respectively assuming both are perpendicular to each other. The servo motor moves the webcam towards the centre of Sun with the help of Image centre shown in Figure 5.12.

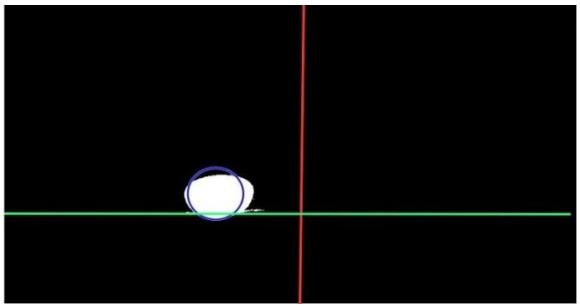

Figure 5.12 Traced Image

The degree of rotation is reducing so the pan servo motor lines cross the centre, than the Sun is traced. At 90 degrees, the Raspberry Pi send PWM signal of 1.49 ms. According to this, when the pulse width signal directed to the driver is lower, which is 1.28 ms, the orientation will be equal to 70 degrees. The same is repeated with tilt of servo motor.

Line of tilt should pass the blue circle which is present slightly left to the circle hence rotation degree of the servos should be reduced. The tilt lines are at 90^0 so now

lines are hence decreased to 750 and the signal has taken 1.32ms. Various images data were given in respected chapter. The observed results represented in Figure 5.13 where Image and Sun centre coincide and pan & tilt line cross each other at image centre.

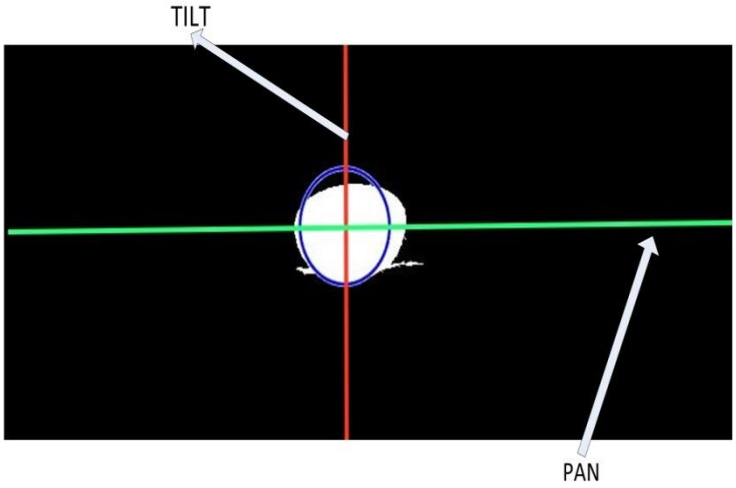

Figure 5.13 Centroid of Sun located

The high signal of the PWM which given to drivers to calculate the rotation degree of motor shown in Figure 5.14.

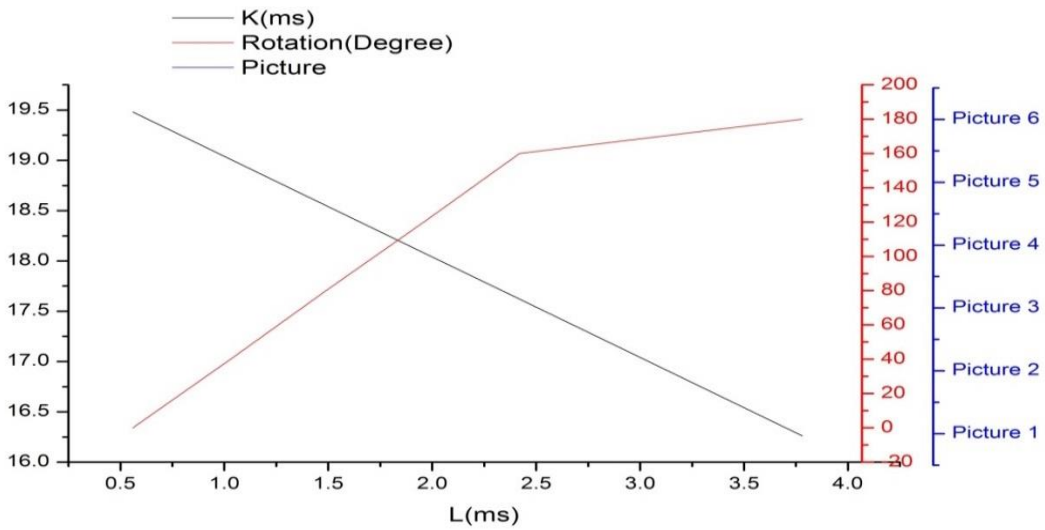

Figure 5.14 Result analysis

The proposed work based on solar tracking by the raspberry pi 4 B board systems. The system consist of webcam with image processing by raspberry pi board which is effective and works very well in tracking the Suns position during the cloudy days. This has effectively increased the efficiency of the solar power output. The

system has the capability to track and to find the centroid of the Sun by the Sun's picture which initiates the motors to rotate according to the position of the Sun.

9.3 Vision Based Solar Tracking System for Efficient Energy Harvesting

Single day reading for 17 hours of sunlight is taken by the proposed model, based on LDR and fixed panel. Figure 6.10 shows a contrast of power outcome from stable, LDR, and suggested (LDR & IP) modals, with the proposed system generating more power than the other two. Figure 6.11 shows a graphical representation of the short circuit current for all three systems, and it was shown that the I_{SC} is the same across the modes. In Figure 6.12, the V_{OC} of all of the above-mentioned models is calculated and examined, and it is noted that the Voc of LDR and IP-based systems is higher than that of stable and LDR systems. The results demonstrate that IP & LDR based trackers create increased power compare to the other two system, as illustrated in Figure 6.13, which shows their combined parameter analysis.

Efficiency of LDR & IP compare to LDR is 12.50%
Efficiency of LDR & IP compare to SS is 30.05%

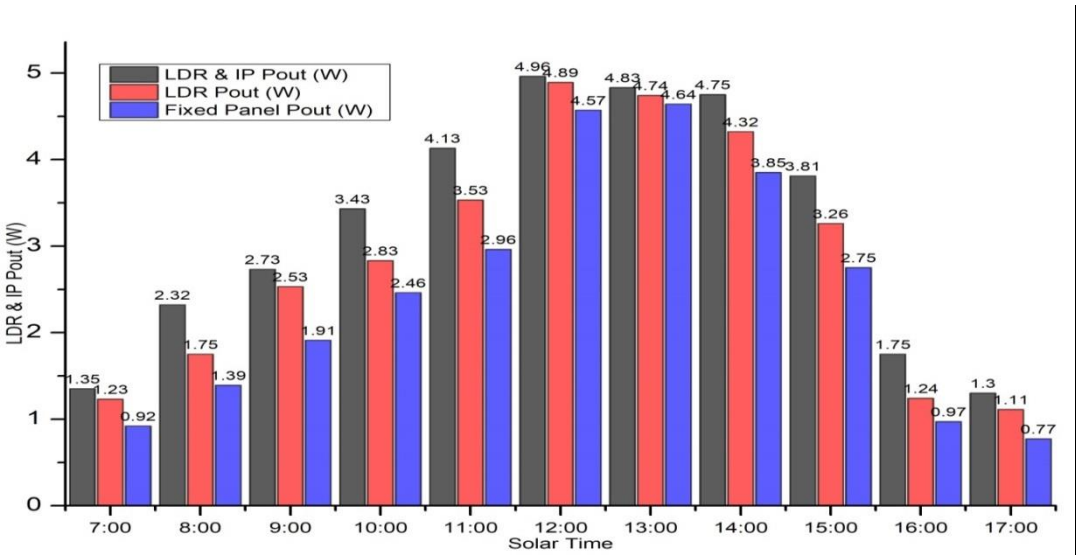

Figure 6.10 Power comparisons of all three systems

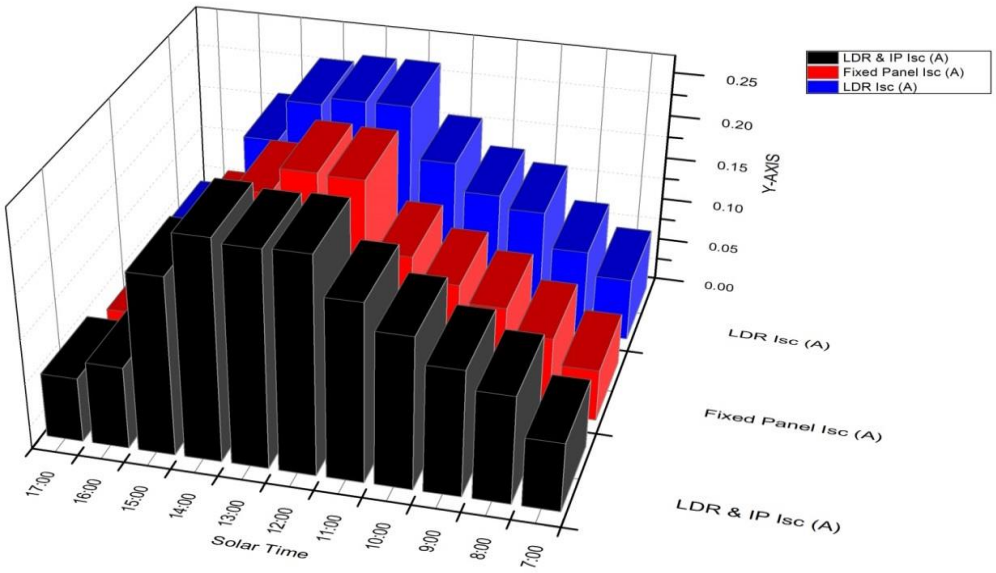

Figure 6.11 Short circuit current comparisons of all three systems

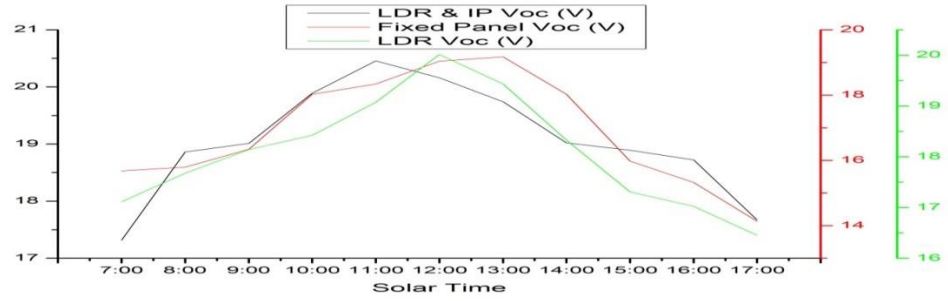

Figure 6.12 Open circuit voltage comparison of all three systems

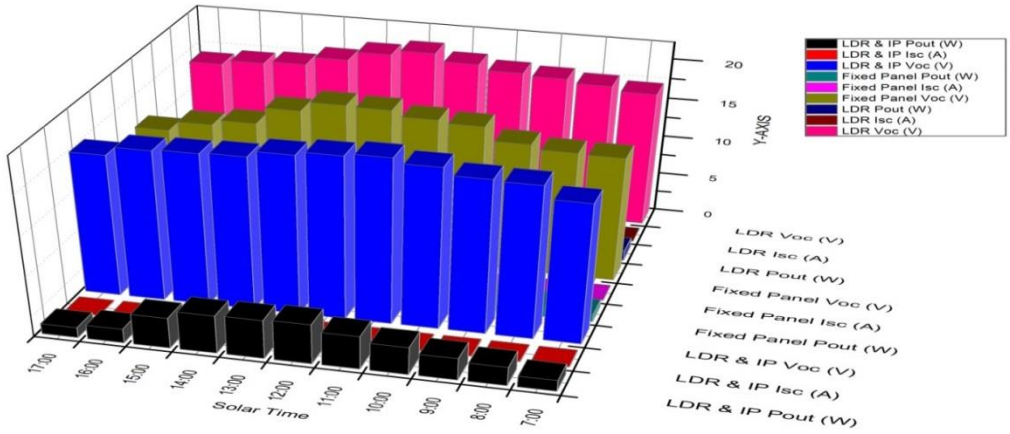

Figure 6.13 Power, I_{SC} & V_{OC} analysis of all three systems

After examining the all system, we discovered that the IP & LDR based solar trackers yield the best results compared to the other two. When only a few panels need to be tracked, LDR is the best option; however, when hundreds or thousands of panels need

to be tracked, IP & LDR is the most cost-effective option. If we utilise a higher resolution camera, the solar panel's efficiency will increase.

9.4 Two Axis GPS and LDR based Sun Follower and Static Base Photo Voltaic Panel working Analysis on Various Weather Conditions

All of the trials were carried out at Greater Noida City, India (28^0 34' 48"N 77^0 19' 47.999E). The amount of energy engrossed was found to be highest in the months of May to July, and then began to decline in the months of August to December, before rising again in January. During these three seasons, the solar tracker and fixed systems behaved differently.

Based on the outcome observed from the solar tracking power system, the values were tabulated and graphs were created. On the specific month, the absorbed energy during sunny, overcast, and rainy days was tabulated for six days. The actual readings were taken and recorded in a 20-minute interval

The highest and minimum monthly energies produced as a expressed by Figure 7.13. The TASFS-GPS system produced more absorbed energy than the TASFS_LDR and SS type arrangement. The GPS solar tracker's energy collection was calculated to be 45.85 % higher than SS and 14.93% greater than TASFS_LDR. The tracking error of TASFS_GPS and TASFS_LDR are 0.10% and 0.11% respectively.

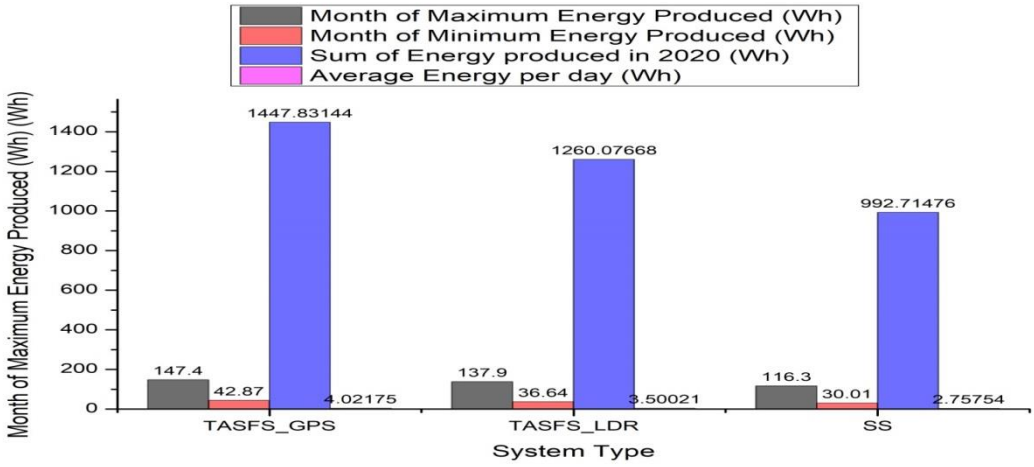

Figure 7.13 System comparison graph

The efficiency of above system where expressed in Figure 7.14.

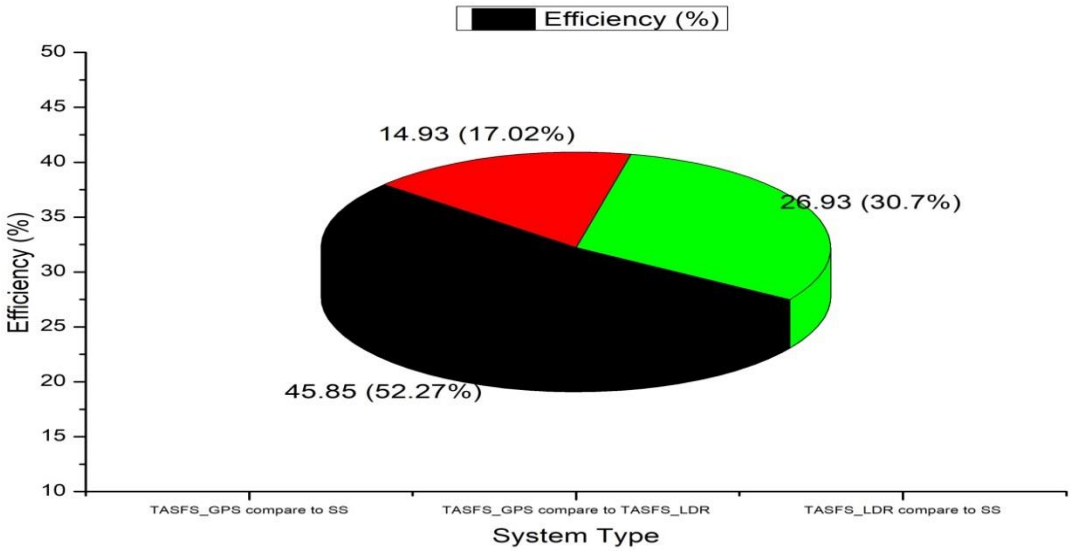

Figure 7.14 Output efficiency of three systems

Solar Energy Produced on Sunny Days-Figure 7.15 displays TASFS_GPS (May 26 & 27, 2021) exceptional solar energy trapping capabilities.

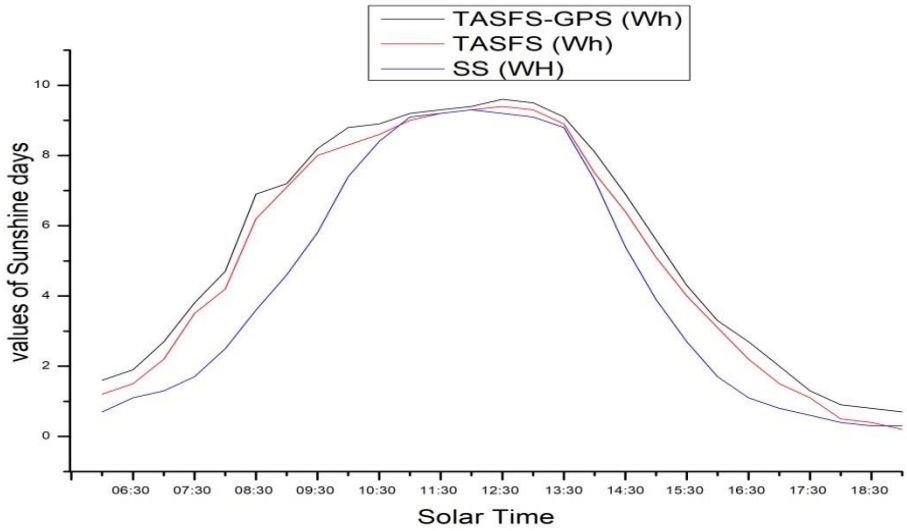

Figure 7.15 Average energies produced by the TASTS_GPS, TASFS_LDR and SS during two sunny days

Solar Energy Produced on Cloudy Days-Figure 7.16 reveals significant differences in energy harvesting within the TASFS_GPS, TASFS_LDR and the SS on cloudy days (August 3 & 4, 2021), with the SFS obtaining more energy.

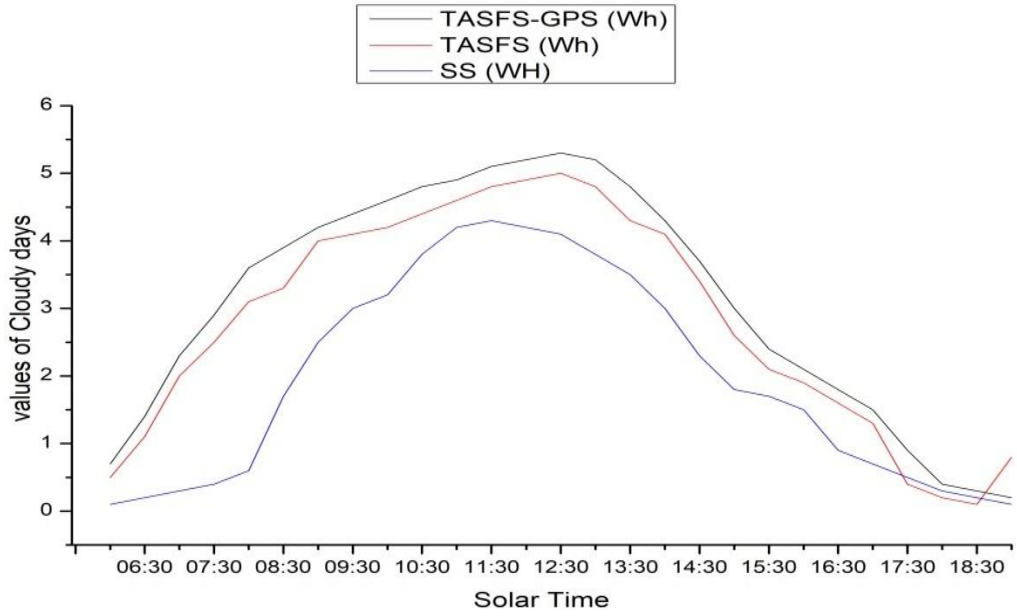

Figure 7.16 Average energy generated by the TASFS_GPS, TASFS_LDR and SS during the two cloudy days

Solar Energy Produced on Rainy Days-The data on energy harvested during wet days (June 6 & 7, 2021) from 6:00 to 19:00 solar time, when the sun rose swiftly in the morning, shows that the TASFS_GPS values are substantially bigger than the TASFS_LDR and SS values, as shown in Figure 7.17.

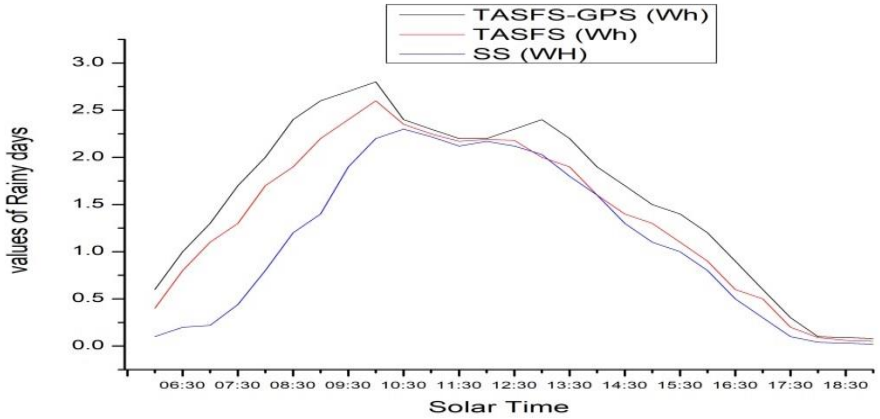

Figure 7.17 Average energy generated by the TASTS_GPS, TASFS_LDR and SS on the two rainy days

The TASFS_GPS absorbed more energy than the TASFS_LDR and SS solar system, even during wet days. The TASFS_GPS was only nearly equal to the TASFS_LDR and SS from 11:30 A.M to 12:30 PM. Figure 7.18 compares total energy production under three different weather conditions.

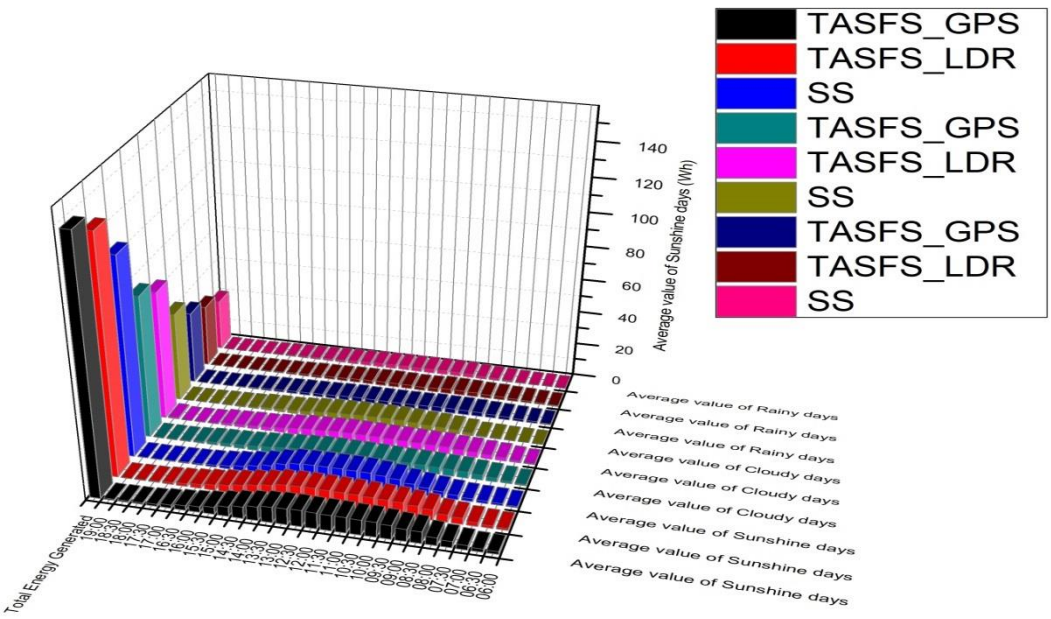

Figure 7.18 Comparison of the energies generated from the TASFS_GPS, TASFS_LDR and SS on different weather conditions

Even on cloudy days, the two-axis sun following with GPS delivered better energy yield than the SS and TASFS_LDR. The energy yield of the GPS two-axis sun following was 45.85% higher than the fixed mount system and 14.93% more than TASFS_LDR. The tracking error of TASFS_GPS and TASFS_LDR is 0.10 and 0.11 respectively. The most crucial element to consider when evaluating a solar tracking system is its energy yield. The use of lightweight materials for the building of the GPS solar tracker is another area of research that can be pursued to improve the performance of GPS solar tracker. Furthermore, more research with the use of artificial intelligence approaches to regulate the GPS location of the PV panel for the solar tracker and PV panel, employing flexible monocrystalline materials.

9.5 Soft Computing & IoT Based Solar Tracker

Figure 8.8 depicts the experimental outcome of a 10 watt stable system, a dual axis solar tracker, and an IoT-based TASF.

IoT has a 59.21 % higher average panel output efficiency than SS and a 10.32 % higher average panel output efficiency than TASF.

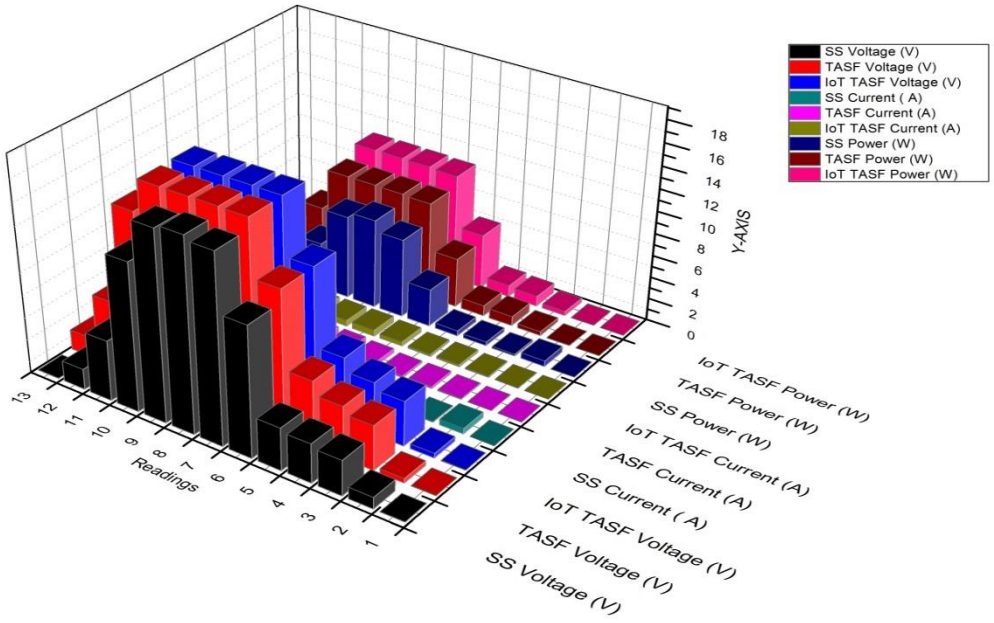

Figure 8.8 Comparison SS, TASF and IoT TASF parameter

It is effectively re-enacted a modernised method of dealing with constructing a classifier to examine and control the sunlight-based system. When synchronised with other conventional classifiers, the back propagation (BPA) classifier is lively. The proposed approach had the ability to summon all of the photographs of the sun at various tendencies with precision whose values are individually, according to the goal fulfilment for the planned classifier. As a result of the image analysis, a smart feed forward controller for tracking the sun's position in terms of azimuth point is now possible. Furthermore, electricity generation is mainly reliant on high light generation intercity. As a result, the output power is estimated using information from the sun's image. Energy gain is 59.21% when compared to SS and 10.32 % when compared to TASF. The GPS plus ANN-DIP system reduced azimuth angle error by 0.20° and increased efficiency by about 59.21 %. The main goal of this investigation is to identify the unfavourable weather conditions that drive system during shady and windy days. Because of the Internet of Things, it is now possible to monitor output remotely.

CHAPTER 10

SUMMARY AND CONCLUSION

10.1 Summary of Research Work

The research work carried out during course of this thesis can be summarized is detailed below:

The current research involves examining and addressing the problem of Stable and LDR based solar panel's low efficiency. Here we also go through Hybrid approach so as to improve the efficacy of energy by combining PV and wind energy approach. In existing Stable panel the panel is fixed with some angle because of that the energy harvesting is limited to some value. This happen because the sun radiation incident is not maximum all the time. The Two axis LDR based solar trackers have many disadvantages out of with is their electronic part which is really effected by the geographical environmental condition. The electronic discharge affects the tracking accuracy of system and it requires more intense maintenance. In order to solve this above said issue we examined here different energy harvesting system and produce there result.

The various discussed systems are

- Hybrid system
- Image processing (IP) Based system
- IP and LDR system
- GPS based system
- GPS, IP and Artificial neural network (ANN) system.

Modelling And Simulation of Hybrid System-Perhaps a hybrid power model uses two non-conventional power resources, such as PV and wind turbine systems, to provide single phase AC load. Then, using Simulink / MATLAB, each system was planned and modelled separately before being combined to compare voltage and power variance. In reality, the simulation's results show how efficient the intended hybrid power system is in terms of generating maximum electricity. This system based on the Array-power predictive -P&O MPPT technique.

In IP system the LDR is not used to grab or trace the sun location but the Image is used to find the centroid Co-ordinate of sun within image using image processing technique. This type of system is basically very useful in solar farming where lakhs of solar panel get instruction from single tracking sensor called camera. So energy saving is shown there. The LDR who's tracking error (Single axis-0.14, two-axis-0.12) increase because of electronic discharge caused by environmental condition is also solved there. It also harvests solar energy greater than stable PV & LDR (one and two axis) based solar tracker. So it is better than the LDR based tracker by improving efficiency and reducing tracking error during haze or cloudy day.

In IP and LDR system LDR and IP use back to back to increase energy efficacy of harvesting system. Compare to stable panel system the applied system improve energy by 30.05% and compare to LDR based two axis systems their energy efficiency increased by 12.50%.

In GPS based system, the work investigates the result of GPS, LDR and stable system. Here we conclude that GPS system improve energy harvesting by 45.85% compare to stable system and 14.93% compare to LDR based two axis system.

In IP, GPS and ANN based system we conclude that this system improve energy efficiency by 59.21% compare to stable system.

So finally we conclude that with the use of GPS, IP ANN the system efficiency increased up to 59.21 % and tracking error reduce to 0.1 and GPS system improve efficiency up to 45.85% and tracking error reduce to 0.1. In this system continuous tracking is prohibited and tracking is done on 20 minute interval because of that the energy consumption is reduced. The LDR tracker limitation is also removed in applied approach because of that the tracking error is reduced. So it is overall an energy efficient system for large scale solar energy harvesting by using lakhs of solar panel.

10.2 Future Scope

The demand of renewable energy increasing continuously and solar is the best reliable resource of renewable power. For this purpose many study is going on in improving the efficiency of solar energy. The new material is introducing in order to improve panel

efficiency. Many MPPT technique algorithms are discovered to improve the system output. Different tracking technique is also introduced to increase to harvest of solar energy. Out of this tracking technique our approach carries soft computing and GPS system. In future this system injected with soft computing to add forecasting based solar tracker, where the 10 year data of tracker system can be used to forecast the tracker path. This system generally successful on solar farming where the single sensor or controller control thousands of solar panel to track the sun and the monitoring process is done online through IoT and these all work can be done on real time basis.

REFERENCES

1. (IRENA) TIREA, 'Renewable energy statistics 2020'. IRENA; 2020. https://www.irena.org/Statistics, 2020.
2. Nsengiyumva, W., Chen, S.G., Hu, L. and Chen, X., 2018. "Recent advancements and challenges in Solar Tracking Systems (STS)", A review. *Renewable and Sustainable Energy Reviews*, *81*, pp.250-279.
3. Ritchie Hannah RM, Comparison graph of Annual change in renewable energy generation expressed in terawatt-hours (TWh). BP Statistical Review of Our World in Data; 2020. http://www.bp.com/statisticalreview, 2020.
4. Ritchie Hannah RM, Comparison graph of Annual change in solar energy generation, 2019 expressed in terawatt-hours (TWh). BP Statistical Review of Our World in Data; 2020. http://www.bp.com/statisticalreview, 2020.
5. The National Institute of Solar Energy (NISE) and Ministry of New & Renewable Energy (MNRE), Annual Report 2018-19, MNRE:2019, https://mnre.gov.in/img/documents/uploads/file_f-1597797108502.pdf, 2019.
6. The National Institute of Solar Energy (NISE) and Ministry of New & Renewable Energy (MNRE), Grid connected solar energy of about 36.62 GW, MNRE: 2019, https://mnre.gov.in/solar/solar-ongrid. 2019.
7. Green, A M, Warta YW, Ewan, Levi DH, Hohl-Ebinger J, et al., 2017, "Solar cell efficiency tables (version 50).", *Progress in photovoltaic: research and applications*, 25, pp.668–676.
8. Report, data, Solar Tracker Market By Product (Single Axis and Dual Axis), Technology (Solar PV, Concentrated Solar Power (CSV) and Concentrated Photovoltaic (CPV)), By Application (Utility and Non-utility) and Segment Forecasts, 2016-2026. Solar -tracker-market, https://www.reportsanddata.com/report-detail/solar-tracker-market, 2020.
9. (IRENA) TIREA, 'Solar Energy Could Meet up to 13% of Global Power Needs by 2030'. Inter Solar Europe, Letting in the Light, https://www.irena.org/newsroom/pressreleases/2016/Jun/Solar-Energy-Could-Meet-up-to-13-of--Global-Power-Needs-by-2030, 2016.

10. Hafez, A.Z., Yousef, A.M. and Harag, N.M., 2018, "Solar tracking systems: Technologies and trackers drive types–A review", *Renewable and Sustainable Energy Reviews, 91*, pp.754-782.
11. Ritchie Hannah RM, Comparison graph of World and India electricity production from Sun expressed in terawatt-hours (TWh) annually, BP Statistical Review of World Energy, http://www.bp.com/statisticalreview, 2019.
12. Ritchie Hannah RM, Percentage variation in solar energy production, BP Statistical Review of World Energy, http://www.bp.com/statisticalreview\%0A, 2019.
13. Patel, M.R. and Beik, O., 2021, *Wind and solar power systems: design, analysis, and operation*. CRC press.
14. Clifford, M.J. and Eastwood, D., 2004, "Design of a novel passive solar tracker", *Solar Energy*, *77*(3), pp.269-280.
15. Ritchie, E., Argeseanu, A. and Leban, K.M., 2009, *Robust solar position sensor for tracking systems,* In *Proceedings of 9th WSEAS International Conference on Power Systems (PS'09), 9,* pp. 49-54.
16. Nayak, S.R. and Pradhan, C.R., 2012, "Solar tracking application", *IOSR J. Eng*, *2*(12781281), p.4.A.
17. Yamin, A.H., Ibrahim, M.N., Idroas, M. and Zin, A.R., 2013, *June. Embedded solar tracking instrumentation system*, In 2013 IEEE 7th International Power Engineering and Optimization Conference (PEOCO), pp. 223-227.
18. Hossain, M.I., Khan, S.A. and Shafiullah, M., 2012, December, "Power maximization of a photovoltaic system using automatic solar panel tracking along with boost converter and charge controller", In *2012 7th International Conference on Electrical and Computer Engineering,* pp. 900-903.
19. Andrew, Software, two dimensional projected Sun-path diagrams, http://andrewmarsh.com/apps/releases/sunpath2d.html, 2014.
20. Sharma, M. and Jilte, R., 2021, "A review on passive methods for thermal performance enhancement in parabolic trough solar collectors", *International Journal of Energy Research, 45*(4), pp.4932-4966.
21. Mohammad, N. and Karim, T., 2013. "Design and implementation of hybrid automatic solar-tracking system", *Journal of solar energy engineering*, *135*(1), p.011013.

22. Tina, G.M. and Gagliano, S., 2011, “Probabilistic modelling of hybrid solar/wind power system with solar tracking system”, *Renewable Energy*, *36*(6), pp.1719-1727.
23. Natarajan, S.K., Thampi, V., Shaw, R., Kumar, V.S., Nandu, R.S., Jayan, V., Rajagopalan, N. and Kandasamy, R.K., 2019, “Experimental analysis of a two-axis tracking system for solar parabolic dish collector”, *International Journal of Energy Research*, *43*(2), pp.1012-1018.
24. Lubitz, W.D., 201,.”Effect of manual tilt adjustments on incident irradiance on fixed and tracking solar panels”, *Applied energy*, *88*(5), pp.1710-1719.
25. Koussa, M., Cheknane, A., Hadji, S.M.H.S.N., Haddadi, M. and Noureddine, S., 2011, “Measured and modelled improvement in solar energy yield from flat plate photovoltaic systems utilizing different tracking systems and under a range of environmental conditions” ,*Applied Energy*, *88*(5), pp.1756-1771.
26. Pen, E.F., 2019, “Energy efficiency of photovoltaic panels when using holographic gratings as passive solar trackers”, *Optoelectronics, Instrumentation and Data Processing*, *55*(3), pp.271-279.
27. Gaspar, F., Deac, T., Tutunaru, L.V.F. and Moldovanu, D., 2016, “Experimental study on the sun tracking ability of a spherical solar collector”, *Energy Procedia*, *85*, pp.220-227.
28. Peng, S., Hong, H., Jin, H. and Zhang, Z., 2013, “A new rotatable-axis tracking solar parabolic-trough collector for solar-hybrid coal-fired power plants”, *Solar energy*, *98*, pp.492-502.
29. León, N., García, H. and Ramírez, C., 2014, “Semi-passive solar tracking concentrator”, *Energy Procedia*, *57*, pp.275-284.
30. Gordon, J.M., Kreider, J.F. and Reeves, P., 1991, “Tracking and stationary flat plate solar collectors: yearly collectible energy correlations for photovoltaic applications”, *Solar energy*, *47*(4), pp.245-252.
31. Cammarata, A., 2015, “Optimized design of a large-workspace 2-DOF parallel robot for solar tracking systems”, *Mechanism and machine theory*, *83*, pp.175-186.
32. Sahu, S.K. and Natarajan, S.K., 2021, “Design and development of a low-cost solar parabolic dish concentrator system with manual dual-axis tracking”, *International Journal of Energy Research*, *45*(4), pp.6446-6456.

33. Zengwei, Z., Zhen, Z., Yongfeng, J., Haolin, L. and Shengcheng, Z., 2019, "Performance Analysis on Bifacial PV Panels With Inclined and Horizontal East–West Sun Trackers", *IEEE Journal of Photovoltaics*, *9*(3), pp.636-642.
34. Tchakounté, H., Fapi, C.B.N., Kamta, M. and Woafo, P., 2019, "Experimental Assessment of a Smart Sun Tracking System Consumption for the Improvement of a Crystalline Silicon Photovoltaic Module Performance under Variable Weather Conditions", *Applied Solar Energy*, *55*(6), pp.385-396.
35. Asiabanpour, B., Almusaied, Z., Aslan, S., Mitchell, M., Leake, E., Lee, H., Fuentes, J., Rainosek, K., Hawkes, N. and Bland, A., 2017, "Fixed versus sun tracking solar panels: an economic analysis", *Clean Technologies and Environmental Policy*, *19*(4), pp.1195-1203.
36. Diaz, A., Garrido, R. and Soto-Bernal, J.J., 2018, "A filtered sun sensor for solar tracking in HCPV and CSP systems", *IEEE Sensors Journal*, *19*(3), pp.917-925.
37. Ram, J.P., Pillai, D.S., Rajasekar, N. and Strachan, S.M., 2019, "Detection and identification of global maximum power point operation in solar PV applications using a hybrid ELPSO-P&O tracking technique", *IEEE Journal of Emerging and Selected Topics in Power Electronics*, *8*(2), pp.1361-1374.
38. Tekumalla, D.V., Pal, D. and Bajpai, P., 2019, "Comprehensive performance evaluation of various solar PV system configurations", *IET Renewable Power Generation*, *13*(8), pp.1261-1270.
39. Hammoumi, A.E., Motahhir, S., Ghzizal, A.E., Chalh, A. and Derouich, A., 2018", A simple and low-cost active dual-axis solar tracker", *Energy Science & Engineering*, *6*(5), pp.607-620.
40. Kumar, V.S.S. and Suryanarayana, S., 2014' "Automatic dual Axis sun tracking system using LDR sensor", *International Journal of Current Engineering and Technology*, *4*(5), pp.3214-3217.
41. Corp Z, Photovoltaic Tracking Racks. http://www.zomeworks.com/photovoltaic-tracking-racks/, 2014.
42. Roong, A.S.C. and Chong, S.H., 2016, "Laboratory-scale single axis solar tracking system: Design and implementation", *International Journal of Power Electronics and Drive Systems*, *7*(1), p.254.
43. Sallaberry, F., Pujol-Nadal, R., Larcher, M. and Rittmann-Frank, M.H., 2015, "Direct tracking error characterization on a single-axis solar tracker", *Energy Conversion and Management*, *105*, pp.1281-1290.

44. Bhattacharjee, R. and Bhattacharjee, S., 2020, “Viability of a concentrated solar power system in a low sun belt prefecture”, *Frontiers in Energy*, *14*(4), pp.850-866.
45. Li, Z., Liu, X. and Tang, R., 2010, “Optical performance of inclined south-north single-axis tracked solar panels”, *Energy*, *35*(6), pp.2511-2516.
46. Chang, T.P., 2009, “Performance study on the east–west oriented single-axis tracked panel”, *Energy*, *34*(10), pp.1530-1538.
47. Tomson, T., 2008, “Discrete two-positional tracking of solar collectors”, *Renewable energy*, *33*(3), pp.400-405.
48. Grass, C., Schoelkopf, W., Staudacher, L. and Hacker, Z., 2004, “Comparison of the optics of non-tracking and novel types of tracking solar thermal collectors for process heat applications up to 300 C”, *Solar Energy*, *76*(1-3), pp.207-215.
49. Ai, B., Shen, H., Ban, Q., Ji, B. and Liao, X., 2003, “Calculation of the hourly and daily radiation incident on three step tracking planes”, *Energy Conversion and Management*, *44*(12), pp.1999-2011.
50. Huang, B.J., Ding, W.L. and Huang, Y.C., 2011, “Long-term field test of solar PV power generation using one-axis 3-position sun tracker”, *Solar energy*, *85*(9), pp.1935-1944.
51. Chin, C.S., Babu, A. and McBride, W., 2011, “Design, modeling and testing of a standalone single axis active solar tracker using MATLAB/Simulink”, *Renewable Energy*, *36*(11), pp.3075-3090.
52. Oner, Y., Cetin, E., Ozturk, H.K. and Yilanci, A., 2009, “Design of a new three-degree of freedom spherical motor for photovoltaic-tracking systems”, *Renewable Energy*, *34*(12), pp.2751-2756.
53. Rahimi, M., Banybayat, M., Tagheie, Y. and Valeh-e-Sheyda, P., 2015, “An insight on advantage of hybrid sun–wind-tracking over sun-tracking PV system”, *Energy Conversion and Management*, *105*, pp.294-302.
54. Khan, A. and Javaid, N., 2020, “Jaya Learning-Based Optimization for Optimal Sizing of Stand-Alone Photovoltaic, Wind Turbine, and Battery Systems”, *Engineering*, *6*(7), pp.812-826.
55. Padmagirisan, P. and Sankaranarayanan, V., 2019, “Powertrain control of a solar photovoltaic-battery powered hybrid electric vehicle”, *Frontiers in Energy*, *13*(2), pp.296-306.

56. Kumar, K., Aggrawal, T., Verma, V., Singh, S., Singh, S. and Varshney, L, 2020, "Modeling and Simulation of Hybrid System", *International Journal of Advanced Science and Technology*, 29(4s), pp. 2857 -2867.
57. Quesada, G., Guillon, L., Rousse, D.R., Mehrtash, M., Dutil, Y. and Paradis, P.L., 2015, "Tracking strategy for photovoltaic solar systems in high latitudes", *Energy conversion and Management*, *103*, pp.147-156.
58. Eldin, S.S., Abd-Elhady, M.S. and Kandil, H.A., 2016, "Feasibility of solar tracking systems for PV panels in hot and cold regions", *Renewable Energy*, *85*, pp.228-233.
59. Moharram, K.A., Abd-Elhady, M.S., Kandil, H.A. and El-Sherif, H., 2013, "Influence of cleaning using water and surfactants on the performance of photovoltaic panels", *Energy Conversion and Management*, *68*, pp.266-272.
60. Gholinejad, M., Bakhtiari, A. and Bidi, M., 2016, "Effects of tracking modes on the performance of a solar MED plant", *Desalination*, *380*, pp.29-42.
61. Roth, P., Georgiev, A. and Boudinov, H., 2004, "Design and construction of a system for sun-tracking", *Renewable energy*, *29*(3), pp.393-402.
62. Njoku, H.O., 2016, "Upper-limit solar photovoltaic power generation: Estimates for 2-axis tracking collectors in Nigeria", *Energy*, *95*, pp.504-516.
63. Yao, Y., Hu, Y., Gao, S., Yang, G. and Du, J., 2014, "A multipurpose dual-axis solar tracker with two tracking strategies", *Renewable Energy*, *72*, pp.88-98.
64. Zhang, P., Zhou, G., Zhu, Z., Li, W. and Cai, Z., 2013, "Numerical study on the properties of an active sun tracker for solar streetlight", *Mechatronics*, *23*(8), pp.1215-1222.
65. Jamroen, C., Komkum, P., Kohsri, S., Himananto, W., Panupintu, S. and Unkat, S., 2020, "A low-cost dual-axis solar tracking system based on digital logic design: Design and implementation, "*Sustainable Energy Technologies and Assessments*, *37*, p.100618.
66. Zhang, J., Yin, Z. and Jin, P., 2019, "Error analysis and auto correction of hybrid solar tracking system using photo sensors and orientation algorithm", *Energy*, *182*, pp.585-593.
67. Asim, M., Tariq, M., Mallick, M.A., Ashraf, I., Kumari, S. and Bhoi, A.K., 2018, "Critical evaluation of offline MPPT techniques of solar PV for stand-alone applications", In *Advances in Smart Grid and Renewable Energy* (pp. 13-21). Springer, Singapore.

68. Ram, J.P. and Rajasekar, N., 2016, "A novel flower pollination based global maximum power point method for solar maximum power point tracking", *IEEE Transactions on Power Electronics*, *32*(11), pp.8486-8499.
69. Pillai, D.S., Ram, J.P., Ghias, A.M., Mahmud, M.A. and Rajasekar, N., 2019, "An accurate, shade detection-based hybrid maximum power point tracking approach for PV systems", *IEEE Transactions on Power Electronics*, *35*(6), pp.6594-6608.
70. Pellet, N., Giordano, F., Ibrahim Dar, M., Gregori, G., Zakeeruddin, S.M., Maier, J. and Grätzel, M., 2017, "Hill climbing hysteresis of perovskite-based solar cells: a maximum power point tracking investigation", *Progress in Photovoltaics: Research and Applications*, *25*(11), pp.942-950.
71. Ramli, M.A., Twaha, S., Ishaque, K. and Al-Turki, Y.A., 2017, "A review on maximum power point tracking for photovoltaic systems with and without shading conditions", *Renewable and Sustainable Energy Reviews*, *67*, pp.144-159.
72. Mei-xia, Z. and Xiu, Y., 2012, "May. Efficiency optimization of photovoltaic arrays based on distributed max power point tracking", In *IEEE PES Innovative Smart Grid Technologies*, pp. 1-6.
73. Kheldoun, A.B.R.B., Bradai, R., Boukenoui, R. and Mellit, A., 2016, "A new Golden Section method-based maximum power point tracking algorithm for photovoltaic systems", *Energy Conversion and Management*, *111*, pp.125-136.
74. Ahmed, J. and Salam, Z., 2016, "A modified P&O maximum power point tracking method with reduced steady-state oscillation and improved tracking efficiency", *IEEE Transactions on Sustainable Energy*, *7*(4), pp.1506-1515.
75. Brahmi, H. and Dhifaoui, R., 2013, "Dynamic characteristics and improved MPPT control of PV generator. *Frontiers in Energy*", *7*(3), pp.342-350.
76. Kahoul, N., Houabes, M. and Neçaibia, A., 2015, "A comprehensive simulator for assessing the reliability of a photovoltaic panel peak power tracking system", *Frontiers in Energy*, *9*(2), pp.170-179.
77. Rakesh, N. and Madhavaram, T.V., 2016, "Performance enhancement of partially shaded solar PV array using novel shade dispersion technique", *Frontiers in Energy*, *10*(2), pp.227-239.

78. Rao, P.S., Dinesh, P., Ilango, G.S. and Nagamani, C., 2015, "Optimal Su-Do-Ku based interconnection scheme for increased power output from PV array under partial shading conditions", *Frontiers in Energy*, *9*(2), pp.199-210.
79. Fathy, A., Rezk, H. and Yousri, D., 2020, "A robust global MPPT to mitigate partial shading of triple-junction solar cell-based system using manta ray foraging optimization algorithm", *Solar Energy*, *207*, pp.305-316.
80. Eke, R. and Senturk, A., 2012,"Performance comparison of a double-axis sun tracking versus fixed PV system", *Solar Energy*, *86*(9), pp.2665-2672.
81. Bentaher, H., Kaich, H., Ayadi, N., Hmouda, M.B., Maalej, A. and Lemmer, U., 2014, "A simple tracking system to monitor solar PV panels", *Energy conversion and management*, *78*, pp.872-875.
82. Nadia, A.R., Isa, N.A.M. and Desa, M.K.M., 2020, "Efficient single and dual axis solar tracking system controllers based on adaptive neural fuzzy inference system", *Journal of King Saud University-Engineering Sciences*, *32*(7), pp.459-469.
83. Fares, D., Fathi, M., Shams, I. and Mekhilef, S., 2021," A novel global MPPT technique based on squirrel search algorithm for PV module under partial shading conditions", *Energy Conversion and Management*, *230*, p.113773.
84. Pervez, I., Shams, I., Mekhilef, S., Sarwar, A., Tariq, M. and Alamri, B., 2021, "Most Valuable Player Algorithm Based Maximum Power Point Tracking for a Partially Shaded PV Generation System", *IEEE Transactions on Sustainable Energy*, 12(4), pp.1876-1890.
85. Kermadi, M., Mekhilef, S., Salam, Z., Ahmed, J. and Berkouk, E.M., 2020, "Assessment of maximum power point trackers performance using direct and indirect control methods", *International Transactions on Electrical Energy Systems*, *30*(10), p.e12565.
86. Rodríguez-Gallegos, C.D., Gandhi, O., Panda, S.K. and Reindl, T., 2020, "On the PV tracker performance: tracking the sun versus tracking the best orientation", *IEEE Journal of Photovoltaics*, *10*(5), pp.1474-1480.
87. Kasburg, C. and Stefenon, S.F., 2019, "Deep learning for photovoltaic generation forecast in active solar trackers", *IEEE Latin America Transactions*, *17*(12), pp.2013-2019.

88. Wu, J., Chen, X. and Wang, L., 2015, "Design and dynamics of a novel solar tracker with parallel mechanism", *IEEE/ASME Transactions on Mechatronics*, *21*(1), pp.88-97.
89. Stefenon, S.F., Kasburg, C., Nied, A., Klaar, A.C.R., Ferreira, F.C.S. and Branco, N.W., 2020, "Hybrid deep learning for power generation forecasting in active solar trackers", *IET Generation, Transmission & Distribution*, *14*(23), pp.5667-5674.
90. Ghazali, A.M. and Rahman, A.M.A., 2012, "The performance of three different solar panels for solar electricity applying solar tracking device under the Malaysian climate condition", *Energy and environment Research*, *2*(1), p.235.
91. Choi, Y.K. and Lee, Y.G., 2014, "A study on development of rotary structure for tracking-type floating photovoltaic system", *International journal of precision engineering and manufacturing*, *15*(11), pp.2453-2460.
92. Wu, J., Hou, H. and Yang, Y., 2016, "Annual economic performance of a solar-aided 600 MW coal-fired power generation system under different tracking modes, aperture areas, and storage capacities", *Applied Thermal Engineering*, *104*, pp.319-332.
93. Hong, T., Jeong, K., Ban, C., Oh, J., Koo, C., Kim, J. and Lee, M., 2016, "A preliminary study on the 2-axis hybrid solar tracking method for the smart photovoltaic blind", *Energy Procedia*, *88*, pp.484-490.
94. Vijayalakshmi, K., Narendra, B. and Anjaneyulu, K.S.R., 2016, "Designing a dual axis solar tracking system for maximum power", *J Electr Electron Syst*, *5*, pp.1-3.
95. Bhaskar, K. and Yuvaraj, K., 2016, "Solar powered vehicle under GSM network by using solar tracking & monitoring", *Int. J. Eng. Dev. Res*, *4*(1), pp.263-270.
96. Sallaberry, F., de Jalón, A.G., Torres, J.L. and Pujol-Nadal, R., 2015, "Optical losses due to tracking error estimation for a low concentrating solar collector", *Energy Conversion and Management*, *92*, pp.194-206.
97. Parmar, N.J., Parmar, A.N. and Gautam, V.S., 2015, "Passive solar tracking system", *International Journal of Emerging Technology and Advanced Engineering*, *5*(1), pp.138-145.
98. Lazaroiu, G.C., Longo, M., Roscia, M. and Pagano, M., 2015, "Comparative analysis of fixed and sun tracking low power PV systems considering energy consumption", *Energy Conversion and Management*, *92*, pp.143-148.

99. Fathabadi, H., 2016, "Novel online sensorless dual-axis sun tracker", *IEEE/ASME transactions on mechatronics*, *22*(1), pp.321-328.
100. Pelaez, S.A., Deline, C., Greenberg, P., Stein, J.S. and Kostuk, R.K., 2019, "Correction: Model and Validation of Single-Axis Tracking with Bifacial PV", *IEEE Journal of Photovoltaics*, *9*(6), pp.715-721.
101. du Plessis, A.A., Strauss, J.M. and Rix, A.J., 2020, "Application of dust mitigation strategies to single-axis-tracking photovoltaic modules in the semi-arid areas of South Africa", *IET Renewable Power Generation*, *14*(15), pp.2781-2790.
102. Achuthan, K., Freeman, J.D., Nedungadi, P., Mohankumar, U., Varghese, A., Vasanthakumari, A.M., Francis, S.P. and Kolil, V.K., 2020, "Remote triggered dual-axis solar irradiance measurement system", *IEEE Transactions on Industry Applications*, *56*(2), pp.1742-1751.
103. Zhao, D., Xu, E., Wang, Z., Yu, Q., Xu, L. and Zhu, L., 2016, "Influences of installation and tracking errors on the optical performance of a solar parabolic trough collector", *Renewable energy*, *94*, pp.197-212.
104. Fathabadi, H., 2016, "Novel high accurate sensorless dual-axis solar tracking system controlled by maximum power point tracking unit of photovoltaic systems", *Applied Energy*, *173*, pp.448-459.
105. Parthipan, J., Raju, B.N. and Senthilkumar, S., 2016, "Design of one axis three position solar tracking system for paraboloidal dish solar collector. *Materials Today", Proceedings*, *3*(6), pp.2493-2500.
106. Kumar, N.K., Subramaniam, V. and Murugan, E., 2018, "Power analysis of non-tracking PV system with low power RTC based sensor independent solar tracking (SIST) PV system", *Materials Today: Proceedings*, *5*(1), pp.1076-1081.
107. Avarand, S. and Pirmoradian, M., 2016, "Solar tracking system with momentary tracking based on operational amplifiers in order to be used in photovoltaic panels for following the sun", *Bull. la Société R. des Sci. Liège*, *85*, pp.269-277.
108. Li, L., Li, H., Xu, Q. and Huang, W., 2015, "Performance analysis of azimuth tracking fixed mirror solar concentrator", *Renewable Energy*, *75*, pp.722-732.
109. Hussain, M.I. and Lee, G.H., 2015, "Experimental and numerical studies of a U-shaped solar energy collector to track the maximum CPV/T system output by varying the flow rate", *Renewable energy*, *76*, pp.735-742.
110. Patel, R.R. and Shewale, A.N., 2015, "Intelligent sun tracking system using FLC implemented on FPGA", *Int. J. Adv. Found. Res. Comput*, *2*(10), pp.260-263.

111. Das, S., Chakraborty, S., Sadhu, P.K. and Sastry, O.S., 2015, "Design and experimental execution of a microcontroller (μC)-based smart dual-axis automatic solar tracking system", *Energy Science & Engineering*, *3*(6), pp.558-564.
112. Saymbetov, A.K., Nurgaliyev, M.K., Tulkibaiuly, Y., Toshmurodov, Y.K., Nalibayev, Y.D., Dosymbetova, G.B., Kuttybay, N.B., Gylymzhanova, M.M. and Svanbayev, Y.A., 2018, "Method for increasing the efficiency of a biaxial solar tracker with exact solar orientation", *Applied Solar Energy*, *54*(2), pp.126-130.
113. Safaraliev, M.K., Odinaev, I.N., Ahyoev, J.S., Rasulzoda, K.N. and Otashbekov, R.A., 2020, "Energy Potential Estimation of the Region's Solar Radiation Using a Solar Tracker", *Applied Solar Energy*, *56*(4), pp.270-275.
114. Rambhowan, Y. and Oree, V., 2014, "Improving the dual-axis solar tracking system efficiency via drive power consumption optimization", *Applied Solar Energy*, *50*(2), pp.74-80.
115. Reges, J.P., Moreira, F.D.L., Bezerra, L.D.S., de Alexandria, A.R. and Reboucas Filho, P.P., 2015, "Thermographic image processing application in solar followers", *IEEE Latin America Transactions*, *13*(10), pp.3350-3358.
116. Hammad, B.K., Fouad, R.H., Nijmeh, S.D., Mohsen, M. and Tamimi, A., 2014, "Adaptive control of solar tracking system", *IET Science, Measurement & Technology*, *8*(6), pp.426-431.
117. Akhlaghi, S., Sangrody, H., Sarailoo, M. and Rezaeiahari, M., 2017, "Efficient operation of residential solar panels with determination of the optimal tilt angle and optimal intervals based on forecasting model", *IET Renewable Power Generation*, *11*(10), pp.1261-1267.
118. Fazlizan, A., Abdulmula, A., Amran, A.N., Lim, C.H. and Sopian, K., 2019, "Performance evaluation of maximum light detection solar tracking system in the tropics", *Journal of Mechanical Science & Technology*, *33*(3).
119. Oh, S.J., Burhan, M., Ng, K.C., Kim, Y. and Chun, W., 2015, "Development and performance analysis of a two-axis solar tracker for concentrated photovoltaics", *International Journal of Energy Research*, *39*(7), pp.965-976.
120. B H Khan, 2009, *Non-Conventional Energy Resources*, Tata McGraw-Hill Pub. Co., New Delhi, ISBN 0-07-060654-4, pp. 1-451, 2009, Chap.
121. Gazia Manzoor, Kamalkant Sharma, Satyanand Vishwakarma, 2019, "PSO-GSA based MPPT Algortihm for Photovoltaic Sytems", *International Journal of*

Recent Technology and Engineering (IJRTE), 7(6S4), pp. 259-263.

122. Renaudineau, H., Donatantonio, F., Fontchastagner, J., Petrone, G., Spagnuolo, G., Martin, J.P. and Pierfederici, S., 201,." A PSO-based global MPPT technique for distributed PV power generation", *IEEE Transactions on Industrial Electronics*, *62*(2), pp.1047-1058.
123. Vpiasha Sharma, Harpreet Kaur, Inderpreet Kaur, 2019, Design and Implemetation of Multi Junction PV cell for MPPT to improve the Transformation efficiency, Chap.
124. Sundareswaran, K., Vigneshkumar, V., Sankar, P., Simon, S.P., Nayak, P.S.R. and Palani, S., 2015, "Development of an improved P&O algorithm assisted through a colony of foraging ants for MPPT in PV system", *IEEE transactions on industrial informatics*, *12*(1), pp.187-200.
125. Teshome, D.F., Lee, C.H., Lin, Y.W. and Lian, K.L., 2016, "A modified firefly algorithm for photovoltaic maximum power point tracking control under partial shading", *IEEE Journal of Emerging and Selected Topics in Power Electronics*, *5*(2), pp.661-671.
126. Liu, X., Wang, P. and Loh, P.C., 2011, "A hybrid AC/DC microgrid and its coordination control", *IEEE Transactions on smart grid*, *2*(2), pp.278-286.
127. Ahmed, J. and Salam, Z., 2015, "A critical evaluation on maximum power point tracking methods for partial shading in PV systems", *Renewable and Sustainable Energy Reviews*, *47*, pp.933-953.
128. Lodin, O., Kaur, I. and Kaur, H., 2019, "Predictive-P&O Mppt Algorithm for Fast and Reliable Tracking of Maximum Power Point in Solar Energy Systems", *International Journal of Recent Technology and Engineering (IJRTE)*, *7*, pp.264-268.
129. Haruni, A.O., Negnevitsky, M., Haque, M.E. and Gargoom, A., 2012, "A novel operation and control strategy for a standalone hybrid renewable power system", *IEEE transactions on sustainable energy*, *4*(2), pp.402-413.
130. Paz, F. and Ordonez, M., 2014, "Zero oscillation and irradiance slope tracking for photovoltaic MPPT", *IEEE Transactions on Industrial electronics*, *61*(11), pp.6138-6147.
131. Shefali, Harvinder Singh, Sachin Kumar, Inderpreet Kaur, 2019, "Designing and Imulation of Solar module in the Islanded network of a solar PV microgrid",

International Journal of Recent Technology and Engineering (IJRTE), 7(6S4), pp. 254-258.

132. Kumar, K., Varshney, L., Ambikapathy, A., Saket R.K. and Mekhilef, S., "Solar Tracker Transcript – A Review", *International Transactions on Electrical Energy Systems (ITEES)*. Accepted, 2021.
133. Despotou, E., 2012, *Vision for Photovoltaics in the Future, Comprehensive Renewable Energy*, 1, ISBN 9780080878737, PP. 179-198, Chap.
134. (IRENA) TIREA,' 2020 report on Solar energy generated electricity of world and India 'https://www.irena.org/-/media/Files/IRENA/Agency/Publication/2020/Jul/IRENA_Renewable_Energy_Statistics_2020.pdf, 2020.
135. Prinsloo, G. and Dobson, R., 2015, *Sun Tracking and Solar Renewable Energy Harvesting: Solar Energy Harvesting, Trough, Pinpointing and Heliostat Solar Collecting Systems*, Prinsloo, Dobson, South Africa, 2, ISBN 978-0-620-61576-1, pp. 3-401,Chap.
136. Said, S.A., Hassan, G., Walwil, H.M. and Al-Aqeeli, N., 2018, "The effect of environmental factors and dust accumulation on photovoltaic modules and dust-accumulation mitigation strategies", *Renewable and Sustainable Energy Reviews*, *82*, pp.743-760.
137. Abdollahpour, M., Golzarian, M.R., Rohani, A. and Zarchi, H.A., 2018, "Development of a machine vision dual-axis solar tracking system", *Solar Energy*, *169*, pp.136-143.
138. Kumar, K., Varshney, L., Ambikapathy, A., Mittal, V., Prakash, S., Chandra, P. and Khan, N., 2021, "Soft computing and IoT based solar tracker", *International Journal of Power Electronics and Drive Systems*, *12*(3), p.1880.
139. Lee, C.D., Huang, H.C. and Yeh, H.Y., 2013, "The development of sun-tracking system using image processing", *Sensors*, *13*(5), pp.5448-5459.
140. Wei, C.C., Song, Y.C., Chang, C.C. and Lin, C.B., 2016, "Design of a solar tracking system using the brightest region in the sky image sensor", *Sensors*, *16*(12), p.1995.
141. Kumar, K., Varshney, L., Ambikapathy, A., Ali, I., Rajput, A., Bhatnagar, A. and Omar, S., 2021, "Vision based solar tracking system for efficient energy harvesting", *International Journal of Power Electronics and Drive Systems*, *12*(3), p.1431.

142. Carballo, J.A., Bonilla, J., Berenguel, M., Fernández-Reche, J. and García, G., 2019, "New approach for solar tracking systems based on computer vision, low cost hardware and deep learning", *Renewable energy*, *133*, pp.1158-1166.
143. Kumar, K., Saurabh, Devendra and Gaur, N., 2013, "A Review on Image Processing", *National Conference on Emerging Trends in Electrical, Instrumentation & Communication Engineering*, 4(7), pp. 47-55.
144. Kumar, K. and Khan, AA., 2011, "A Review on Face Recognition Using Genetic Algorithm and Back-Propagation Neural Network", *National conference on Recent Advances in Computational Techniques in Electrical Engineering(RACTEE),* ;PP. 84-1-84-4.
145. Kumar, K., Anand, S., Gurjar, S. and Saxena, V., 2012, "Image denoising based on wavelet transformation", *International Conference on Recent Trends of Computer Technology in Academic (ICRTCTA),* Janardan Rai Nagar Rajasthan Vidyapeeth University; pp. 1-7.
146. Martins, F., Felgueiras, C., Smitkova, M. and Caetano, N., 2019, "Analysis of fossil fuel energy consumption and environmental impacts in European countries", *Energies*, *12*(6), p.964.
147. Lee, Y.J., Kim, B.S., Ifitiquar, S.M., Park, C. and Yi, J., 2014, "Silicon solar cells: Past, present and the future", *Journal of the Korean Physical Society*, *65*(3), pp.355-361.
148. Asim, M., Khan, M.S., Ahmad, J., Umar, T. and Riyaz, A., 2020, "Efficiency Enhancement of Solar Panel Using Photodiode", In *Energy Systems, Drives and Automations* (pp. 215-223). Springer, Singapore.
149. Sinha, S., Agarwal, P., Gupta, N.K., Asim, M. and Riyaz, A., 2020, "Performance of Solar Cell Under Changing Atmospheric Condition", In *Energy Systems, Drives and Automations* (pp. 225-234). Springer, Singapore.
150. Mirdanies, M., 2015, "Astronomy algorithm simulation for two degrees of freedom of solar tracking mechanism using Clanguage", *Energy Procedia*, *68*, pp.60-67.
151. Mousavi Maleki, S.A., Hizam, H. and Gomes, C., 2017, "Estimation of hourly, daily and monthly global solar radiation on inclined surfaces: Models re-visited", *Energies*, *10*(1), p.134.
152. Tahseen, M., Charan, P., Maurya, S. and Asim, M., 2018, "Life Cycle Performance & Analysis of 100kw Solar PV Plant", *Life*, *8*(7).

153. Yan, X., Wen, L. and Gao, L., 2019, "A fast and effective image preprocessing method for hot round steel surface", *Mathematical Problems in Engineering*, *2019*.
154. Kumar, K., 2013, "Enhancement of image contrast using histogram Equalization", *National conference on Emerging Trends in Engineering & Technology (ETEAT).* VIT, Dadri , UP; pp. 1-4, 2013.
155. Lee, C.Y., Chou, P.C., Chiang, C.M. and Lin, C.F., 2009, "Sun tracking systems: a review", *Sensors*, *9*(5), pp.3875-3890.
156. Akhtar, I., Asim, M., Yadav, R.K., Agarwal, P. and Kirmani, S., 2019, "August. Design of Effective Grid-Connected Solar System", In *International Conference on Inventive Computation Technologies,* Springer, Cham, pp. 606-614.
157. Virmani, D., Jain, N., Parikh, K. and Upadhyaya, S., 2018, "Boundary Outlier Centroid Based Reduced Overlapping Image Segmentation", *Journal of Engineering Science & Technology Review, 11*(5).
158. Kumar, K., Anand, S. and Yadava, R.L., 2012, "Advanced dsp technique to remove baseline noise from ecg signal", *International Journal of Electronics and Computer Science Engineering,* vol. 1, no. 3, pp. 1013-1019.
159. Asim, M., Mallick, M.A., Malik, A. and Saaqib, M., 2015, "Modelling and simulation of 5 parameter model of solar cell", *International Journal of Electronics, Electrical and Computational System,* 4, pp. 38-42.
160. Solarin, S.A., Bello, M.O. and Bekun, F.V., 2021, "Sustainable electricity generation: the possibility of substituting fossil fuels for hydropower and solar energy in Italy", *International Journal of Sustainable Development & World Ecology*, *28*(5), pp.429-439.
161. Fouad, M.M., Shihata, L.A. and Morgan, E.I., 2017, "An integrated review of factors influencing the perfomance of photovoltaic panels", *Renewable and Sustainable Energy Reviews, 80,* pp.1499-1511.
162. Sumathi, V., Jayapragash, R., Bakshi, A. and Akella, P.K., 2017, "Solar tracking methods to maximize PV system output–A review of the methods adopted in recent decade", *Renewable and Sustainable Energy Reviews*, *74,* pp.130-138.
163. Hafez, A.Z., Yousef, A.M. and Harag, N.M., 2018, "Solar tracking systems: Technologies and trackers drive types–A review", *Renewable and Sustainable Energy Reviews, 91,* pp.754-782.

164. Abdollahpour, M., Golzarian, M.R., Rohani, A. and Zarchi, H.A., 2018' "Development of a machine vision dual-axis solar tracking system", *Solar Energy*, *169*, pp.136-143.
165. Al-Ammri, A.S., Al-Attar, F.I.M. and Ahmad, F.F., 2015, "Performance test of two-axis solar tracker system with distinct tracking strategies", *AASCIT Journal of Energy*, *2*(5), pp.57-60.
166. Kumar, K., Khan, AA. , 2012, *Fast Face Recognition using Back Propagation Neural- Network*, National conference on Green Technology: Smart and efficient Management, SLIET Longowal, pp.GT21-1-GT25-5.
167. Kumar, K., 2012, "Artificial neural network based face detection using gabor feature extraction*", Int J Adv Technol Eng Res. ,* 2(4), pp. 220 -225.
168. Sidek, M.H.M., Azis, N., Hasan, W.Z.W., Ab Kadir, M.Z.A., Shafie, S. and Radzi, M.A.M., 2017, "Automated positioning dual-axis solar tracking system with precision elevation and azimuth angle control", *Energy*, *124*, pp.160-170.
169. Yılmaz, M. and Kentli, F., 2015, "Increasing of electrical energy with solar tracking system at the region which has Turkey's most solar energy potential", *Journal of Clean Energy Technologies*, *3*(4), pp.287-290.
170. Jacobson, M.Z. and Jadhav, V., 2018, "World estimates of PV optimal tilt angles and ratios of sunlight incident upon tilted and tracked PV panels relative to horizontal panels", *Solar Energy*, *169*, pp.55-66.
171. Yuan, J., Farnham, C., Emura, K. and Lu, S., 2016, "A method to estimate the potential of rooftop photovoltaic power generation for a region", *Urban Climate*, *17*, pp.1-19.
172. Maddison, R. and Mhurchu, C.N., 2009, "Global positioning system: a new opportunity in physical activity measurement", *International Journal of Behavioral Nutrition and Physical Activity*, *6*(1), pp.1-8.
173. K, Kumar. and AA, Khan., 2011, *A Review on Face Recognition Using Genetic Algorithm and Back Propagation Neural Network*, Recent Advances in Computational Techniques in Electrical Engineering, SLIET, Longowal, pp. 1–5, 2011.
174. Hafez, A.Z., Yousef, A.M. and Harag, N.M., 2018, "Solar tracking systems: Technologies and trackers drive types–A review", *Renewable and Sustainable Energy Reviews*, *91*, pp.754-782.
175. Tirmikci, C.A. and Yavuz, C., 2015, "Comparison of solar trackers and

application of a sensor less dual axis solar tracker", *Journal of Energy and Power Engineering*, *9*, pp.556-561.

176. Monika, Year-end review-2020, PIB Delhi, [Online] Available: https://www.pib.gov.in/PressReleseDetailm, 2020.
177. B. M. Tayal, Which States Have the Highest Solar Energy Potential in India-Saur Energy International, https://www.saurenergy.com/solar-energy-blog/which-states-have-the-highest-solarenergy-potential-in-india, 2021.
178. Cotfas, D.T. and Cotfas, P.A., 2019, "Multiconcept methods to enhance photovoltaic system efficiency", *International Journal of Photoenergy*, 2019, pp. 1-15.
179. Sungur, C., 2009, "Multi-axes sun-tracking system with PLC control for photovoltaic panels in Turkey", *Renewable energy*, *34*(4), pp.1119-1125.
180. Mamlook, R., Nijmeh, S. and Abdallah, S.M., 2006, "A programmable logic controller to control two axis sun tracking system", *Information Technology Journal*, *5*(6), pp.1083-7.
181. Muhammad, B., Seung, J.O., Ng, K.C. and Chun, W.O.N.G.E.E., 2016, "Experimental investigation of multijunction solar cell using two axis solar tracker", In *Applied mechanics and materials* (Vol. 818, pp. 213-218). Trans Tech Publications Ltd.
182. Sneineh, A.A. and Salah, W.A., 2019, "Design and implementation of an automatically aligned solar tracking system", *International Journal of Power Electronics and Drive Systems*, *10*(4), p.2055-2064.
183. Mohaimin, A.H., Uddin, M.R. and Khalil, A., 2020, "Self-sustaining and externally-powered fixed, single, and dual-axis solar trackers", *International Journal of Power Electronics and Drive Systems*, *11*(2), p.1031-1039.
184. Loon, C.M. and Daud, M.Z., 2020, "Sensorless dual axis solar tracker using improved sun position algorithm", *International Journal of Power Electronics and Drive Systems*, *11*(3), p.1305.
185. Rubio, F.R., Ortega, M.G., Gordillo, F. and Lopez-Martinez, M., 2007, "Application of new control strategy for sun tracking", *Energy Conversion and Management*, *48*(7), pp.2174-2184.
186. Awasthi, A., 2020, "Review on sun tracking technology in solar PV system", Energy Rep 6: 392–405.
187. Kumar, S., Tiwari, P. and Zymbler, M., 2019, "Internet of Things is a

revolutionary approach for future technology enhancement: a review", *Journal of Big data*, *6*(1), pp.1-21.

188. Kakar, Saboor., Sheikh, Naveed., Naseem, Adnan., Iqbal, Saleem., Rehman, Abdul., ullah, Aziz., Ahmad, Bilal., Ali, Hazrat. and Khan, Bilal, 2018, "Artificial Neural Network based Weather Prediction using Back Propagation Technique", *International Journal of Advanced Computer Science and Applications*, 9(8), pp. 462-470.
189. Louis, L., 2016, "working principle of Arduino and using it", *International Journal of Control, Automation, Communication and Systems (IJCACS)*, *1*(2), pp.21-29.
190. Abdalla, M., Dr. Zhijun P. and Faustini L. 2015, "Image Noise Reduction and Filtering Techniques*", International Journal of Science and Research (IJSR)*, *6*(3), pp.2033-2038.
191. Al-Naima, F.M., Ali, R.S. and Abid, A.J., 2013, May. Solar tracking system: design based on GPS and astronomical equations. In *IT-DREPS Conf. Exhib* (pp. 1-6).